National Library
of Canada

Acquisitions and
Bibliographic Services Branch

395 Wellington Street
Ottawa, Ontario
K1A 0N4

Bibliothèque nationale
du Canada

Direction des acquisitions et
des services bibliographiques

395, rue Wellington
Ottawa (Ontario)
K1A 0N4

Your file Votre référence

Our file Notre référence

NOTICE

The quality of this microform is heavily dependent upon the quality of the original thesis submitted for microfilming. Every effort has been made to ensure the highest quality of reproduction possible.

If pages are missing, contact the university which granted the degree.

Some pages may have indistinct print especially if the original pages were typed with a poor typewriter ribbon or if the university sent us an inferior photocopy.

Reproduction in full or in part of this microform is governed by the Canadian Copyright Act, R.S.C. 1970, c. C-30, and subsequent amendments.

AVIS

La qualité de cette microforme dépend grandement de la qualité de la thèse soumise au microfilmage. Nous avons tout fait pour assurer une qualité supérieure de reproduction.

S'il manque des pages, veuillez communiquer avec l'université qui a conféré le grade.

La qualité d'impression de certaines pages peut laisser à désirer, surtout si les pages originales ont été dactylographiées à l'aide d'un ruban usé ou si l'université nous a fait parvenir une photocopie de qualité inférieure.

La reproduction, même partielle, de cette microforme est soumise à la Loi canadienne sur le droit d'auteur, SRC 1970, c. C-30, et ses amendements subséquents.

Canada

Studies of the Kinetics of Cluster Redistribution in CCl_3F Vapours

By

ZHIKAI CHENG

A thesis presented to the University of Ottawa

in partial fulfilment of the requirements for the degree of

DOCTOR OF PHILOSOPHY

Department of Chemistry

University of Ottawa

Ottawa, Canada

Ph. D. Candidate

Zhikai Cheng

Research Supervisor

Dr. Heshel Teitelbaum

ISBN 0-315-95899-5

Canada

UNIVERSITÉ D'OTTAWA
UNIVERSITY OF OTTAWA

ACKNOWLEDGEMENT

I would like to thank Professor Teitelbaum, my research supervisor, for his invaluable advice, scientific guidance, enormous encouragement, continuous support and patience throughout my studies, and for his proofreading. Without his precious help this thesis could not be finished. My thanks are extended to all the professors whose courses I have taken, and to the support staff who helped me at various stages of this study.

I would like to acknowledge the helpful discussions and the friendship of my group-mates Del Permann and Zhichun Su.

I would like to thank my father, Wenyu Cheng, and my mother, Baozhen Li, for their unwavering support and understanding throughout my studies, and my wife, Zhun Zheng, for her help.

ABSTRACT

A shock tube coupled to a laser-schlieren detection system in conjunction with computer simulation was used to study the formation of small clusters in nearly saturated Freon-11 vapour. When a shock wave passed through Freon-11 vapour a temperature and pressure jump was produced. A new equilibrium cluster distribution at the new temperature and pressure was reached by formation and stabilization of clusters, this being an exothermic reaction. This process is accompanied by a temperature and density change. The laser-schlieren technique records a signal proportional to the density gradient. In the experimental studies the initial pressure of CCl_3F was varied from 26 mm Hg to 762 mm Hg and the speed of the shock wave was changed from 141.1 m/s to 320.7 m/s. Several carefully chosen gases (Ar, CH_4, CCl_4 and SF_6) were used for comparison studies. The time scale for the observed process was 10 - 100 μs. Characteristic of bond formation, the observed process displayed a negative activation energy suggesting a strong competition between cluster formation, dissociation and stabilization. Oscillatory signals were observed in those cases where the initial pressure was high, the postshock temperature was low and the postshock pressure was high. It was found that the oscillatory signal was biperiodic at an early stage. Then this oscillatory signal became a chaotic one. The experimentally reproducible chaotic signals are proof that the processes occurring in our system are nonlinear kinetic processes. A computational model for the rate of formation of clusters (cluster size <5) based on the

scheme $A_{n-1} + A = A_n^*$ and $A_n^* + M = A_n + M$, was built and constrained by experimental observation, thermodynamics and nonlinear kinetics. With the help of computer simulation it was confirmed that the negative signal observed is caused by the cluster formation process followed by exothermic cluster collisional stabilization. The oscillation is a direct result of thermal feedback affecting the equilibrium cluster distribution.

CONTENTS

List of Figures

List of Tables

CHAPTER 1

INTRODUCTION

1.1 Phase Transformation , Nucleation and Clustering

Phase transformations are involved in many branches of science and technology including physics, chemistry, astrophysics, meteorology, metallurgy, medicine and biology. Some phase transformations appear to occur without hinderance whenever conditions change such that a new phase becomes stable, for example, the evaporation of a pure liquid or the melting of a pure crystal. These phase transitions occur so reproducibly that they are often used as thermometric fixed points. In organic chemistry the melting point of a compound is measured to check its purity. If a substance is pure, it melts at its normal melting point, otherwise it melts below its melting point. However, there are other phase transitions for which this is not the case, for example, the condensation of a vapour or the crystallisation of a melt. The dew point of water vapour at 0.22 atm is 20 °C , but at 20 °C water vapour can be supersaturated to 0.75 atm pressure before condensation occurs[1]. Also while the melting point of Aluminum is 660 °C, it can be cooled to 200 °C before solidification occurs[2]. The difference between phase changes which occur at equilibrium and those which do not occur at equilibrium is apparently the result of the presence of

"free" surfaces on which a new phase can form in the form case. If we let vapour be in contact with its bulk liquid, vapour can condense at equilibrium. We cannot get supersaturated vapour because bulk liquid provides a free surface. The reason why a crystal melts at equilibrium is that the crystal always provides a free surface to its melt under ordinary conditions. Experiments have shown that if crystals are poorly wetted by their melts, crystals can be superheated[3,4].

Why does the free surface make so big a difference to phase transformations? The answer can be found from thermodynamics. When a liquid is dispersed as droplets of radius r, its vapour pressure is given by the Kelvin equation[5]

$$P=P^{o}\exp\left(\frac{2\sigma V_m}{RTr}\right) \qquad (1.1.1)$$

P^o is the vapour pressure of the bulk liquid at temperature T; V_m is the molar volume of liquid; r is the radius of a droplet; σ is the surface free energy; T is in Kelvin; and R is the universal gas constant. In the case of droplets of water of radius 10^{-3}mm and 10^{-6} mm the ratios of P/P^o are about 1.001 and 3.0 respectively. The latter value, although quite large, is not quite exact because at that radius the droplet is less than 56 molecules in size, and the Kelvin equation is not valid in that regime. However, for "large" droplets the effect is usually small. To see the significance of these vapour processes on condensation consider a pure vapour, initially unsaturated at sufficiently high temperature, i.e. the pressure of the vapour is lower than its vapour pressure. Now decrease the

temperature. When the system becomes saturated, the pressure of the vapour equals the bulk vapour pressure. Decrease the temperature further. Then the pressure of the vapour is higher than the vapour pressure at that low temperature. This is a supersaturated system that is thermodynamically unstable with respect to its liquid phase. In order to convert the unstable vapour into stable liquid the first step must be the sticking together of a number of vapour molecules to form a microscopic droplet. This process is called nucleation. Since the radius of the initial droplets is so small they have an enhanced vapour pressure according to the Kelvin equation. Therefore, they evaporate as soon as they form. This effect prevents stabilization of the thermodynamically unstable vapour, because an initial tendency to condense is overcome by a heightened tendency to evaporate. However, if the tiny droplets can continue to stick together to form larger droplets before they evaporate, then "large" low vapour pressure droplets can form. Clearly kinetic effects determine if a supersaturated vapour phase can exist, If, however, there is a free surface provided by dust or other kinds of foreign matter, vapour molecules can attach to the free surface. The radius of this surface is big enough to make the enhanced pressure negligible. Consequently, vapour can easily condense into stable liquid. If the bulk liquid phase coexists with its vapour, when the temperature is decreased the molecules in the vapour phase attach to the liquid surface, i.e. the transformation will advance on the free surface, where the radius of the bulk liquid is essentially infinite. Therefore, no enhanced pressure can exist under these conditions and the phase transformation can be carried out at equilibrium.

In the case of the melting of a crystal it is well known that under ordinary conditions overheating the crystal, similar to overheating a liquid, is impossible. The basis of the Lindemann (1910) theory[3,6] of melting is that as the solid is heated the atoms start to vibrate with greater and greater amplitudes until, at some critical value, the interaction of adjacent atoms 'shakes the solid to pieces'. It had been widely assumed that a crystal cannot exist above its melting temperature, and the free energy curve of the solid phase terminates discontinuously at the melting point. In 1937 this theory of melting was proved to be wrong by experiment[7]. The relation[3] of the melting temperature with the radius of a melt droplet can be derived in following way. Suppose that the transformation of solid to liquid advances so that the sphere of the melt reaches an increased radius r+dr, where dr is very small. The chemical potentials of a molecule in solid and melt are μ_s and μ_l, respectively and dn moles of molecule transfer from the solid to the melt. Then there is a change in the Gibbs free energy, $(\mu_s - \mu_l)dn$. For equilibrium this is equated with the increased free interfacial energy, γ_{sl} dA. For a sphere melt $dA=8\pi rdr$ and $dv=vdn=4\pi r^2 dr$ where v is the molar volume of the melt. Then for equilibrium

$$\mu_l - \mu_s = \frac{2\gamma_{sl}}{r} v \qquad (1.1.2)$$

This shows that there is an increase in the chemical potential of the melt phase due to presence of a spherical interface. For equilibrium of a spherical melt droplet with the solid phase, the temperature must be above the normal melting point by $\Delta T=T'-T_m$. This is shown schematically in fig. 1.1, in which the chemical potential of the two bulk phases are given by the solid line, the broken line is the chemical potential of the spherical melt

droplet of radius, r, and T_m is the normal melting point .

However, since a molecule in fluid can attach onto its solid free surface, the melting of a crystal kept at a homogeneous temperature always begins on the free surface[8]. A flat embryo of the liquid phase is formed on the free surface. There are no micro-droplets or spherical interfaces; r tends to infinity. Therefore ΔT equals zero. This results is a natural consequence of the fact that the surface free energy of a liquid is smaller than that of any face of the corresponding crystal and that the surface free energy between the two phases is very small.

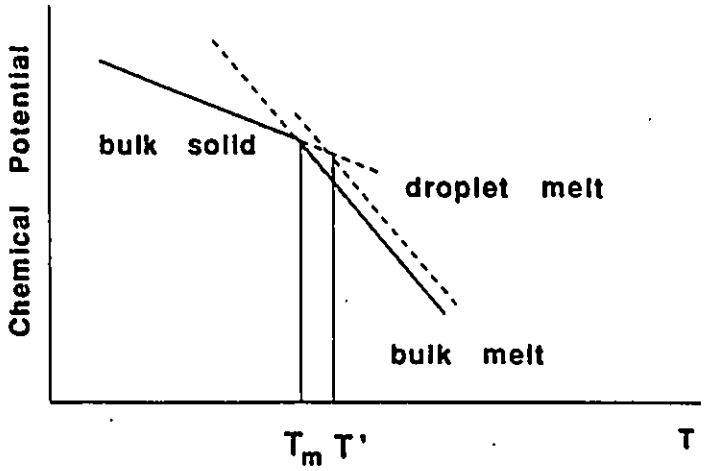

Fig 1.1 Schematic figure to illustrate melting temperature increase for droplets.

The proof that an overheated crystal can exist is given by the experiment performed by Khaikin[7] in which the crystal is cooled down from its surface so that the temperature of

the surface lies below the melting-point. Then the internal temperature is raised (by concentrating radiant heat with the help of a lens) far above the melting-point without any trace of internal melting. This shows that in the absence of surface effects, melting can occur under non-equilibrium conditions, newly born liquid must form small droplets. Therefore, a crystal can be overheated. The presence of a free surface during a phase transformation changes the mechanism, avoiding the formation of small clusters.

These curious phenomena are manifestations of nucleation. Nucleation can be divided into two classes, heterogeneous and homogeneous, depending on whether foreign nuclei are present or not. If the phase transformation takes place in the presence of dust, a wall, ions, or micro-crystals etc, it is termed heterogeneous nucleation. It is difficult to characterize accurately the crucial experimental parameters in heterogeneous nucleation. Conversely, homogeneous nucleation is accurately characterizable, but it is difficult to study experimentally since it is difficult to provide an environment free of walls, dust, ions, bubbles, etc. However, there are cases where homogeneous nucleation is the dominant mechanism. Examples are condensation in supersonic nozzles, explosions that occur when a cold liquid comes in contact with a much hotter one, and the formation of heavily micro-crystallized ceramics.

In the absence of free surfaces a transformation from a phase α to a phase β does not occur the instant the free energy of β becomes lower than that of α. Rather, very small nuclei of β (having a critical size) must form initially in the α phase. The first step in

the transformation, the nucleation step, can be extremely slow. Once the initial nucleation step has occurred, though, the β-phase clusters will grow to form droplets. These droplets continue to grow or combine until the transformation is complete. The initial step of the phase transformation is nucleation, which is the process of cluster formation and growth staring from a small cluster leading to one of critical size. Nucleation theory attempts to describe the rate at which the first very small clusters nucleate at a given state of supersaturation.

In this chapter we shall discuss the basic concept of nucleation theory. The second section is devoted to the classical theory of nucleation. The drawbacks of this theory are discussed in the third section. Then some recent kinetic nucleation models are introduced. The experimental methods used for studying nucleation are discussed in the section 1.5, followed by an introduction to chemical oscillation.

1.2 Classical Homogeneous Nucleation Theory (CNT)

Nucleation theory is the theory of formation of critical clusters or nuclei. In the period 1876-1878, J. Willard Gibbs[9] developed the thermodynamic theory of curved surfaces and calculated the free energy of formation of a critical size cluster from supersaturated vapour. In 1926, Volmer and Weber[10] recognized that the metastability of a supersaturated phase is a question of kinetics, and they realized the relation between the free energy and the rate of formation of critical nuclei by spontaneous natural fluctuations in the parent

phase. However, Volmer and Weber did not develop a kinetic model. A kinetic approach was made by Farkas[11] in 1927. He developed a quantitative theory for the steady-state nucleation rate. On this basis, laid by Volmer and by Farkas, Becker and Doring[12], Zeldovich[13] and Frenkel[8] developed the so-called classical nucleation theory. Some good agreement between this theory and experiments has been obtained[14,15]. Nevertheless, many experimental results do not agree with the prediction of the classical theory[16-19]. Furthermore, many of the fundamental problems of nucleation theory cannot solved with the classical theory. Since then, some of the drawbacks and inconsistencies have been pointed out and corrected (see section 1.3). In the last twenty years new kinetic approaches have been proposed (see section 1.4). In this section we shall discuss the classical theory of nucleation, first, the thermodynamics, and then the kinetics .

1.2.1 Thermodynamics of Nucleation

The state of a macroscopic system in equilibrium can be described by thermodynamic theory. It is postulated that a system in equilibrium with its surroundings can be described by a number of extensive parameters, usually the entropy, S, the volume, V, and the total number of chemically different molecules, N_1, N_2,$\cdots$, N_m. For any equilibrium state there exists a function U(S, V, X_1, X_2 ,$\cdots$, X_{m-1}), the internal energy, in which X_i is the mole fraction of different components. The value assumed by the extensive parameters in the absence of an internal constraint are those that minimize the internal energy over the manifold of the constrained equilibrium state. The internal energy of the composite

system is additive over the constituent subsystems. The internal energy is continuous and differentiable and is a monotonically increasing function of the entropy. The internal energy of an equilibrium state can be written as follows

$$U(S, V, N_1, N_2, \cdots N_m) = TS - PV + \sum_{i=1}^{m} \mu_i N_i \tag{1.2.1}$$

Temperature is given by

$$T = \left(\frac{\partial U}{\partial S}\right)_{V, N_1, N_2 \cdots N_m} \tag{1.2.2}$$

Pressure is given by

$$P = -\left(\frac{\partial U}{\partial V}\right)_{S, N_1, N_2, \cdots N_m} \tag{1.2.3}$$

and chemical potential is given by

$$\mu_i = \left(\frac{\partial U}{\partial N_i}\right)_{S, V, N_j, j \neq i} \tag{1.2.4}$$

T, P and μ_1, μ_2, $\cdots$ μ_m are the intensive parameters of a system, which are not functions of the number of moles of substances. Combining the first and the second thermodynamic laws the following thermodynamic potentials can be defined:

Helmholtz free energy

$$A = U - TS \tag{1.2.5}$$

Gibbs free energy

$$G=U-TS+PV \tag{1.2.6}$$

With the above thermodynamic potentials and the state equation PV=nRT (assuming the vapour phase obeys the ideal gas law), we can show how classical theory explains the existence of a supersaturated vapour state and define the free energy of formation of clusters.

First let us show that the supersaturated vapour state is unstable. The thermodynamic system we consider is n moles of a vapour initially equilibrated at pressure P_1 and temperature T_1, where P_1 is less than the vapour pressure P_∞ at the same temperature. Then the pressure is increased isothermally so that the new pressure P exceeds the equilibrium vapour pressure of the condensed phase P_∞.

At the initial condition the vapour's chemical potential can be derived from

$$\left(\frac{\partial \mu}{\partial P}\right)_T = V \tag{1.2.7}$$

$$\mu=\mu_o(T)+RT\ln P_1 \tag{1.2.8}$$

If the vapour is not ideal, fugacities must be used instead of pressure. When the pressure of the system equals the vapour pressure at the same temperature, the chemical potential is given by

$$\mu_\infty=\mu_o(T)+RT\ln P_\infty \tag{1.2.9}$$

Because at P_∞ the vapour is at equilibrium with the corresponding liquid, μ_∞ is equal the chemical potential of the liquid state of that substance. When the pressure is higher than its vapour pressure, P_∞, at the same temperature, a supersaturated state is reached Assuming that the vapour can still be treated as an ideal gas, the chemical potential is given by

$$\mu=\mu_o(T)+RT\ln P \tag{1.2.10}$$

The chemical potential of the supersaturated vapour, μ, is higher than that of the corresponding liquid phase, μ_∞, because $P>P_\infty$, and the difference of the chemical potential, $\Delta\mu$, between the supersaturated vapour and liquid phase at the same temperature is given by

$$\Delta\mu=RT\ln\left(\frac{P}{P_\infty}\right)=RT\ln S \tag{1.2.11}$$

where S is the degree of supersaturation of the system. From this we see that $\Delta\mu=\mu-\mu_\infty>0$, meaning that the transformation of supersaturated vapour to liquid is a spontaneous process. Supersaturated vapour is a thermodynamically unstable system.

How can a supersaturated state exist even though it is unstable thermodynamically? The explanation is given by the classical theory as follows. The physical origin of stability of a supersaturated vapour is central to the development of a nucleation theory. Although condensation of supersaturated vapour to form the liquid phase will lower the free energy

of the system, the onset of condensation actually increases the free energy of the system before the subsequent decrease, and this prevents immediate condensation. The process of formation of a liquid phase within the old gaseous one must start by the formation of droplets (or clusters). As soon as embryonic droplets form, the surface-free-energy of the interfaces between the droplets and the surrounding vapour must be considered. There are two factors which determine the change of the total free energy of the system:

(1) The decrease in the bulk free energy due to condensation into liquid. The contribution is proportional to the number of molecules forming droplets.

(2) The increase of the surface free energy due to the formation of the droplets. It is proportional to the surface area of the droplets formed.

Assuming that the shape of a droplet is spherical, and that the bulk liquid is nearly incompressible, we can describe the change in the number of isothermally formed droplets from the supersaturated vapour mathematically by calculating the free energy change of the system, ΔF. The initial state is the supersaturated vapour ($P>P_\infty$) at temperature T. For the isothermal formation of a droplet from vapour molecules the free energy change is given by[20]

$$\Delta F=4\pi r^2\sigma-(\frac{4}{3})\pi r^3\rho RTln(\frac{P}{P_\infty}) \qquad (1.2.12)$$

where σ is the bulk surface tension having dimension J/m^2, r is the radius of the droplet, ρ is the density of the droplet, and $RTln(P/P_\infty)$ is the excess free energy of the supersaturated vapour over the saturated vapour as calculated in (Eq. 1.2.11). It is

multiplied by the total mass of the droplet. This free energy change of the system equals the free energy change of formation of the droplet. If the pressure of the vapour at the initial and final states for the process of isothermal formation of a droplet have the same value, as is assumed in classical nucleation theory, we have ΔA equal to ΔG. Since supersaturated vapour is not an equilibrium system, the calculation of ΔG is problematic. This question will be discussed later in section 1.3.

In equation 1.2.12, the first term on the right is the intrinsically positive contribution of the surface-free energy. The second term on the right is the free energy decrease caused by transferring molecules from the vapour to the liquid phase. The equation specifies the free energy change, ΔG, as a function of the radius of a droplet, r, and of the degree of supersaturation, S, for a fixed temperature, T. For the limiting case, S=1, the second term becomes zero, and ΔG rises monotonically as the square of r. For a sub-saturated vapour the ΔG curve would rise even more steeply, because a fractional S makes the second term on the right positive. Droplets cannot be formed in a subsaturated vapour system. For $S>1$, the second term is a negative contribution to ΔG. The higher the degree of supersaturation, the larger the absolute value of the second term. It is this term that assures the existence of a maximum in ΔG at a certain value of the droplet radius, r^*, which denotes the critical cluster radius. As the degree of supersaturation increases, r^* decreases. This is shown in the following derivation. We differentiate both sides of Eq. 1.2.12 with respect to r, holding T and S constant (assuming that cluster growth will not deplete the vapour stock by an amount producing measurable changes in P), and we let

the derivative equal zero. Solving for the critical radius, we find

$$r^* = \frac{2\sigma}{\rho RT \ln S} \tag{1.2.13}$$

Substituting r* into equation 1.2.12 the maximum value of ΔG (i.e. ΔG*) corresponding to r* is

$$\Delta G^* = \frac{16\pi\sigma}{3(\rho RT \ln S)^2} \tag{1.2.14}$$

We see from the above equation that the larger the degree of supersaturation, the smaller is the free energy of formation of the critical cluster. Also we can take ΔG* as a free energy barrier which must be surmounted for condensation to proceed. Increasing the degree of supersaturation will decrease this barrier. It can be deduced from Eq. 1.2.12 that formation of droplets or clusters of size $r < r^*$ will increase the total free energy of the system. In other words, a small subcritical ($r<r^*$) droplet is unstable with respect to the metastable supersaturated gas. It is the instability of small clusters that makes the supersaturated vapour exist for a long time. Paradoxically, a droplet can become stable only if $r>r^*$. It can grow irreversibly at the expense of supersaturated vapour. Its growth decreases the total free energy of the system. The final effect of this growth is the phase transition.

It is worth noting that equation 1.2.13 is just Kelvin's equation which we used in section 1.1. From the point of view of this equation we can say that the reason that small

clusters ($r<r^*$) are not stable in supersaturated vapour is that the vapour phase is subsaturated with respect to the cluster whose radius is smaller than r^*. The small cluster will evaporate. The supersaturated vapour is just saturated with respect to clusters that have radius r^*. This size of cluster is at equilibrium with the vapour phase. The vapour phase is really supersaturated with respect to clusters that have radius $r>r^*$. They will grow irreversibly.

According to CNT, ΔG is always >0 for subsaturated vapours forming any size cluster. (It is also >0 for supersaturated vapours forming sufficiently small (subcritical) clusters). Therefore,in subsaturated vapours there should be no clusters at all, even at equilibrium. McDonald[20] nevertheless calculated cluster distributions for both subsaturated and saturated vapour using CNT's ΔG. He argued that there exists a statistical steady-state population of clusters characterized by the Boltzmann-like distribution function[8,20]

$$N_n=N_1 e^{-\frac{\Delta G_n}{RT}} \qquad (1.2.15)$$

where N_n is the number of n-mers per unit volume of vapour, n is the size of the cluster, and ΔG_n is the Gibbs free energy of formation of the n-mer. For the case of $S<1$ ΔG_n always has a positive value and increases dramatically with increasing cluster size, n, as described above. The number of n-mers per unit volume in a subsaturated system decreases monotonically with an increase in cluster size, n. McDonald's calculation[20] shows that for half-saturated water vapour in one cm^3 at 0°C there exist 10^4 pentamers at any instant. The concentration of 20-mers is less than 10^{-17} per cm^3. Band[21] also

developed a theory of a saturated vapour based on the model that, in a real gas, clusters of molecules of various sizes actually exist, and he pointed out that the compressibility factor depends upon the surface energy of the clusters and the temperature. Kung and Bauer[23] found small clusters, such as dimers trimers tetramers and so on in unsaturated iron vapour using a spectral method. Finally, the kinetic approach[24] to nucleation theory proposed by Katz and Donohue is based on the fact that there is an equilibrium cluster distribution in the saturated vapour phase.

A finite cluster distribution is a direct challenge to CNT's prediction of zero-cluster concentrations. It is a contradiction in terms. How do we resolve the discrepancy between CNT and statistical thermodynamics? We shall reserve this question for discussion in Section 1.3.

To conclude this section let us note that although the thermodynamic approach is useful in describing the equilibrium properties of the stable and metastable states (supersaturated vapour system) of the gas, it cannot describe the time dependent phenomenon of the formation or decay of a metastable state. The kinetic approach based on the thermodynamic description of the metastable supersaturated state was proposed by classical nucleation theory in order to find an expression for the nucleation rate. It will be discussed in the next section.

1.2.2 Kinetics of Nucleation

Clusters grow and decay by absorbing monomers onto or evaporating from other clusters. This process of growth and decay can be represented by a set of reactions in which clusters of a certain size, n, play the role of chemical species.

$$A_n + A_1 \leftrightharpoons A_{n+1} \tag{1.2.18}$$

From this chemical reaction-like model and additional assumptions the nucleation rate, J, (the number of nuclei formed per unit volume per unit time) can be calculated. Below we shall give an outline of this derivation.

Classical nucleation theory makes three basic assumptions in the derivation of the nucleation rate. The first one is monomer addition. A detailed microscopic model for nucleation can be obtained by looking at the stochastic process by which embryos of condensed phase are formed through a series of bimolecular reactions between the set of species A_n. In the system the number of clusters is very small compared to the number of monomers. To a good approximation cluster growth via the addition of another cluster can usually be neglected with respect to reaction between cluster and monomer. The nucleation process can be expressed as an infinitely long series of reactions

$$\begin{aligned} A + A + M &= A_2 + M \\ A_2 + A + M &= A_3 + M \\ &\cdots \\ A_{n-1} + A + M &= A_n + M \\ &\cdots \end{aligned} \tag{1.2.19}$$

The second assumption is the fixed droplet free energy. The free energy of formation of a cluster of n molecules may be written in terms of molecular number,n, as

$$\Delta G_n^o = An^{2/3} - Bn \qquad (1.2.20)$$

in which A and B are constants. Comparing with equation 1.2.12 the first term, A, is the contribution of the surface energy of clusters in the vapour phase. The second term, B, corresponds to the difference in free energy between n liquid molecules and n vapour molecules. The free energy of cluster formation calculated using the above formula does not include the contributions of translational or rotational motion of a droplet. It is called the fixed droplet free energy. We shall discuss this later in section 1.3. The third assumption is that the monomer concentration is constant.

We employ Eq. 1.2.19 to write the time dependent equation for the concentration of the cluster A_n . Any n-mer can be created either by addition of a molecule to an (n-1)-mer or by evaporative loss of a molecule from an (n+1)-mer. Concurrently, n-mers can be destroyed either by growing into (n+1)-mers by addition of a monomer, or by decaying into (n-1)-mers through loss of a molecule. Denoting the concentration of clusters of size n at any instant by $[A_n]$, we get

$$\frac{\partial [A_n]}{\partial t} = (k_{n-1}[A_{n-1}] - k_{-(n-1)}[A_n]) - (k_n[A_n] - k_{-(n)}[A_{n+1}]) \qquad (1.2.21)$$

Here k_n is the condensation rate coefficient; k_{-n} is the evaporation rate coefficient. In the

classical theory k_n is set equal the gas kinetic collision frequency multiplied by a sticking coefficient, α_n.

$$k_n = \frac{a_n \alpha_n P}{\sqrt{2\pi m k T}} \qquad (1.2.22)$$

where P denotes the pressure of the monomer, and a_n is the surface area of the n-mer.

Since microscopic reversibility holds for individual cluster formation reactions, E. 1.2.19, k_{-n} can be expressed in terms of the rate constant for the forward reaction and of the equilibrium concentrations, ie.

$$\frac{k_n}{k_{-n}} = \frac{[A_{n+1}]_e}{[A_n]_e}$$

where the subscript e denotes equilibrium. For a stable unsaturated vapour $[A_n]_e$ decreases rapidly with n, and the above ratio is always smaller than one. In a supersaturated vapour, however, the ratio is less than unity if $n<n^*$, If $n>n^*$ the condensation rate becomes greater than the evaporation rate.

The equilibrium concentration, $[A_n]_e$, is calculated in the following way in classical theory. Formation of the cluster A_n can be written as the reaction $nA = A_n$. Its equilibrium constant is related to the Gibbs free energy of formation of the n-mer according to

$$K_p(n) = e^{-\frac{\Delta G_n^o}{kT}} \tag{1.2.24}$$

and the equilibrium constant presumably can be written as

$$K_x(n) = \frac{X(A_n)}{(X_A)^n} = \frac{[A_n] / ([A] + \sum_{i=2}^{n'} [A_i])}{([A] / ([A] + \sum_{i=2}^{n'} [A_i]))^n} \tag{1.2.25}$$

in which $X(A_n)$ is the mole fraction of A_n, and n' is a molecular number somewhat greater than the critical size. Usually

$$[A] > \sum_{i=2}^{n'} [A_i] \tag{1.2.26}$$

and hence $K_x=[A_n]/[A]$. CNT commonly assumes that $[A_n]=[A]\exp(-\Delta G_n^o/kT)$. Furthermore, it assumes that ΔG_n^o is given by Eq.1.2.20. (As we shall see later this is all highy quesionable.)

Equation 1.2.21 is derived for the general non-steady-state case. Since the probability of a condensation reaction becomes much greater than that of evaporation for $n>n^*$, the set of equations can be truncated at the critical size, n^*, by assuming the transition from A_{n^*} to A_{n^*+1} to be irreversible. If the concentration of single molecules (monomers) in the

system is constant for the time of interest, all the equations are quasi-linear with constant coefficients, and it is possible in principle to investigate the complete kinetic behaviour of the system analytically.

Defining J_n to be the following net rate of transition from A_{n-1} to A_n,

$$J_n = k_{n-1}[A_{n-1}] - k_{-(n-1)}[A_n] \tag{1.2.27}$$

then Eq. 1.2.21 becomes

$$\frac{\partial [A_n]}{\partial t} = J_n - J_{n+1} \qquad n=2,3,\cdots \tag{1.2.28}$$

In fact, because of the nature of the activation barrier a significant simplification is usually possible. If the concentration of monomer is held constant, a kinetic steady state occurs after a short induction period. Assuming that this condition is established instantaneously the rate of nucleation can be set equal its easily computed steady state value. This approximation was first applied by Farkas[11] and by Becker and Doring[12]. In the steady state $[A_n]$ does not change with time because the J_n have one and the same value for all n.

$$J = J_n = J_{n+1} = \cdots = k_{n-1} f_{n-1} - k_{-(n-1)} f_n = k_n f_n - k_{-n} f_{n+1} = \cdots \tag{1.2.29}$$
$$J = Constant$$

Here we use f_n to indicate the concentration of clusters of size n at the steady state, and

f_n does not change with time. But a uniform non-zero current J "flows" through the embryo chain due to a statistical excess of condensational growth over evaporative decay of embryos at each link of the chain.

Condensational formation of (n+1)-mer from n-mer can exceed evaporative decay of the (n+1)-mer in spite of the fact that $k_n < k_{-n}$, because $f_n > f_{n+1}$. Hence J can be positive for all n within the range of concern. We rewrite the general term , J, as

$$\begin{aligned} J &= k_n [A_n]_e \left(\frac{f_n}{[A_n]_e} - \left(\frac{k_{-n}}{k_n} \right) \left(\frac{f_{n+1}}{[A_n]_e} \right) \right) \\ &= k_n [A_n]_e \left(\frac{f_n}{[A_n]_e} - \frac{f_{n+1}}{[A_{n+1}]_e} \right) \end{aligned} \qquad (1.2.30)$$

where we used the principle of detailed balance. Two more assumptions must be made: (1) $f_1 = [A]_e$ and (2) for some large g, $f_g=0$. The first one is the same as the assumption that the growth of clusters has not depleted the number of monomers. The second assumption is that no very large clusters (say $g = 2n^*$) have formed during nucleation. In classical nucleation theory both of these requirements are imagined as being met by having a Maxwell demon break up clusters of size g into monomers. With these two assumptions, we can write J in terms of the concentration of clusters of size n= 2 to g-1.

$$\frac{J}{k_1[A]_e}=(1-\frac{f_2}{[A_2]_e}),\ \frac{J}{k_2[A_2]_e}=(\frac{f_2}{[A_2]_e}-\frac{f_3}{[A_3]_e}),$$
$$\vdots \qquad (1.2.31)$$
$$\frac{J}{k_{g-1}[A_{g-1}]_e}=(\frac{f_{g-1}}{[A_{g-1}]_e}-0)$$

In the above equation we used $f_1=[A]_e$ and $f_g=0$. Now if we sum the left and right side of each equation, we obtain an expression for the steady state homogeneous vapour nucleation rate, J:

$$\sum_{n=1}^{g-1}\frac{J}{k_n[A_n]_e}=1 \qquad (1.2.32)$$

or

$$J=(\sum_{n=1}^{g-1}\frac{1}{k_n[A_n]_e})^{-1} \qquad (1.2.33)$$

The equilibrium concentration of the critical size cluster, n*, is very much smaller than that of the very large clusters. Hence, the largest clusters will contribute very little to the sum in Eq. 1.2.33. Therefore, Eq. 1.2.33 can just as well be replaced by

$$J=(\sum_{n=1}^{\infty}\frac{1}{k_n[A_n]_e})^{-1} \qquad (1.2.34)$$

Since J is given in terms of the capture rate and the Boltzmann thermodynamic equilibrium concentration Eq. (1.2.34) is often referred to as a thermodynamic expression for the nucleation rate. Another expression containing only kinetic parameters can be derived by replacing $[A_n]_e$ with

$$[A_n]_e = \frac{k_{n-1}[A_{n-1}]_e}{k_{-(n-1)}} = [A_1]_e \prod_{i=1}^{n-1} \frac{k_i}{k_{-(i+1)}} \tag{1.2.35}$$

and so

$$J = [A_1]_e \left(\sum_{n=1}^{\infty} \frac{1}{k_n \prod_{j=1}^{n-1} k_j / k_{-(j+1)}} \right)^{-1} \tag{1.2.36}$$

The above equation contains only the kinetic parameters, $k_{\pm n}$. It is called the kinetic expression of the nucleation rate.

Replacing the summation with integration in Eq. 1.2.33, as did Lothe and Pound[25], the result is

$$J^{ss} = Z k_{n^*} [A] e^{-\frac{\Delta G^{\circ}_{n^*}}{kT}} \tag{1.2.37}$$

where

$$Z=\left(\frac{\Delta G^{o}_{n*}}{3\pi kTn^{*2}}\right)^{1/2}$$

The physical interpretation of the above formula is clear. It describes the rate at which supercritical clusters (i.e. n*+1) are formed from the critical cluster. The additional factor, Z, is a non-equilibrium factor, or the Zeldovich factor which accounts for the departure of the steady-state concentration from the equilibrium concentration of the critical cluster.

Feder[26] et al used the same approach to estimate the induction period required to attain the stationary distribution of critical clusters and the steady-state nucleation rate. They integrated the transient expression, Eq.1.2.21 in an approximate manner and obtained

$$J(t)=J\left[1-e^{-\frac{t}{\tau}}\right] \tag{1.2.38}$$

in which the induction period τ is given by

$$\tau=-2\pi kT/k_{n*}\left[\frac{\partial^2\Delta G^{o}}{\partial n^2}\right]_{n=n*} \tag{1.2.39}$$

Abraham[27] has carried out extensive computer calculations of the time dependence of the cluster concentrations and the nucleation rate for homogeneous nucleation of water vapour. The crucial result of his calculations is that in typical gas phase nucleation experiments the cluster concentration and the nucleation rate become independent of time after a time period of the order of microseconds in fluid phases. But Turnbull[28] has shown

that it may be of the order of days in the solid phase where the mobility of the monomer is very low.

Substituting the free energy of formation of critical clusters, $\Delta G^{o}_{n^*}$, into the equation for J (Eq. 1.2.37) we can obtain J in terms of the supersaturation ratio, S.

$$J=k_{n^*}[A]\,Z\,\exp\left(-\frac{16\pi\sigma^3}{3k^3T^3\rho^2(\ln S)^2}\right) \qquad (1.2.40)$$

As $(\ln S)^2$ appears in the exponential in E. 1.2.40, the nucleation rate, J, depends very strongly on the degree of supersaturation, S. The homogeneous nucleation rate will rise from a very low to a very high value in a narrow increment of supersaturation. Accordingly, the critical supersaturation may be meaningfully defined as that at which the logarithm of the rate equals zero, i.e. at which J = 1 nucleus per cm^3/sec. The critical supersaturation can be measured experimentally and can be calculated using the above equation. This provides an opportunity to verify classical nucleation theory experimentally. In Table 1 we compare the critical supersaturation measured in experiments with the predictions of classical theory for a variety of materials. In some cases, such as H_2O, C_2H_5OH and the alkanes, classical theory seems to provide satisfactory results. However, in other systems, like C_6H_6, $CHCl_3$ and CCl_3F, the classical theory predicts much too high a critical supersaturation. This is not surprising. Since the classical nucleation theory arises basically from a continuum thermodynamic description

TABLE 1

The Critical Supersaturation, S, Calculated from Classical Theory Compared With Experimental Values.

Vapour	Temperature (K)	Critical Supersaturation		Reference
		Experiment	Theory	
H_2O	272.2	4.2	4.2	29
CH_3OH	270.0	5.0	5.0	29
C_2H_5OH	273.0	2.3	2.3	29
C_2H_5OH	240.0	8	11	29
n-Propanol	270.0	3.0	3.2	29
H_2O	260	11	15	30
NH_3	200.0	4.5	7.5	30
C_6H_6	210.0	110.0	390.0	14
$CHCl_3$	200.0	40.0	170.0	14
CCl_3F	170	100	440	14
CCl_4	270	7.2	6.35	38
$C_2H_2Cl_2$	300	10	10	38
C_6H_{14}	230	11	11	31
C_7H_{16}	250	10	11	31
C_8H_{18}	250	15	17	31
C_9H_{20}	280	13	13	31

of a very large cluster, we really cannot expect that classical theory will give good agreement with experiment for all systems. It is clear from the equation 1.2.40 that a very precise knowledge of micro-cluster thermodynamic properties is required if nucleation behaviour is to be predicted accurately. In Eq. 1.2.40 σ^3 appears in the exponential. As a result J depends strongly on the assumed value of the surface free energy per unit area. Unfortunately σ is the least well known thermodynamic parameter specially for small clusters. A 10% change in σ changes J by a factor of 10^{10}. In the next section we shall discuss the drawbacks of the classical theory.

1.3 The Inconsistencies and Drawbacks of Classical Homogeneous Nucleation Theory

As we have indicated previously the classical theory of nucleation has extended the thermodynamic description of a vapour to the microscopic range. The concepts of free energy, pressure, temperature and surface tension have been used for clusters consisting of less than 500 molecules. It is not surprising that a number of investigators [32-39], most notably Lothe and Pound, Wegener, Cohen, Reiss, and Katz, have pointed out the inconsistencies and drawbacks of this theory, and various alternative models of homogeneous nucleation theory have been proposed. We shall devote this section to a discussion of the drawbacks of the classical theory. The alternative models will be discussed in the next section.

1) The Capillarity Approximation

Classical nucleation theory assumes that a cluster is a small spherical object with the characteristics of liquid droplets. In particular, it has been assumed that the surface free energy of the bulk liquid (σ) can be used for a small cluster, that σ depends only on temperature and does not depends on the size of the cluster. The assumption that certain intensive parameters of the microscopic drops equals experimentally measured intensive parameters of macroscopic drops is referred to as the capillarity approximation. This may not be true for cluster sizes smaller than a certain value. Since the surface free energy, σ, appears in the argument of the exponential of equation 1.2.41, a small uncertainty in σ can cause a dramatic uncertainty in the calculated nucleation rate. Furthermore, the concept of a cluster surface is difficult to define for clusters composed of only a few molecules. This is the most serious drawback of the classic nucleation theory.

This problem can be attacked from two directions. The first one is to build a kinetic nucleation model (see the next section) and avoid using the surface free energy of a cluster in the calculation of the nucleation rate. The other one is to try to find the relationship between cluster size and the cluster surface free energy. In this part we discuss the method which some investigators used to find the micro-surface free energy. The most important, and at the same time the most controversial question is the nature of the dependence of the surface free energy of the cluster, σ, on the size of the cluster since it is not possible to measure surface free energy of clusters experimentally. It has not even been conclusively established whether the surface free energy increases or decreases with a decreasing cluster size. The calculation carried out by Nishioka[40]

indicates that, for a Lennard-Jones gas, σ is not even a monotonic function of particle number, n. For $100< n <\infty$ the surface free energy of clusters first decreases slowly; for n less than 100 it increases, and eventually it exceeds the value of bulk surface free energy. Band[21] showed that the compressibility factor of a real gas is a function of the temperature, pressure, molar volume, molecular weight and the surface free energy of clusters. Therefore it is possible to use the experimental compressibility data to calculate the microscopic surface free energy σ. As the compressibility is determined by the properties of mixtures of very small clusters, the surface free energy, σ, obtained in this way is appropriate to a mixture of small clusters and not to the bulk material. It is called the microscopic surface free energy. Abraham's calculation of nucleation rates using the microscopic surface free energy, σ, obtained from Band's compressibility equation were in good agreement with experiment for all of the materials he discussed[22,27]. Two conclusion from Abraham's work are important. (1) The microscopic surface energy, σ, is not necessarily identical to the macroscopic surface free energy (for water, microscopic σ is 1.5 times the macroscopic one, for NH_3 they are equal.) (2) For some vapour systems, when the microscopic σ is used good agreement with experimental data is obtained[27].

Hamill, Stuffer and Kiang[42] showed that the microscopic surface free energy can be calculated from the second virial coefficient combined with the Fisher[43] droplet model. They calculated equilibrium cluster concentrations and thence nucleation rates using the microscopic surface free energy obtained from the second virial coefficient. Good

agreement was obtained between their prediction and experiments, for some of which the classical nucleation theory fails badly (eg. C_6H_6, $CHCl_3$ and CCl_3F).

2) Thermal Non-Accommodation

The classical theory does not consider the energy difference between nascent clusters and stable clusters. In other words classical theory assumes that newly formed clusters can be de-energized instantly. This requires the vapour phase monomers to form a good heat bath. Monomers will play such a role only when non-reactive collisions of monomers with clusters are much more frequent than the reactive ones. This is not necessarily true in a real pure clustering vapour system, and in effect growing clusters may be expected to be somewhat hotter or energetic than the surrounding monomers. The nascent cluster has sufficient energy to redissociate even without collisions. The energy-removing collision must take place within the lifetime of a nascent cluster. The lifetime of newly-born clusters increases rapidly with cluster size[44]. Therefore the stabilization requirement becomes less serious for large n. However, the small clusters must be stabilized first before large clusters can form. Consequently the whole nucleation process is affected.

3) Constrained Equilibrium

The supersaturated gas is a metastable state, and is not in thermodynamic equilibrium, since condensation can spontaneously take place, that is, the Gibbs free energy decreases.

Strictly speaking, we can not calculate thermodynamic functions for a supersaturated state. In classical nucleation theory the rate of nucleation is related to the "equilibrium distribution" of a supersaturated system which is a hypothetical state that is constrained to be in equilibrium at the same temperature and pressure. To further constrain the distribution, a Maxwell demon is sometimes used. This demon is imagined to take all clusters larger than some given size and break them into individual monomers. Katz and Wiedersich[45] has showed that it is completely unnecessary to invoke a constrained equilibrium distribution in calculating the nucleation rate. Their kinetic model will be discussed in the next section.

4) Translation-Rotation Correction to the Free Energy of Formation of Clusters

Lothe and Pound[32] first pointed out that the contribution to the free energy of formation of clusters from both translational and rotational degrees freedom were neglected in classical theory. They incorporated these directly into the droplet model which, they assumed, correctly describes the internal properties of a small cluster. Their formula was derived in a thought experiment in which reversible homogeneous nucleation is accomplished by the following steps (1) condensation of the vapour into a bulk liquid; (2) cutting the bulk liquid into small droplets of equal size, n; and (3) energizing the n droplets to make a "gas" of embryos of size n. After the translational and rotational correction, the Gibbs free energy of formation of a critical cluster was given by

$$\Delta G^* = \Delta G^{*\prime} + \Delta G_s + \Delta G_c + \Delta G_r \qquad (1.3.1)$$

in which $\Delta G^{*\prime}$ is the same as obtained by the classical theory, ΔG_t corresponds to the translational degree of freedom, ΔG_r corresponds to the rotational degree of freedom, and ΔG_s, which is called the replacement free energy, arises from the requirement for the conservation of degrees of freedom. Six degrees of freedom are needed for energizing the embryo. Accordingly, six degrees of freedom in the molecules of the embryo must be deactivated.

Reiss[35,39,46] , Katz and Cohen took a similar approach to that of Lothe and Pound. They obtained an additional factor in the nucleation rate expression beyond that which appeared in classical theory. However, they do not agree with Lothe and Pound's treatment of the rotational and replacement factor contributions.

5) Multi-step Clustering

The classical theory assumes that clusters grow by sequential addition of monomers. The process in which clusters react with clusters is ignored. This approximation is based on the observation that the concentration of monomers is much larger than the concentration of clusters. However, cluster-cluster reactions lead to a much more rapid and effective growth of droplets. When the degree of supersaturation is very high, close to the critical supersaturation, and the concentrations of small clusters are not very small, the usual argument for monomer addition is simply incorrect.

6) Non-Applicability to Small Clusters

A successful nucleation theory should provide the whole picture of formation of clusters, but classical nucleation theory cannot be applied to cluster sizes less than 1000 because by its very nature nucleation is the formation of critical clusters and because macroscopic thermodynamic properties are used in it[8]. In classical theory a surface free energy is calculated by multiplying the cluster's surface area with the bulk surface free energy per unit area. This can be interpreted as the number of molecules on the cluster surface times the surface energy per surface molecule in the bulk material. When this is done, one can calculate the number of surface molecules on clusters of n-mers. Abraham[47] pointed out the ludicrous result that the droplet model then regards a 10-molecule cluster as having 20 surface molecules. This drawback can be corrected using kinetic models[24,48-52] to be discussed in the next section, in which the rate of formation and dissociation of small clusters can be estimated otherwise.

7) Use of ΔG for Calculating Equilibrium Cluster Distributions

In section 1.2.2 we described a contradiction between statistical thermodynamics and classical nucleation theory's prediction that the Gibbs free energy of formation of clusters of any size in a subsaturated gas or of subcritical clusters in a saturated vapour is larger than zero (Eq. 1.2.20). The problem can be resolved by noting CNT's basic assumption that clusters are treated as liquid droplets. As such their molar free energy is (except for

a negligible PΔV term) unaffected by their partial pressure (or by the amount of clusters), unlike the case of monomers for which $\mu = \mu_o + RT\ln P$. Because of this CNT predicts that $\Delta G_n = C_n - D_n \ln P/P_{vap}$ for the formation of clusters of size n. This leads to $\Delta G > 0$ if $P < P_{vap}$. Had one treated the clusters of size n as vapour phase particles, then one would have obtained $\Delta G_n = \Delta G_n^\circ + RT\ln P_n/P^n$ where P_n is the partial pressure of cluster size n and P is the pressure of monomers. The second term on the right is the free energy change of mixing the pure monomer and pure n-mer at constant T and P, and ΔG_n° is the standard free energy change which includes surface free energy effects. Then, one can see, at equilibrium ($\Delta G_n = 0$), $(P_n/P^n)_e = \exp(-\Delta G_n^\circ/RT)$. Therefore, a statistical thermodynamic calculation of cluster concentration is indeed in order, if one were to treat the clusters as gas phase species. This highlights a failing of the CNT. Note that the hand-waving argument of McDonald (Eq. 1.2.15) uses ΔG_n rather than ΔG_n°. Strictly speaking, ΔG_n only relates to spontaneity and not to equilibrium properties. [Furthermore N_n/N_1 is used, ignoring the stoichiometry, rather than N_n/N_1^n]. A positive ΔG_n° is not problematical in that it does not predict zero cluster concentrations.

1.4 Other Kinetic Theories of Homogeneous Nucleation

From thermodynamics we know that supersaturated vapour is an unstable system. The formation of a new liquid phase from unstable supersaturated vapour is a spontaneous process. Homogeneous nucleation or condensation in a supersaturated vapour is a kinetically controlled process. Some theories have been proposed. These kinetic

approaches try to avoid the inconsistencies and drawbacks of classical nucleation theory which we discussed in the last section.

A complete nucleation theory should[50] (1) provide a practical relationship between the supersaturation($[A_1]/[A_{1,e}]$) and the nucleation rate; (2) give the critical supersaturation at which a recognizable condensation starts; (3) give the rates of condensation of a monomer to and evaporation of a monomer from a cluster as a function of temperature and cluster size; (4) give a relation between critical cluster size and supersaturation; and (5) give the distribution of clusters at supersaturation.

In this section we shall give a brief summary of some kinetic approaches to homogeneous nucleation. These include the approach proposed by Katz and Donohue[24] (1978) and extended by Grishick and Chiu[48] (1990), the kinetic theory proposed by Nowakowski[49] and Ruckenstein (1991), the self-consistent kinetic model of homogeneous nucleation (SCKN) proposed by Bauer[44,50] and Wilcox (1991) , the kinetic model used by Creasy[51] (1990) and the chemical kinetic view of nucleation developed by Yang and Qiu[52] (1986).

1.4.1 The Kinetic Approach

Katz[24] and Donohue proposed a kinetic approach to nucleation theory in 1977. Grishick[48] and Chiu extended it in 1991. The assumptions of this theory are: (1) the rate coefficients for the decay of clusters does not depend on the density of the vapour; (2) the growth of

clusters occurs almost entirely by the addition of single molecules, and the decay of clusters also occurs almost entirely by the loss of single molecules; and (3) the difference between the bulk condensed phase and a cluster lies in the surface to volume ratio. Then the rate, J, at which clusters containing n molecules at time t become clusters containing (n+1)-molecules is given by the equation

$$J(n,t) = k_n[A_n] - k_{-(n+1)}[A_{n+1}] \tag{1.4.1}$$

where k_n is the forward rate constant for n-mer formation, i.e. for monomer condensation on an (n-1)-mer; and $k_{-(n+1)}$ is the backward rate constant for the (n+1)-mer dissociating into an n-mer, or the rate that a molecule evaporates from an (n+1)-mer. $[A_n]$ is the concentration of n-mer. The nucleation rate, J(n,t), can be calculated if k_n and $k_{-(n+1)}$ are known. k_n is approximated as the product of $\beta a(n)$, where β is the rate at which vapour molecules impinge and condense on a surface of unit area at time t, and a(n) is the surface area of an n-mer. For an ideal gas

$$\beta = \frac{\alpha P(t)}{\sqrt{2\pi mkT}} \tag{1.4.2}$$

P(t) is the pressure of the monomers at time t. α is the sticking coefficient. The backward rate coefficients are determined in terms of the equilibrium distribution, $[A_{n,e}]$, and the forward equilibrium rate coefficient, $k_{n,e}$. At equilibrium the vapour is in contact with its own liquid, and the nucleation rate J=0. Then

$$J(n,t) = k_{n,e}[A_{n,e}] - k_{-(n+1),e}[A_{n+1,e}] = 0 \qquad (1.4.3)$$

and

$$k_{-(n+1),e} = \frac{k_{n,e}[A_{n,e}]}{[A_{n+1,e}]} \qquad (1.4.4)$$

Because of assumption (2) $k_{-(n+1),e} = k_{-(n+1)}$. Substituting k^e_{n+1} into the Eq. 1.4.1

$$J(n,t) = k_n[A_{n,e}]\left(\frac{[A_n]}{[A_{n,e}]} - \frac{[A_{n+1}]\,k_{n,e}}{[A_{n+1,e}]\,k_n}\right) \qquad (1.4.5)$$

Since the forward rate coefficient, k_n , is the product of the arrival rate β and the area of the cluster, the ratio, $k_n / k_{n,e}$, simplifies to the ratio of the arrival rates, β/β_e . Rearranging Eq. 1.4.5 and dividing both sides by $(\beta/\beta_e)^n$

$$\frac{J(n,t)}{k_n[A_{n,e}]\,(\beta/\beta_e)^n} = \frac{[A_n]}{[A_{n,e}]\,(\beta/\beta_e)^n} - \frac{[A_{n+1}]}{[A_{n+1,e}]\,(\beta/\beta_e)^{n+1}} \qquad (1.4.6)$$

Summing from n=1 to some sufficiently large size, $n=n_g$, successive terms cancel.

$$\sum_{n=1}^{n=n_g} \frac{J(n,t)}{k_n[A_{n,e}]\,(\beta/\beta_e)^n} = \frac{[A_1]}{[A_{1,e}]\,(\beta/\beta_e)} - \frac{[A_{n_g}]}{[A_{n_g,e}]\,(\beta/\beta_e)^{n_g}} \qquad (1.4.7)$$

If the steady state is very rapidly achieved J becomes a constant for all sizes of clusters. In addition, the numerator of the last term on the right hand side of the above equation

is a very slowly decreasing function of n, but the denominator is an ever-increasing function of n, ($\beta/\beta_e > 1$ for supersaturated vapour), so for large clusters, n_g , the last term is negligible compared with first term. Consequently,

$$J^{ss} = \frac{[A_1]}{[A_{1,e}](\beta/\beta_e)} / \sum_{n=1}^{n_g-1} [k_n [A_{n,e}] (\beta/\beta_e)^n]^{-1} \qquad (1.4.8)$$

To calculate the steady state nucleation rate, J^{ss}, we have to know the arrival ratio β/β_e and the concentrations of clusters in equilibrium with the bulk condensed phase. The former is a kinetic problem; the latter one is a thermodynamic problem. The equilibrium concentration of cluster is given by $[A_{n,e}] = N\exp(-\Delta G_n/RT)$ where N is a normalization factor, and ΔG_n is the difference in Gibbs free energy between n molecules in a cluster of size n and the bulk condensed phase. According to assumption (3) ΔG_n equals $\sigma a(n)$ where σ is the surface free energy, the surface area $a(n) = a_o n^{2/3}$ where $a_o = 4\pi(3v_1/4\pi)^{2/3}$, and v_1 is the volume of a single molecule. Then $[A_{n,e}] = N\exp(-\sigma a_o n^{2/3}/RT)$. Converting the summation in Eq. 1.4.8 into an integral, expanding the argument of the exponential in a Taylor series about $n = n^*$ (at which the argument's first derivative equals zero), and neglecting terms higher than the quadratic term, we then obtain

$$J^{ss} = \frac{[A_1]}{[A_{1,e}](\beta/\beta_e)} N\beta a_o \left(\frac{a_o\sigma}{9\pi kT} - \frac{1}{3n^{*2/3}}\right)^{1/2} e^{\left(\frac{a_o\sigma n^{*2/3}}{3kT} - \frac{2}{3}\right)} \qquad (1.4.9)$$

n^* is conventionally known as the critical size. The definition of the critical size is the same as that in CNT. It is given by

$$n^* = \frac{2}{3}\frac{\sigma a_o}{kT \ln \beta/\beta_e} \qquad (1.4.10)$$

There are two differences between CNT and the kinetic approach proposed by Katz et al. First, in the kinetic approach the evaporation rate constants are obtained by reference to the stable equilibrium of a saturated vapour (S=1) at the same temperature as the vapour in question, while in CNT it is obtained by reference to a metastable equilibrium. The other is that in the kinetic approach the appropriate driving force for nucleation is the ratio of arrival rates, β/β_e, a kinetic property, while in CNT the driving force is the degree of supersaturation, a thermodynamic property. In the kinetic approach the macroscopic surface free energy is still used for calculating the cluster distribution at equilibrium. The assumption that the rate of evaporation of molecules from a cluster is independent of the density of the vapour is the most questionable assumption.

Grishick and Chiu[48] pointed out that since there is a true equilibrium between the vapour and the bulk condensed phase, molecules in the vapour phase and the bulk liquid have the same chemical potential. Therefore, ΔG_n can be evaluated simply as the difference in Gibbs free energy between an n-mer and a monomer, both considered to be in the condensed phase; so $\Delta G_n = \sigma a_o (n^{2/3}-1)$. The equilibrium concentration of n-mers is given by $[A_{n,e}]=[A_1]\exp(-\sigma a_o (n^{2/3}-1)/RT)$. The modified nucleation rate is given by

$$J^{ss} = v_1 \left(\frac{2\sigma}{\pi m_1}\right)^{1/2} [A_1]^2 \frac{\beta}{\beta_e} \exp\left(\frac{\sigma a_o}{RT} - \frac{4(\sigma a_o)^3}{27(\ln(\beta/\beta_e))^2}\right) \qquad (1.4.11)$$

Taking the vapour as an ideal gas the relation between the nucleation rates obtained using the kinetic and the classical theories is

$$J_{kin}=\exp(\sigma a_o/RT)\frac{J_{cl}}{\beta/\beta_e}. \qquad (1.4.12)$$

Grishick and Chiu compared the nucleation rates predicted by both kinetic and classical theories with the experimental data for ethanol[53], toluene[54] and n-nonane[55]. For n-nonane at lower temperatures (less than 280K) the kinetic nucleation rate is much closer to the experimental result than the classical theory, but at higher temperatures (higher than 280K) this situation is reversed. For toluene the kinetic theory does dramatically better than the classical theory over the full temperature rage of the experiment from 220 to 270 K. For pentanol and hexanol the kinetic nucleation rate is closer to experiment than is the classical rate[56]. For methanol and ethanol the data from Wagner and Strey[56] indicate that both theories tend to overestimate the nucleation rate, but the classical rate is closer. They ascribed the discrepancies between theory and experiment to the physical assumptions, mainly that the physical properties of microscopic clusters are the same as those of the bulk liquid.

1.4.2 The Kinetic Theory Proposed by Nowakowski

Nowakowski[49] and Ruckenstein(1991) proposed a new kinetic approach to nucleation

theory which avoided the use of the macroscopic surface free energy and detailed balance. In contrast to the classical theory the rates of condensation and evaporation of clusters were calculated independently of each other in Nowakowski's kinetic theory.

The attractive intermolecular forces between molecules in clusters produce a potential well of depth Φ_o in the gas layer around the cluster. If a molecule is confined to this layer it has a total energy E ($0 > E > \Phi_o$). That means this molecule is bound to the cluster. This molecule can escape from the cluster only when it receives sufficient energy from collisions with other molecules. This is the evaporation process. They treat the escape of a molecule from a cluster using the Fokker-Planck equation under the constraint of slowly changing energy. Then the rate of evaporation of molecules from a cluster is obtained directly by calculating the mean passage time of the molecules that escape from the potential well. The evaporation rate, k_{-n}, of a spherical n-mer cluster of radius, R_n, is $4\pi R_n^2 \lambda n_d e_n$ in which $4\pi R_n^2 \lambda n_d$ is the number of molecules in the potential well of thickness λ. e_n is given by

$$e_n = \left[\int_{\Phi_o}^{0} dE P_{eq}(E) \int_{E}^{0} \frac{dE'}{D(E') P_{eq}(E')} \right]^{-1} \qquad (1.4.13)$$

in which P_e (E) is the equilibrium distribution of molecular energy, and D(E') is the diffusion coefficient in energy space which depends on the dynamics governing the motion of a molecule. The quantity e_n decreases with the size of the cluster because the

potential well is deeper for larger clusters. The rate of condensation of the clusters is given by gas kinetic theory $k_n=a(n)\beta$, just as in the classical theory.

The critical size, n*, is determined by the condition of unstable equilibrium between evaporation and condensation and depends on the concentration of monomer. The nucleation rate is given by

$$J^{ss}=\frac{1}{2}[A_1]k_1(-\frac{H''(n*)}{2\pi})^{1/2}e^{-H(n*)} \qquad (1.4.14)$$

in which H'' is the second order derivative of H and

$$H(n)=\sum_{i=2}^{n-1}[\ln(\frac{k_{-i}}{k_i})+\ln(\frac{k_{-i}}{k_i+k_{-i}})] \qquad (1.4.15)$$

They showed that for small supersaturation (lnS<0.2), i.e., for large critical clusters the rates of nucleation predicted by their kinetic theory and by the classical theory coincide, but for larger supersaturation their kinetic theory predicts much larger nucleation rates than the classical theory does. They attributed this to the use of the microscopic surface free energy in the classical theory, which overpredicts the surface free energy of small clusters and consequently provides lower values for the nucleation rate. They compared the theoretical results with experimental data for methanol, ethanol and propanol in argon[57] in the form of graphs of temperature vs supersaturated vapour pressure for a

nucleation rate of 10^8 cm^{-3} s^{-1}. Consistency with experimental results was better for the lower alcohols using their kinetic theory than for higher alcohols. They explained that this was because the lower alcohols are closer to spherical shapes, and their kinetic theory assumes clusters to be spheres.

In the application of this kinetic theory the depth of the potential well of a cluster and the diameter of a molecule in a cluster are needed. It was noted that the interaction among molecules is complex, and there is no reliable and accurate universal method to calculate these parameters (except for monatomic systems[153]). In their calculation the interaction constant, ε, in the binary interaction potential was determined so as to provide the correct values of the surface free energy; the diameter of a hypothetical spherical molecule was calculated from the density of the liquid.

1.4.3 A Chemical Kinetic View of Nucleation Theory

C. H. Yang[52] and H. Qiu proposed a chemical kinetic view of homogenous nucleation in which a simple function with two undetermined parameters has been used to relate the activation energy of the vaporization reaction to cluster size. The use of surface free energy was avoided. The kinetic scheme for the nucleation process was as follows:

$$A_1 + A_{n-1} \rightleftharpoons A_n \qquad (1.4.16)$$

The nucleation flux, J, between any two neighbouring steady state cluster concentrations is expressed as follows:

$$J=\alpha\beta a(n)\,[A_n]-k_{-(n+1)}a(n+1)\,[A_{n+1}] \tag{1.4.17}$$

where α is the sticking coefficient, a(n) is the surface area of the n-mer, β is the condensation rate of monomer onto the surface of the n-mer, given by

$$\beta=\frac{[A_1]}{\sqrt{2\pi mkT}} \tag{1.4.18}$$

and $k_{-(n+1)}$ is the vaporization rate of monomer from the surface of the (n+1)-mer. Assuming that the vaporization rate can be written in the Arrhenius form,

$$k_{-(n+1)}=Ae^{-\frac{E_n}{RT}} \tag{1.4.19}$$

and using the relation $S=P/P_\infty$ the nucleation rate is given by

$$J^{ss}=\frac{\alpha\beta_e[A_{1,e}]\,a_o}{1+1/Se^{-(E_2-E_e)/RT}+1/S^2e^{-(E_2+E_3-2E_e)/RT}+\cdots+1/S^{N-1}e^{-\sum_{i=2}^{N}(E_i-E_e)/RT}}$$

where β_e is the condensation rate of the monomer onto the bulk liquid surface, E_e is the activation energy for vaporization at the equilibrium vapour pressure, and $[A_{1,e}]$ is the monomer concentration at the equilibrium vapour pressure. It is clear from the equation above that the flux would be fully determined if E_n were to be known as a function of

cluster size. Yang and Qiu assumed $E_n = (1-B/n^{\gamma})E_c$ in which B and γ were undetermined parameters. Substituting E_n into the flux expression they obtained

$$J^{ss} = \frac{\alpha \beta_e [A_{1,e}] a_o}{1+1/S\Theta^{BE_e/RT2^{\gamma}}+1/S^2\Theta^{BE_e/RT(1/2^{\gamma}+1/3^{\gamma})}+\cdots+1/S^{N-1}\Theta^{BE_e/RT\sum_{2}^{N}(1/n^{\gamma})}}$$

If B and γ are given the rate of nucleation can be calculated. In the case of the classical theory B and γ assume the values $2\sigma/\rho E_c(4\pi\rho/3m)^{1/3}$ and 1/3 respectively. Since surface free energy is a function of temperature, B also varies with temperature. The optimum values of B and γ are obtained in practice by numerical fit to the best experimental data. Their calculation showed that this approach closely predicts and correlates available experimental data for water[29,58,59,60], benzene[61-63], and ethanol[14,29,61,62].

This kinetic approach to nucleation follows the classical theory very closely. The only departure from it is the use of a simple parametric function for the activation energy of the evaporation rates instead of using detailed balance and the surface free energy. As the rate parameters can only be selected according to the criterion of a best fit to nucleation data, an amount of uncertainty is introduced. This approach is regarded as another crude approximation to nucleation kinetics.

1.4.4 The Self-consistent Kinetic Model of Homogeneous Nucleation

In 1977 Bauer[41] and Frurip proposed a self-consistent kinetic model of homogenous nucleation (SCKM). Bauer[44,50] and Wilcox extended it. The growth of a cluster is a two-step process in this model. The first step is the accretion of n-mer and i-mer(i=1,2,3···). The nascent cluster is unstable because it has sufficient energy for reevaporation; The second step, energy-removing collisions, must be followed within the lifetime of the unstable cluster. This can be expressed as follows:

(a) $$A_{n-i} + A_i \rightleftharpoons A_n^*$$

(k_{-n} is the backward rate constant and k_{n+i} is the forward rate constant); and

(b) $$A_n^* + M \rightleftharpoons A_n + M$$

(k_n^s is the forward rate constant and k_{-n}^s is the backward rate constant).

Imposing the steady state approximation for the short lived A_n^*, and letting i=1 the rate of production of A_n is given by

$$J_n = [\frac{k_n^s [A_1]}{1 + (k_n^s / k_{-n})[M]}\{\frac{k_n [A_{n-1}]}{k_{-n} [A_n]} + \frac{[k_{-n}^s [M]}{k_{-n} [A_1]}\} - k_{-n}^s] [M] [A_n] \quad (1.4.22)$$

J_n is the net flux of clusters passing from the n-population to (n+1)-population. The concentration of n-mer as a function of time can be obtained by integrating the coupled master differential equations constrained by the mass conservation condition

$$\frac{d[A_n]}{dt} = \sum_1^i \{k_n [A_{n-i}] [A_i] + k_{-(n+i)} [A_{n+i}] - k_n [A_n] - k_{-(n+i)} [A_n] [A_i]\}$$

The k's are expressed in terms of molecular parameters and fundamental constants. The

k_n's are calculated as the frequency of collisions between monomers and (n-1)-mers, each at unit concentration, interacting along an attractive Lennard-Jones (L-J) potential with a hard repulsive core:

$$k_n=\pi\sigma_n^2\left(\frac{8kT}{\pi\mu_n}\right)^{1/2}\left(\frac{4\varepsilon_n}{kT}\right)^{1/3}\Gamma(5/3) \qquad (1.4.24)$$

They expressed the ratio of k_n/k_{-n} as an equilibrium constant for pairwise interaction via the L-J potential

$$D_n\equiv\left(\frac{k_n}{k_{-n}}\right)=\frac{8\pi h\sigma_n^2}{(2\pi\mu_n kT)^{1/2}}\left(\frac{\varepsilon_n}{kT}\right)^{1/3}\Gamma(5/3) \qquad (1.4.25)$$

Here k is Boltzmann's constant, h is Planck's constant and σ_n is the sum of the radii of n-mer and monomer. They proposed that σ_n is a function of n and of the density of n-mers :

$$\sigma_n=\left(\frac{3(n-1)}{4\pi\theta_{n-1}}\right)^{1/3}+a_o \qquad (1.4.26)$$

where

$$\theta_n=\left(\frac{\rho}{W}\right)N_o\frac{n^{2/3}}{2+n^{2/3}} \qquad (1.4.27)$$

in which N_o is Avogadro's number, ρ is the density of the liquid , and W is the molecular

weight of the monomer. ε_n is the depth of the L-J potential for the n-mer estimated using the enthalpy change, $\varepsilon_n=(1/5)\{|\Delta H_n^o|-|\Delta H_{n-1}^o|-kT\}$. Then $k_{-n}=k_n(D_n)^{-1}=0.7937(kT/h)$. The stabilization constant, k_n^s, is the binary collision rate between the unstable cluster, A_n^*, and stabilizing collision partners, M. It is controlled by a hard sphere $+r^{-6}$ attractive potential but modulated by a relative efficiency factor for energy transfer that depends both on n and T. k_n^s is given by

$$k_n^s=\omega\,(SP) \tag{1.4.28}$$

where SP is a single adjustable parameter. Its magnitude increases as temperature decreases, and it ranges from 0.2 to 1.0. This favourably biases stabilization at lower temperatures, since then the mean duration of the encounters is longer.

$$\omega=\pi\sigma_{ns}^2\left(\frac{8kT}{\pi\mu_n'}\right)^{1/2}\left(\frac{4\epsilon_{n+1}}{kT}\right)^{1/3}\Gamma(5/3) \tag{1.4.29}$$

in which

$$\sigma_{ns}=\left(\frac{3n}{4\pi\delta_n}\right)^{1/3}+a_o \tag{1.4.30}$$

The destabilization rate constant, k_{-n}^s, is given by

$$k_{-n}^s=\omega\left(\frac{\epsilon_n}{kT}\right)e^{-\frac{3\epsilon_n}{kT}} \tag{1.4.31}$$

With these equations the k's can be calculated, and hence the concentration of clusters

as a function of time can be deduced by integrating the coupled differential equations subject to conservation of mass.

In Wilcox and Bauer's kinetic treatment a significant parameter appears, τ_n, the time for the onset of a steady-state concentration of n-mer. They estimated τ_n for larger n-mers (n>50). The mean incubation time for an n-mer, $\langle\tau\rangle$, is approximately given by $(k_n[M][A_1])^{-1}$.

The cluster equilibrium distribution was calculated using thermodynamic functions (ΔH_n^o, ΔG_n^o, ΔS_n^o). For the overall step $nA \rightleftharpoons A_n$

$$\frac{[A_{n,e}]}{[A_{1,e}]^n} = (RT)^{n-1} e^{-\frac{\Delta G_n^o}{RT}} \qquad (1.4.32)$$

where $\Delta G_n^o = \Delta H_n^o - T\Delta S_n^o$. ΔS_n^o is given by

$$\Delta S_n^o - \Delta S_{n-1}^o = \frac{\Delta H_n^o - \Delta H_{n-1}^o}{T} + R\ln\left(\frac{k_n^s}{k_{-n}^s}\right) + R\ln\left(\frac{D_n}{RT}\right) \qquad (1.4.33)$$

where

$$-\frac{\Delta H_n^o}{nQ_T} = 1 - An^{-B} \qquad (1.4.34)$$

Here B=1/3, A is about 0.85, and Q_T is the standard heat of vaporization at T. Wilcox and Bauer defined a 'constrained' equilibrium by postulating that the above equation applies to a supersaturated vapour, as a transient state. In practice, an upper limit (n=m) must be assigned to calculate the equilibrium concentration of clusters using the above equation in conjunction with the mass balance equation. For any specified m the calculated values $[A_{n,e}]$ pass through a minimum (L). For low values of m the value of L is independent of the upper limit (m). The L-mer cluster was considered in a similar way as the critical cluster was in classical theory. Letting v=L+1, and substituting the equilibrium concentration into the expression for J_n, Eq. 1.4.23, an approximate condensation flux at steady state can be calculated

$$J^{ss} \approx \left[\frac{k_v^s [A_1]}{1+(k_v^s/k_{-v})\,[M]}\left\{\frac{k_v [A_{v-2}]}{k_{-v}[A_{v-1}]}+\frac{[k_{-v}^s [M]}{k_{-v}[A_1]}\right\}-k_{-v}^s\right]\,[M]\,[A_{v-1}] \qquad (1.4.35)$$

The calculated J^{ss}, as a function of temperature and supersaturation, for n-nonane was compared with an extended set of experimental data over the range 233 to 315 K (4<S<26) obtained by Katz[64] et. al, supplemented with J_{exp}^{ss} values by Adams and Schmitt[54], and Wagner and Strey[65] up to S=600. Overall the agreement between the computed and the experimental values fell well within the current uncertainties of the three sets of data. However, there are clear differences at high log J^{ss} levels ($J^{ss} = 10^7$ to 10^{10}) where the experimental magnitudes consistently do not increase as rapidly with log S, as they do in the lower range.

The SCKM theory does not suffer from the conceptual flaws that characterize classical nucleation theory. The difficulties with this model lie in finding the association enthalpy and entropy as a function of cluster size, and in finding accurate molecular parameters, such as the geometric cross sections, and the potential energy well depth needed for calculating the rate constants.

1.4.5 The Simple Kinetic Model for Carbon Clusters

Creasy and Brenna[51,66] used a simple kinetic model to account for large-mass carbon clusters produced by laser ablation of graphite. Since experimental results indicate that the predominant species formed by laser vaporization or thermal vaporization of graphite are small species, mostly C_3[67,68,69], the basis of the mechanism involves only stepwise addition of small species(C_1 to C_3). The kinetic equations are given below:

(a) $$A_{n-x} + A_x \rightleftharpoons A_n^*$$

for which k_1 and k_{-1} are the forward and backward rate constants respectively; and

(b) $$A_n^* + M \rightarrow A_n + M$$

for which k^s is the stabilization rate constant. Applying the steady state approximation to the concentration of the cluster, A_n^*, the differential equation for the formation of A_n is given by

$$\frac{d[A_n]}{dt} = \frac{k_1 k^s [A_x]\ [M]\ [A_{n-x}]}{k_1 + k^s [M]} \qquad (1.4.36)$$

Creasy and Brenna integrated the above system of equations under the following assumptions:

(1) The concentration of large clusters, $[A_n]$, is much smaller than that of the small species, $[A_x]$. Therefore, $[A_x]$ is not depleted by the formation of $[A_n]$ to a great extent. Pseudo-first-order kinetics was used. The values of [M] and $[A_x]$ were assumed to be constant during the 10 ns laser pulse, due to a constant rate of formation by ablation. After the laser pulse, they decrease only because of the increase in volume, given by the function V(t)

$$V(t)=1, \qquad t \leq 10ns$$
$$V(t)=\{[r_o+v(t-10)]/r_o\}^3, \quad t>10ns \qquad (1.4.37)$$

where r_o is the initial radius of the sphere of ablated material and v is the velocity of the expanding material.

(2) The rate constants were estimated to be consistent with gas kinetic considerations and adjusted as parameters to obtain good agreement with experimental observations.

(3) The growth of clusters occurs only by addition of small species, x=1 to 3.

Using this simple model they explained several aspects of the experimental observations. The calculated cluster distributions corresponded well to the experimental mass spectral distributions for several conditions. It provided some possible mechanisms for the formation of magic numbers and for the predominantly even cluster distribution.

Several kinetic approaches to homogenous nucleation theory have been discussed in this section. Since nucleation in supersaturated vapour is a kinetically controlled process, the kinetic approach provide a more consistent picture than classical nucleation theory. The kinetic models discussed above overcome some inconsistencies and drawbacks which appear in classical theory. Some of these models avoid using the constrained equilibrium assumption and Maxwell demons. Some avoid the use of the concept of macroscopic surface free energy for the equilibrium cluster distribution calculation. A complete kinetic analysis is limited by the lack of reliable estimates of the many rate constants involved and of their dependence on temperature and cluster size. As Reiss et al[55] pointed out there is no simple expression for the rate constant for evaporation of monomer from clusters. The difficulty in estimating the rate constants lies in obtaining molecular parameters such as the diameter of molecules within clusters and the interaction forces among the molecules within clusters. These are the most important yet least established parameters used in the kinetic approach.

Although every model can find some experimental data to support it, such data do not provide a very sensitive quantitative test of a theory, due to the difficulties of performing homogeneous nucleation experiments. It is very difficult to make sure that nucleation is completely homogeneous. Trace quantities of dust or small ion concentrations can cause a big difference in the nucleation rate. It is also very difficult to determine the pressure, P, that yields the observed nucleation rate. Due to the very steep dependence of nucleation rate on supersaturation, the corresponding deviations encompass many orders

of magnitude. An example was given by Bauer[44]. Because of these considerations there are no experimental criteria to determine which model is better than others.

1.5 Experimental Studies of Nucleation

There are four main experimental methods for the study of nucleation from the vapour phase. They are the expansion cloud chamber, the diffusion cloud chamber, the supersonic nozzle and the shock tube. In the piston cloud chamber and the supersonic nozzle, the supersaturated vapour state is reached by adiabatic expansion of a vapour. The diffusion chamber employs a different way of generating the supersaturated state, that is, by the diffusion of vapour molecules from a high temperature region to a low temperature region of the apparatus. The shock tube is a versatile method for studying nucleation. It can be used to study either heterogeneous or homogeneous nucleation. It can generate the supersaturated vapour either by an adiabatic expansion wave or by an incident compression shock wave, or by a reflected expansion wave. In this section we shall discuss these methods.

1.5.1 The Expansion Cloud Chamber

The first observation of homogeneous nucleation was made by Wilson[70] using a piston expansion chamber. A chamber filled with nearly saturated vapour is expanded adiabatically by moving a piston rapidly. The vapour in the chamber is cooled and

becomes supersaturated. Larger and larger expansions are performed until a raining of droplets is observed as deduced by light scattering. The temperature can be either measured or calculated. The pressure of the vapour can be monitored by means of a fast piezoelectric pressure transducer. Critical supersaturation ratios at different temperatures can be determined in this way.

Using this method it is hard to measure or estimate the nucleation rate, and vapour can be rapidly depleted while forming droplets that are too small to see. Heat released during condensation can increase the temperature and thus affect the nucleation rate. Furthermore, it is hard to distinguish between heterogeneous nucleation on ions or dust and homogeneous nucleation.

P. E. Wagner and R. Strey[33] modified this method. The modified chamber has two spring-operated pistons. One is called the expansion piston, the other is called the compression piston. Both pistons can be released with a selectable delay time >1ms. First, the expansion piston is released. The vapour is adiabatically expanded until a supercritical condition is achieved in the measuring chamber and homogeneous nucleation occurs. At the end of the selected delay time a small recompression is achieved by releasing the compression piston. This causes a reduction of the supersaturation to a subcritical value, and nucleation stops. The already-formed nuclei grow to visible sizes and the droplet concentration, C, can thus be determined by comparison with Mie theory. Therefore an average experimental nucleation rate can be determined from a knowledge of the delay

time. From the position of the first Mie maximum, Wagner and Strey could uniquely determine whether homogeneous or heterogeneous nucleation occurred. In their investigation they found that when filtered gas was used, visible droplets were never observed before the end of the expansion process. However, upon introducing heterogeneous condensation nuclei the onset of condensation occurred significantly earlier than for the case of homogeneous nucleation. With the two-piston cloud chamber homogeneous nucleation was observed during a short well-defined, supercritical expansion pulse with a duration as short as about 1 ms.

1.5.2 The Upward-Diffusion Cloud Chamber

In 1939, Langsdorf[36] proposed a novel "diffusion" chamber which eliminates the adiabatic expansion of a Wilson-type cloud chamber and replaces the transient operation and complicated fluid mechanics of this device with a simple diffusive flow. Katz and Ostermier have refined the method to make it into a very promising experimental tool in vapour nucleation studies[62]. The chamber is designed so that, to a high degree of approximation, one dimensional diffusion takes place.

The vapour molecules under investigation diffuse from a lower heated pool of liquid via a carrier gas to an upper "cold" metal plate at which vapour condenses. A light carrier gas is used so that the total gram density of the vapour and carrier gas mixture decreases from the bottom of the chamber to the top, thus preventing convection. Between the two plates

the temperature and partial pressure of the vapour are approximately linear with distance. Since the equilibrium pressure of the vapour, P_∞, varies exponentially with temperature, the supersaturation is unity at the top and bottom plate surfaces, and is greater than unity in between the two surfaces. S reaches its maximum value near the top of the chamber. By increasing the temperature gradient the supersaturation maximum can be made as large as desired. The onset of homogeneous nucleation is determined visually by observing the forward scattering of light by droplets. Local thermodynamic conditions in the chamber are calculated from the values of the temperature at the boundaries of the chamber. The critical chamber state is that which just produces homogeneous nucleation. This state is defined as the point at which the temperature difference across the chamber is sufficient to yield about 2-3 drops per second per cubic centimetre. For each critical chamber state, a curve of supersaturation ratio vs. temperature is calculated for the region in the chamber at which the supersaturation is a maximum. The envelope of these individual supersaturation curves gives the experimentally observed critical supersaturation as a function of temperature. Katz and his co-workers studied homogeneous nucleation with the upward diffusion chamber extensively. They obtained good agreement with the classical theory for CCl_4 CCl_3H, $C_2H_2Cl_4$, CCl_3F[37], H_2O, methanol, ethanol, hexane[38], and n-alkyl benzene[62] over the temperature region they measured.

The upward thermal diffusion cloud chamber has several advantages[37] over the expansion cloud chamber in homogeneous nucleation studies. First, it is a steady state device with long diffusion time constants, so one can be certain that the steady state assumption of

nucleation theory is fulfilled. Second, the depletion of the vapour phase due to nucleation is not a problem, since a fresh supply of vapour always diffuses into the nucleation zone. This condition is required in classical nucleation theory. Perhaps this is a partial explanation why the experimental data from upward thermal diffusion cloud chambers is in good agreement with the prediction of CNT. Finally, the chamber is self-cleaning; it effectively has no walls since the nucleation region probed is between the top and bottom plate. The main limitation is that the substance studied must be liquid at both the bottom and the top plate. Therefore, the temperature region in nucleation measurements must be below the critical temperature and above the triple point.

1.5.3 The Supersonic Nozzle

Cluster formation and nucleation rates have also been studied by supersonic nozzles[151]. A vapour and carrier gas mixture is expanded adiabatically when it flows through a converging-diverging nozzle. The number of clusters is measured by several techniques based on light scattering by droplets. This method has several advantages: (1) It can be used to study not only nucleation from vapour to liquid, but also nucleation from vapour to solid. The temperature region here is less restricted than in the upward thermal diffusion cloud chamber. (2) The condensation process is spread out spatially instead of temporally, thus permitting measurements of the time history of condensation. And (3), the expansion is sufficiently rapid that dust and ions are insignificant as nucleation sites under typical supersonic nozzle experimental conditions. The disadvantages of this

technique are: (1) a complicated analysis is required to calculate nucleation rates, requiring the incorporation of the kinetics of nucleation and growth along with the equations of mass, momentum and energy conservation for the flow. (2) The expansion is so fast that it raises the question of whether the distribution of new-phase embryos can attain a steady state, and the question of the validity of local thermodynamic equilibrium.

1.5.4 The Shock Tube Method

P. Wegener and G. Lundquist[71] were the first to use the shock tube to study the nucleation of water at a temperature of 129 °C in 1950. There are several different ways to generate a supersaturated state using a shock tube. We shall discussed these different techniques.

Wegener and Lundquist produced the supersaturated vapour with an unsteady expansion wave. They filled the compression chamber of the shock tube with filtered air of controlled humidity at 1 atm and room temperature. The expansion chamber was then evacuated. When the diaphragm was punctured, a shock wave was generated and allowed to propagate into the expansion chamber. The air in the compression chamber underwent an isentropic unsteady fast expansion from its controlled initial conditions. Consequently, it cooled. The presence or absence of condensation was detected by a sensitive electronic method in which the light scattered from droplets was observed and recorded.

J. B. Homer[72] studied the nucleation and growth of metallic clusters from supersaturated metallic vapour produced by an incident shock wave. In his approach an organometallic vapour, tetramethyl-lead (TML), was highly diluted in argon. The mixture was placed in the test (compression) section and then heated and compressed dramatically by incident shock waves to temperatures of 600 to 1200 K. At shock wave temperatures the TML molecules were rapidly pyrolysed, and supersaturated lead vapour was produced. The process of formation of small clusters of lead was monitored by recording the turbidity of the hot gas as a function of time. The TML was so dilute in the test gas that temperature changes due to the pyrolysis and condensation process were insignificant. Shock wave attenuation was minimal, less than one percent per meter; so Homer concluded that the condensation occurred essentially under conditions of constant temperature and total pressure.

Kung and Bauer[23] studied iron condensation. They observed the formation of iron clusters in the expansion region following the reflected shock wave. Their samples consisted of 0.5% $Fe(CO)_5$ in Kr or in (1:1) Xe + Ar mixtures. The samples were shocked-heated to temperatures of 2500 to 2680 K behind the reflected shock wave. $Fe(CO)_5$ decomposed into atomic Fe vapour completely even behind the incident shock wave at temperatures of about 1100 K. Under these conditions iron vapour was supersaturated. Therefore, clusters of iron formed behind the incident shock front. When the reflected shock front arrived at the test sample, the temperature jumped to about 2700 K. The clusters evaporated completely because the iron was subsaturated at this high

temperature. In the expansion wave where the temperature fell to approximately 2000 K, cluster formation occurred again. Cluster formation was observed by recording non-characteristic emissions at two wave-lengths (5940 and 4945 Å). In contrast with Homer's technique nucleation occurred here under conditions where both temperature and pressure were falling.

In the approach of Peters and Paikert[73,74], the nucleation rate is given by $J_{exp} = N/(v\Delta t)$, where N is the number of nuclei found in a volume, v, and the nucleation period, Δt, is delineated by the reflected tail of the centred expansion wave and the reflected shock wave. The mixture of vapour under investigation plus Ar is put into the driver side of the shock tube. The driven side contains pure argon at lower pressure. The observation station is placed near the end wall of the driver side. In this arrangement, after the diaphragm separating the two sections is broken, a shock wave is generated and allowed to propagate to the driven side. At the same time, an adiabatic expansion wave propagates to the end wall of the driver side. Its head reaches the end wall at the speed of sound in the driver gas. Its tail however travels slower than the speed of sound because the local temperature is lower. The temperature of the vapour dramatically decreases after the expansion wave passes. The expansion wave is terminated when the tail is reflected at the wall. This is defined as the initial point of the nucleation period, Δt. Because of the boundary condition at the end wall the vapour is at rest during and after the nucleation period and thus a stationary sample of growing nuclei is observed. A constant pressure builds up, the duration of which is precisely adjustable by the initial condition. But only

when the reflected shock arrives at the observation window are the pressure and temperature dramatically raised to a higher level. The vapour then ceases to be supersaturated, and the nucleation period, Δt, is terminated. The length of the nucleation period, Δt, was controlled in Peters' and Paikert's apparatus by the distance between the diaphragm and a constriction in the driven section. Before the nucleation period started, the vapour was already cooled to a supersaturated state by the expansion wave, and pre-nucleation had already started. They believed this pre-nucleation could be minimized by placing the observation station close to the end wall, and the rate of expansion of the wave was increased considerably after the centred expansion wave reflected from the closer end wall. Thus the period of pre-nucleation was shortened. The nucleation and growth rate were measured by a 90° Mie light scattering technique. In contrast to the method used by Wegner and Lundquist, Peters and Paikert's method measured nucleation in a constant pressure region while the vapour is at rest. This method resembles the two-piston cloud chamber in principle without physical pistons. Therefore, the nucleation period can be very short. The average experimental value of the nucleation rate, $J_{exp}=N/(v\Delta t)$, can reach the true value more closely as Δt approaches zero. The difficultly with this method lies in evaluating the importance of the pre-nucleation effect.

The shock tube cannot only be used for studying homogeneous nucleation as shown above, but also for investigating the effect of surfaces on heterogeneous condensation e.g. film-wise condensation. Goldstein[75] was the first one to conduct this kind of study with a shock tube in 1964. Later, Smith[76] also studied film condensation of water vapour with

a shock tube. Fujikawa and co-workers[77] have carried out many studies of non-equilibrium vapour condensation at the end-wall of a shock tube. The mechanism of film-wise condensation on the end wall behind a reflected shock wave is briefly described below. The vapour under investigation is in the driven section, the driver side containing helium at higher pressure. After the breaking of the diaphragm, a compression shock wave is produced and allowed to propagate towards the end wall of the driven section. At the moment when the incident shock wave reflects from the end-wall surface, the pressure, temperature and density of the vapour in the compressed region are increased instantaneously and held at a higher value . Because of the large heat capacity of the end wall of the shock tube, however, the vapour very close to the surface of the wall is heated very little, and a thermal boundary layer is thus formed. The gas very near the end-wall thus experiences, essentially, an isothermal compression. The vapour then begins to condense on the end-wall surface in the form of liquid film. The film grows in thickness with time. Smith found[76] that film growth is linear in time, t, when $t<10\mu s$. This was later confirmed and explained theoretically by Fujikawa et al[78]. In this region the film growth rate is governed by the condensation parameter, defined by Fujikawa[79], that depends on the initial conditions and thermal properties of the vapour and the film. Beyond that time period film growth is dependent on $t^{1/2}$, and the growth of the film depends on the thermal properties of the vapour film and of the end wall.

In this section we have discussed four methods used to study nucleation. These methods can be divided into two types. The upward diffusion chamber and the supersonic nozzle

are of the continuous type; the expansion cloud chamber and the shock tube are of the transient type. The latter two use rapid expansion and compression processes to generate a supersaturated state of short duration. No nucleation occurs before and after this period theoretically. Despite the progress made by these methods there are still some limitations. First, no method can provide any detailed kinetic information on cluster formation processes directly, and no method can identify the critical cluster or nucleus. What one monitors in these methods using scattered light are droplets. The droplet production rate is measured, rather than the nucleation rate. No existing theory can guarantee that the droplet formation rate is equal to the nucleation rate of critical clusters. Second, none of the methods so far provides data over wide enough ranges of temperature and supersaturation, as is necessary for testing the theory thoroughly. In fact, using different methods different results are obtained. For example, in the case of water, Katz and Ostermier[62] measured the critical supersaturation ratio as a function of temperature using the upward diffusion cloud chamber at 285 to 305 K. Good agreement between their results and classical theory was obtained, within 5%. Kassner and Schmitt[79] got the same result with the expansion cloud chamber. The results obtained by Jaeger et al[30] using a supersonic nozzle for water at temperatures between 215 and 255 K agreed with classical theory's prediction. Good agreement with classical theory was also obtained by Barschdorff[80] using an unsteady, isentropic expansion in a shock tube experiment at 220 to 280 K with Ar or He as a carrier gas. But the nucleation rates of water at 276.15, 289.35 and 301.65 K measured in a two-piston expansion chamber by Wagner and Strey[33] were considerably lower than predicted by classical theory. Their results were in good

agreement with one-piston cloud chamber measurements performed by Miller[81] and by Anderson et al[82]. The shock tube experiment of Peters and Paikert[73,74] at 204 to 220 K confirmed the results of Strey and Wagner. With these experimental data it is not possible to conclude which experimental method is best, let alone evaluate the classical nucleation theory.

1.6 Requirements for Chemical Oscillation

We know that any closed chemical system must come to equilibrium. Equilibrium is a stable and unique state, and there are some thermodynamic functions to describe the change from one equilibrium to another equilibrium state, such as the change in the Gibbs free energy, ΔG. G decreases monotonically when a chemical reaction takes place at constant pressure and temperature. The reactant concentrations decrease monotonically, and product concentrations increase monotonically. However, some oscillatory reactions have been observed and studied. In these kinds of reactions the concentrations of intermediates or products rise and fall periodically[83]. In this section we briefly describe conditions for observing an oscillatory reaction.

Here we consider two types of chemical oscillators: one is the isothermal oscillator; the other is the thermokinetic oscillator. Studies show that a chemical oscillator must satisfy the following three requirements, which can be divided into two classes: thermodynamics

and kinetics. Thermodynamics requires that a system must be far from thermodynamic equilibrium i.e. the Gibbs free energy change, ΔG, for the overall reaction must be large and negative. Also, oscillation is a transient phenomenon. In a closed system oscillations cannot be sustained because any reaction will approach equilibrium eventually. In experiments an oscillatory system can be maintained far from equilibrium indefinitely by continuously adding fresh reactants into a continuous flow stirred tank reactor (CSTR). Kinetically there are two requirements. One is non-linearity. For an isothermal oscillator the polynomial differential rate equations that describe a chemical reaction must be non-linear, that is, the differential equation must contain terms that depend on the product of two concentration terms or on the nth power of the concentration of a single species ($n \geq 2$). If a set of differential rate equations corresponding to a chemical reaction are linear, and reaction takes place at constant temperature, its kinetic behaviour is simple. As discussed in any physical chemistry text book the concentrations of reactants decrease monotonically with time, while the concentrations of the products will increase monotonically with time. The concentration of intermediates may pass through a single maximum during reaction. But for nonlinear differential rate equations, although the concentrations of reactants and products will change just as in the linear system, the concentrations of intermediates will change in a much more complicated way. Non-linearity is a necessary but not a sufficient condition for a system to have oscillatory behaviour. The second condition is that there be some mechanism for "feedback". This means that species formed during the reaction must affect the rate of earlier reaction steps. The mechanism for feedback is realized by auto-catalytic reactions. If there is a

feedback mechanism in a chemical reaction then its dynamical law, i.e. the set of differential rate equations must be nonlinear.

The most famous chemical oscillator is called the Belousov-Zhabotinskii (BZ) reaction[84], an organic reaction, in which oxidation is carried out by bromate and catalyzed by inorganic ions. An example is the oxidation of malonic acid represented by the equations

$$CH_2(COOH)_2 + 6Ce(IV) + 2H_2O \rightarrow 2CO_2 + HCOOH + 6Ce(III) + 6H^+$$
$$2Ce(III) + BrO_3^- + 3H^+ \rightarrow 2Ce(IV) + HBrO_2 + H_2O$$

Ceric ion is reduced in the first step, and cerous ion is oxidized in the second. It exhibits oscillations in colour and in overall redox potential as measured by a Pt electrode as well as in the potential measured by a bromide-ion-selective electrode[84]. It was found that the oscillations in colour result from oscillations in [Ce(IV)] and that free Br_2 does not appear in detectable amounts.

The first thorough analysis of the mechanism of temporal oscillations in the BZ reaction was presented by Field[85], Koros and Noyes (FKN) in 1972. The FKN mechanism is quite complicated and involves no less than 18 steps and 21 intermediates. According to the FKN mechanism the oscillation in the BZ oscillator is based on two sets of essentially non-interacting reactions, process A and process B. These two processes taken together represent a sort of bistability (two stable steady states between which the system can be flipped by a suitable perturbation). These are coupled by a third process, C, that allows the dominant process of the reacting system to be process A or B alternately. The study

shows that bromide ion is the critical intermediate whose concentration determines whether the process A (high [Br^-]) or process B (low [Br^-]) is the dominant process. [Ce(III)] is oxidized in process B, and [Ce(IV)] is reduced in process C. The FKN mechanism can be reduced to a much simpler model, usually called the Oregonator[86] that has been remarkably successful in interpreting the behaviour of the BZ reaction and in understanding the dynamic structure. It is summarised by

$$\begin{array}{ll} \textit{process A:} & A+Y \rightarrow X+P \\ & X+Y \rightarrow 2P \\ \textit{process B:} & A+X \rightarrow 2X+Z \\ & 2X \rightarrow A+P \\ \textit{process C:} & Z \rightarrow fY \end{array}$$

k_1, k_2, k_3, k_4 and k_5 are the rate constants of the five equations respectively, and f is a stoichiometric factor. When [Y] is very large A is the control process in which X is formed in the first step and most of it is removed in the second step. Y is depleted in process A. When the concentration of Y is low enough, X is formed mainly by the third reaction and removed by the fourth reaction. Process B then becomes the major process. Z is produced in process B. The third reaction involves autocatalytic production of X. This is positive feed-back. All of the presently understood examples of chemical oscillators contain such feedback. It is process C (reaction 5) that makes this model oscillate. Its function is, after a delay during which Z accumulates via process B, to "poison" process B by the production of Y. This completes a delayed negative-feedback loop. The concentration of Y increases; the system returns to restart process A again. k_5 is very small. If k_5 were sufficiently large, the system would not oscillate but would approach a stable steady state.

For the thermokinetic oscillator the thermodynamic requirement is the same as for the isothermal oscillator. However here non-linearity for a chemical reaction arises naturally in the relationship between a rate constant and temperature. Most chemical reaction rate constants obey the Arrhenius law, k=Aexp(-E/RT), where E is the activation energy, A is the pre-expontial factor, and R is the universal gas constant. "Feedback" is realized by the self-heating process. The heat produced during an exothermic reaction increases the temperature of the reaction system. Then the temperature affects the rate constant nonlinearly. The simplest model of a thermokinetic oscillator is composed of two first order-reaction steps given by

$$A \rightarrow B \qquad rate = k_1[A] \qquad (1)$$
$$B \rightarrow C + Q \qquad rate = k_2[B] \qquad (2)$$

It was first studied by Sal'nikov[87], and later by Gary[88,89]. The oscillation of the temperature and of the concentration of B could be monitored. A qualitative description of the oscillation of a thermokinetic oscillator is given as follows.

As exothermic reaction (2) proceeds, heat is released. The result of self-heating is to increase the system temperature. Since the rate constant, k_2 increases dramatically with temperature, according to $k_2 \propto \exp(-E_2/RT)$, positive feed-back of heat is present. Suppose $E_1 \ll E_2$, or $E_1 \approx 0$. A "stationary state" in B can be reached when $d[B]/dt \approx 0$ and $dT/dt \approx 0$. A fluctuation or heat diffusion to the surroundings causes a temperature drop. Then the local stability of the stationary state is lost. Subsequently the rate of reaction(2) decreases and less heat is released. The system temperature decreases further,

and the rate constant, k_2, decreases dramatically. This is negative feedback. At a certain point another stationary point is reached. However, the concentration of the intermediate [B] increases since $E_1 < E_2$. The rate of reaction (2) will increase again due to the accumulation of B, releasing heat again. The result is the loss of local stability of the second stationary state. Then the cycle begins again, resulting in a thermokinetically oscillating system.

Several thermokinetic oscillators, most of them oxidation reactions of hydrocarbons, have been studied [90], such as $CH_3CHO + O_2$, $2C_3H_8 + O_2$ and $C_4H_{10} + O_2$ etc. Although much more complicated mechanisms were applied to these systems, the basic requirements of thermodynamics and kinetics must be satisfied by all of them.

1.7 Summary and Justification of the Present Study

In this chapter we have discussed classical nucleation theory, some kinetic models and experimental methods for the study of nucleation. The classical nucleation theory is an equilibrium rate theory. The steady state nucleation rate is given by $J = Zk_{n^*}[A_{n^*}]$ in which $[A_{n^*}]$ is the equilibrium concentration of the critical cluster, A_{n^*}; $k_{n^*}[A_{n^*}]$ is the rate of the growth of critical clusters at equilibrium. The Zeldovich factor, Z, is used to relate the steady state with the equilibrium state. In the calculation of the equilibrium distribution macroscopic thermodynamic functions are employed. Therefore, in classical

theory the key piece of information is the equilibrium size distribution of clusters; yet this is treated in a casual way. Kinetic approaches avoid using the macroscopic surface tension for small clusters by treating clusters (n<100) as large gas phase molecules formed by the reaction $A_{n-1} + A = A_n$. The fundamental problem in kinetic models is how to determine all of the rate constants for each reaction.

The essential part of nucleation theory is the kinetics of formation of the critical cluster. The experimental methods discussed in the last section measure the rate of formation of droplets rather than the nucleation rate ——— the relation between the nucleation rate and the rate of droplet formation being unknown. Therefore, none of these experiments can, at present, resolve any of the difficulties of the theory of nucleation, as the truly microscopic world is beyond their reach. It is the purpose of this dissertation to explore the kinetics of truly cluster formation and dissociation in the vapour phase using shock tube experiments and computer simulation. The present shock tube is equipped with a laser-schlieren detector that is highly sensitive to the vapour density gradient. It is orders of magnitude more sensitive than Mie scattering, and can follow changes in real time with submicrosecond resolution. Consequently, information on production rates of subcritical clusters (n<10) is accessible. The experiments are based on the assumption that there is an initial cluster distribution in CCl_3F vapour determined by the initial conditions such as pressure and temperature, even in subsaturated gases. When a shock wave passes through the vapour, there is a temperature and pressure jump. The new equilibrium distribution of clusters will be reached by the process of formation and stabilization of

clusters. The laser schlieren technique can record a signal proportional to the density gradient (proportional to the rate of heat evolution) caused by the exothermic and endothermic reactions ($A_{n-1}+A = A_n$) and their allied stabilization reactions in the vapour phase. The schlieren signal is the total change caused by all of these reactions. Hopefully with computer simulation the contribution of each reaction can be determined, i.e. the rate constant for cluster formation can be found. The perturbation caused by the incident shock wave is essentially instantaneous. Therefore, an additional advantage exists in that one can avoid reliance on finite rates of thermal conductivity or adiabatic expansion for establishing a non-equilibrium initial state, as in other methods we have discussed. A unique feature of the present experiments, though, exploits the sensitivity to heat release allowing the study of the effects of thermal feedback on condensation —— an unexpected property of the microscopic kinetics of condensation.

CHAPTER 2

EXPERIMENTS

The shock wave technique is very useful for the study of physical and chemical processes[92]. This is largely due to three advantages. The first one is the wide range of temperatures and pressures that can be covered in shock tube experiments. When observations are made on the incident shock wave temperatures as high as about 5000 K can be achieved. In reflected shock waves temperatures as high as 20,000 K can be reached[93]. In the expansion wave temperatures below 150 K can be reached[71]. The second advantage is that the change of temperature and pressure is instantaneous, on a time scale that corresponds to a few molecular collisions. Translational heating at the shock front occurs in less than 5 collisions. The last advantage is the shock processes' amenability to be monitored by very sensitive instrumental methods of detection, for example, the schlieren technique. Therefore, it is not surprising that this method has been used extensively for the study of the chemical kinetics of a variety of reactions such as the decomposition of hydrocarbons[94,95,96], radical reactions[97,98], vibrational relaxation processes[99,100] and nucleation in vapour over a very wide range of temperature. In the last chapter we already saw that the shock tube technique is very versatile and powerful for studying nucleation over a large range of temperature.

In this chapter we shall describe our experimental method for studying the kinetics of cluster formation. First, the shock tube equipment and the formation of shock waves will be discussed, then the measurement of the shock velocity and of the reaction rate, and the experimental procedure will be described. The properties of CCl_3F vapour will also be given in this chapter. In the final section we shall examine the schlieren signal.

2.1 Equipment Description

2.1.1 Shock Waves and the Shock Tube

In order to understand the formation of shock waves in a shock tube, it is necessary to introduce the concept of a sound wave.

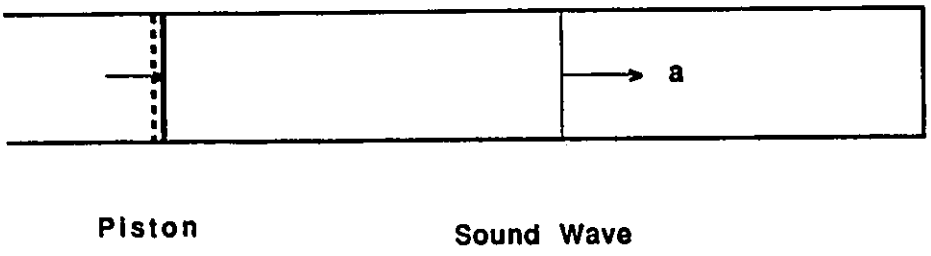

Fig. 2.1.1 Generation and propagation of a sound wave.

If a gas is confined to a long tube with a piston at one side, as shown in fig.2.1.1, and

if the impulse produced by suddenly pushing a piston is infinitesimally small, the compression wave produced by the impulse is called a sound wave. It moves through the gas at a velocity equal to the velocity of sound. Sound consists of a succession of rarefaction and compression waves, across which the fluid properties, such as temperature and pressure, change only infinitesimally. Therefore the process occurring in the wave is reversible. Furthermore, the wave front itself is extremely thin. Changes in fluid properties occur very rapidly. The rapidity of the process precludes the possibility of any heat transfer between the system particles and its surroundings. Therefore the sound wave process is isentropic i.e. reversible and adiabatic. The velocity of sound depends on the nature and physical state of the gas. For an ideal gas the sound speed[92,101] ,a, is given by

$$a=\sqrt{\frac{\gamma P}{\rho}}=\sqrt{\frac{\gamma RT}{M}} \qquad (2.1.1)$$

where γ is the specific heat ratio.

If a piston in a tube is given a steady velocity of magnitude dV towards the right (fig. 2.1.2), a sound wave travels ahead of the piston through the medium in the tube at speed a_1. Suppose the piston is now given a second increment of velocity dV, generating a second sound wave. It moves into the compressed gas behind the first wave at speed a_2. Each wave travels at the velocity of sound with respect to the gas into which it is moving. Since the second wave is moving into a compressed gas having a slightly more elevated temperature, the second wave travels with a greater absolute velocity than the first wave,

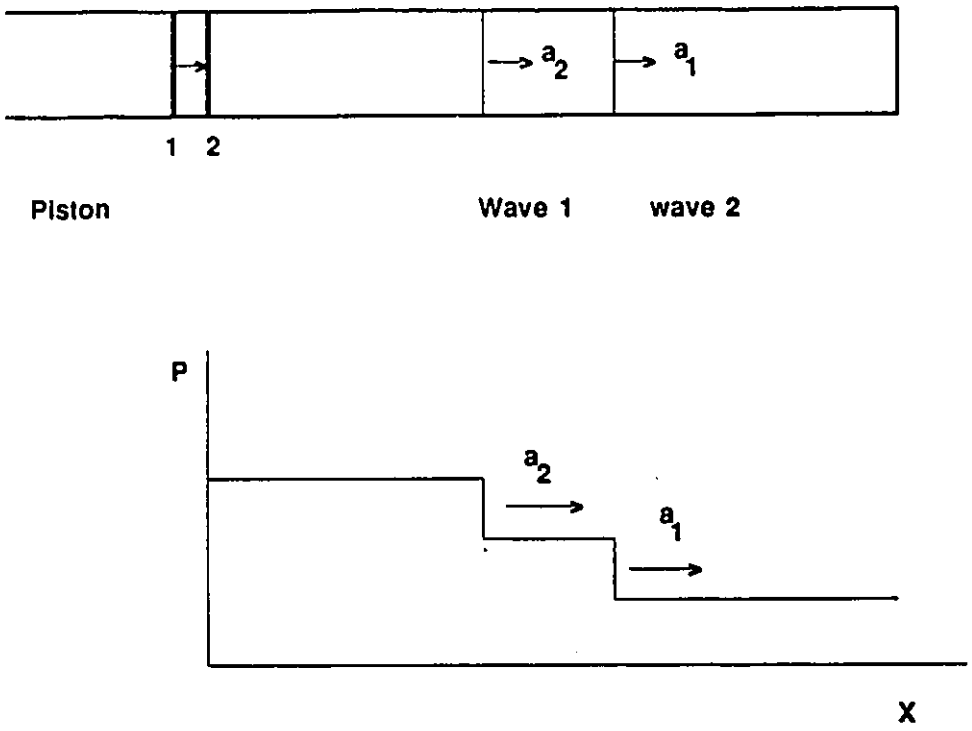

Fig. 2.1.2 Generating a shock wave at time t1

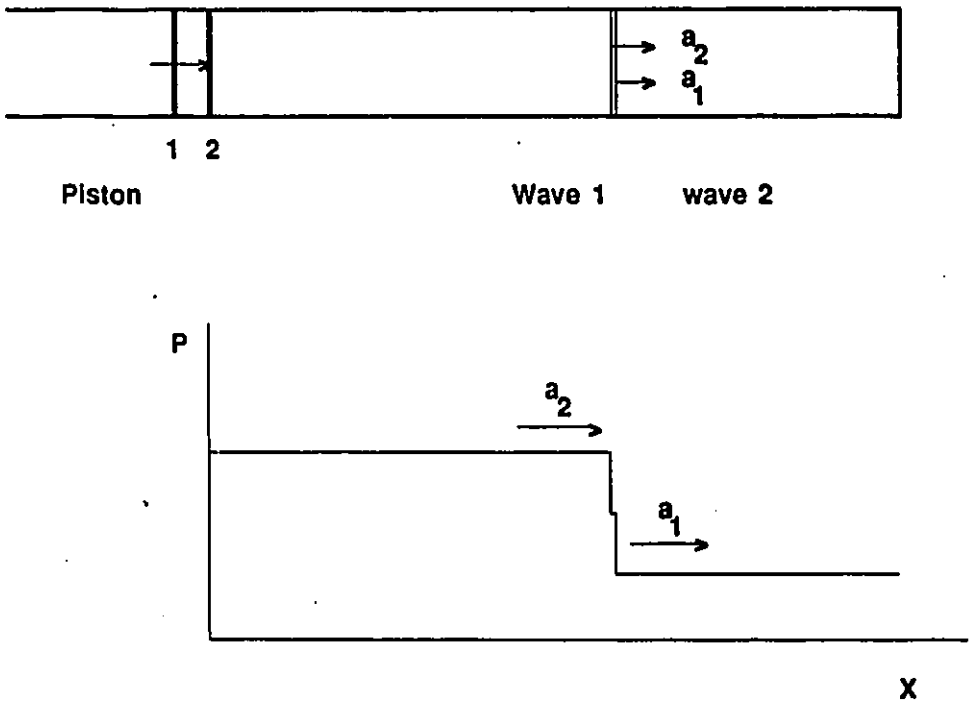

Fig. 2.1.3 Generating a shock wave at time t2

$a_2 > a_1$, and gradually catches up with it. In a similar way accelerating the piston by an amount dV again, a third sound wave is produced, which propagates at the sound velocity a_3. As explained above a_3 is bigger than a_2. The third wave will eventually catch up to the first wave too. No overtaking is possible because it would imply moving at the slow velocity, a_1, subsequently. A succession of these accelerations then gives a series of increasingly rapid wavelets which catch up to each other, producing at the end a single abrupt change where the small changes coalesce. This is a shock wave which moves into the undisturbed gas with a speed greater than either the speed of sound in the original unheated gas or of the piston itself. In fig. 2.1.3 the dramatic rise of pressure due to the shock wave is shown.

In contrast to a sound wave, a shock wave is an adiabatic but irreversible process because across the shock wave there is a big change in fluid properties. Another difference between a sound wave and a shock wave is that the sound wave is transmitted in the gas by collisions between gas molecules; there is no net flow. However, in a shock wave molecules will be carried along with the flow in the direction of propagation. The shock wave has a Mach number greater than unity. Mach number, M_a, is defined by the equation[101]

$$M_a = \frac{u_1}{a} \qquad (2.1.2)$$

where u_1 is the shock velocity and a is the speed of sound in the test gas.

If the piston moves in the opposite direction, an expansion wave will be generated, which moves at sound speed in the same direction as the piston. When the piston is given a second increment of velocity, a second expansion wave is produced and moves into the expanded gas behind the first wave. In this case the second expansion wave is travelling at a lower speed because it is moving into the already expanded and cooled fluid in which the sound speed is lower. In this manner the expansion wave spreads out.

The simplest shock tube is a long metal pipe of constant internal cross-section. It is divided into two sections (test and driver) by a thin plane diaphragm. The experimental sample is filled into the test section at the desired pressure, P_1, and temperature T_1. In the other section a high pressure, P_4, of a light gas, such as helium, is introduced. When the diaphragm is suddenly removed or broken, a shock wave is generated since the driver gas pressure is much higher than that of the test gas and the driver gas acts as an accelerated piston. This shock wave is called an incident normal shock wave which propagates into the test section. If the translational temperature of the gas is not perturbed by chemical processes, or the effect of this process is so small that it can be neglected, the ideal theory predicts that region 2, the incident shock region, is a hot zone of moving gas of uniform pressure, P_2, and temperature, T_2. When the shock wave reaches the end wall in the test section, it is reflected backwards. Region 5 denotes the reflected shock region which is an even hotter zone of stagnant gas of uniform pressure, P_5 and temperature, T_5 (see fig. 2.1.4.) At the same time that the shock wave is generated, an adiabatic expansion wave is produced and propagates to the driver side, forming an expansion fan. Region 3 denotes

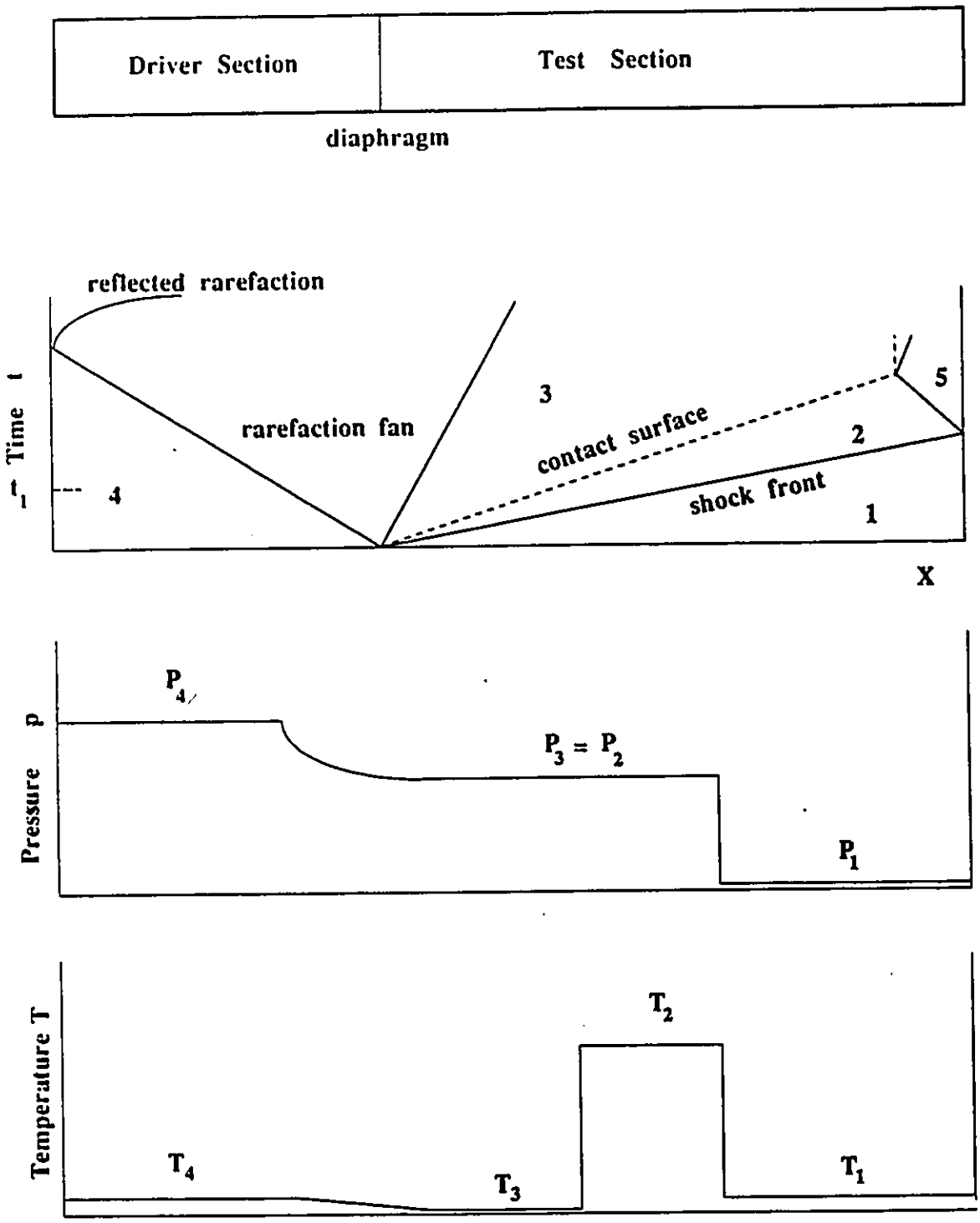

Fig 2.1.4 (a) conventional shock tube, (b) An (x-t) diagram showing progress of the shock wave, the rarefation fan and the contact surface separating driver and experimental gases, (c) The pressure distribution along the tube at time t_1. (d) The temperature distribution at time t_1 (adapted from reference 92)

the expansion fan in which the temperature and pressure is not constant, both of them decreasing as the expansion fan grows. In principle, if the velocity of the shock wave is known the properties of all of the different regions can be calculated using the conservation laws of gas dynamics and the equation of state of the gas[102]. The desired temperature and pressure in regions 2 and 5 can be realized by adjusting the pressure ratio, P_4/P_1. There are upper limits to the temperature ratios, T_2/T_1, which are determined by the thermodynamic properties of the test gas as $P_4/P_1 \rightarrow \infty$. In our study the incident shock region is monitored. Behind the incident shock, the gas molecules are always moving, and therefore, observation time at a fixed station is always less than true heating time. The maximum observation time is limited by the arrival of the contact surface (separating test gas and driver gas) at the station.

All of the 190 experiments reported in this study were done with two different size shock tubes. One was a nickel coated-steel shock tube. The internal dimensions of the test section measured 6.8 cm by 6.8 cm, and it was 318 cm long. The high pressure driver section (9.5 cm internal diameter) was 123 cm long. These two sections were separated by an aluminum foil diaphragm. Experiment No.1 to 130 were performed with this so-called "old tube". The remainder were performed with a "new tube". It was a stainless steel tube shown schematically in fig. 2.1.5. The test section was 730.0 cm long, and its cross section was 9.3 cm by 8.3 cm. The length of the driver section was 380.0 cm, and its diameter was 15.3 cm. The test section of each tube could be connected to the sample container or to the pump or to the mixing tank, depending upon which valves were

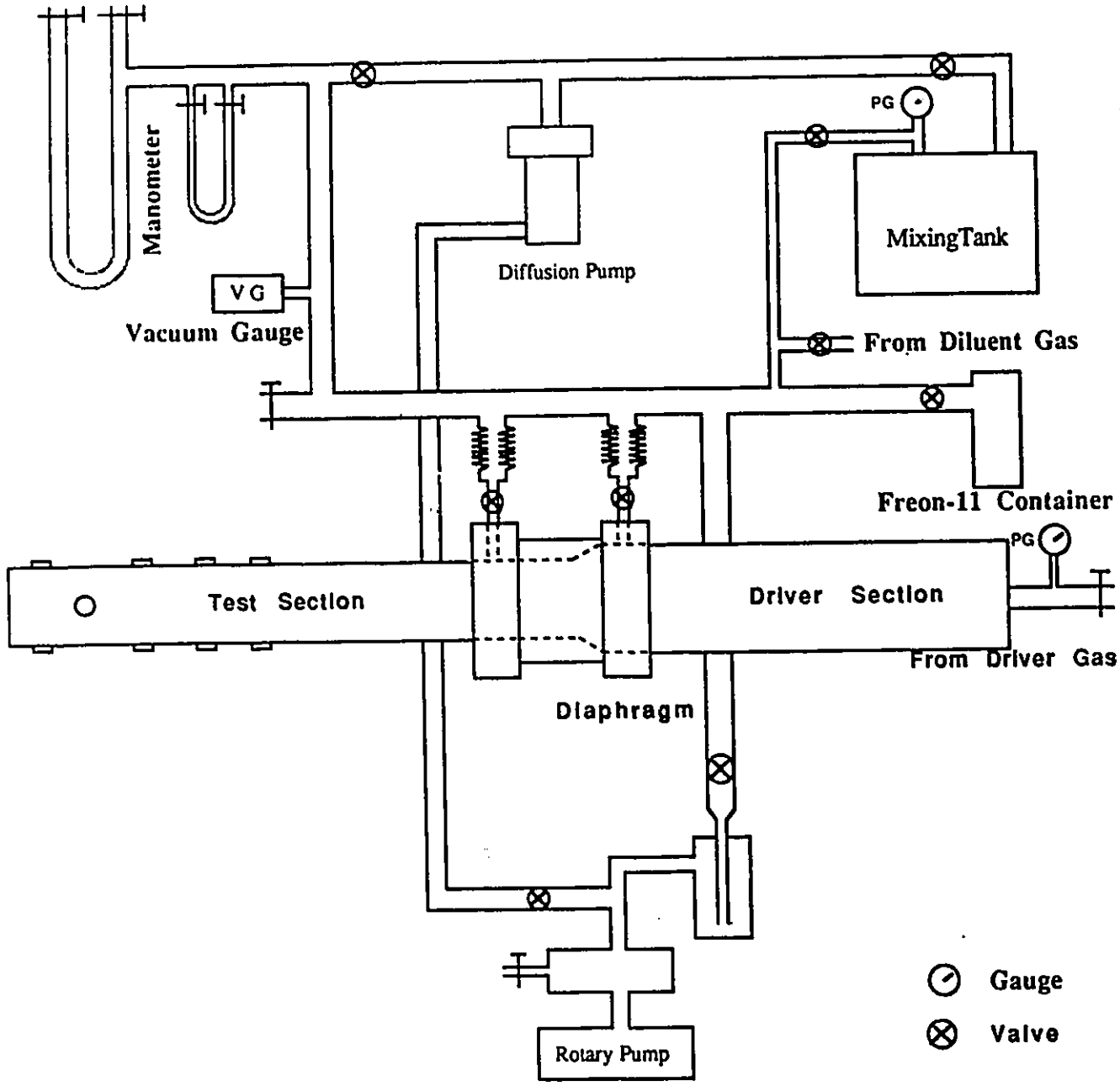

Fig. 2.1.5 Experimental arrangement

opened. A mercury manometer could also be connected to the test section, when the pressure of the sample to be introduced into the test section was to be measured. The driver section of the tubes was connected directly to a high pressure helium cylinder. The vacuum in the system was measured with an Edwards Vacustat high vacuum gauge.

In the test section of each tube, there was a main observation window for the measurement of the main schlieren signal in the axial direction. The distances between the observation station and the diaphragm position were 617.0 cm and 258.3 cm for the new and old tubes respectively. There were several observation windows located upstream and downstream of the main observation window of each tube for the measurement of shock wave velocity.

In order to approximate to a one dimensional flow both test sections had constant cross-sectional areas throughout. The tubes were straight and the interior surfaces of both tubes were smooth. The test sections themselves were clamped to the concrete floor of the laboratory to avoid recoil.

2.1.2 Gas Handling and Gas Mixture Preparation

Liquid CCl_3F (trichlorofluormethane) was stored in a glass container that was connected to the test section of the shock tube and the mixing tank. Valves controlled the gas flow between the test section and the CCl_3F container and between the mixing tank and the

container. Pure CCl_3F (99.9%) manufactured by DuPont de Nemours as C.P. Grade "Freon-11" was used in experiments without further purification. The dissolved air was removed by two cycles of freezing, pumping, and melting. Liquid Freon-11 was first frozen using liquid nitrogen. Then, the air in the top part of the container was pumped out. After this, the frozen CCl_3F was melted at room temperature. This process was repeated three times. After removing the air and after the CCl_3F sample returned to room temperature, the sample could be evaporated either directly into the pre-evacuated test section for shock wave experiments or into a pre-evacuated steel mixing tank for mixture preparation.

Steel storage tanks of 180 L capacity were used to prepare the mixture of CCl_3F with argon or the mixture of SF_6 with CCl_3F . The leak rate in the tank was less than 10^{-3} mm Hg per minute. The amount of CCl_3F in the mixture was determined by the partial pressure. First, the degassed CCl_3F was evaporated into a tank. After reaching the desired pressure as measured by a mercury manometer ultrahigh purity Argon (>99.99% purity from Matheson) was introduced into the tank directly from the cylinder without any further purification until a pre-determined total pressure was reached. After this step the mixture was allowed to stand in the tank for at least 24 hours before use. The mixture could be directly introduced into the test section of the shock tube. The pressure of the gas in the test section was measured using a mercury manometer.

2.1.3 Detection System

2.1.3.1 Laser Schlieren System

Even though the laser schlieren technique is a simple method, it is capable of detecting fast changes in gas density, [dρ/dy], that result from endothermic and exothermic reactions. In the experiments we expect the following heat exchange process to take place. CCl_3F vapour at or close to the vapour pressure is shock compressed. The translational temperature and pressure increase instantly. Rotational and vibrational relaxation, which are endothermic processes, take place. Consequently, the translational temperature drops somewhat, but after the initial temperature jump and pressure-jump. The cluster distribution is perturbed, and approaches a new equilibrium distribution. Condensation releases heat and generates another rotational and vibrational relaxation. All of these heat exchange processes can be measured directly by the laser-schlieren technique which is highly sensitive to rapid density changes and has excellent temporal resolution. Since a detailed and thorough discussion of this technique has been given by Teitelbaum[103] and by Kiefer[104,105], here we only give a brief outline.

The laser-schlieren technique is based on geometric optics. Because of the dependence of the speed of light on the refractive index, n, if a ray of light traverses a medium having a refractive index gradient (schlieren), ∇n, normal to the propagation direction, it will be deflected in the direction of increasing refractive index. In shock tube experiments the ray is replaced by a narrow laser beam. The refractive index gradient is caused by the density gradient. Therefore, the recorded deflection of light determines the density gradient

established in the post-shock gas. The density gradient can be related to the rate of reaction in the post-shock flow[105] .

Under conditions where (a) the refractive index n≈1, (b) deflections are small and (c) the laser beam is initially perpendicular to the axial flow, the deflection of the laser beam by a refractive index gradient, dn/dy, is given by

$$\theta = W\frac{dn}{dy} \tag{2.1.3}$$

in which W is the internal width of the test section of the shock tube and y is the coordinate of the laser beam corresponding to the axis of the shock tube, (see fig 2.1.6). The index of refraction is related to density, ρ, by the Gladstone-Dale law[106]

$$n = 1 + \kappa\rho \tag{2.1.4}$$

where κ is called the specific refractivity or Gladstone-Dale constant. For CCl_3F monomer its value[107] is 0.229 $cm^3\ g^{-1}$.Then the angular deflection of a ray will be

$$\theta = \kappa W\frac{d\rho}{dy} \tag{2.1.5}$$

Condition (a) is satisfied well for gases: κρ is negligible compared to 1. The second condition (b) is also satisfied under our experimental conditions. Condition (c) is easily satisfied and checked routinely in our experiments (see section 2.2).

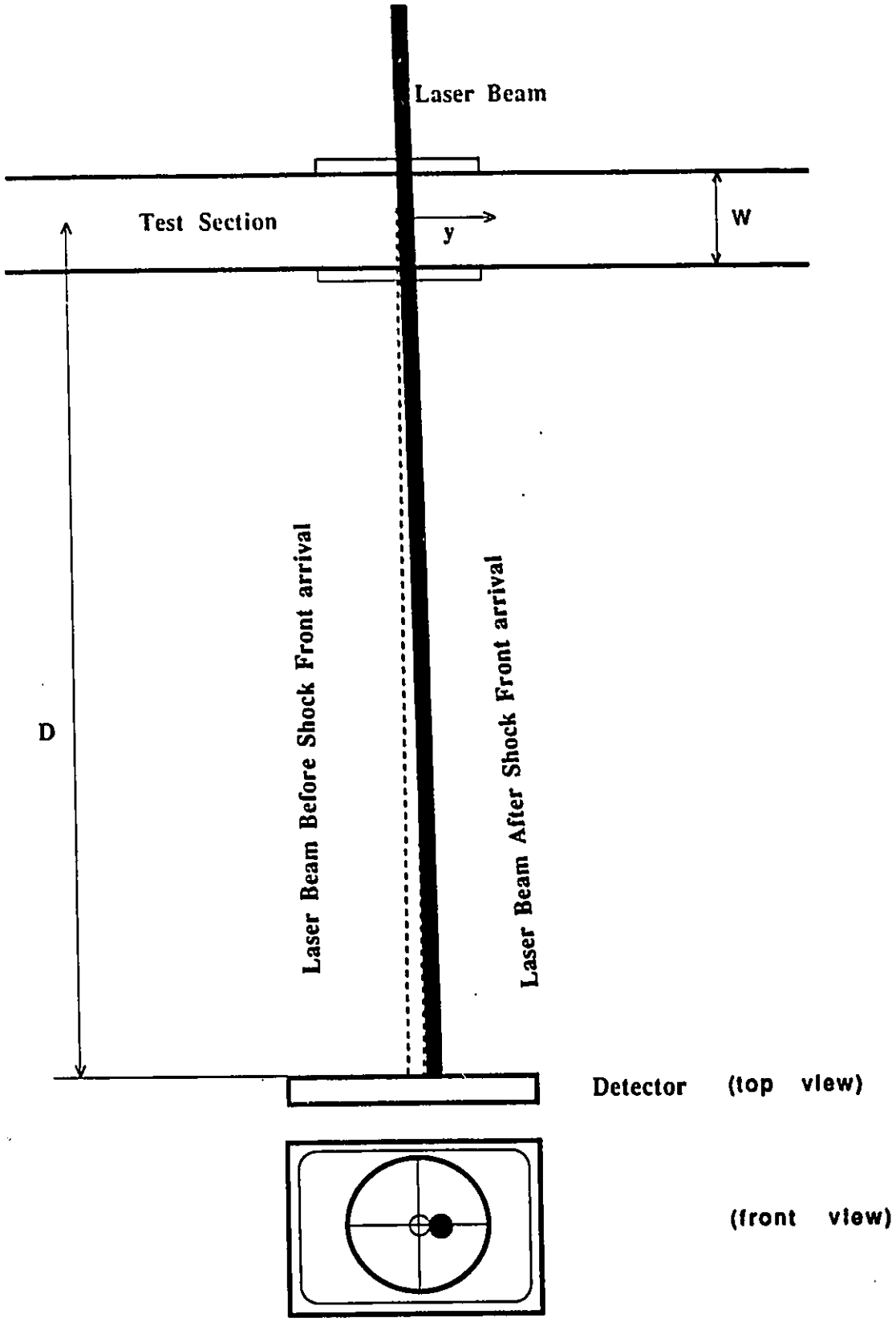

Fig. 2.1.6 Generation of schlieren signals

A small angular deflection, θ, can nevertheless cause a big lateral displacement of the laser beam on the surface of a photodiode detector. The displacement, Δ, is given by

$$\Delta = D\theta = D\kappa W \frac{d\rho}{dy} \tag{2.1.6}$$

where D is the distance between the centre of the shock tube and the detector surface. For the old tube D = 293 cm, and for the new tube, 271 cm.

When the test sample is a mixture of several gases the specific refractivity, κ, of the sample can be calculated from the following weighted average

$$\kappa = \frac{\sum_i \kappa_i X_i M_i}{\sum_i X_i M_i} \tag{2.1.7}$$

where X_i is the mole fraction of component i, κ_i is its specific refractivity and M_i is its molar weight.

The laser schlieren system used in our experiments is shown in fig. 2.1.7. It consists of a laser, a photodiode detector and a digital waveform recorder. A low noise Spectra Physics Model 120 He-Ne laser (at 632.8 nm) supplies a TEMϕ beam of 8 mW total power. The beam diameter is 0.81 mm (distance between e^{-2} points) and its divergence is 1.0 mrad. The laser beam passes through the shock tube perpendicular to its axis and then hits the photodiode detector. Before the experiment the beam is centred on the diode

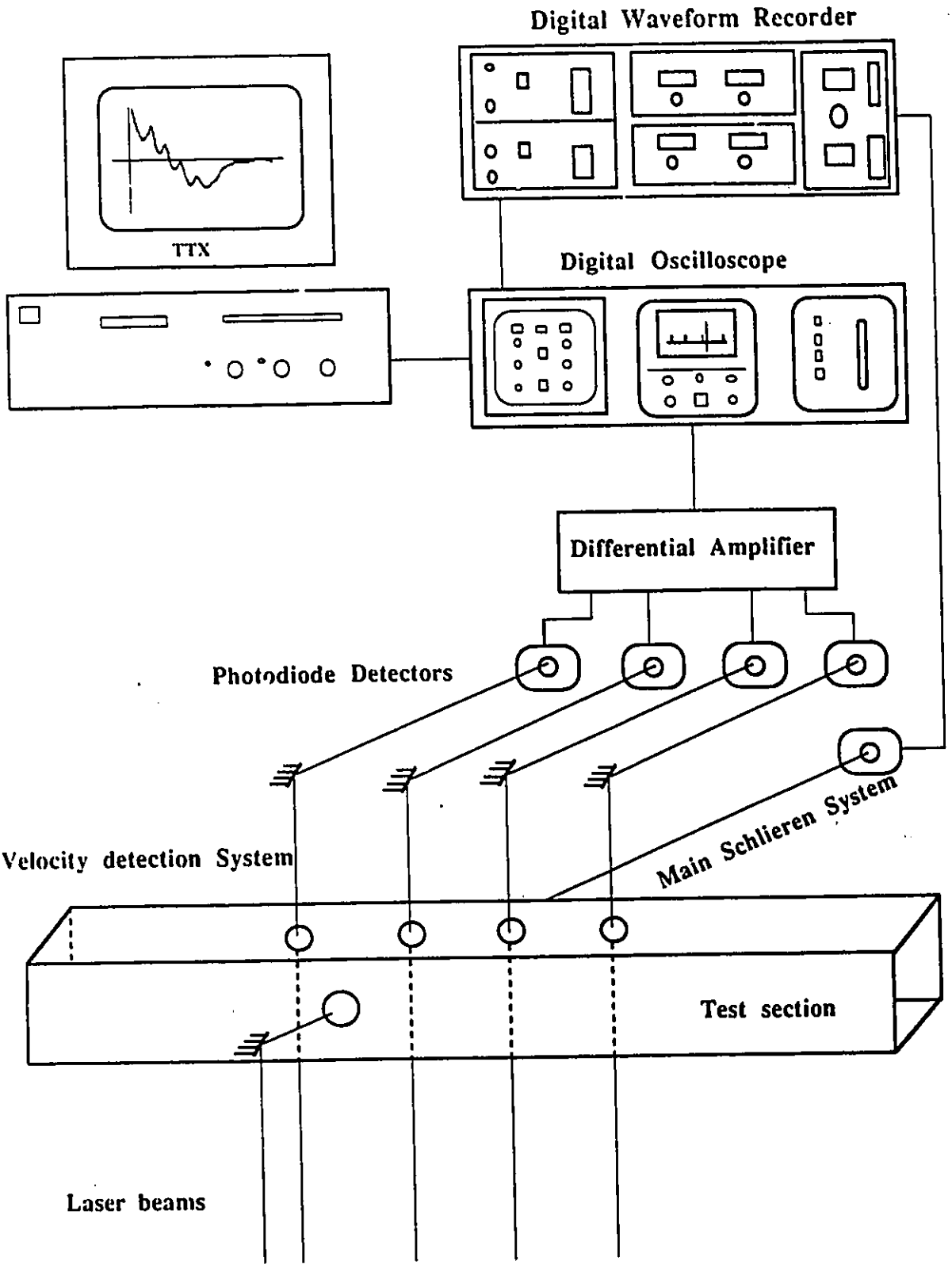

Fig. 2.1.7 The detection system

(see fig 2.1.6). The output of the diode is null. When the shock wave reaches the window the laser beam experiences a density change caused by the chemical reaction (in our experiment caused by vibrational relaxation and the formation, stabilization and dissociation of clusters). The gradient of the index of refraction caused by the density change deflects the laser beam through a small angle. The detector then generates a voltage signal which is differentially amplified, recorded by the digital waveform analyzer, and later analyzed with a computer.

The detailed description of photodiode detector including the electronic circuit can be found in reference 103. It was constructed in this laboratory. It is a quadrant-connected photodiode (United Detector Technology PIN-Spot/9). The main characteristics of the photodiode are : 1 cm^2 active area, 0.5 mA/mV sensitivity with linearity better than 1%, 0.25μA dark current, 25 pf capacitance and a noise-equivalent power of 2×10^{-8} watts. A 0.01 μs high efficiency response to visible light can be obtained with a signal-to-noise ratio better than 20,000 to 1[103]. The voltage generated from each quadrant, v_i, which is proportional to the light power that falls on it, can be measured with an oscilloscope. This measurement is done routinely to check if each quadrant generates the same voltage. With this detector three kinds of signal can be measured. First is the difference between the signals generated by the right half of the detector and the left half of the detector, (v_1-v_2). This signal is produced by deflection of the laser beam in the horizontal direction, and it is the signal we measure in each experiment. The second signal, (v_1-v_3) is produced by the beam deflection in the vertical direction. The third signal is the sum of all voltage

signals generated by the four quadrants. The source of that signal is the bias potential of the photodiode. If the deflection of the laser beam is small, and assuming that the laser beam remains on the active area of the diode during the measurement this output signal should be a constant. If the beam is deflected out of the active area, by eg. the passage of the shock front then the total current generated is a function of time. In order to avoid pick-up or interference from other electronic equipment, the photodiode and the electronic circuit of the amplifiers are placed in a single metal box, which are fixed onto a translation stage mounted on an optical bench. Therefore the box can be moved in both vertical and horizontal directions and can be rotated. Before each experiment the signals are used to confirm that the laser beam is on the centre of the surface of the detector. While simultaneously measuring (v_1-v_2) and (v_1-v_3) on two oscilloscopes (Telequipment Oscilloscope Type D1011) the position of the detector is adjusted until the signals are zero.

The digital waveform recorder is a Gould Biomation model 8100 waveform analyzer. The sampling interval is selectable from 0.01μs to 10 s. The resolution of the digital converter is 8 bits(1 part in 256) at all sampling rates. The memory of the recorder is 8 bits x 2049 words.

The laser, mirrors and photo-detector are mounted on the same large heavy concrete bench. Therefore, the laser source and the detector oscillate in phase if at all and extraneous vibration does not affect the schlieren signal measurement, since the shock

tube is not in physical contact with the optical system.

2.1.3.2 Measurement of Shock Velocity

The shock wave velocity is the most important parameter measured in the experiments, because the physical properties of the shock wave are calculated from it. The shock velocity is determined by measuring the time that is taken by the shock wave to move from one observation window to another, separated by a precisely known distance. The arrival of the shock front at each window is detected by the schlieren optical method. A laser beam from a He-Ne laser (632.8 nm) (Uniphase Model 1105P) passes through each window. Since there is a very abrupt change in density from unshocked gas to shocked gas, the laser beam is deflected when the shock front arrives at the window. The deflection of the laser beam is detected by a quadrant-connected photodiode. Four velocity measuring stations were used in each shock tube. Three of them are upstream of the main window and one downstream of the main window in the new tube. In the old tube two velocity measuring stations were located before the main window, and the two behind it. The signals generated by the four photodiodes were amplified and summed in a unit constructed by the electronics shop at the Department of Electrical Engineering at the University of Ottawa. Finally the signal is displayed and stored on a digital oscilloscope (NICOLET 290-111). The four peaks on the oscilloscope correspond to the arrival of the shock front at the four velocity measuring stations. The time of arrival is read directly from the oscilloscope. The shock velocities between stations are calculated by dividing

the known distances by the measured time intervals. These velocities could be determined in this way. Generally, it was found that the shock speed was constant with a slight deceleration of 1.1% per meter.

2.1.4 The Properties of CCl_3F Vapour.

In this section we shall discuss the deviation of CCl_3F vapour from an ideal gas. Since the pressure of CCl_3F vapour is close to its vapour pressure in our experiments the vapour of CCl_3F should be treated as a real gas. Its enthalpy is a function of both temperature and volume. The ideal gas law is not valid for CCl_3F vapour under our experimental conditions. Since the shock parameters, T_2 and P_2, are quite sensitive to the enthalpy change the most accurate enthalpy functions are required. The thermodynamic data for CCl_3F used in the shock parameter calculation and computer simulations are from "Tables on the Thermophysical Properties of Liquids and Gases"[108]. In that book, the volume per kg (vapour and liquid), enthalpy and entropy of liquid and vapour, vaporization enthalpy and vapour pressure of CCl_3F are tabulated for temperatures between -60° and 140 °C and for selected pressures (see Appendix 2.1.6). In fig. 2.1.8 the vaporization enthalpy is shown as a function of temperature. The vaporization entropy as a function of temperature is given in fig. 2.1.9.

The P-V-T data for CCl_3F at low pressures agrees with the ideal gas law, but as the pressure of the vapour approaches its equilibrium vapour pressure the disagreement

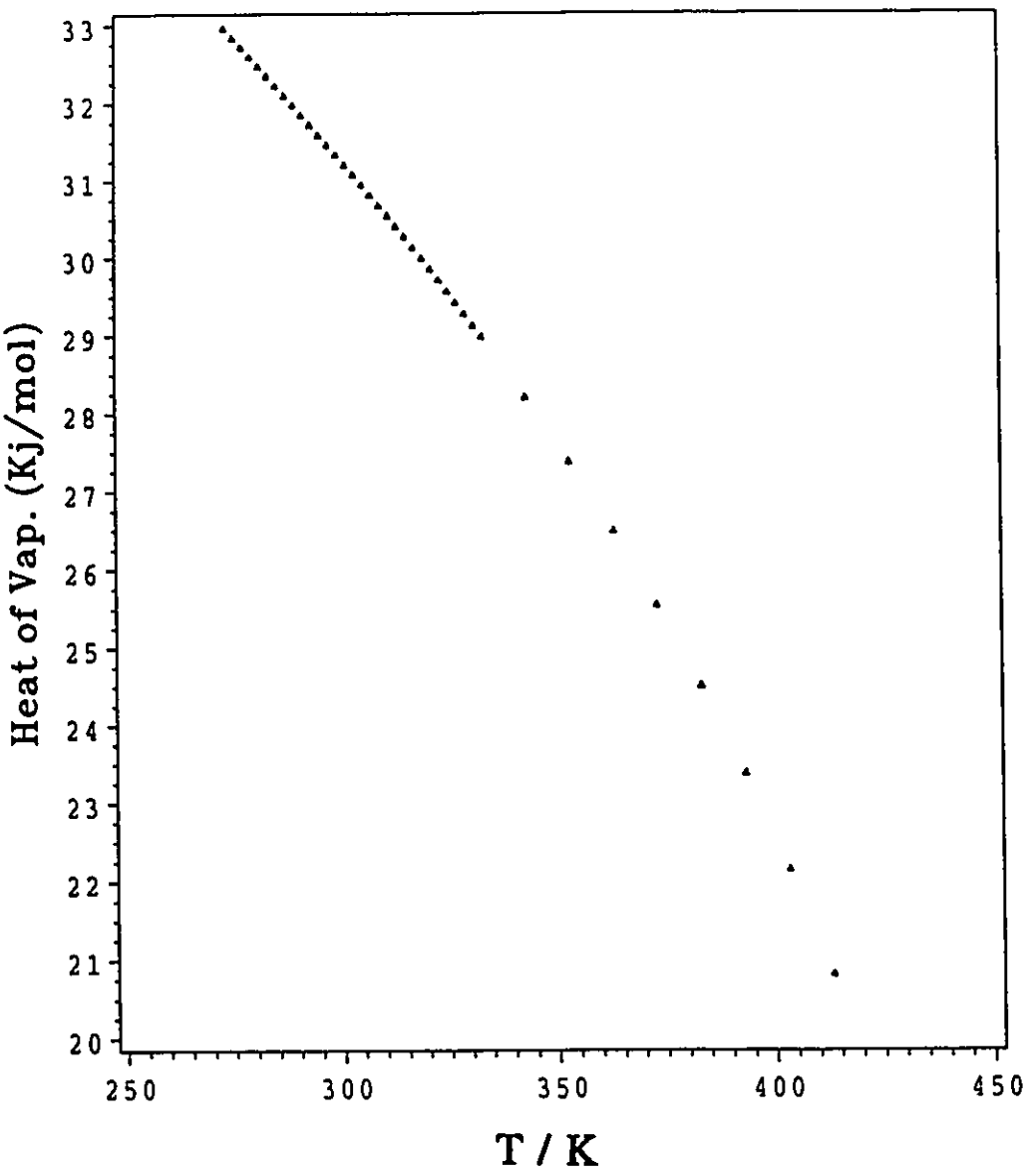

Fig. 2.1.8 Heat of vaporization vs temperature for CCl_3F from reference 108.

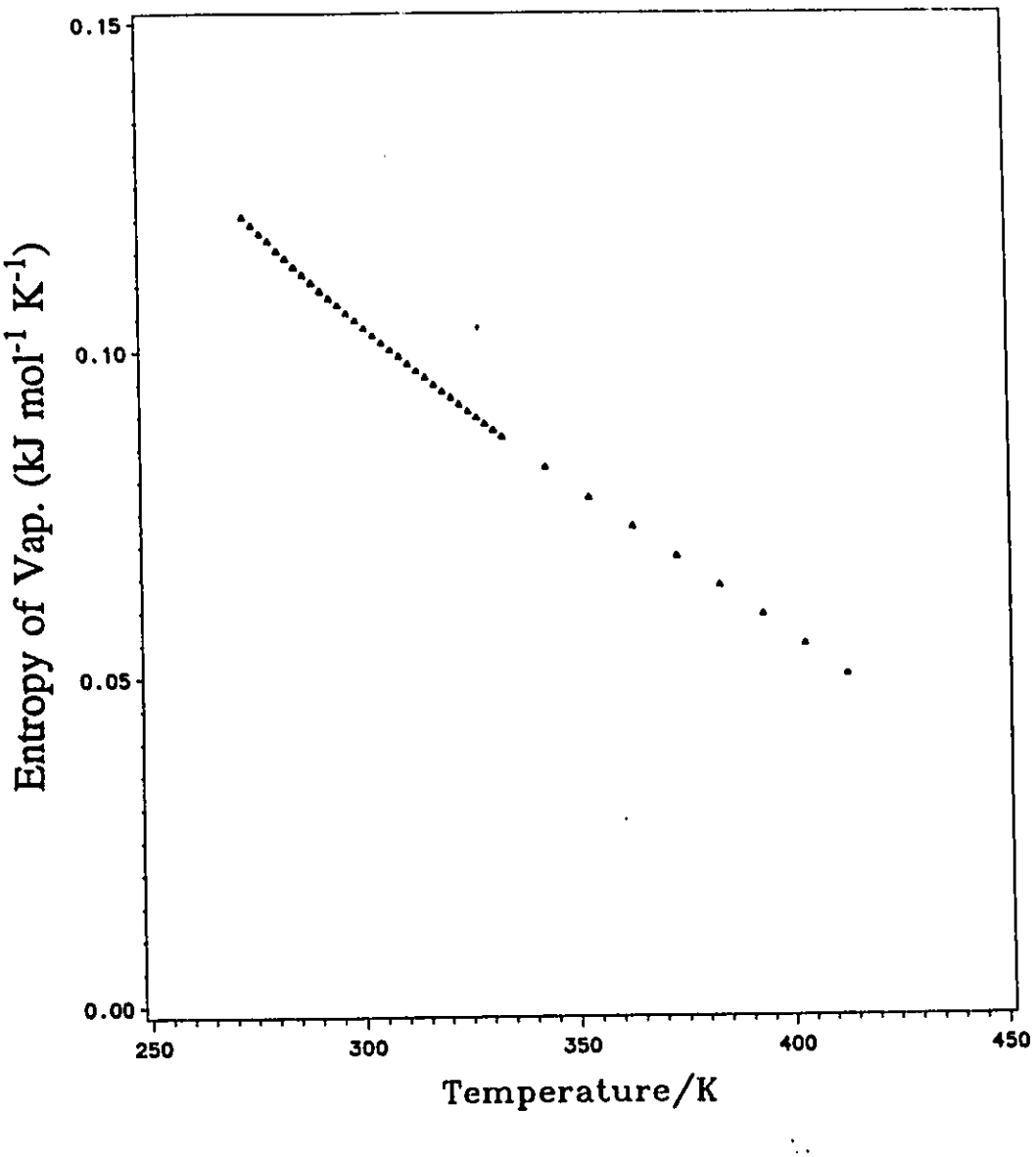

Fig. 2.1.9 Entropy of vaporization vs temperature for CCl_3F from reference 108.

increases. The percentage error is as big as 10% at 343 K and 3000 mm Hg. This is shown in fig. 2.1.10, in which the broken line is calculated from the ideal gas law and the solid line from the published data. In order to condense the information the P-V data at a given temperature (from T= 273 K to 520 K) was fit, in the present study, to the equation P = RT/(V+b). The parameter b which best fits the data is a function of temperature and is shown in Table 2.1.1. P could then be evaluated from the equation P=RT/(V+b) for a given volume and temperature if b is known at that temperature. Similarly, V could be found with known P, T and b. Good agreement between the fitted data and the reference data was obtained with the error less than 3%.

The table of values for b and the corresponding temperatures were used as input data for the computer program used to calculate the shock wave parameters. In the present calculation at any temperature between 273 and 520 K, b(T) was obtained using a cubic spline interpolation method[109]. The interpolation was used in the shock parameter calculation and the computer simulation. It is a piece-wise polynomial approximation achieved by fitting a cubic polynomial between each successive pair of data. This is done by constructing a cubic function on $[x_0, x_1]$ agreeing with the function at x_0 and x_1, another cubic on$[x_1, x_2]$ agreeing with the function at x_1 and x_2 and so on. Since a general cubic polynomial involves four constants ($f = a_0 + a_1x + a_2x^2 + a_3x^3$), there is sufficient flexibility in the cubic spline procedure to ensure not only that the interpolation is continuously differentiable on the interval but also that it has a continuous second derivative on the interval. The data interpolated with this method agrees with the reference data within 0.2%.

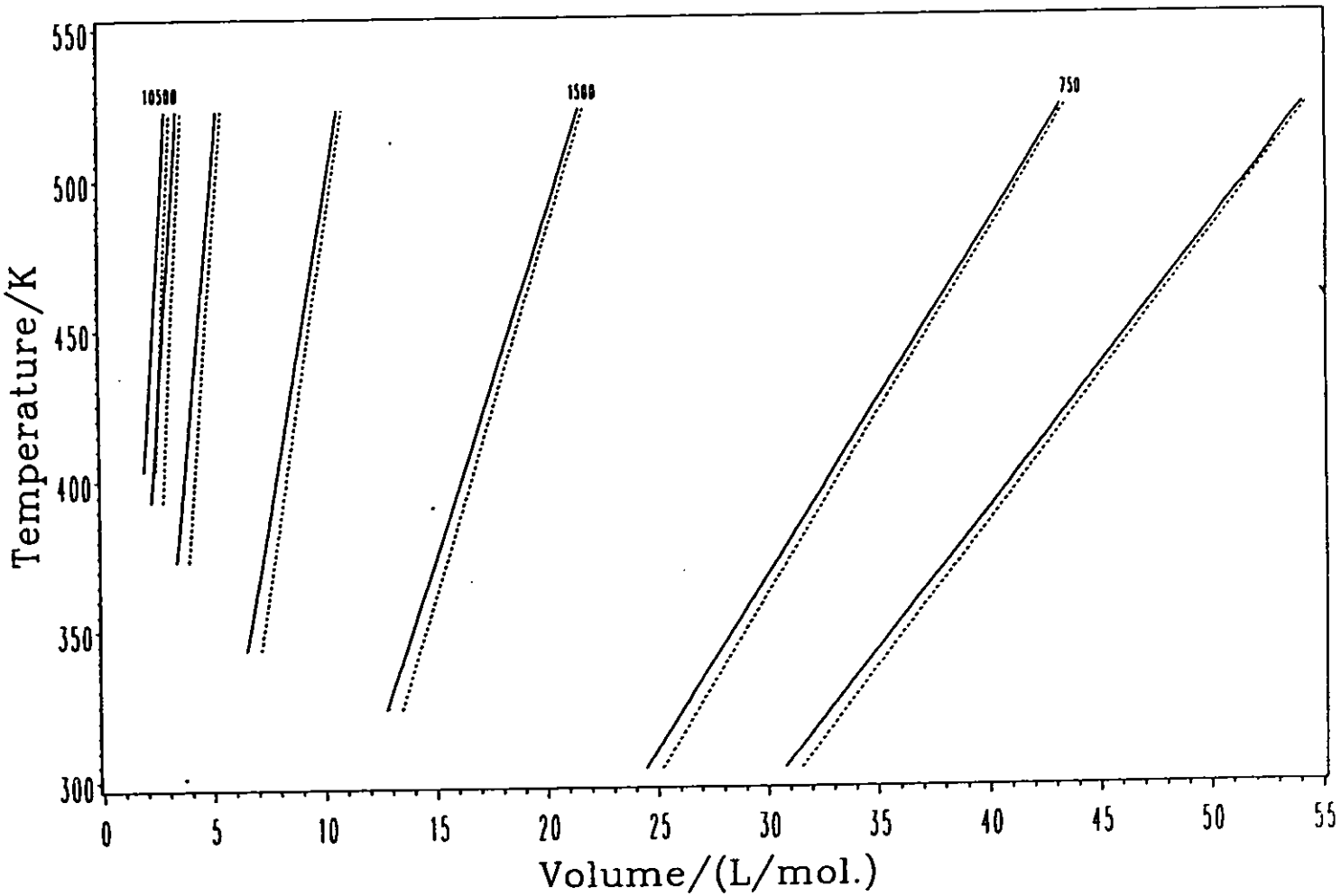

Fig. 2.1.10 Temperature vs the molar volume of Freon-11 vapour at P=600, 750, 1500, 3000, 6000, 9000, and 10500 mm Hg. Data from reference 108. Broken lines are for ideal gas.

Table 2.1.1 The fitted parameter (b) of the P-V-T equation of state for CCl_3F.

T (K)	b (dm^3/mol)
273.15	0.9000243770
283.15	0.8505771536
293.15	0.8087479663
303.15	0.7638705989
313.15	0.7358700700
323.15	0.6988121712
333.15	0.6695868990
343.15	0.6421926883
353.15	0.6019880373
363.15	0.5867150207
373.15	0.5678202321
383.15	0.5485156511
393.15	0.5284387617
403.15	0.5064686259
413.15	0.4697285245
423.15	0.4368257251
433.15	0.4099875814
443.15	0.3781677787
453.15	0.352211574
463.15	0.3265756462
473.15	0.3063187738
483.15	0.2854921011
493.15	0.2654888679
503.15	0.2469125506
513.15	0.2294547639
523.15	0.2129328637

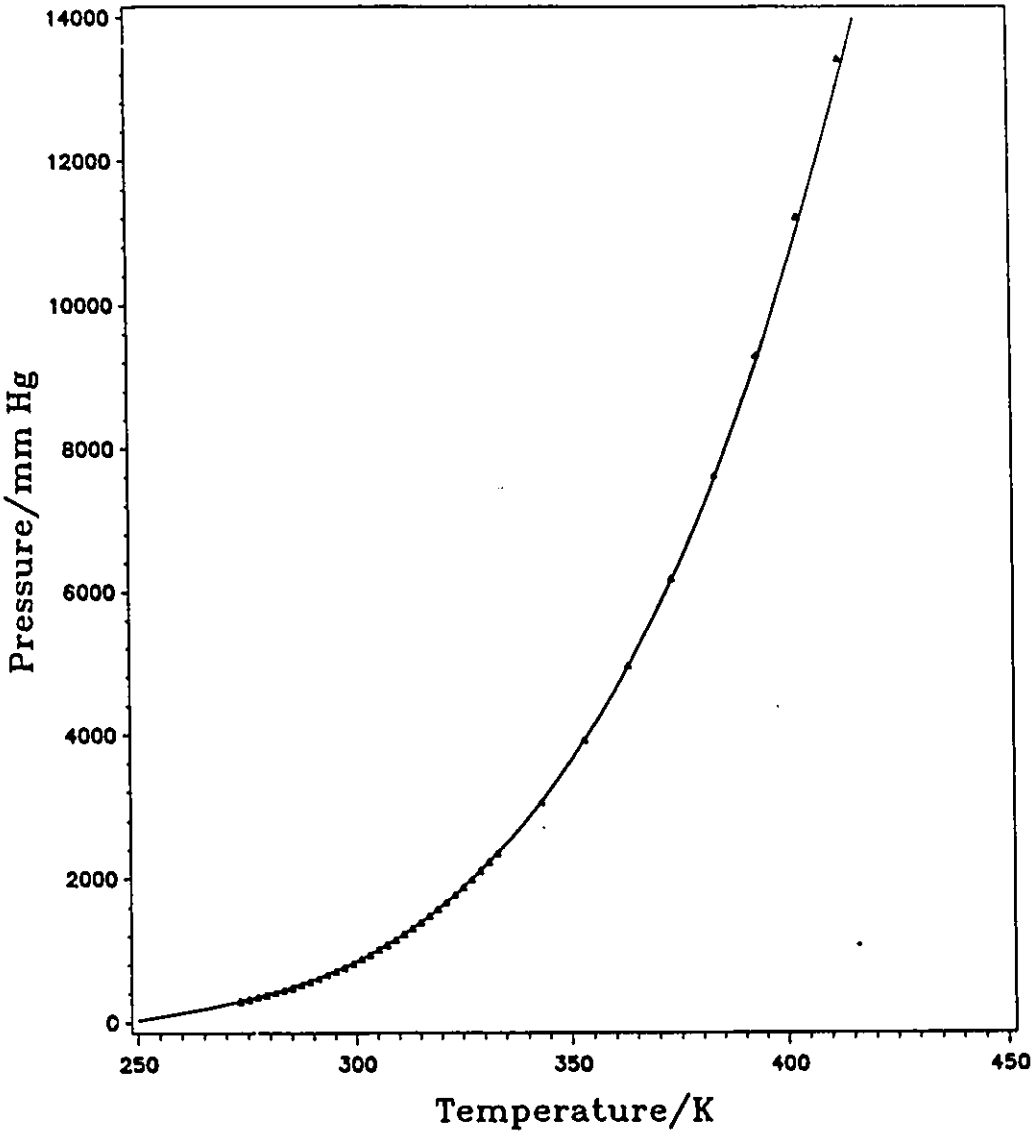

Fig. 2.1.11 Vapour pressure vs temperature for CCl_3F. Line is calculated from formula given in reference 110. Δs are data from reference 108.

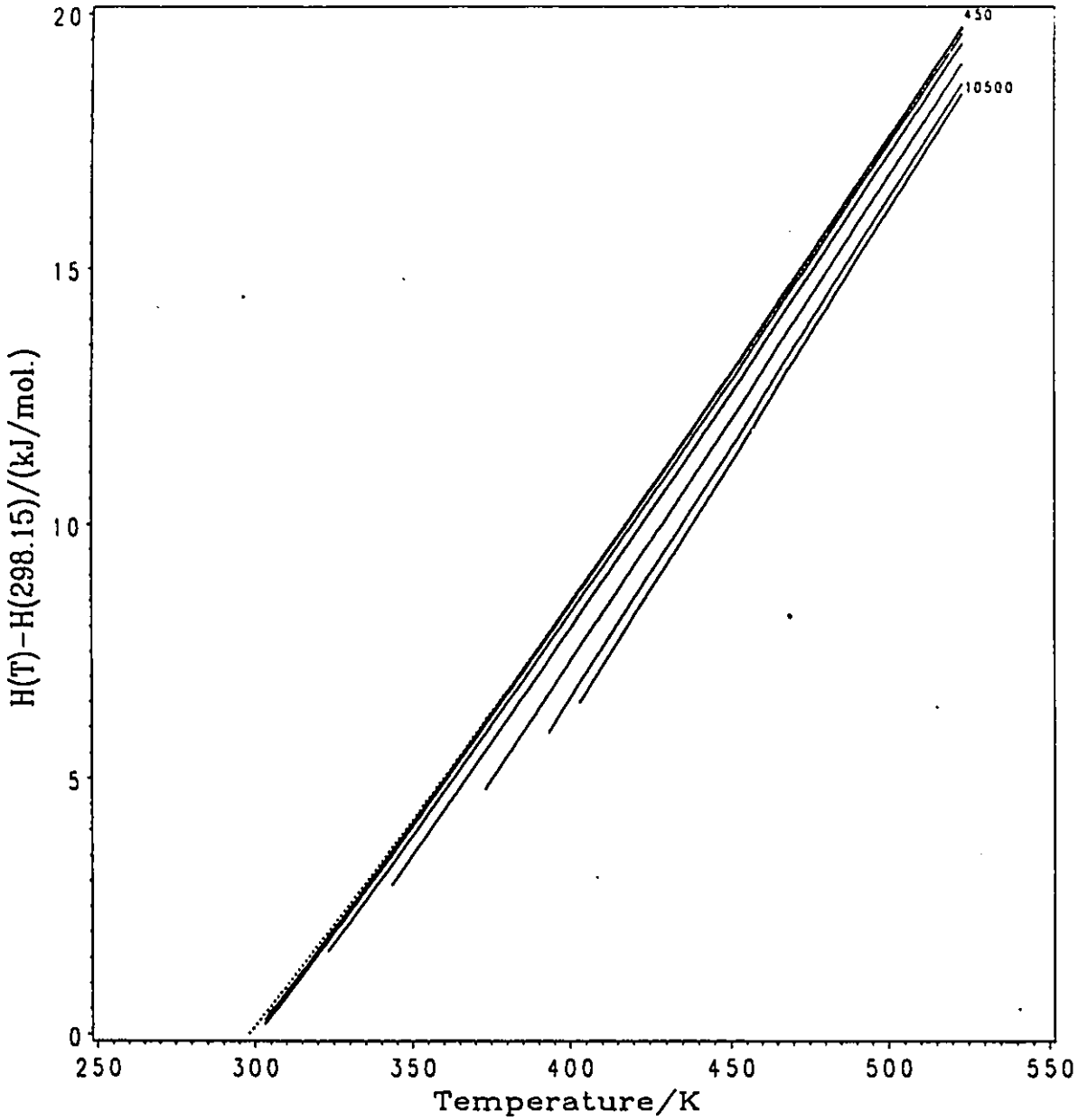

Fig. 2.1.12 The enthalpy of Freon-11 vapour vs temperature for P=400, 750, 1500, 3000, 6000, 9000, and 10500 mm Hg. Data are from reference 108. Broken lines is for ideal gas from JANAF.

The equilibrium vapour pressure was calculated using the formula given by T. Boublik et. al[110]. The results were checked with the data from reference 108. Good agreement was obtained between the calculated value and reference data. In fig. 2.1.11 the line shows the calculated vapour pressure of CCl_3F as a function of temperature, while the points show the data from reference 108.

The enthalpy-temperature data is given at the pressures 22.5, 37.5 75, 150, 300, 450, 600, 750, 125, 1500, 2500, 3000, and 4500 mm Hg in reference 82. Some of these data are plotted in fig. 2.1.12, in which it is clear that the enthalpy of CCl_3F vapour is a function of both temperature and pressure. The enthalpy and temperature data from reference 108 was fitted to the equation $H = a_0 + a_1T^{\alpha}$ at each given pressure. First a value of α was guessed and then substituted into the equation. Then, a least squares method was used to find the values of a_0 and a_1. Then, the value of α was changed (either increased or decreased), to find new values of a_0 and a_1. After comparing the difference between the calculated values with different α and reference values, we could zero in on the value of α, by iteration. Since the enthalpy of a real gas is a function of pressure, the parameters a_0, a_1 and α also vary with pressure, as shown in Table 2.1.2. The values of a_0, a_1 and α at any intermediate pressure were calculated by cubic spline interpolation between the entries in Table 2.1.2. The comparison of the fitted values with the reference data show a percentage error of less than 2% .

Table 2.1.2 Parameters for fitted enthalpy of CCl_3F vs pressure.

P (mm Hg)	a_0 (kJ/mol)	a_1 (kJ/mol K)	α
22.5	584.3214800	0.0386221	1.412400
37.5	584.1109242	0.0390109	1.410900
75	583.9658229	0.0390555	1.410800
150	575.8664086	0.0633401	1.337100
300	574.9772786	0.0647575	1.334000
450	573.7518356	0,0670800	1.329000
600	571.7684459	0.0719276	1.318900
750	570.1260789	0.0758353	1.311300
1125	567.2664054	0.0818157	1.300600
1500	564.0077966	0.0895526	1.287800
2250	558.6028258	0.1017952	1.2699500
3000	551.3389198	0.1231841	1.2430500
4500	541.8687340	0.1461620	1.2200500
6000	521.5522235	0.2391646	1.1510000
7500	501.7091485	0.3592392	1.0948800
9000	482.6744033	0.5006909	1.0499000
10500	459.2415242	0.7370550	0.9976502

2.2 Experimental Procedure

2.2.1 Experimental Methods

Accurate alignment of the beam normal to the shock tube axis is important for good spatial resolution. In order to get reliable signals the following calibration and alignment of the schlieren optical system was performed before each experiment.

The beam was aligned normal to the shock tube windows by superimposing reflections from the observation window with the incident laser beam at a distance of several meters. In the same way, the laser beam exiting the shock tube could be made normal to the surface of the detector in the horizontal plane. However, the laser beam was slightly misaligned in the vertical plane to avoid that reflected radiation from the surface of the detector reentered the laser source.

Before each experiment, the unamplified signal from each quadrant was checked using a Telequipment Oscilloscope (Type D1011). This was done by measuring the voltage generated by each quadrant when the laser beam fell onto that quadrant. It was found that the difference of these four signals was less than 0.1%.

One of the most important checks was to make sure that the gains of the two differential amplifiers were identical. This was adjusted when constructed, but it was checked

regularly. The gain, G, was measured by comparing the amplified and unamplified signals generated from each quadrant of the photodiode.

Before every experiment the laser beam was centred on the photodiode very precisely by measuring the two differential signals originating from the quadrants (a,b,c). V_{a-c} and V_{a-b} were measured simultaneously, and the position of the detector, sitting on a y-z translation stage, was adjusted until the outputs of the two differential signals on the oscilloscope were each zero.

Both the test and driver sections of the shock tube were was evacuated to less 10^{-3} mbar (checked with a vacuum meter Edwards Vacustat) using a rotary pump (Edwards High Vacuum Model EDM12). The vapour of the degassed CCl_3F was evaporated into the test section directly from the storage vessel. After the test section was filled, about 10 minutes were spent waiting for the vapour to reach room temperature. During this time the laser beams for both the schlieren system and the velocity measurement system were aligned and centred on the detectors. The Biomation waveform recorder and the Nicolet digital oscilloscope were reset. The initial temperature of the gas was taken to be the temperature of the shock tube as read from a thermometer that was attached to the tube. It was measured before firing the shock as was the initial pressure of the gas in the test section (which was read from the mercury manometer). After this step the driver gas, helium, was introduced into the driver section from the end plate driver section, until the pressure of helium was high enough to burst the aluminum diaphragm separating the test

and driver section. The strength of the shock wave was determined by the pressure ratio, P_4/P_1, of the driver and test sections at the moment of bursting. P_4/P_1 is controlled by the thickness of the diaphragm. (After each experiment the mixture of Freon-11 and Helium was pumped though a cold trap. Freon-11 was collected for recycling.

When the shock front crossed the laser beam used for quantitative measurements at the main observation window, the Biomation waveform recorder was triggered by the signal generated by the shock front itself. The signal was recorded in the Biomation's memory, and could be transferred later to the Nicolet digital oscilloscope for display, and stored on a floppy disk, or transferred to computer for further processing. Since both the Biomation unit and the Nicolet unit are equipped with a pre-triggering function, they were able to record the signal before shock arrival thus providing an unequivocal zero base line in the schlieren signal for each experiment.

175 experiments were performed on CCl_3F vapour at different initial pressures, at different shock strengths, and in two shock tubes of different cross-section and length. A wide range of temperatures and pressures could be accessed for pure CCl_3F. It made it possible to study the kinetics of cluster formation under different experimental conditions. Experiments with several other gases including Ar, CCl_4, SF_6 and CH_4 were also performed as controls. This made it possible for a systematic diagnosis of unexpected observations. These included four experiments with CH_4, 4 experiments with mixtures of CCl_3F and Ar, three with mixtures of CCl_3F and SF_6, one with pure SF_6, one with pure

CCl_4, and several with pure Ar and air.

2.2.2 Calculation of Shock Wave Parameters

In principle, all the physical properties behind the incident shock wave can be directly calculated on the basis of the thermodynamic properties of the shocked gas and the measured incident shock wave velocity. If there are no chemical reactions, and no radiation, the Rankine-Hugoniot equations[101] can be used in the calculation. It is convenient to consider the gas motion relative to the shock front. The shock front is considered to be at rest, and the test gas can be thought of as entering the front with a relative speed u_1 and leaving with a relative speed u_2. The mass flow per unit area is the product of the density and the velocity of the flow. Mass conservation require that we have

$$\rho_1 u_1 = \rho_2 u_2 \tag{2.2.1}$$

Momentum conservation requires

$$P_1 + \rho_1 u_1^2 = P_2 + \rho_2 u_2^2 \tag{2.2.2}$$

in which ρu^2 is proportional to the momentum flow, and P is the pressure. Since a shock wave is an adiabatic process the stagnation enthalpy per unit mass, $h_t = h + u^2/2$, is

conserved[101]. Then

$$h_1 + \frac{u_1^2}{2} = h_2 + \frac{u_2^2}{2} \qquad (2.2.3)$$

In these equations the subscript 1 denotes the initial state of the test gas, i.e. the state before shock arrival, and 2 denotes the properties behind the shock front, after the vapour molecule's vibrational energy has equilibrated. ρ is the density of the vapour in units of kg m^{-3}, h is the enthalpy of the vapour in units of J/kg, and u is the velocity of the shock wave in m/s.

So far, we have three equations with four unknowns, The fourth equation is the P-V-T equation of state. Since in our experiments the gas pressure is close to the vapour pressure of CCl_3F there would be large errors if the ideal gas law were to be used. Therefore, we used the equation which best fit the P-V-T data and which we described above, namely

$$P = \frac{RT\rho}{(M + \rho b)} \qquad (2.2.4)$$

in which b is a function of temperature as shown in the last section and has units of dm^3/mol.

The enthalpy of the vapour was obtained from the fitted equation

$$H=a_0+a_1T^{\alpha} \tag{2.2.5}$$

As we have already pointed out, a_0, a_1 and α are functions of pressure. Their values at any given pressure and temperature can be calculated by employing the cubic spline interpolation method. H is in units of kJ/mol while h is in J/g.

Equations 2.2.1 , 2.2.2, 2.2.3, 2.2.4 and 2.2.5 comprise five equations in the five variables, P, ρ, T, h and u. For CCl_3F we already know H(T,P) as well as the initial conditions (subscript 1). Therefore by solving the above equations the post-shock parameters (subscript 2) can be obtained. This is done as follows.

From Eq. 2.2.1 and 2.2.3 u_1 can be written as a function of h and ρ as

$$u_1=\sqrt{\frac{2(h_2-h_1)}{(1-\rho_1^2/\rho_2^2)}} \tag{2.2.6}$$

From Eq. 2.2.2 and Eq.2.2. 6 P_2 is given as

$$P_2=P_1+\rho_1\frac{2(h_2-h_1)}{1+\rho_1/\rho_2} \tag{2.2.7}$$

Substituting equation 2.2.4 we then obtain

$$\frac{\rho_2 T_2}{M+\rho_2 b_2}=\frac{\rho_1 T_1}{M+\rho_1 b_1}+\rho_1\frac{2(h_2-h_1)}{R(1+\rho_1/\rho_2)} \qquad (2.2.8)$$

Let

$$y=\frac{(h_2-h_1)M}{R} \qquad (2.2.9)$$

and

$$X=\frac{\rho_1}{\rho_2} \qquad (2.2.10)$$

With this a quadratic equation results

$$T_1' X^2+[(1+C_2)T_1'+2y-T_2]X+(T_1'+2y)C_2-T_2=0 \qquad (2.2.11)$$

in which $T_1'=T_1/(1+C_1)$, $C_1=\rho_1 b_1/M$ and $C_2=\rho_1 b_2/M$. C_1 and C_2 are unitless constants. T_1' and y have units of temperature. This equation is the cornerstone of the shock-parameter calculation. Comparing with the equation for an ideal gas shock wave given in reference 111, the difference is that y is a function of both temperature and pressure in our equation. Therefore X depends on both T_2 and P_2. The calculation is more complicated than that for an ideal gas. In the calculation for a given T_2, at first, a trial P_2 is chosen. Then h_2 can be calculated. After X is calculated from eq. 2.2.11, a new

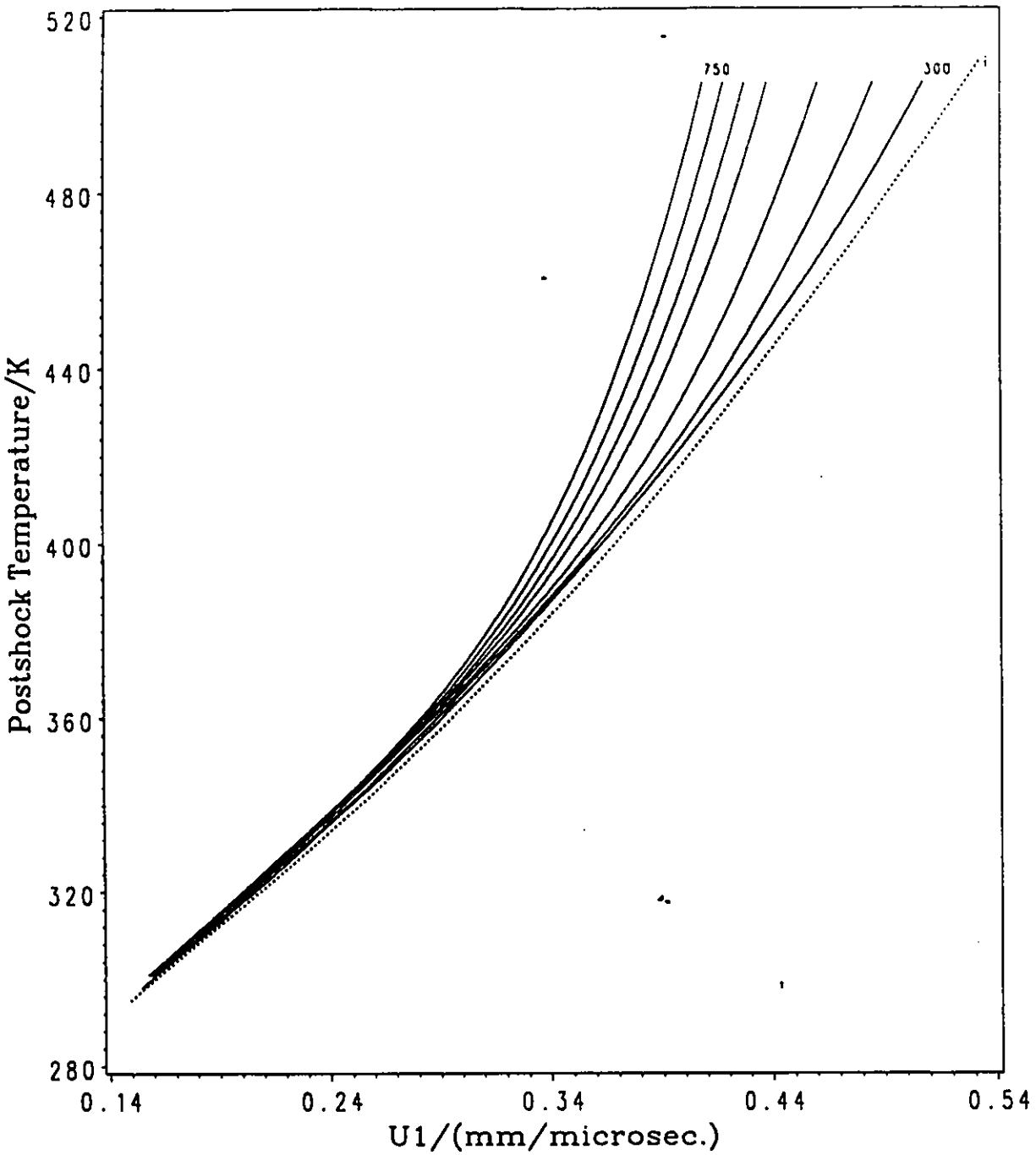

Fig. 2.2.1 Post shock temperature vs shock velocity for initial temperature=291.15 K, and initial pressure = 300, 400, 500, 600, 650, 700, and 750 mm Hg. i (broken line) is for ideal gas at the same initial temperature, but initial pressure=300 mm Hg.

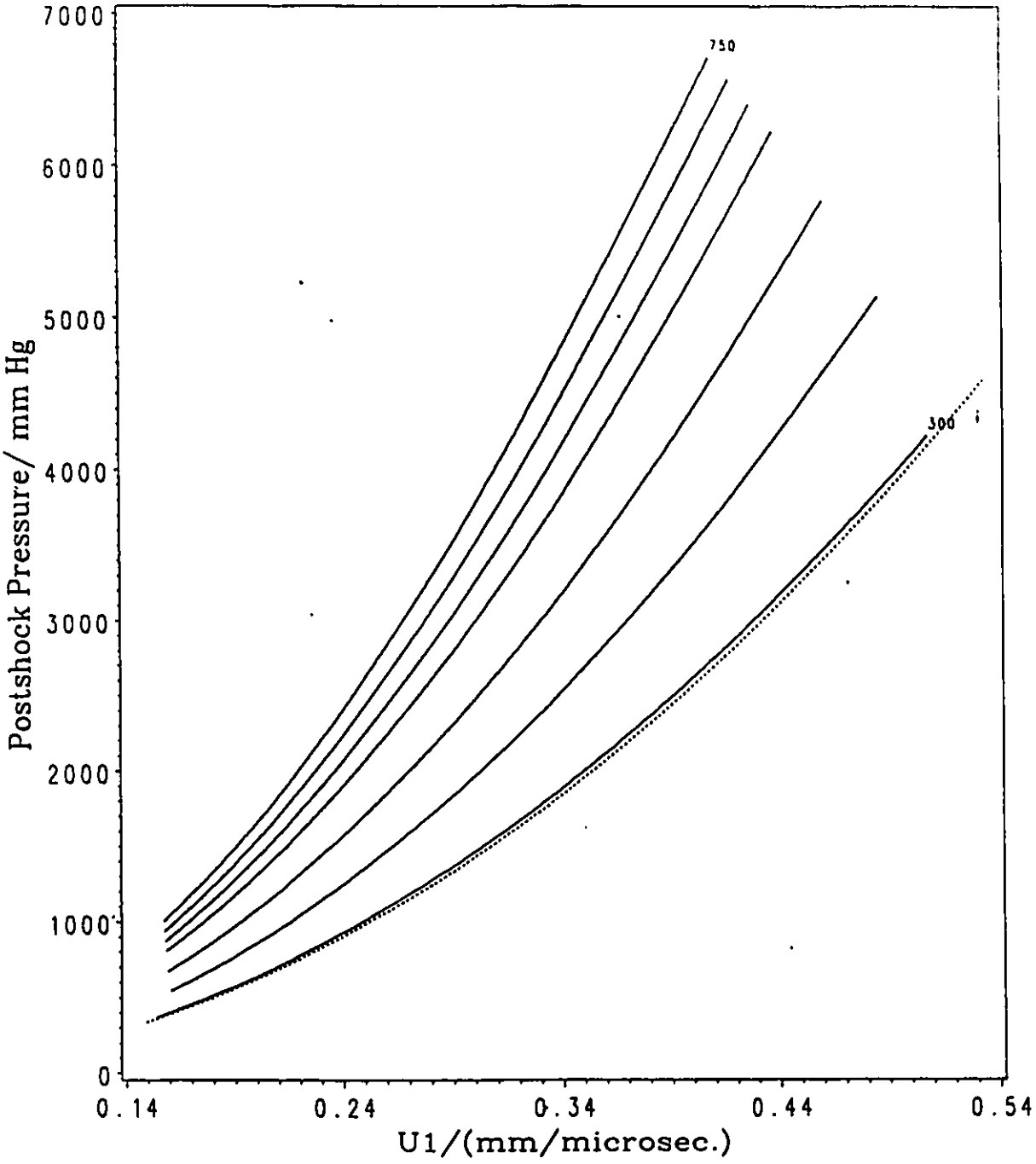

Fig. 2.2.2 Post shock pressure vs shock velocity for initial temperature = 291.15K, and initial pressure = 300, 400, 500, 600, 650, 700, and 750 mm Hg. i (broken line) is for ideal gas at the same initial temperature, but initial pressure=300 mm Hg.

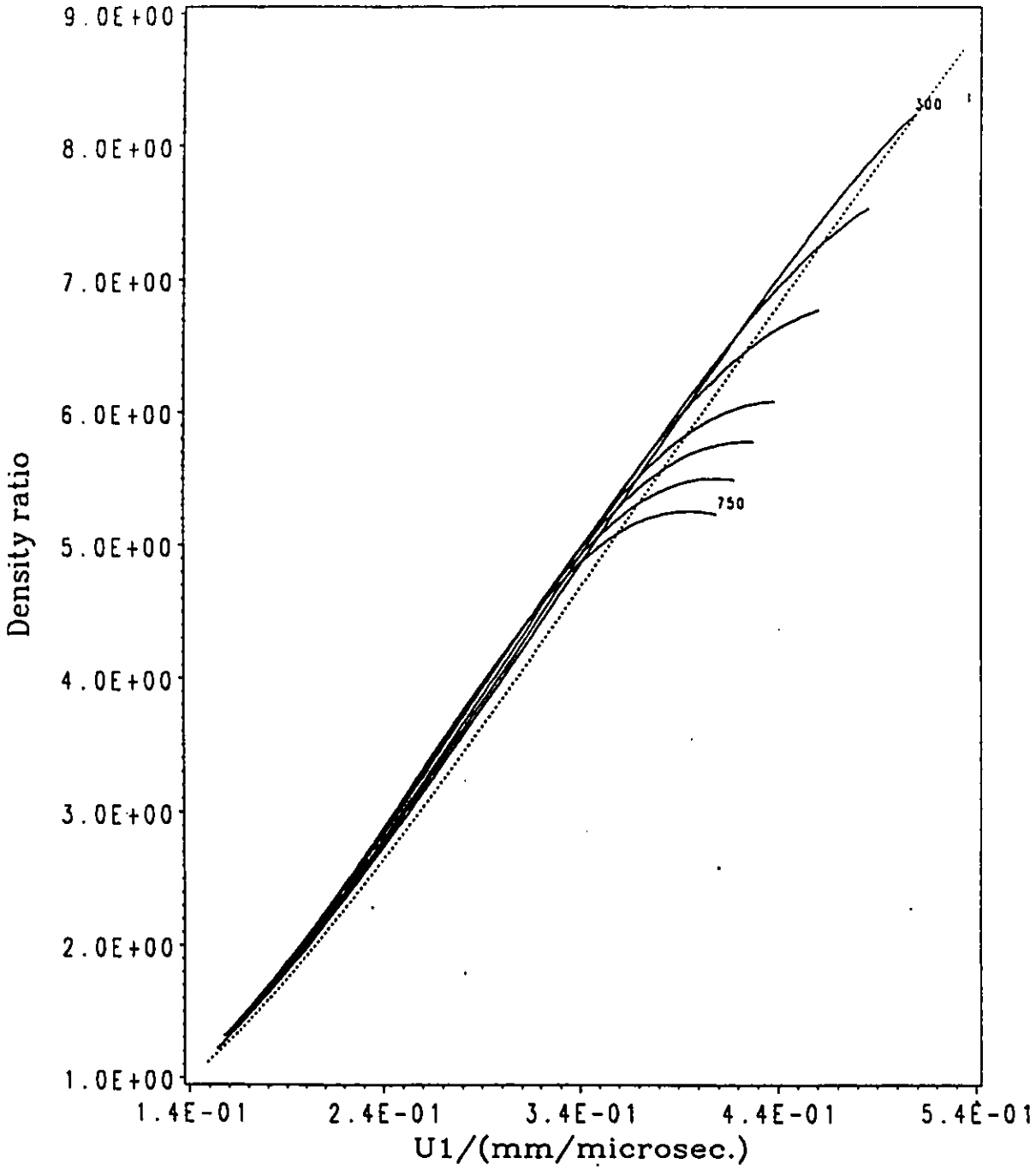

Fig. 2.2.3 The ratio of post-shock density to pre-shock density vs shock velocity for initial temperature=291.15 K, and initial pressure = 300, 400, 500, 600, 650, 700, and 750 mm Hg. i (broken line) is for ideal gas at the same initial temperature, but initial pressure=300 mm Hg.

pressure, P_2' can be calculated from eq. 2.2.7 and compared with the original P_2. P_2' now takes the role of P_2, and the above calculation is repeated until the difference between P_2 and P_2' is less than one part in 10^7. This calculation can be repeated for many choices of T_2 and P_2 spanning a range of experimental interests, from which a calibration graph can be constructed permitting T_2 values to be inferred from given initial P_1, T_1 and shock velocity, u_1. Similarly the corresponding pressure, P_2, and X can be found. ρ_2 can be found easily from equation 2.2.10. Graphs of T_2 as a function of u_1 at the initial temperature of 291 K are shown in Fig. 2.2.1 in which the broken line is for an ideal gas, and the other lines are for the initial pressures of 300, 400, 500, 600, 650, 700 and 750 mm Hg respectively. It can be seen that as the initial pressure increases, the deviation from the ideal gas calculation increases. Fig. 2.2.2 shows how P_2 changes as a function of u_1 for an initial temperature of 291.15 K and initial pressures of 300, 400, 500, 600, 650, 700 and 750 mm Hg. The broken line is for an ideal gas at initial pressure 300 mm Hg. Fig 2.2.3 shows the density ratio, ρ_2/ρ_1, as a function of u_1. As an alternative procedure, we can start from the trial T_2 and P_2 values, and use the experimental values of the initial conditions (P_1, T_1 and ρ_1) and the measured shock velocity u_1. Then we would calculate the shock speed, u_{1c}, compare it to the experimental measured value, u_1, and then change the trial value of T_2 until the difference between u_{1c} and u_1 is small enough. In our calculation the trial values of T_2 and P_2 are the values calculated when treating CCl_3F vapour as an ideal gas. The calculated results for the state immediately after the shock front are listed in Appendix 1. The computer program used to perform the calculation is listed in Appendix 5.

2.3 Experimental Schlieren Signals

Some typical examples of a laser schlieren signal obtained from CCl_3F experiments are shown in figs. 2.3.1 to 2.3.4. These signals, as for all of the other signals, are characterized by large negative and large positive spikes caused by the interaction of the laser beam with the curved shock front[103]. However, this effect dies down within 5 microseconds. Then rotational and vibrational relaxation processes proceed. These endothermic processes cause the temperature to decrease and the density to increase, thus giving a positive signal[103]. Otherwise, if the process is exothermic, such as condensation or clustering, the temperature will increase and the density will decrease. In that case the schlieren signal is negative. There are no bond-breaking reactions since the post-shock temperatures, T_2, for all CCl_3F experiments, are below 450 K. If the initial pressure is far away from the vapour pressure corresponding to the initial temperature, the shock is not too weak, and the signal is similar to the one shown in fig 2.3.1. The positive signal decays very fast to a negative value and stays negative for a short time. No oscillatory signals appear before exothermicity becomes evident. However, if the initial pressure is above a certain value (say 350 mm Hg at a temperature of 291.15 K) or if it is close to the vapour pressure and if the shock is not too strong, (Mach number ~ 1.1 to 1.5) the schlieren signal becomes negative with an oscillatory signal superimposed on it even before exothermicity is evident. This kind of signal is shown in fig. 2.3.2. All of these kinds of signals are quasi-periodic on a short time scale, and irregular on a larger time scale. When the initial pressure is very close to the vapour pressure and the shock is very

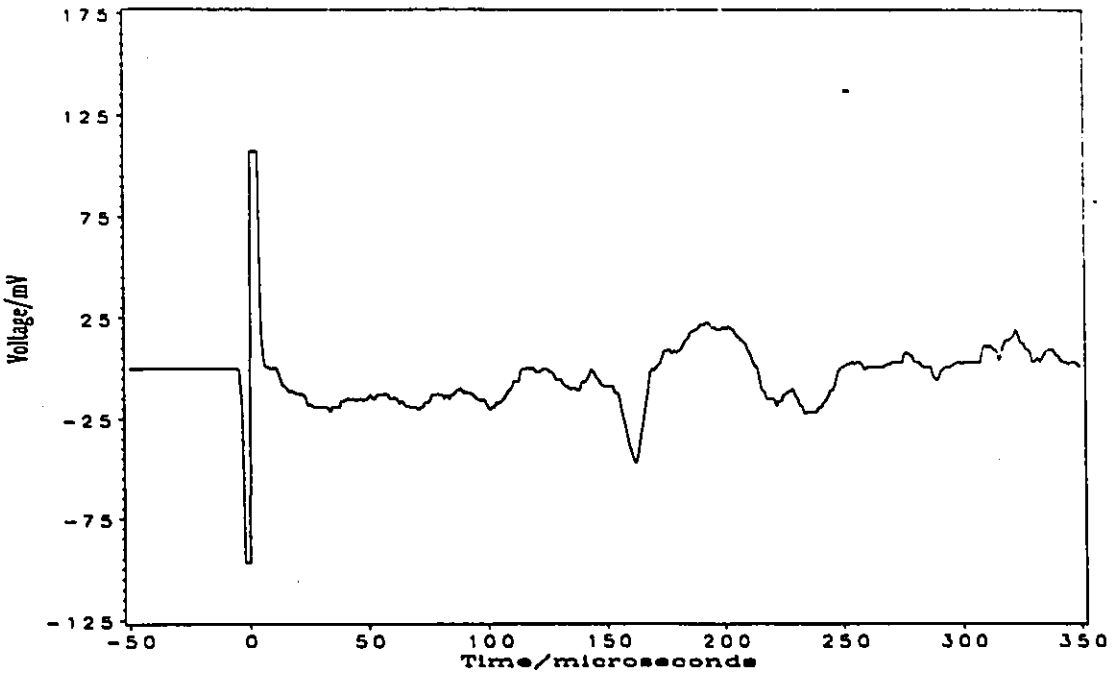

Fig. 2.3.1 Schlieren signal for CCl_2F, Experiment No. 31
T_1=296.2 K, P_1 =30.0 Torr.shock velocity = 243.80 m/s
MACH No. = 1.7224, T_2=339.8 K, P_2 =95.4 Torr.

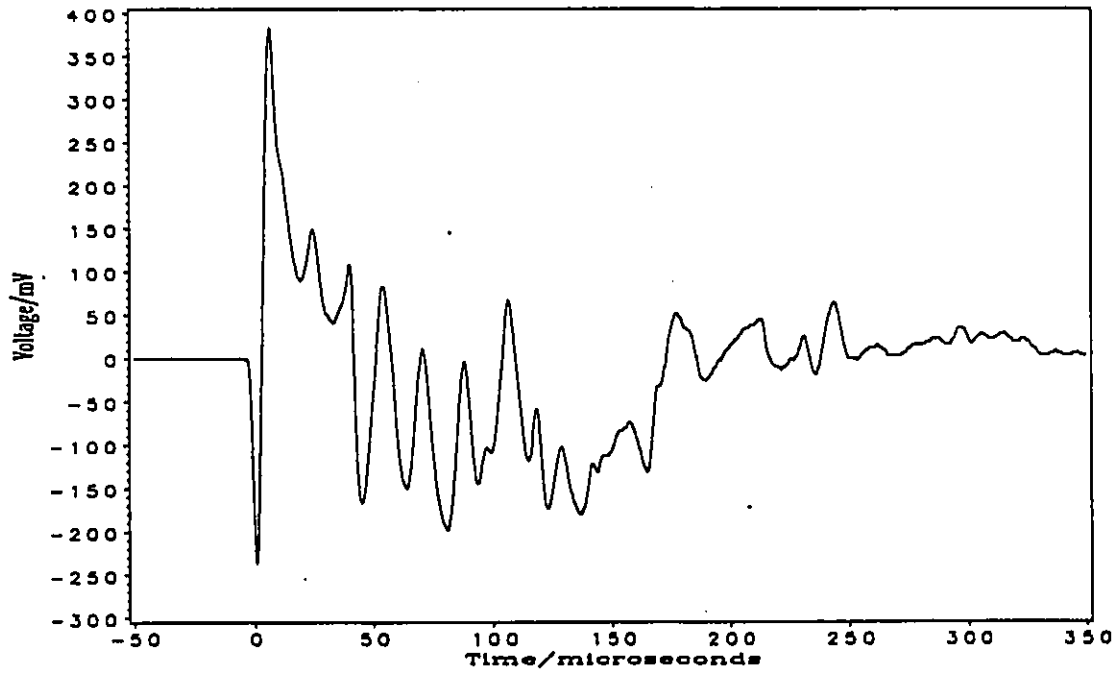

Fig. 2.3.2 Schlieren signal for CCl_2F Experiment No. 122
T_1=294.2 K, P_1 =537.0 Torr, shock velocity = 206.20 m/s,
MACH No. = 1.4533, T_2=324.8 K, P_2 =1229.8 Torr.

weak, oscillatory behaviour disappears leaving only exponential decay as shown in fig. 2.3.3.

A schlieren signal for carbon tetrachloride is shown in fig. 2.3.4. The initial temperature (T_1) is 291.4 K; the initial pressure (P_1) is 85.6 mm Hg; and T_2 is 529 K. It is a quasi-periodic signal superimposed on the exponentially decaying curve. After a short time (about 20 microseconds) the quasi-periodic signal becomes a chaotic signal. At the same time the signal becomes negative overall.

A schlieren signal for methane is shown in fig. 2.3.5. The initial conditions are T_1 = 294.3 K, P_1 = 86.0 mm Hg, T_2 = 350.0 K, and P_2 = 172.4 mm Hg. No oscillations or chaotic signals are observed, but rather a smooth exponentially decaying curve. Another important difference between CCl_3F and CH_4 is that for CH_4 the signal never becomes negative.

Fig. 2.3.6 shows a schlieren signal for sulphur hexafluoride at the initial conditions: T_1 = 293.0 K, P_1 = 361.5 mm Hg, and T_2 = 310 K. There are no oscillations superimposed on an exponentially decaying curve within the first 100 μs. The signal becomes negative within a few microseconds. Only much later do some peaks appear.

A schlieren signal for a mixture of 50% CCl_3F and 50% SF_6 is shown in fig. 2.3.7 at the initial conditions T = 292.0 K and P_1 = 745.3 mm Hg. The signal first becomes negative,

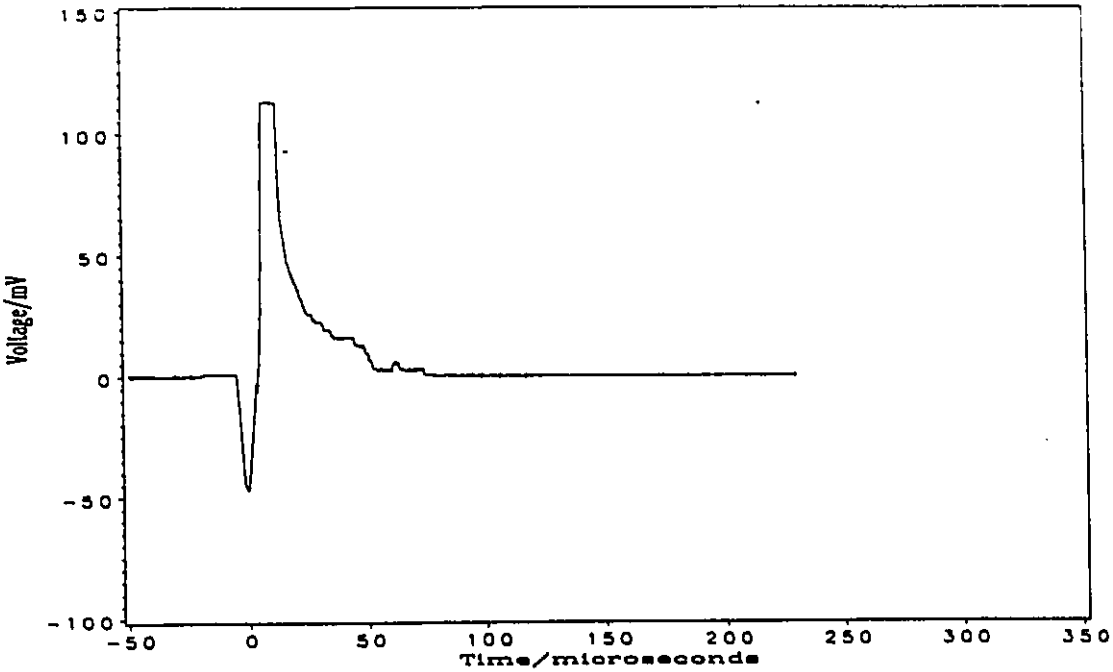

Fig.2.3.3 Schlieren signal for CCl_2F, Experiment No. 157
T_1=294.7 K. P_1 =699.6 Torr.shock velocity = 138.00 m/s
T_s=294.9 K.P_s =702.7 Torr.

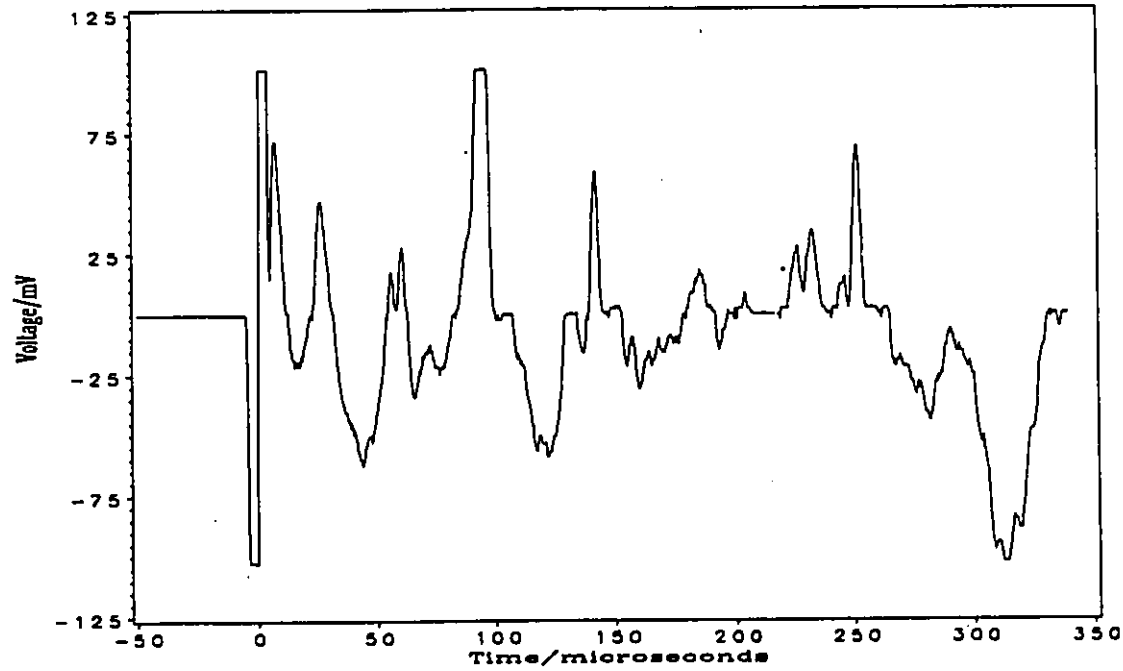

Fig.2.3.4 Schlieren signal for CCl_4, Experiment No. 190
T_1=291.4 K.P_1 =85.6 Torr.shock velocity = 548.00 m/s
MACH No. = 4.2415. T_s=629.0 K. P_s =1515.7 Torr.

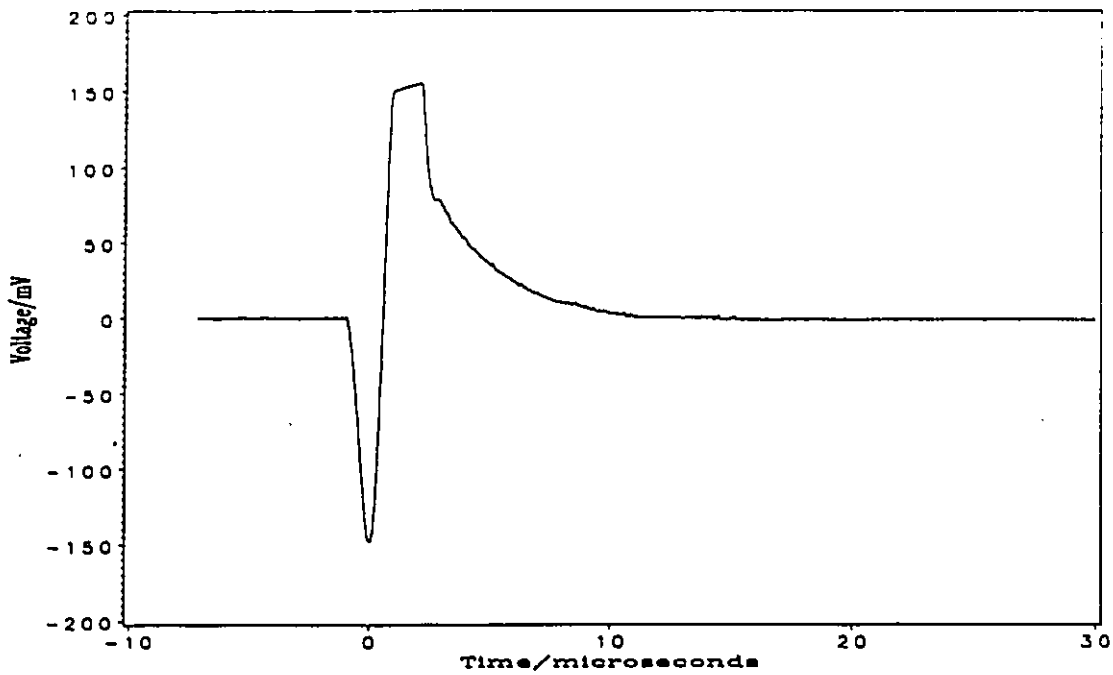

Fig.2.3.5 Schlieren signal for CH_4. Experiment No. 182
T_1=294.3 K.P_1 =80.0 Torr.shock velocity = 617.80 m/s
MACH No. = 1.4330.T_2=350.0 K.P_2 =172.4 Torr.

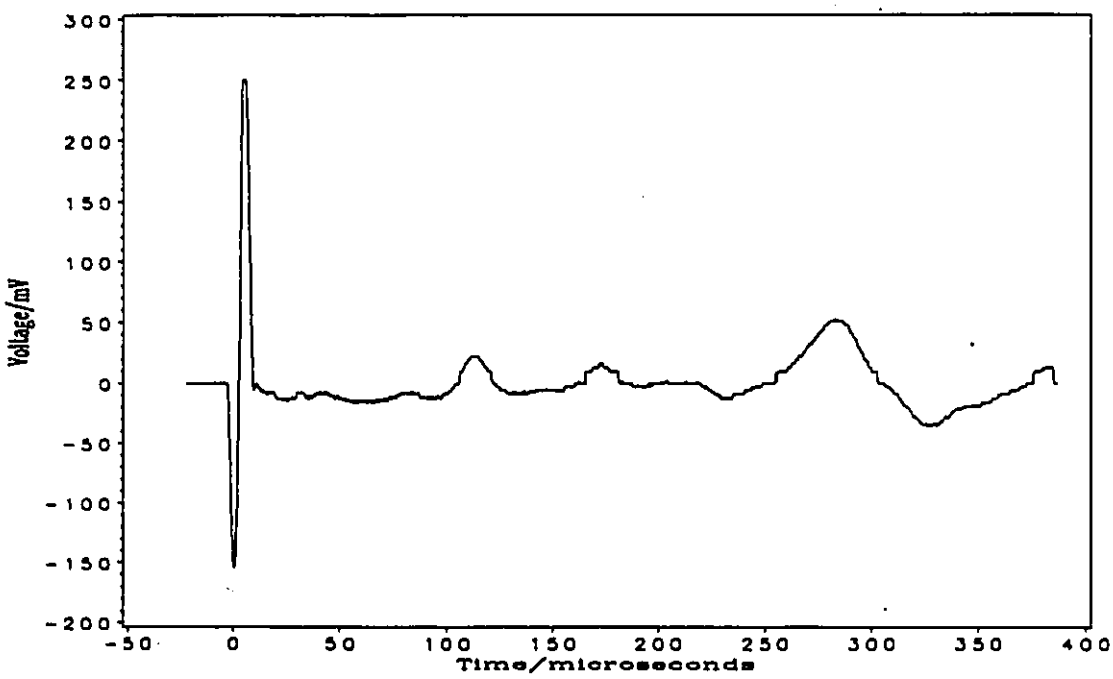

Fig.2.3.6 Schlieren signal for SF_6. Experiment No. 189
T_1=293.0 K. P_1 =361.5 Torr.shock velocity = 181.60 m/s
MACH No. = 1.3440.T_2=310.0 K.P_2 =664.7 Torr.

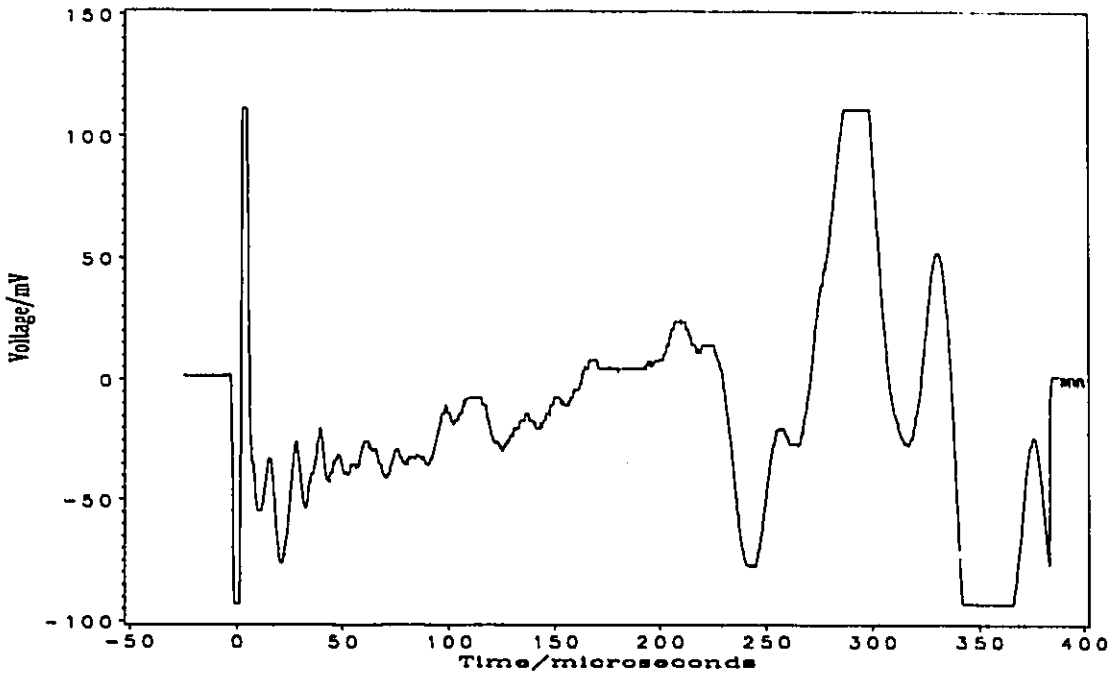

Fig.2.3.7 Schlieren signal for the mixture of CCl_2F and SF_6 . Expt No. 166
T_1=293.0 K, P_1 =730.0 Torr,shock velocity = 329.60 m/s .
T_2=372.4 K, P_2 =4357.1 Torr.

then oscillatory and finally chaotic.

The signals for the experiments are reproducible, as long as the same experimental conditions are employed. These include initial temperature and pressure, the same material and thickness of diaphragms and the same manner of introducing the driving gas. (The speed at which helium enters the driver section and breaks the diaphragm can make a difference in the postshock conditions and hence in the experimental results, and it is actually very difficult to reproduce initial conditions.) As shown in two pairs of experiments, (No. 107 vs No. 108 and No. 8 vs No. 92 , shown in figs 2.3.8, 2.3.9, 2.3.10 and 2.3.11 respectively), identical experimental conditions give rise to essentially the same schlieren signals. As will be discussed later, two experiments governed by non-linear dynamical laws give results which are identical at early times and which gradually diverge either in the chaotic regime, the oscillatory regime, or the monotonic regime. The spectacular similarity of the above two sets of chaotic results is positive proof that the condensation experiments form an example of a non-linear dynamical (kinetic) system.

2.4 Discussion of Experimental Observations

In order to understand the origin of the oscillatory signal, we performed several systematic diagnostic tests. These checks were of two sorts. The first kind of check involved comparing the schlieren signal obtained from two shock tubes of very different dimensions. We checked the total signal, i.e. the summed output of the four quadrants as

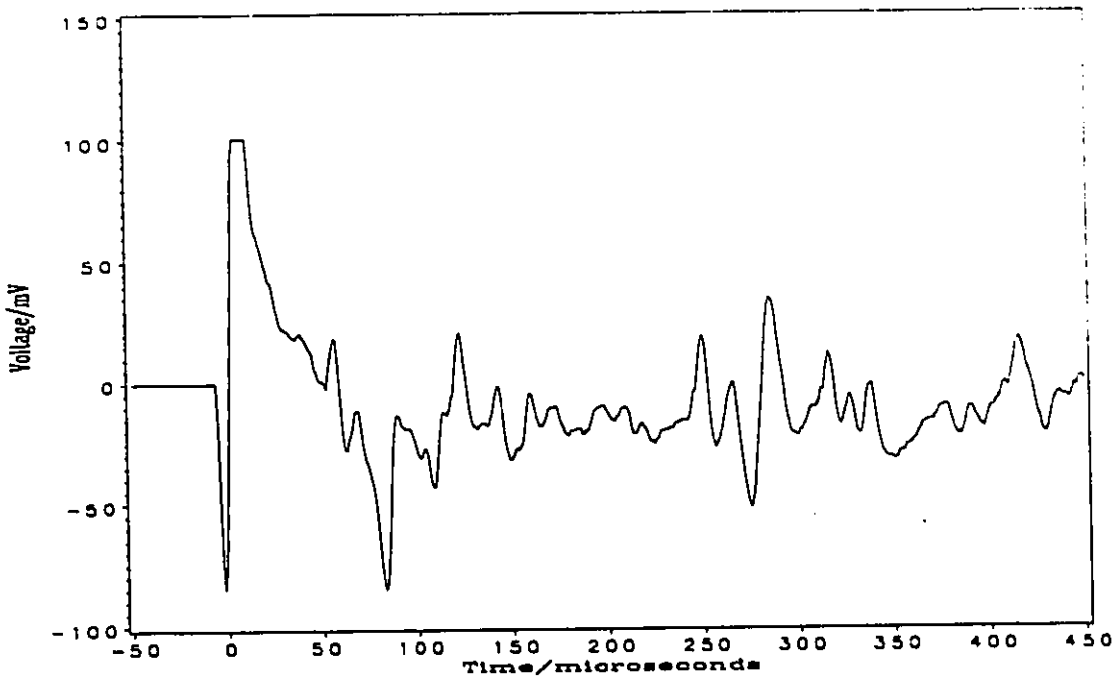

Fig. 2.3.8 Schlieren signal for CCl_3F. Experiment No. 107
T_1=293.2 K. P_1 =615.2 Torr.shock velocity = 180.10 m/s
MACH No. = 1.2141. T_2=312.7 K. P_2 =1114.9 Torr.

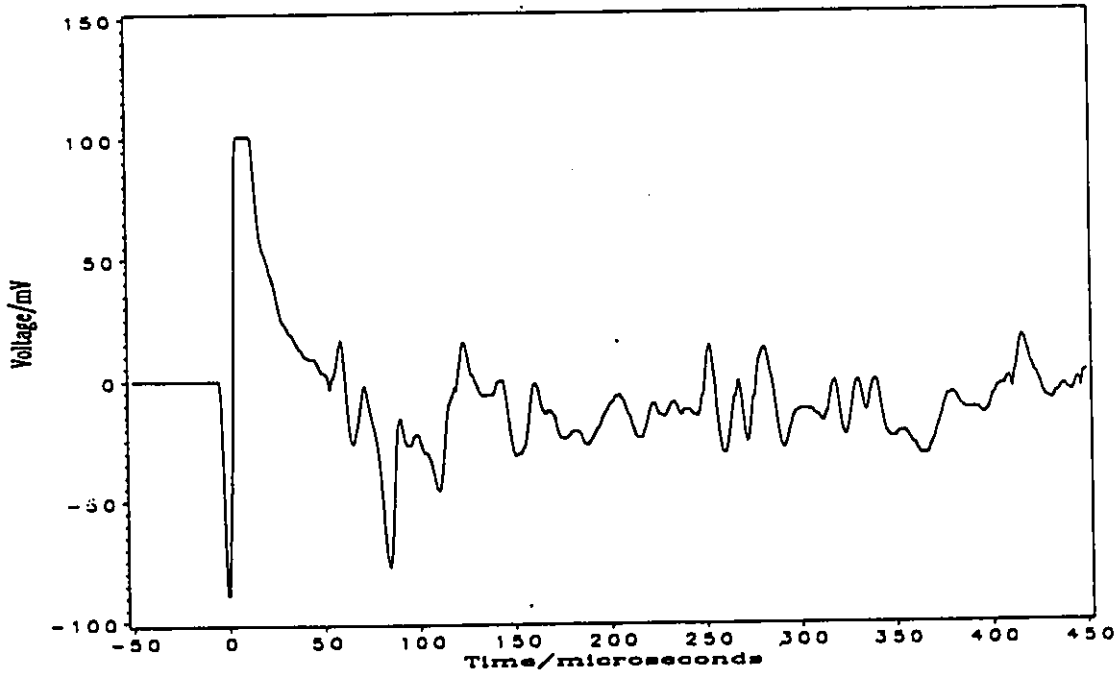

Fig. 2.3.9 Schlieren signal for CCl_3F. Experiment No. 108
T_1=293.2 K. P_1 =609.5 Torr.shock velocity = 179.40 m/s
MACH No. = 1.2128. T_2=312.4 K. P_2 =1056.0 Torr.

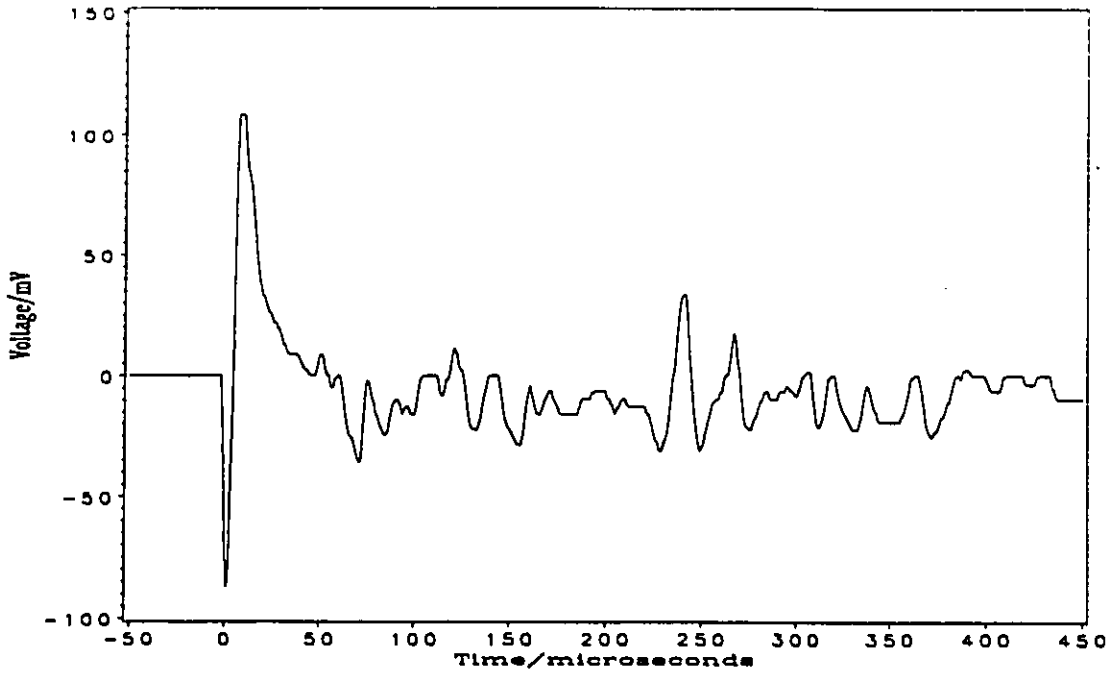

Fig. 2.3.10 Schlieren signal for CCl_3F. Experiment No. 8
T_1=293.2 K, P_1 =651.0 Torr.shock velocity = 179.30 m/s
MACH No. = 1.2906, T_2=312.3 K, P_2 =948.0 Torr.

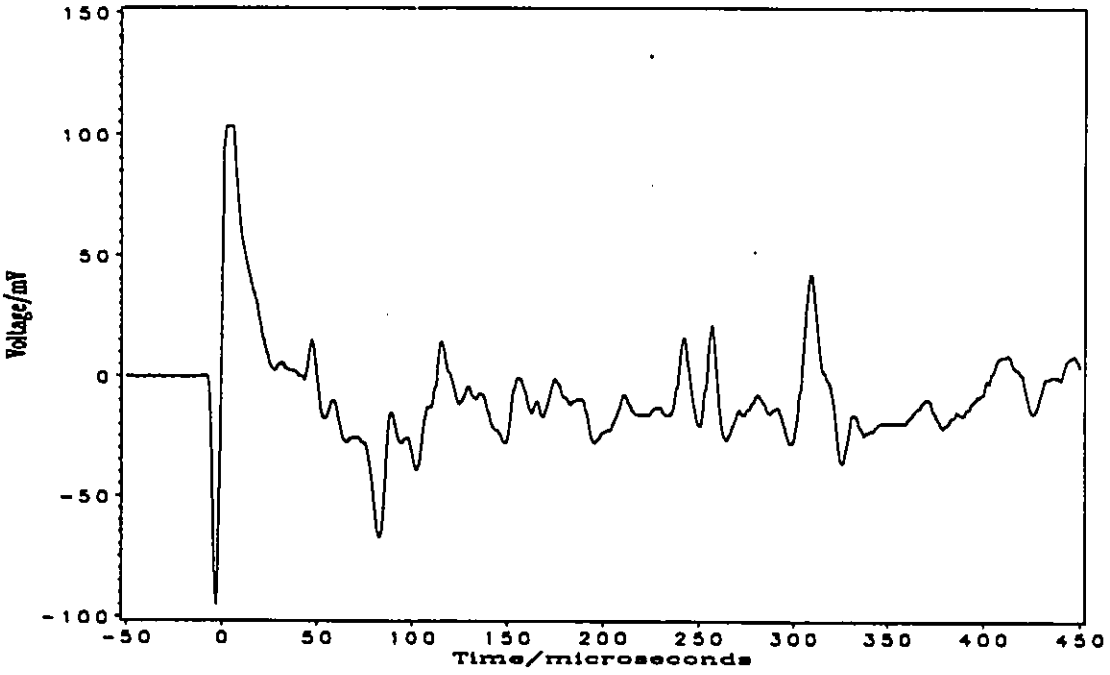

Fig. 2.3.11 Schlieren signal for CCl_3F. Experiment No. 92
T_1=293.2 K, P_1 =664.2 Torr.shock velocity = 186.50 m/s
MACH No. = 1.2590, T_2=315.6 K, P_2 =1056.3 Torr.

well as the differential signal, and we compared the observed oscillation frequencies with the frequency of an acoustic wave in steel and quartz. From these checks we concluded that the observed oscillations are not caused by any physical source, such as mechanical vibration of the shock tube or interference from nearby electronic circuits, or the vibration caused by sound waves propagating in the steel tube or in the quartz observation windows. The second sort of check involved measurement of the schlieren signals for other carefully chosen gases. The result of this check together with the knowledge of the chemical reactivity of pure CCl_3F under our experimental conditions leads to the conclusion that oscillations appear as long as the condensable test pressure of gas is very different from the equilibrium vapour pressure. It is most probably related to an exothermic reaction occurring in the shock compressed gas, such as clustering .

2.4.1 Physical and Acoustic Waves

In our experiments, two different shock tubes were used. The two tubes differ in both length and cross sectional area, as we described in section 2.1. Despite the big difference in tube dimensions, the schlieren signals have the same features. At a certain initial pressure for weak shocks in both of them an oscillatory signal was superimposed on an exponentially decaying curve which went negative; while at low initial pressures and for relatively strong shocks (M>1.6) the oscillatory signal disappeared leaving a quickly decaying curve which became negative. Experiment No. 37 performed using the old tube

and 149 using the new tube (see figs. 2.4.1 and 2.4.2) show that if the initial pressure and temperature and the shock velocity are close, the schlieren signals are similar. The main features are independent of the dimensions of the tubes.

The pre-triggering feature of the waveform recorder allowed the baseline to be recorded for each schlieren signal prior to the big negative spike caused by shock front. The baseline of each signal was stable and smooth. No oscillations or chaotic signals were observed there (see e.g. fig. 2.3.5 or 2.3.2). From this we can conclude that oscillations are not produced by the electronic circuits of the detection system. However, we still cannot exclude the possibility that the oscillations or chaotic signals are caused by interference from other electronic equipment nearby or by the laser beam, if it is unstable. Since the detector system amplifies the difference of voltages generated by the left half and the right half of the photodiode, then if there were some oscillatory interference from other sources or from the laser beam itself, the baseline could still appear to be stable when the laser beam is centred on the detector surface. When the laser beam is deflected to either side, these outside interferences of a chaotic or oscillatory nature would not be cancelled by the differential amplifier. This may cause oscillatory or chaotic signals to appear on the schlieren signal after shock arrival. This possibility can be excluded by checking the total signal generated by the detector. The 4 signals generated from the photodiode quadrants were summed and recorded (see fig. 2.4.3). Whereas the differential arrangement responds to spatially dispersed signal generators (e.g. refractive index gradients) but not to temporal variations in the opto-electronic source, the sum signal

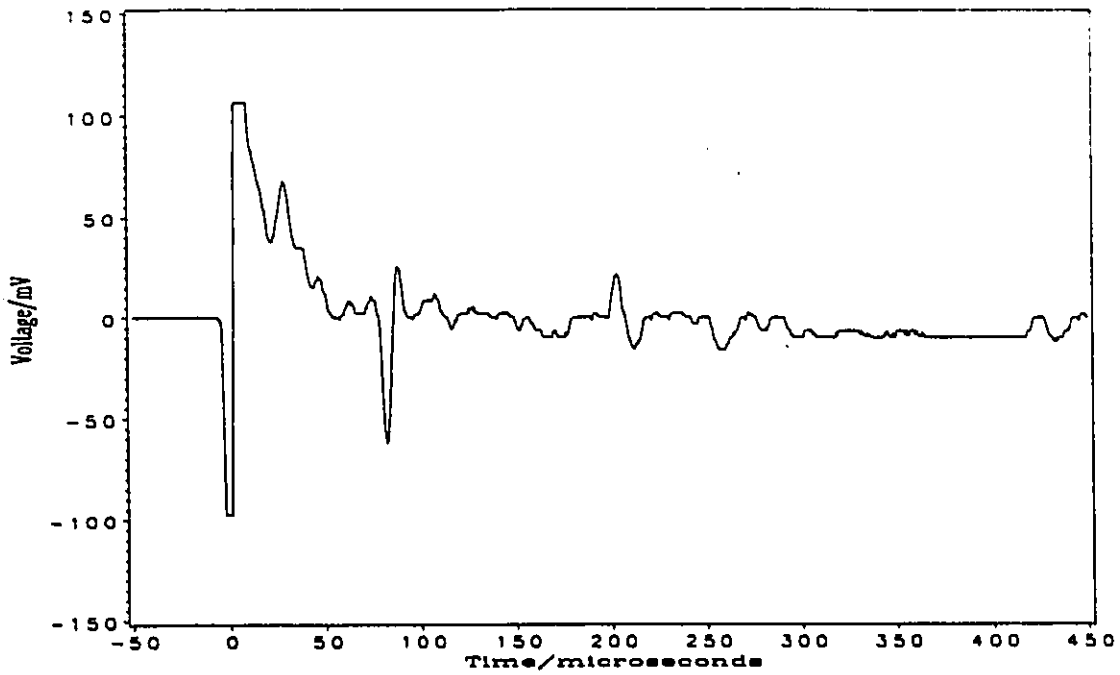

Fig. 2.4.1 Schlieren signal for CCl_3F, Experiment No. 37
T_1=296.2 K, P_1 =607.0 Torr,shock velocity = 149.50 m/s
MACH No. = 1.0690, T_2=300.6 K, P_2 =715.8 Torr.

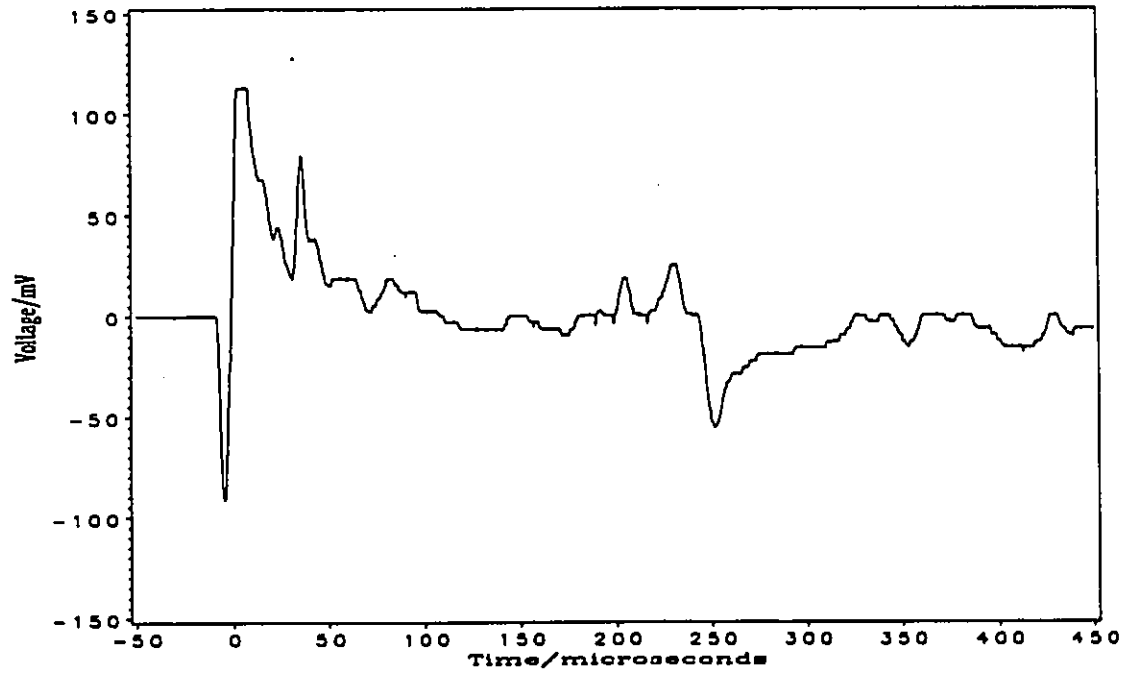

Fig. 2.4.2 Schlieren signal for CCl_3F, Experiment No. 149
T_1=294.7 K, P_1 =606.5 Torr,shock velocity = 159.80 m/s
MACH No. = 1.1300, T_2=302.6 K, P_2 =741.6 Torr.

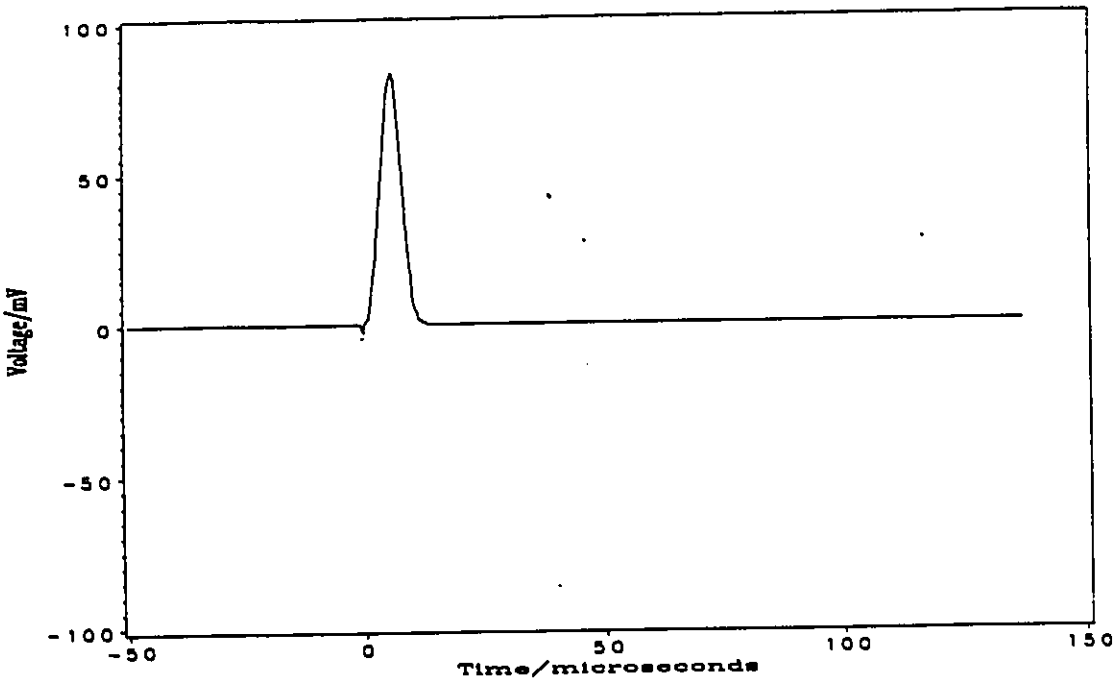

Fig.2.4.3 Total schlieren signal for CCl_2F. Experiment No. 42
T_1=294.2 K, P_1 =659.4 Torr.shock velocity = 148.35 m/s
MACH No. = 1.0449, T_2=298.7 K, P_2 =766.0 Torr.

behaves in a complementary fashion, being sensitive only to temporal variations rather than to spatial variations. This signal did not show any oscillations or noise either before shock arrival or after shock arrival, i.e. before the laser beam was deflected or after. Furthermore, the laser mirrors and the detector system were on the same heavy vibrationally isolated cement support as described in the last section. This rules out the possibility that the oscillatory signal was caused by the relative movement of laser and detectors. Consequently we can conclude that the laser beam was stable, and the oscillatory and subsequent chaotic signal was not the result of any source inside or outside of the detection system.

Are the oscillations caused by acoustic waves propagating in the quartz observation window, i.e. by motions of or in the window relative to the optics ? If this were the case, the frequency of the oscillation of the schlieren signal would be constant at constant room temperature. But the frequency of oscillation, f, varied with the Mach number, the initial pressure and identity of the test gas. The results of a calculation of resonant frequencies are given in Appendix 5, in which a_{steel}, $a_{steel,1}$ and a_{quartz} are the sound speeds[112] in stainless steel, steel and quartz respectively. They are 3100, 3235 and 3764 m/s in the transverse mode respectively, and 5940, 5790 and 5968 m/s in the longitudinal mode respectively. It is worth noting that the value of $a_{quartz}/2f$ for any schlieren signal is not equal to any of the dimensions of the observation window, either thickness or diameter. The thickness of the window is 13 mm. The diameter of the window is 25.4 mm. $a_{steel}/2f$ for any schlieren signal is not equal to any characteristic dimension of the shock

tubes either. The length of the tubes are 3.2 m and 7.3 m for the old and new tubes respectively. The inside widths of the tubes are 6.8 cm and 9.3 cm for the old and new tubes respectively. The thickness of the tube walls are 3.5 and 6.5 mm for the old and new tubes respectively. Furthermore, since the speed of sound in quartz or steel is more than 20 times that in CCl_3F, fast moving disturbances would arrive at the laser beam before the shock front. Yet no disturbances are visible prior to shock arrival. All of this excludes the possibility that the oscillatory signals are caused by acoustic reflections in a solid medium.

It is not possible that the oscillatory or chaotic signals are caused by movement of the shock tube itself. First of all the tube is rigidly mounted onto posts that are firmly bolted to the floor. Only when a thick diaphragm was used, i.e. a strong shock was fired ($M>4$), could a recoil of the tube be observed. The Mach numbers for all of experiments except one were below 2.5. Even if translational motion of the whole tube were occurring, it and the optical windows were physically isolated from the measurement system and could not transfer information to the detector. The stable and unambiguous base line prior to shock arrival is proof. Furthermore, the experiments have shown that the oscillations superimposed on the exponentially decaying signals appear only for weak shocks ($M<2$) and disappear when the shocks are strong. All of these arguments lead to the conclusion that the oscillatory signal is not caused by any kind of movement of the shock tube itself.

We did one more check by performing the same experiments with methane, as with

CCl_3F at the same initial temperatures, over a similar range of initial pressures (from 80 mm Hg to 609.2 mm Hg) and in a similar post shock temperature range(from 301 to 350 K). No oscillations nor chaotic schlieren signals were obtained for CH_4. Rather only smoothly decaying exponential signals were observed see (fig 2.3.5). If oscillation came from the movement of the shock tube during the experiment or from other unknown physical sources, oscillations should have appeared in the schlieren signal for methane, not only CCl_3F, since the initial conditions were similar. This is not the case.

To sum up the above discussion we conclude that the oscillatory and chaotic signals are caused by the density changes occurring in the vapour column behind the shock front. In the next section we shall compare our signals with those obtained from other gases and we shall discuss the boundary layer developed behind the shock front in order to further narrow the argument. Although our arguments so far come from a process of elimination, we shall also present later thermodynamic and kinetic arguments that the perturbed cluster distributions must result in cluster nucleation, heat release and thermal instability.

2.4.2 Diagnostic Testing with Other Gases

In the last section we concluded that the source of the oscillations superimposed on the exponentially decaying signal lies in the gas column behind the shock front. An important question is whether this source is the boundary layer present in the region behind the shock front. The presence of the boundary layer in the moving gas is due to the loss of

heat to the walls by conduction and the loss of momentum due to friction with the wall. Flow in the boundary layer may be either laminar or turbulent. Laminar flow is one in which the mass of fluid may be considered as advancing in separate laminae (sheets) with simple shear existing at the surfaces of contact of the laminae; while turbulent flow is one in which the fluid velocity at a fixed point fluctuates with time in a nearly random way. The motion is essentially rotational, and the rate of mass transfer and momentum transfer is considerably larger than in laminar flow[113]. It is possible that turbulent boundary flow (but not laminar flow) may cause our chaotic signals. What kind of boundary layer does exist in our experiments? This is the question we should consider here. The type of boundary layer is dependent on the shock speed and the roughness of the inner surface of the tube[111]. The properties of boundary layers in shock tubes has been intensively studied by Mirels[114] and a number of other investigators. For weak shocks ($2.5<M<8$), it has been shown that the boundary layer is a region of laminar flow[92,102,115,116], while turbulent boundary layers appear in strong shock waves. Our signals in which the oscillatory signals appeared were obtained in very weak shocks ($M<2.5$). For shock waves whose Mach number is larger than 2 the oscillations actually disappeared in schlieren signal for CCl_3F. This can be seen in experiment No.123 and 156 (see figs. 2.4.4 and 2.4.5). The initial pressure in expt.123 was 441.8 mm Hg. The Mach number is 1.58. Its schlieren signal shows oscillations. However, in expt. 156, the initial pressure was 434.6 mm Hg. The Mach number was 2.27; yet, the oscillations are lost. Even the chaotic signal has disappeared too. If the oscillations were caused by a turbulent boundary layer, an increase in Mach number should have intensified the chaotic signal. Furthermore, since

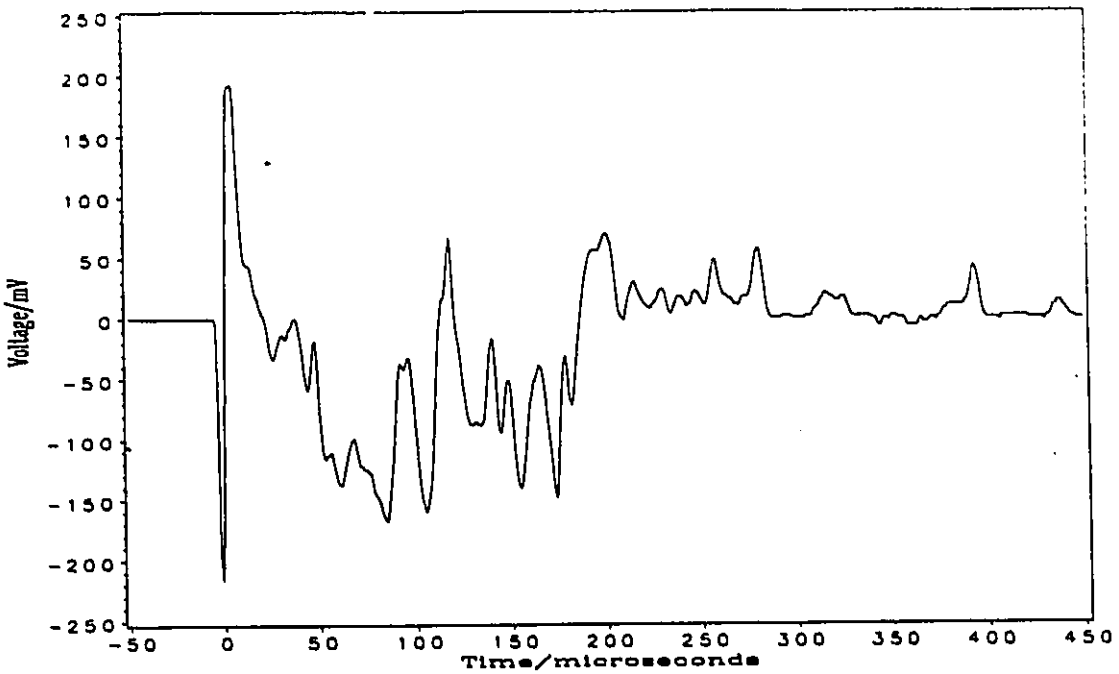

Fig. 2.4.4 Schlieren signal for CCl_3F. Experiment No. 123
T_1=292.8 K, P_1 =441.8 Torr,shock velocity = 230.80 m/s
MACH No. = 1.5794, T_2=331.5 K, P_2 =1103.0 Torr.

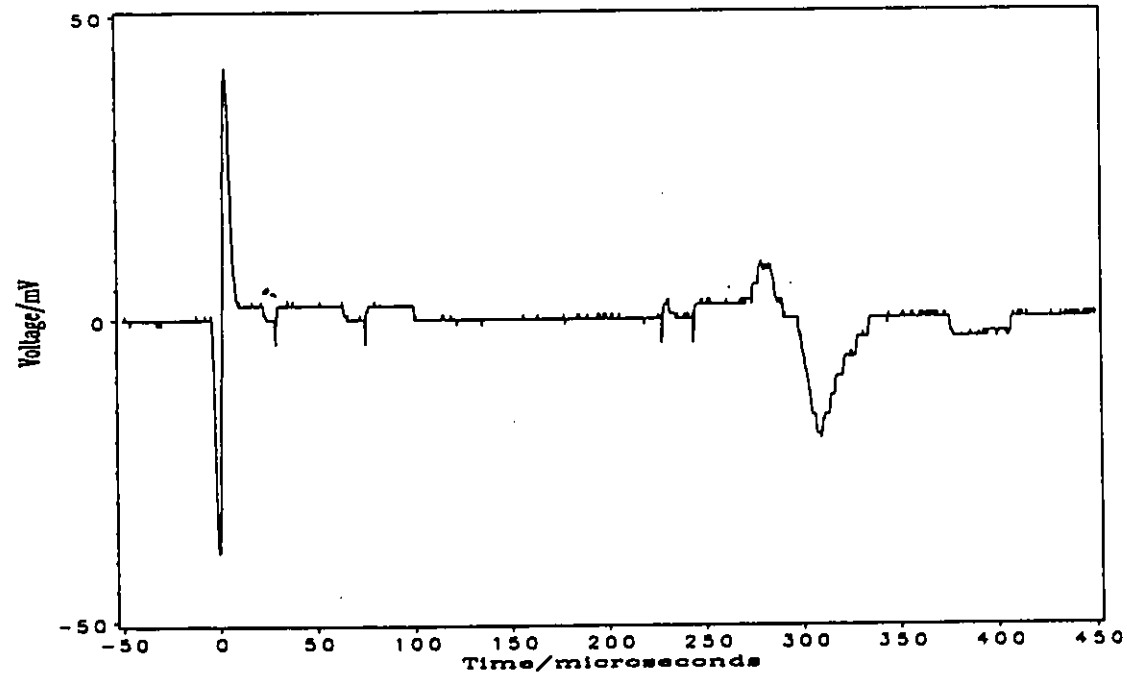

Fig. 2.4.5 Schlieren signal for CCl_3F. Experiment No. 156
T_1=295.0 K, P_1 =434.6 Torr,shock velocity = 320.70 m/s
MACH No. = 2.2690, T_2=380.7 K, P_2 =2418.0 Torr.

the thickness of the boundary layer increases as the distance from the shock front increases, the strength of the oscillatory or chaotic signal should increase with time. This is not the case: as time increases the oscillatory signal actually dies out. As the strength of the shock wave increases the oscillations disappear from the exponentially decaying curve. The turbulent boundary layer cannot give rise to the quasi-periodic signal that we observed in the experiments because the movement of fluid is random in a turbulent boundary layer. The oscillatory signals were observed immediately after arrival of the shock front. That is certainly within the laminar flow region of the boundary layer. Furthermore, our shock tube surface is smooth. The cross section of the new tube is 77.74 cm^2, while the cross section of the old tube is 46.92 cm^2. The area of cross section of the new tube is 1.66 times larger than that of the old tube. The larger the cross section, the longer the duration of laminar flow in the boundary layer, and the lesser the effect of the boundary layer on the schlieren signal. Yet as shown in the last section, if the initial conditions (T_1, P_1 and u_1) of two experiments in two different tubes are similar, the schlieren signals are also similar. There are no dramatic changes in the schlieren signals. Therefore, the effect of the boundary layer on our schlieren signals obtained from the two tubes is apparently not important, i.e. it is negligible. From the above discussion we can exclude the possibility that turbulent flow in the boundary layer causes our oscillatory signal. It must be produced by some chemical process.

The oscillatory signal is not the result of the absorbtion or scattering of laser light by the gas[117] during the measurement. This was checked by monitoring the total laser beam

intensity falling on the detector. If the oscillations were caused by absorbtion or scattering of laser light the oscillatory signal should appear on the total signal. Yet, we observed no modulation.

In order to find out what kind of chemical process was responsible for the oscillatory and chaotic signals we performed experiments with several other gases: argon, methane, sulphur hexafluoride and tetracloromethane. The molecular weight (M.W.), melting point (T_m), boiling point (T_b), critical temperature (T_c), critical pressure (P_c) and heat of vaporization, (H_v) are given[121] in table 2.4.1.

Table 2.4.1

	M.W.	T_m (K)	T_b (K)	T_c(K)	P_c (MPa)	$\tau(10^6)$ (s)	H_v kJ/ mol
Ar	39.98	83.8	87.3	150.9	4.898	-	6.44_b
CH_4	16.04	90.7	111.6	190.5	4.898	$1.68_{(303)}$	8.17_b
SF_6	146.05	222.4	209.2	318.7	3.77	$0.78_{(301.2)}$	8.99
CCl_3F	137.37	162.0	296.9	471.2	4.41	$0.04_{(300)}$	24.9
CCl_4	153.82	250.0	349.9	556.6	4.516	$0.021_{(303)}$	32.43

where the subscript b refers to the normal boiling point. τ is the vibrational relaxation time at the temperature indicated as a subscript .

With pure argon at an initial pressure of 673 mm Hg, u =0.3772 mm/μs, T_2 =345.4 K and P_2=1009.5 mm Hg, the schlieren signal (see fig. 2.4.6) was the same as the one given in reference 85. It is solely the result of the passage of the shock front. Deflections due to the boundary layer were not at all in evidence. Argon is a monatomic gas. Under the experimental conditions of our shock waves no chemical processes occur. This is another proof that the source of the oscillatory signal is not in the apparatus. Methane is a non-polar molecule. At room temperature the stable state is the gas phase. With methane, the initial pressure was varied and the thickness of the diaphragm was changed. No signals similar to CCl_3F's were obtained. Behind the shock front only exponential decay was observed. There was no oscillation superimposed on the decaying curve, and the decaying curve does not become negative (see fig. 2.3.5). In the methane experiments only vibrational relaxation processes take place, and give rise to the exponentially decaying curve. The schlieren signal for an experiment with sulphur hexafluoride is shown in fig. 2.3.6 at an initial pressure of 361.5 mm Hg, an initial temperature of 293.0 K and a shock velocity of 0.1818 km s^{-1}. The post-shock temperature and pressure are 310.0 K and 664.72 mm Hg respectively. There are no oscillations, but the exponentially decaying curve did go negative in distinction from the schlieren signal obtained in experiment No. 166 (see fig. 2.4.6) for CCl_3F (initial pressure = 398.5 mm Hg, T_1 = 293.15 K and shock velocity = 0.1843 km s^{-1}). The latter has an oscillatory signal superimposed on an

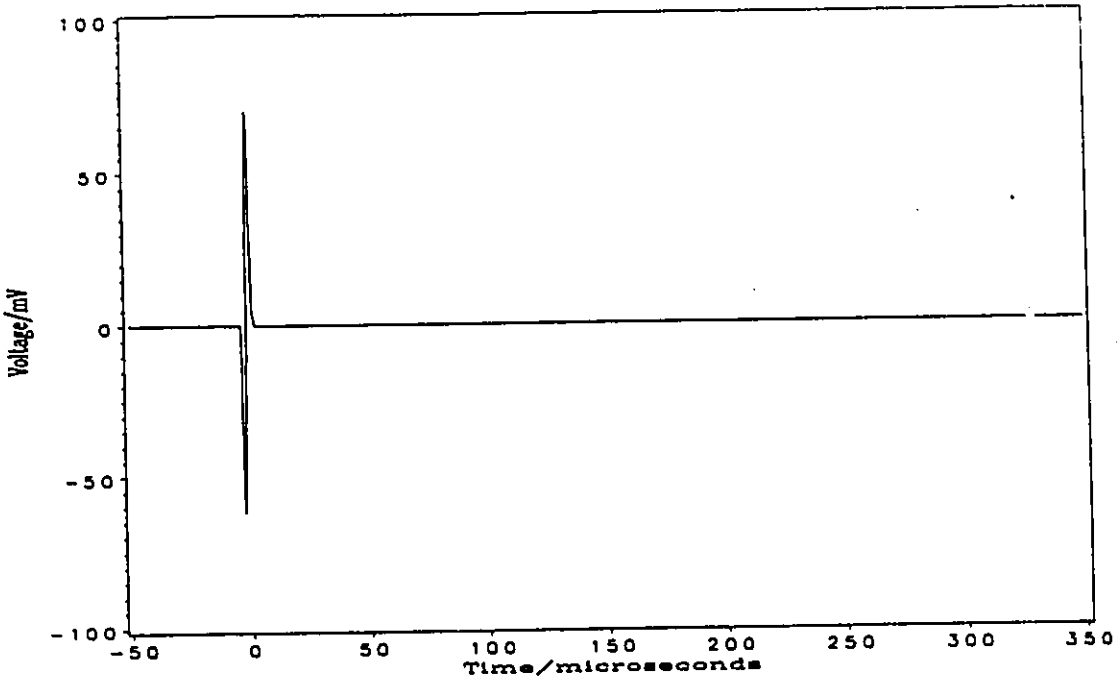

Fig. 2.4.6 Schlieren signal for Ar Experiment No. 185
T_1=293.2 K. P_1 =673.0 Torr.shock velocity = 377.20 m/s
MACH No. = 1.1829, T_2=346.4 K. P_2 =1009.5 Torr.

exponentially decaying curve, and it becomes negative. The schlieren signal for CCl_4, with an initial pressure of 85.6 mm Hg, close to the vapour pressure at an initial temperature of 291.4 K, and a shock velocity 0.5480 km s^{-1}, is shown in fig. 2.3.4. Its post-shock temperature is 529.0 K; its post-shock pressure is 1515.7 mm Hg. There is a large amplitude of oscillation superimposed on the exponentially decaying curve which becomes negative. It is similar to the signal obtained for the experiment with CCl_3F (Expt. 122 and others).

Has any chemical reaction occurred? Carbon tetrachloride is a very stable and inert compound, so it is used as a solvent in organic chemistry. At our experimental temperature and pressure pure CCl_4 does not dissociate, Therefore, this is not the source of the density change in the shock wave. CCl_3F (Freon-11) is also stable and inert under our experimental conditions. It does not dissociate. The mass spectrum of the vapour sample in the test section both before and after shock compression was taken. No new compounds were detected. If molecules of CCl_3F had dissociated behind the shock wave ($T< 450$ K) new compounds should have been produced in the gas phase. This is not the case. Therefore, the endothermic oscillatory signal is not a result of the dissociation of the samples.

What can cause a density change behind a shock wave aside from the rotational and vibrational relaxation? Let us correlate the properties of methane, sulphur hexafluoride, Freon-11 and carbon tetrachloride. Among them methane has the smallest molecular

weight and the smallest relaxing heat capacity, while tetrachloromethane has the largest molecular weight and the largest relaxing heat capacity. Freon-11 should have the second largest relaxing heat capacity. The larger the relaxing heat capacity, the larger the temperature change. Comparing the relaxation time of these compounds we find that CCl_4 relaxes fastest, CCl_3F second fastest, then SF_6; CH_4 is the slowest. This means that the temperature drop caused by vibrational relaxation will occur most quickly in CCl_4. Now, consider the critical temperature, T_c. For both argon and methane T_c is much lower than room temperature. That means that they cannot condense at or above room temperature, no matter how high the pressure is. The molecules of argon and methane have enough kinetic energy to overcome their inter-molecular attractions at temperatures higher than their critical temperatures. The critical temperature of the other three gases all are above room temperature, 318.7, 471.2 and 556.6 K for SF_6, CCl_3F and CCl_4 respectively. It is possible to condense these vapours to liquids below their critical temperatures. The higher the critical temperature, the larger the inter-molecular attractive force. This is an important difference between Ar and CH_4 on the one hand and SF_6, CCl_3F and CCl_4 on the other. Comparing the heats of vaporization we can see that those of argon and methane at the boiling point are the smallest. SF_6 has the smallest heat of vaporization among the other three condensable gases, only 8.99 kJ/mol at 25 ^{0}C, while at the same temperature the heats of vaporization of CCl_3F and CCl_4 are 24.9 and 32.43 kJ/mol. The heat of vaporization of CCl_4 is much larger than that of CCl_3F. The higher the heat of vaporization the larger the amount of energy a liquid molecule needs to overcome intermolecular attractive forces in the liquid in order to enter the gas phase, or the larger

the amount of heat will be released when gas molecules combine into clusters or liquid (Recall that the heat effect is important for the thermokinetic oscillator discussed in chapter 1). Comparing the boiling points we can see a similar pattern. The boiling point of CCl_4 is highest, while that of Ar is lowest.

From the above discussion and our experimental results we can conclude that if the critical temperature of the gas is much lower than the postshock temperature there is no oscillation observed in the schlieren signals of gases such as Ar and CH_4. When the critical temperature is much higher than post-shock temperature, oscillatory schlieren signals can be detected. It seem that there is a relationship between the critical temperature and oscillations. From thermodynamic considerations, the larger the heat of vaporization, the higher the boiling point and heat capacity of relaxation, and the larger the amplitude of the oscillatory schlieren signal. From the kinetic view point the conclusion is that the faster the relaxation process (the smaller the vibrational relaxation time), the earlier the oscillatory signal appears in the schlieren signal(see fig 2.3.4, 2.3.2 and 2.3.6 for CCl_4,CCl_3F and SF_6 respectively).

Next, we shall see the differences between the selected gases in light of their second virial coefficients. The virial equation[118] of state is given by

$$PV_m=RT\left(1+\frac{B}{V_m}+\frac{C}{V_m^2}+\cdots\right) \qquad (2.4.1)$$

in which B, C, etc., are functions of temperature. They are called the second, third, etc., virial coefficients. They reflect the effects of intermolecular forces between the molecules[118]. The second virial coefficient, B, for example, is obtained theoretically by considering only interactions between pairs of molecules. The second virial coefficient is related to the intermolecular pair potential $U_{12}(r)$ by

$$B(T) = \frac{1}{2}\int_{-\infty}^{+\infty}(1-e^{-\frac{U_{12}}{kT}})\,dV \qquad (2.4.2)$$

in which V is the set of relative coordinates. A negative value of B means the pair of molecules attract each other. Comparison of the second virial coefficients of the gases can give a quantitative picture of the interaction of molecular pairs. At 400 K B(T) for CCl_4 is -868 cm^3/mol, the largest among the gases. B(T) for CCl_3F is the second largest one, -431 cm^3/mol; B(T) is -135 cm^3/mol for SF_6, -16 cm^3/mol for CH_4 and -1 cm^3/mol for argon. There is a large difference in the second virial coefficients for SF_6 and CCl_4, although both of them are non-polar molecules and have similar molecular weights. The intermolecular forces for both SF_6 and CCl_4 are London dispersion forces which are the resultant of a temporary dipole on one molecule interacting with the induced dipole on another. This force is proportional to the polarizability of the molecules, which is proportional to the number of electrons in a molecule. CCl_4 has more electrons than SF_6. Consequently the intermolecular force for carbon tetrachloride is much larger than that for SF_6 at the same temperature. This means that when two molecules of CCl_4 come

together they are more easily able to form a cluster. For SF_6 it is much more difficult at the same temperature[122,123]; for CH_4 it is unlikely at all to form clusters at high temperatures since its B(T) is zero at 500 K and +10 at 600 K; similarly for Ar B(T) is -1 at 400 K, and +7 at 500 K. This is more evident when the dimerization constant, K_2, is related[152] to B(T) by $-K_2RT=B(T)$. The smaller the second virial coefficient the smaller the equilibrium constant, K_2, for dimer formation from monomers. The trend in the variations of B(T) is the same as the trend in the capability of forming dimers. It is important to note that B is a function of temperature. The dependence is given[121] by

$$B(T) = \sum_{i=1}^{n} a_i \left(\frac{T_o}{T} - 1\right)^{i-1} \qquad (2.4.3)$$

in which T_o is 295.15 K. The values of a_i are given in Table 2.4.2. Comparing the a_i of the gases we can conclude that dB(T)/dT is largest for CCl_4, second largest for Freon-11, followed by SF_6.

We can arrive at the same conclusion by comparing the Van der Waals' empirical constants for these selected gases. The Van der Waals' equation is an equation of state that is designed to agree with experimental values of P, V, and T for a gas at high pressures and low temperatures. It contains two empirical constants a, and b. The large the value of a, the larger the force of attraction between the gas molecules, and the greater the magnitude of depth of the potential well, ε. The larger value of b, the larger the molecular volume. a for argon is 1.34 L^2atm/mol^2, 2.25 for CH_4, 2.74 for SF_6, 10.8

for CCl_3F, and 20.4 for CCl_4. These values indicate that CCl_4 molecules have the largest attractive forces among the selected gases.

Table 2.4.2

Coefficients for calculating the second virial coefficients of selected gases.

	a(1)	a(2)	a(3)	a(4)
Ar	-16	-60	-0	0
CH_4	-43	-114	-19	-7
SF_6	-279	-647	-335	72
CCl_3F	-789	-1428	-142	0
CCl_4	-1600	-4059	-4653	0

We have compared the boiling points, enthalpies of vaporization, critical temperatures, second virial coefficients, and Van der Waals' empirical constants of selected gases. Oscillatory and negative schlieren signals were observed for CCl_4 and CCl_3F. Both of these gases have relatively higher boiling points, larger enthalpies of vaporization, larger second virial coefficients and empirical Van der Waals' constant, a, than the other selected gases. Their critical temperatures are above experimental temperature. In schlieren signals for Ar and CH_4 there are no oscillations and no negative signals. Both of them have lower boiling points, smaller enthalpies of vaporization, smaller second virial coefficients and Van der Waals' constants, a, than CCl_4 and CCl_3F. The mass

spectrum of CCl_3F after shock wave passage indicates there was no dissociation of CCl_3F, as mentioned above. All of these lead to the conclusion that cluster formation was occurring behind shock waves of CCl_4 and CCl_3F vapour. Does the process of cluster formation generate schlieren signals like those we obtained? Hess[91] et.al. who observed cluster formation using a variety of techniques (such as SEM (scanning electron microscopy) indicated that the particulates have spherical geometry with diameters around 0.2 μm.) also used the technique of photothermal probe beam deflection (PTPD) in studying $(CS)_n$ cluster formation (using a probe laser beam measuring the density variation caused by cluster formation). This is similar to our laser-schlieren technique. If the probe laser beam passes through the cluster formation region, a negative signal is detected. Their experimental signals confirm that our negative signal is generated by cluster formation. The first crossing point of the signal from positive to negative is the time that the cluster formation region arrives at the detecting laser beam. By measuring this cross point in the schlieren signal the incubation time for cluster formation can be deduced. The oscillation in the schlieren signal is generated by an oscillatory diffusive thermal wave which is generated, in turn, by cluster formation processes.

Using the above information we can correlate our schlieren signals for CH_4, SF_6, CCl_3F and CCl_4 with the tendency to cluster and condense and with the tendency to process the evolved heat via vibrational relaxation. Apparently when the shock wave arrives the translational temperature of the vapour molecules CCl_3F, CCl_4, or SF_6, rises nearly instantaneously. The increased kinetic energy (i.e. translational temperature) perturbs the

old cluster distribution. Existing clusters break apart. This requires heat. Then rotational relaxation occurs quickly with vibrational relaxation following. The translational temperature decrease ; dramatically due to the vibrational relaxation. Not only do clusters form in response to the change in the equilibrium cluster distribution, but also the interaction between molecule pairs increases very much since dB/dT is large. At lower temperatures the second virial coefficients of CCl_4 and CCl_3F are much larger than those of CH_4 and SF_6. Small clusters can relatively easily be formed in CCl_4 and CCl_3F vapour. At this point a large heat of cluster formation is released. The heats of cluster formation are related empirically to the heat of condensation of vapour[117] by

$$\Delta H = n\Delta H_{cond}(1-n^{-\frac{1}{4}}) \qquad (2.4.4)$$

in which ΔH is the heat of cluster formation, and ΔH_{cond} is the heat of condensation of vapour to liquid. Both of them are functions of temperature. Since CCl_4 and CCl_3F have larger heats of condensation a large amount of heat is released when clusters are formed in CCl_4 and CCl_3F vapour. Cluster formation occurs via a series of reactions, i.e. a (n-1)-mer, A_{n-1}, reacting with a monomer, A, forming an excited cluster, A_n^*, which has enough energy to break apart. Before the excited n-mer breaks up a stabilization reaction can take place, $A_n^* + M = A_n + M$, in which M is a monomer or cluster. The microscopic rate constants are functions of temperature, but not all four follow $k=Ae^{-E/RT}$. The temperature rises as heat is released, affecting both k and the equilibrium cluster distribution. That is, a self-catalysis process[104]. The released heat then generates a thermal gradient in an already shocked gas propagating along the tube. When it arrives at the observation

window following the main shock front, it is detected by our detection system. On a schlieren signal it shows up as a valley. As the vapour is slightly heated vibrational relaxation of both cluster and monomer proceeds. Then the temperature drops again; more clusters form, and heat is released again in the next stage of the shock wave. A second peak appears on the exponentially decaying curve as the relaxation of clusters and monomers follows. This process can be thought of as a series of weak shocks produced by stagewise heat release due to the formation of small clusters with vibrational relaxation lagging significantly behind. The various processes are widely separeted in time, probably. The events detected by the laser schlieren technique appear as small spikes i.e. as an oscillatory signal. The faster the vibrational relaxation proceeds, the earlier the small spike appears. The greater the initial perturbation to the cluster distribution, the more pronounced are the oscillatory consequences.

When the shock wave is too strong, the temperature behind the shock front is fairly high, dB/dT is small and B is small. Few clusters form in the shock wave. In other words the equilibrium cluster distribution is not disturbed significantly. The process occurs close to equilibrium. More important, the incubation time is much shorter at higher temperature. Local clustering starts before the thermal wave arrives. There are no spikes on the exponentially decaying curve. Cluster formation and heat release change the density of the vapour so the density decreases as the distance increases from the shock front, after the molecules vibrationally relax. As a result, a negative schlieren signal is observed[91,119]. The negative schlieren signal indicates an exothermic reaction[120]. This is the case for

CCl_3F experiments in which low initial pressure and relatively strong shock waves are employed. In these cases the signal decays exponentially (see fig. 2.3.1).

Recalling that processes occurring far from equilibrium can show periodic and even chaotic behaviour (see Section 1.6) if the governing differential rate equations are nonlinear, our observations imply that vapour condensation is an example of nonlinear kinetics. As mentioned earlier the reproducible chaotic signals alone are proof of nonlinear kinetics laws.

The experiment with SF_6 was performed at an initial temperature of 293.15 K and an initial pressure 361.5 mm Hg. The temperature behind the shock front was 310 K at which both B and dB/dT are small. We know that the heat of vaporization at 298.15 K, is very small compared with that of CCl_4 and CCl_3F. When the temperature changed clusters were formed, but no large amount of heat was released. Consequently there were no spikes on the exponentially decaying curve. After vibrational relaxation, the temperature decreased, clusters were formed, heat was released, the density decreased, and a negative signal was observed in exp. 189 (see fig. 2.3.6). This is similar to the experiments with low initial pressure and a strong shock wave in CCl_3F (see fig. 2.3.1). On the other hand, for Exp. 166 (see fig. 2.4.7) occurring under similar initial conditions (T_1 = 293.15 K, P_1 = 398.5 mm Hg, T_2 =313.68 K, P_2=721.6 mm Hg) we can see spikes in the schlieren signal. This is because at the same temperature both second virial coefficients B and dB/dT for CCl_3F are larger than for SF_6, the vapour pressure of

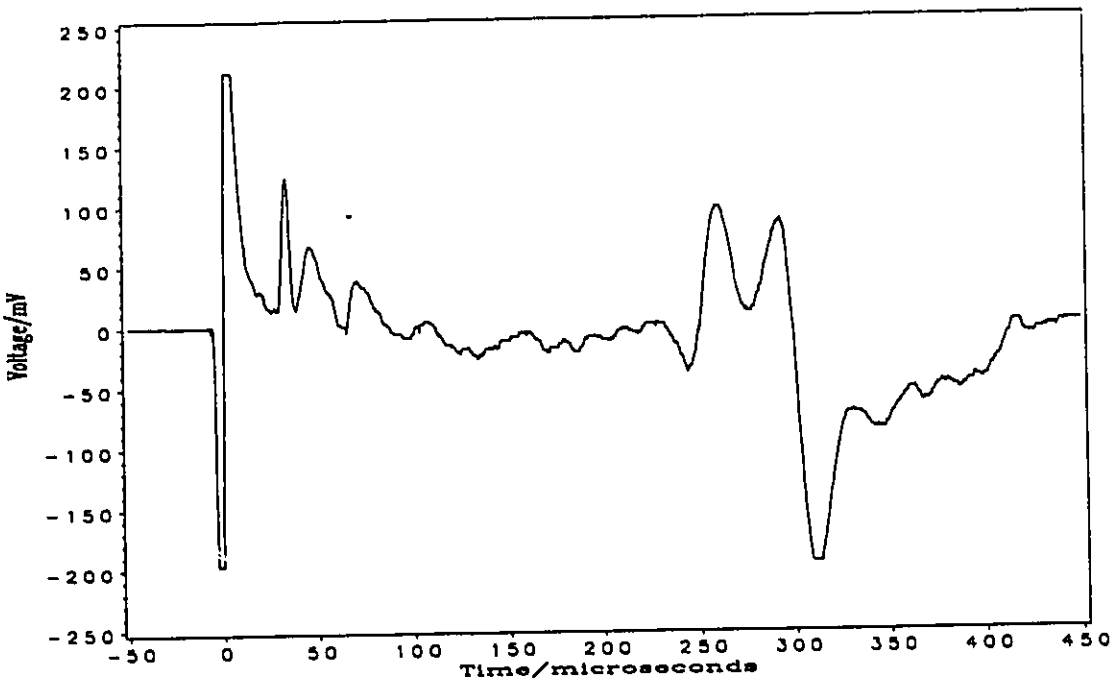

Fig. 2.4.7 Schlieren signal for CCl_2F. Experiment No. 166
T_1=293.2 K, P_1 =398.5 Torr,shock velocity = 184.50 m/s
MACH No. = 1.3080, T_2=313.6 K, P_2 =721.6 Torr.

CCl_3F is much lower than for SF_6 and the heat of evaporation is much larger than for SF_6, corresponding to a relatively large perturbation.

The initial conditions for the experiment with CCl_4 (fig.2.3.4) are T_1 = 291.35 K, and P_1 = 85.6 mm Hg, i.e. close to the vapour pressure. The temperature behind the shock front is 529 K. We do not have the data for the heat of condensation, ΔH_{cond}, and the second virial coefficient at 529 K. However, from the data given in the table we can conjecture that ΔH, B and dB/dT are large compared with the values for CCl_3F, SF_6 and CH_4. A large drop in temperature caused by the vibrational relaxation of CCl_4 causes a formation of clusters. The heat released by cluster formation is large enough to produce the series of pulses that can be detected by the laser schlieren technique. An oscillating schlieren signal was observed. In contrast, Exp. 33 at a similar initial pressure and temperature to the CCl_4 experiment showed no oscillatory signal. Instead, chaotic exothermic cluster formation occurred.

We have done several experiments with CH_4, No oscillatory or negative signal was observed. This is because the critical temperature is very low (190.5 K). No clusters can form under these experimental conditions.

In this section we examined our signals in detail. We reasoned that the spikes or oscillations superimposed on the exponentially decaying curve can be produced by a series of weak pulses of heat released by cluster formation caused by a shock compressed

perturbation and followed by a lagging heat uptake caused by a "slow" vibrational relaxation. We referred to the cluster formation mechanism in order to explain our schlieren signals obtained from several different gases. The conditions for producing oscillatory signals are that, first, the experimental temperature must be below the critical temperature; second, the cluster distribution must be greatly perturbed from the equilibrium distribution; third, there must be a large heat of cluster formation; and last, an endothermic process must couple with the exothermic cluster formation process. There are also indications that vibrational relaxation of clusters must be incapable of keeping in phase with the cluster formation stages. All of these conditions imply that the system of nucleation of CCl_3F and CCl_4 in shock tube is a nonlinear kinetic system and it satisfies the requirements for a thermokinetic oscillator, which we have discussed in section 1.6.

CHAPTER 3

EXPERIMENTAL RESULTS

In the last chapter we concluded that the oscillatory and negative schlieren signals are caused by cluster formation processes. In our experiment we varied the initial pressure of trichloromonofluorometnane from as low as 29 mm Hg to as high as 747 mm Hg, for which at an initial temperature of 296.8 K, it is close to its equilibrium vapour pressure of 750 mm Hg. We also used different thicknesses of aluminum diaphragm to vary the strength of the shock wave and hence the degree of supersaturation. Three different thickness were used. They were 0.1000 mm, 0.0130 mm and 0.0020 mm. Therefore the experiments provided a wide variety of conditions for systematic studies.

In this chapter we try at first to correlate the main characteristics of the schlieren signal with the over-pressure, $(P_{vap}(T_2) - P_2)$, and T_2. In the second part of this chapter we shall use the Fourier transform technique to analyze the oscillatory signal and to correlate the associated frequencies with temperature and over-pressure. In the third section we shall discuss whether CCl_3F cluster formation, as observed here, fits the criteria of a chemical oscillator.

3.1 The Characteristic Time Scale and the Maximum Rate of Heat Release

There are two characteristic points observed in the experimental schlieren signals. One is the crossing point of the signal with the baseline. We define the time interval from zero to this point as t_0. The second is the point at which the signal reaches its most negative value. The time interval from zero to this point is termed t_{min}. The value of the voltage corresponding to t_{min} is called V_{min}, and represents the maximum rate of heat release.

The time sampled by the digital waveform analyzer, appearing as the horizontal axis on the schlieren signal, is the laboratory time. This differs from the gas particle time (some times called heating time) which is the time for which the gas particles have actually been processed by the shock wave. Because the fluid behind the incident shock front is always set into motion, the lab observation time at a fixed observation window is always less than the gas particle time. The relationship between gas particle time (t_p) and laboratory time (t_l) is schematically shown in fig. 3.1.1. The characteristic times measured in the laboratory time frame can easily be converted into the particle time frame, if the ratio of the post-shock and pre-shock densities are known, using the following equation[92]

$$dt_p = dt_l \left(\frac{\rho_2}{\rho_1}\right)$$

The values of t_0 and t_{min} in appendix 4 are given in the gas particle time frame.

For bimolecular reactions like ours the characteristic times (t_0 and t_{min}) are inversely

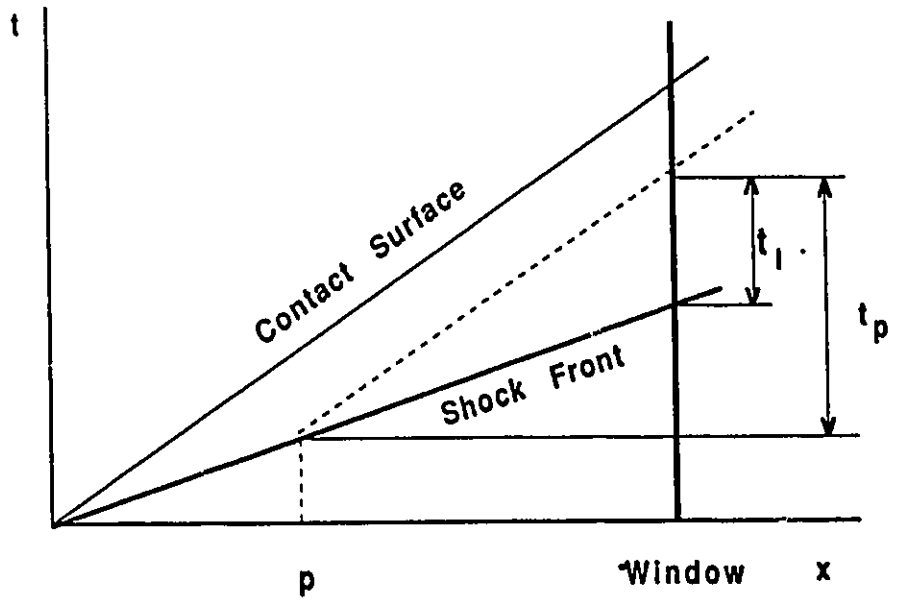

Fig. 3.1.1 The relation between laboratory time (t_l) and gas particle time (t_p).

proportional to the gas concentration, whereas V_{min} of the schlieren signals is proportional to the square of the concentration. Therefore, the invariants for our reaction (second order rate constants) should be related to t_0P_2, $t_{min}P_2$ and V_{min}/P_2^2. These were plotted against the over-pressure, ΔP, i.e. $(P_{vap}(T_2)-P_2)$, for different fixed T_2 respectively. These are shown in figs. 3.1.2a to 3.1.4b. The plots of t_0P_2, $t_{min}P_2$ and V_{min}/P_2^2 against $1/T_2$ for different fixed over-pressures are shown in figs. 3.1.5a to 3.1.7b respectively.

Some subjectivity was necessary for choosing t_0, t_{min} and V_{min} because of the oscillatory nature of the signal. Our procedure was to draw an envelope for each signal, and choose t_0, t_{min} and V_{min} appropriate to the envelope. Even this was subjective, and some of the scatter in fig. 3.1.2a to 3.1.7b is due to this arbitrariness. However, by far the greatest contribution to the scatter is the inability to select initial conditions reproducibly at will. Although the precision in calculating (from measured shock speeds) T_2 and P_2 is ~0.1% (±0.1 μs, uncertainty in an overall 200 μs time interval) we could not guarantee that e.g. a series of experiments with different P_2 could be chosen with all of them at the same temperature better than ±2 K. Yet, the dependence of the observables on T_2, as seen in figs 3.1.5a - 3.1.7b, is so dramatic that considerably greater stringency is required to remain on a particular contour of figs 3.1.2a to 3.1.4b. Similarly figs. 3.1.5a to 3.1.7b's scatter reflects the lack of selectability of constant $(P_{vap}-P_2)$ rather than the imprecision. Notwithstanding this vexing problem, the observed precision is rather remarkable and is most impressive for the most extreme conditions.

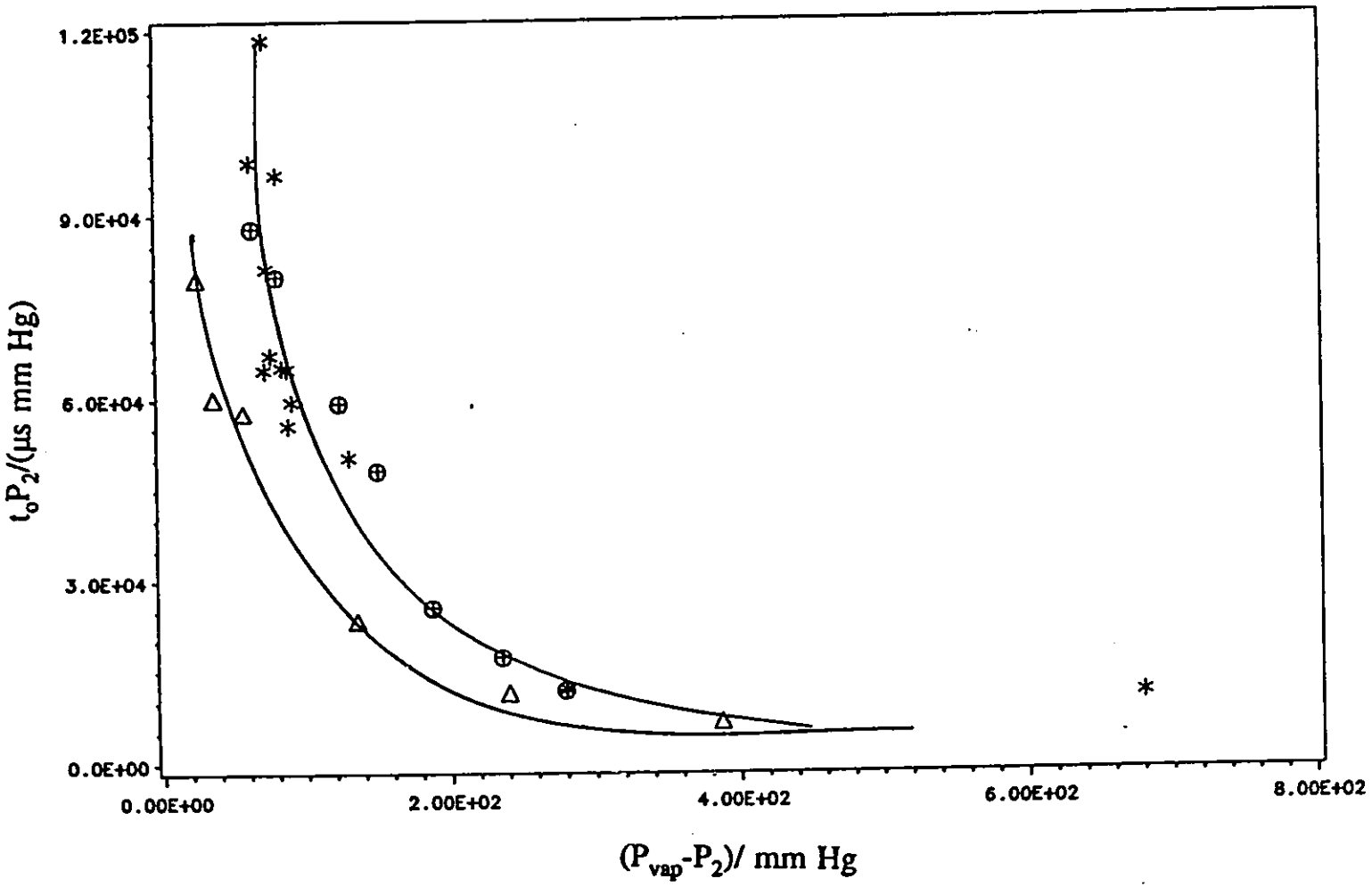

Fig. 3.1.2a t_oP_2 vs $(P_{vap}-P_2)$. △ T=298 ±0.5 K, ⊕ T=301±1 K, and * T=304 ±1 K.

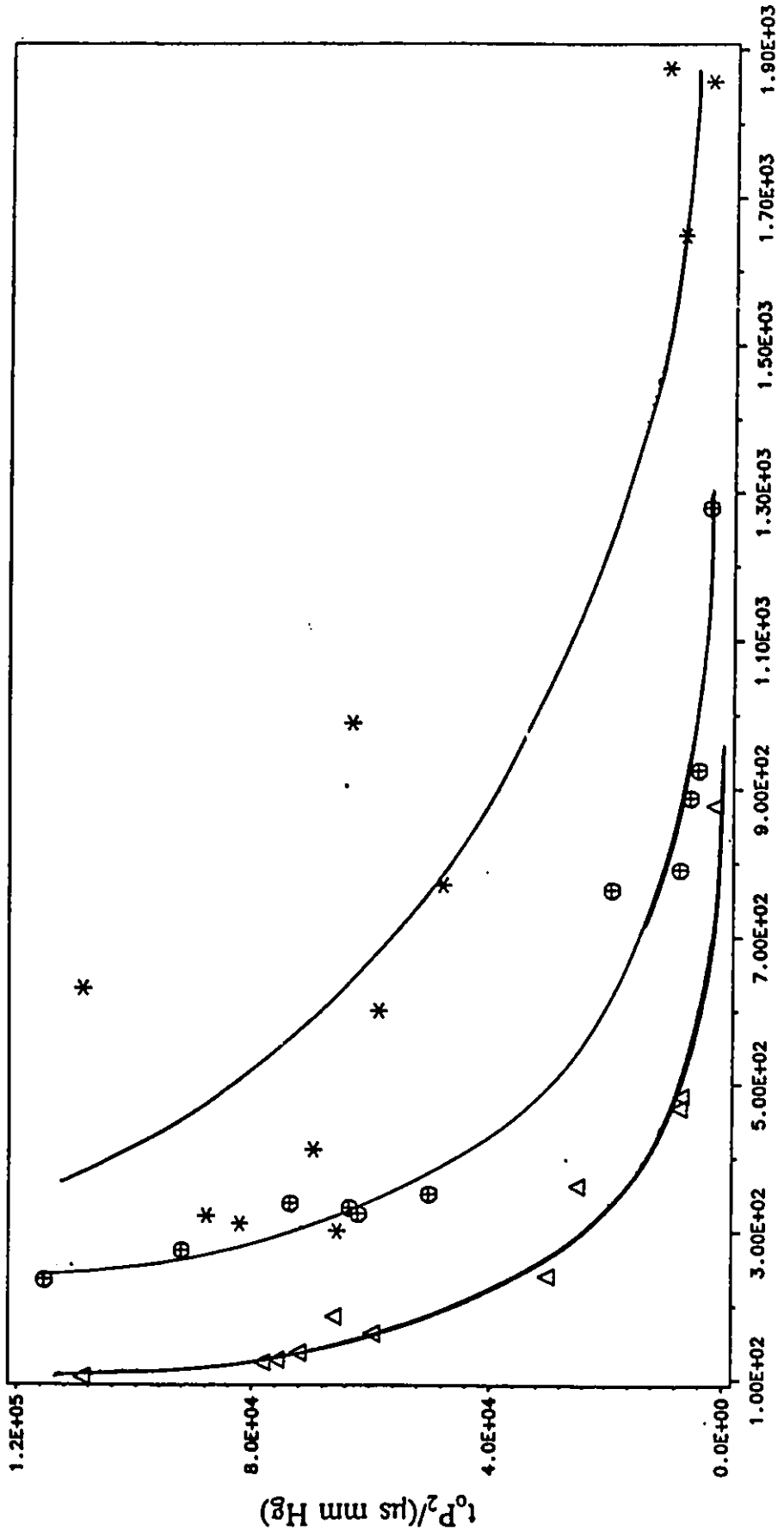

Fig. 3.1.2b t_oP_2 vs $(P_{vap}-P_2)$. ▲ T=308 ±2 K, ⊕ T=315±2 K, and * T=327±6 K.

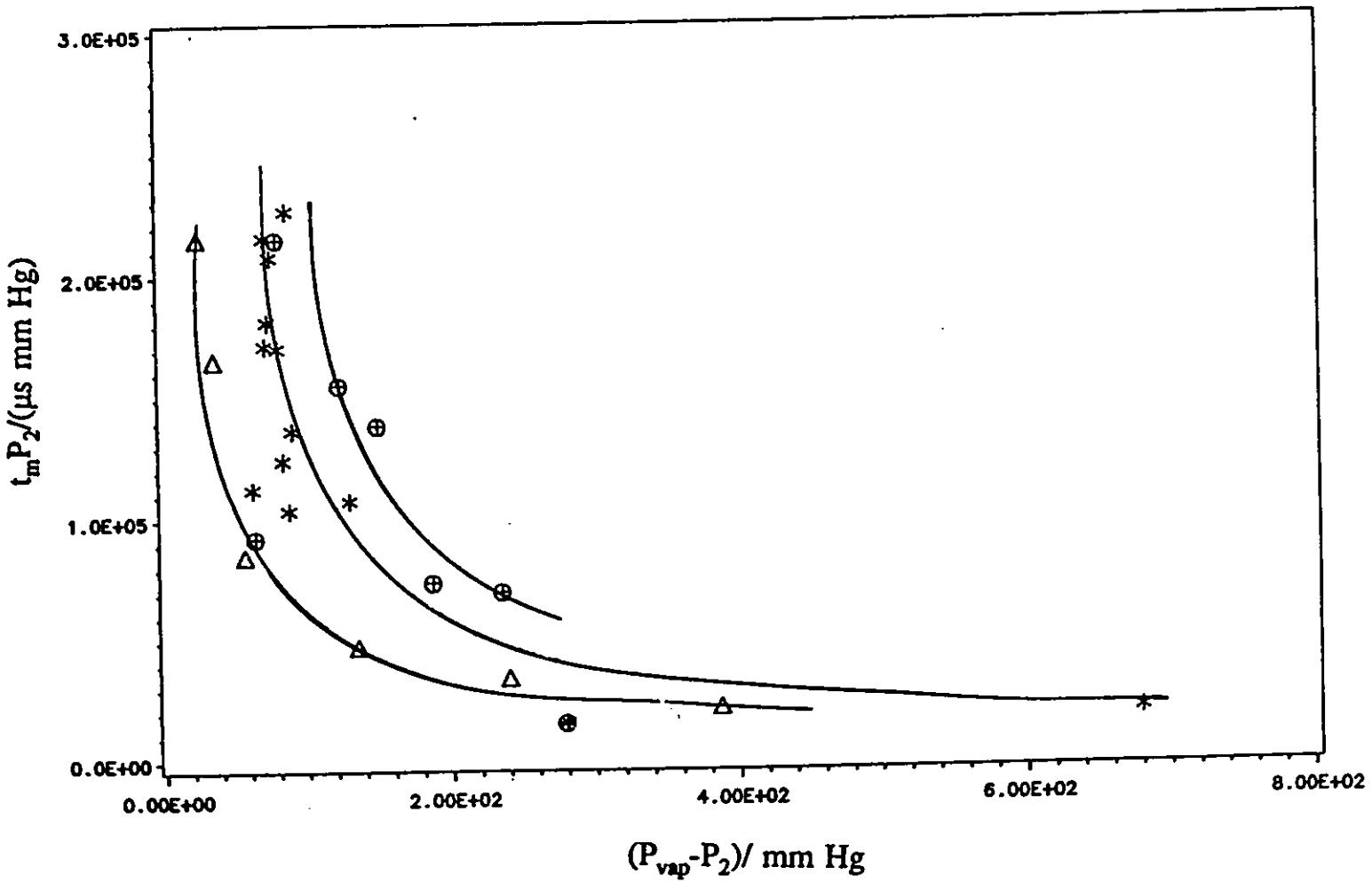

Fig. 3.1.3a $t_m P_2$ vs $(P_{vap}-P_2)$. △ T=298 ±0.5 K, ⊕ T=301±1 K, and * T=304 ±1 K.

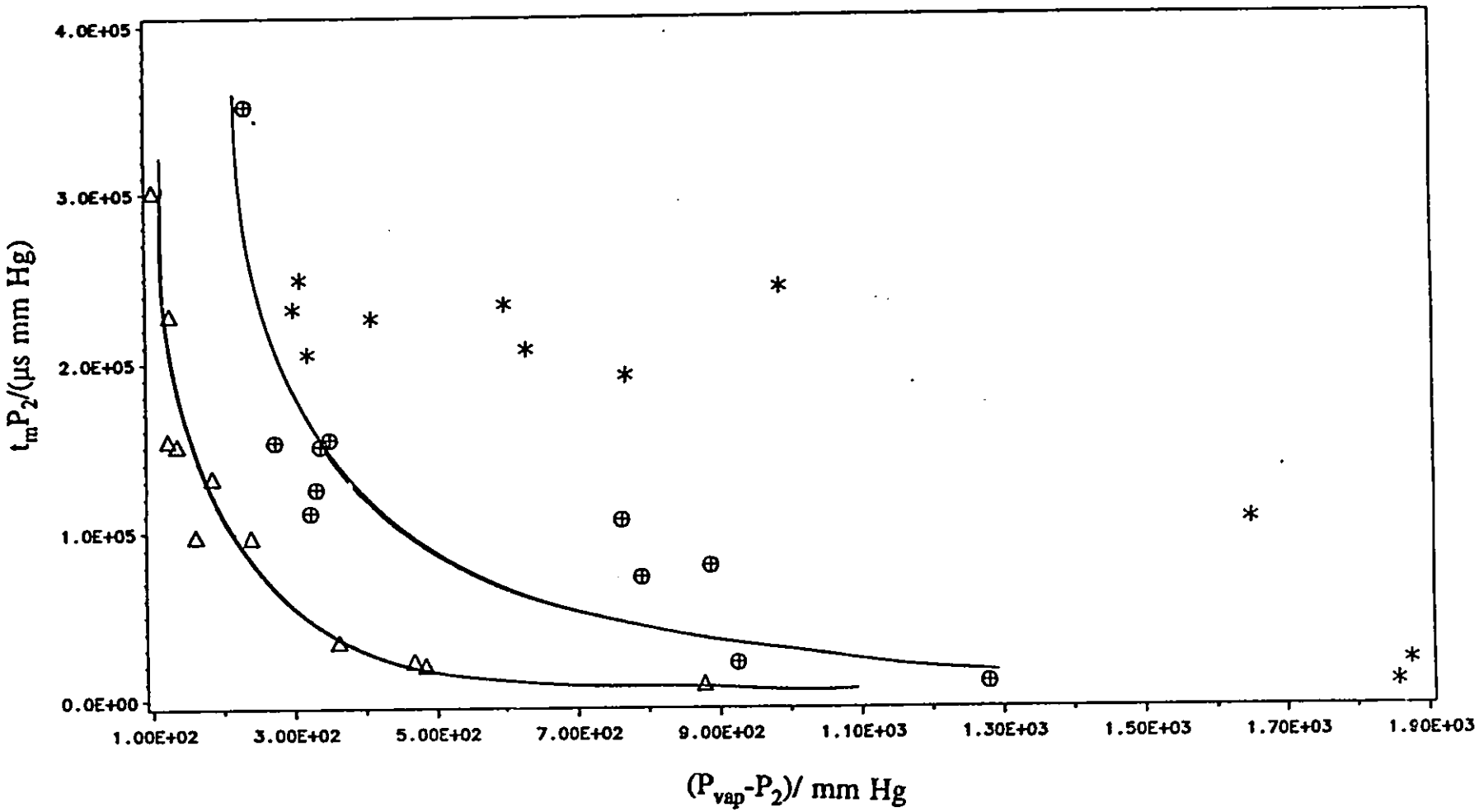

Fig. 3.1.3b $t_m P_2$ vs $(P_{vap}-P_2)$. △ T=308 ±2 K, ⊕ T=315±2 K, and * T=327±6 K.

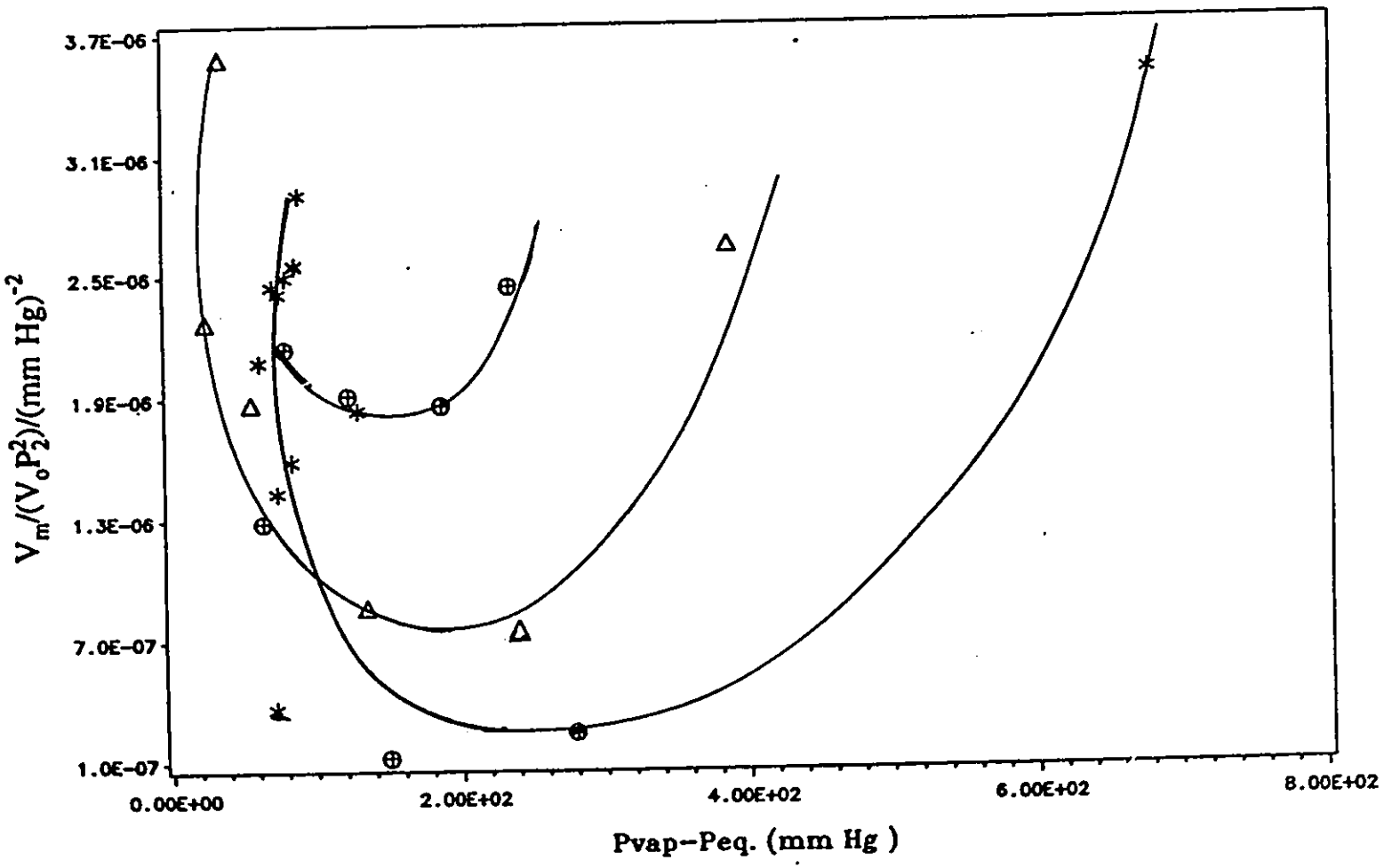

Fig. 3.1.4a $V_m/(V_oP_2^2)$ vs $(P_{vap}-P_2)$. △ T=298 ±0.5 K, ⊕ T=301±1 K, and * T=304 ±1 K.

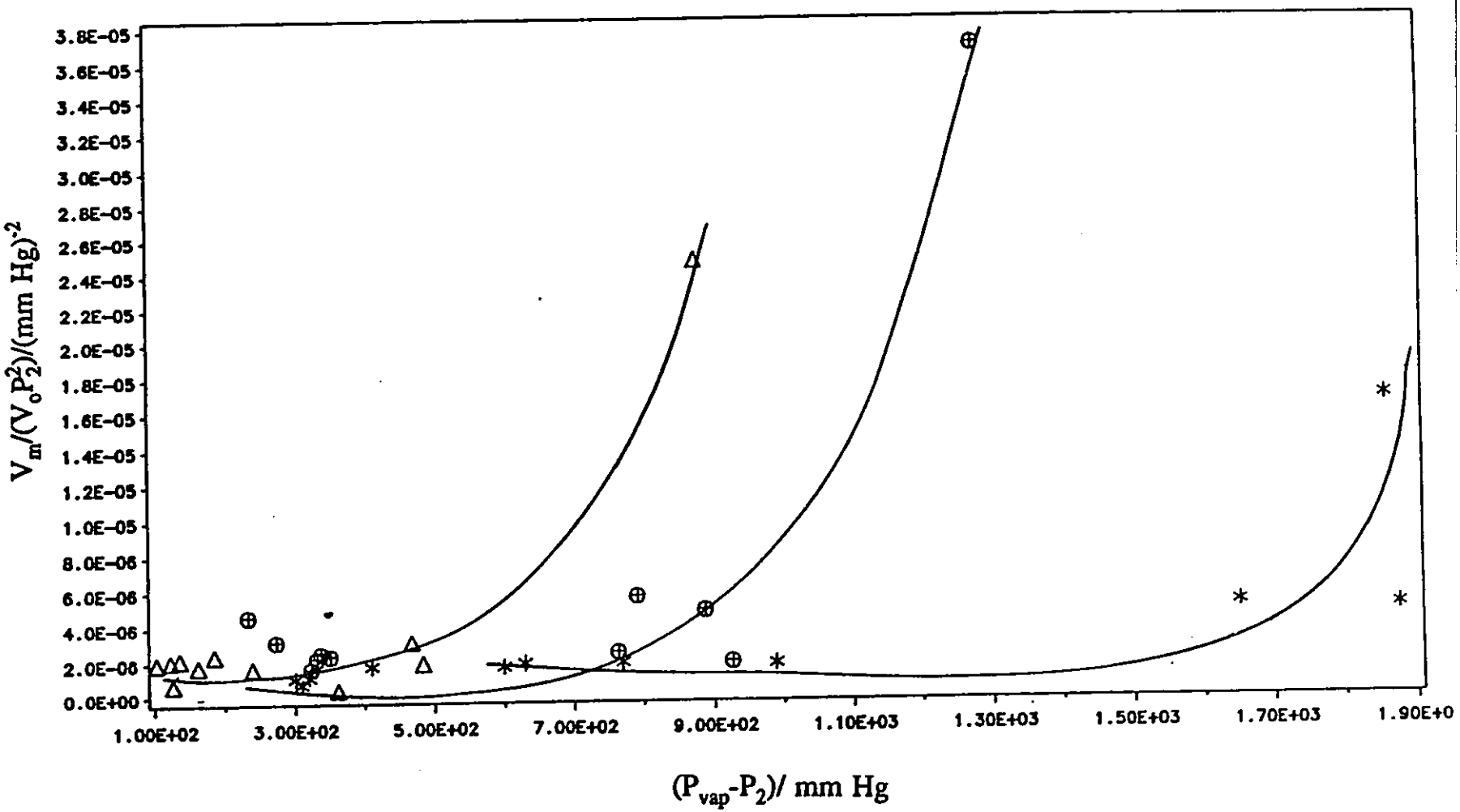

Fig. 3.1.4b $V_m/(V_oP_2^2)$ vs $(P_{vap}-P_2)$. ▵ T=308 ±2 K, ⊕ T=315±2 K, and * T=327±6 K.

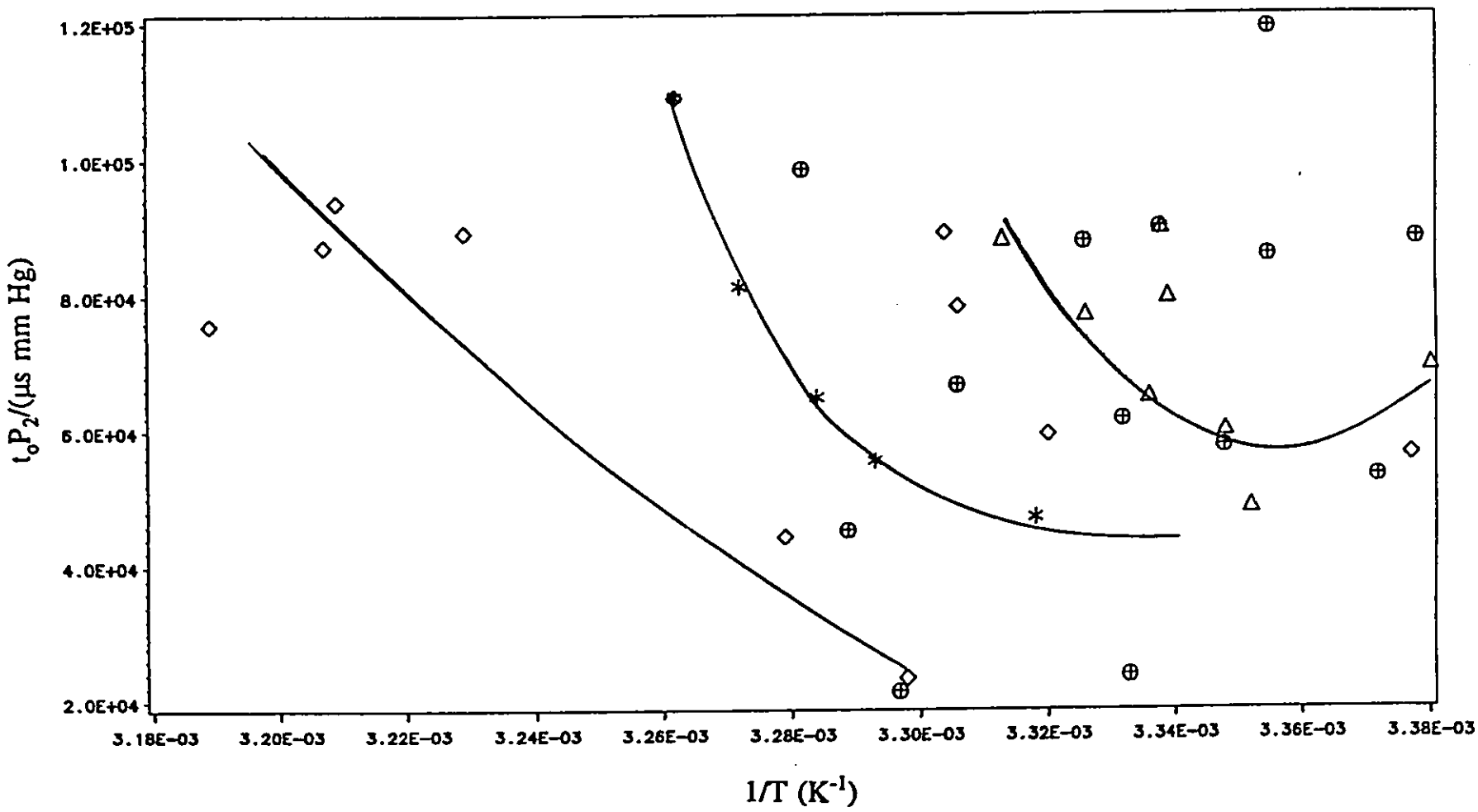

Fig. 3.1.5a t_oP_2 vs 1/T. △ (P_{vap}-P_2)= 32 ±7 mm Hg, ⊕ 50 ±4 mm Hg, * 77 ±7 mm Hg, ◊ 125 ±13 mm Hg.

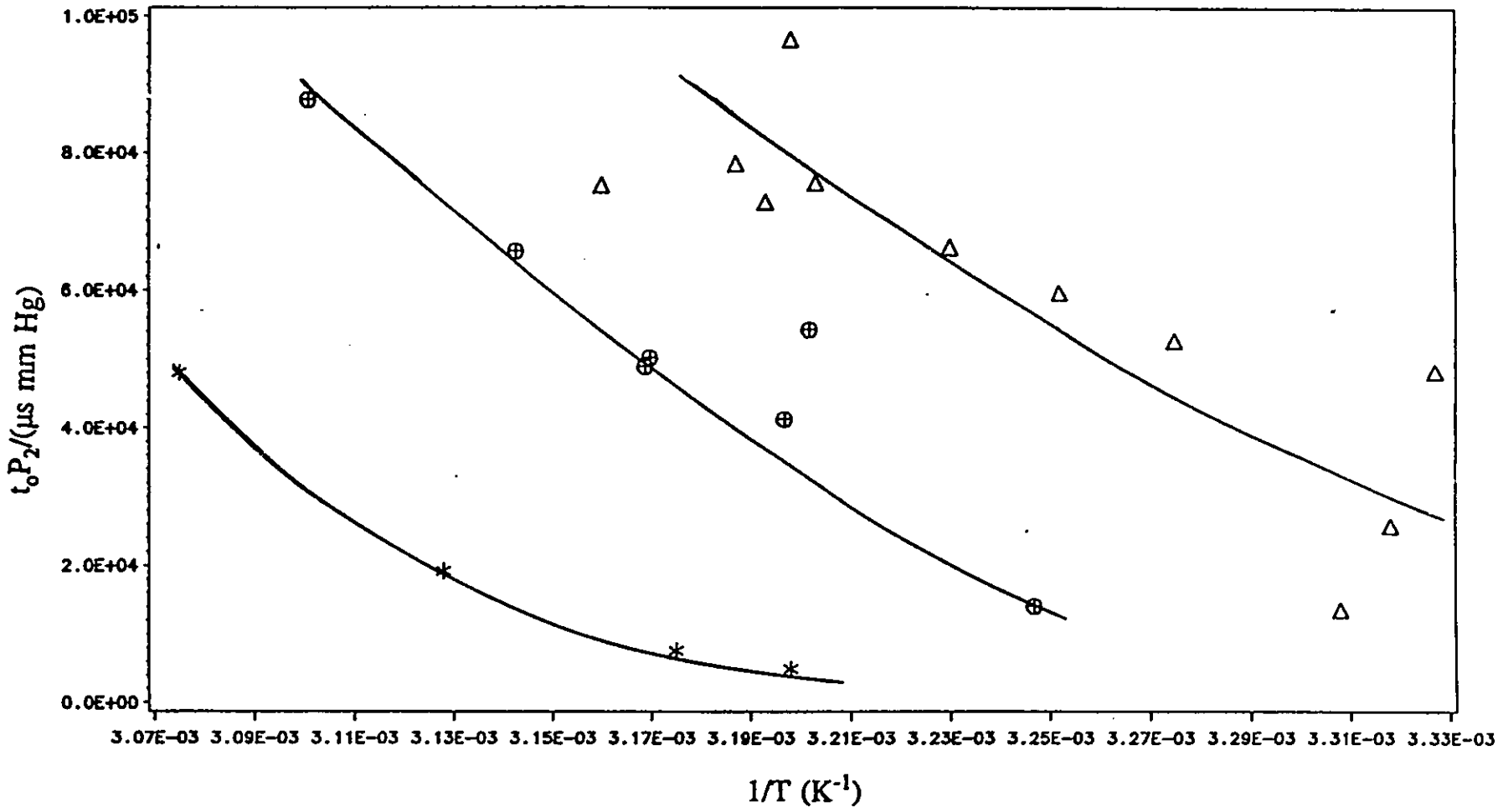

Fig. 3.1.5b t_oP_2 vs 1/T. △ (P_{vap}-P_2)= 174 ±14 mm Hg, ⊕ 335 ±15 mm Hg, * 760 ±35 mm Hg.

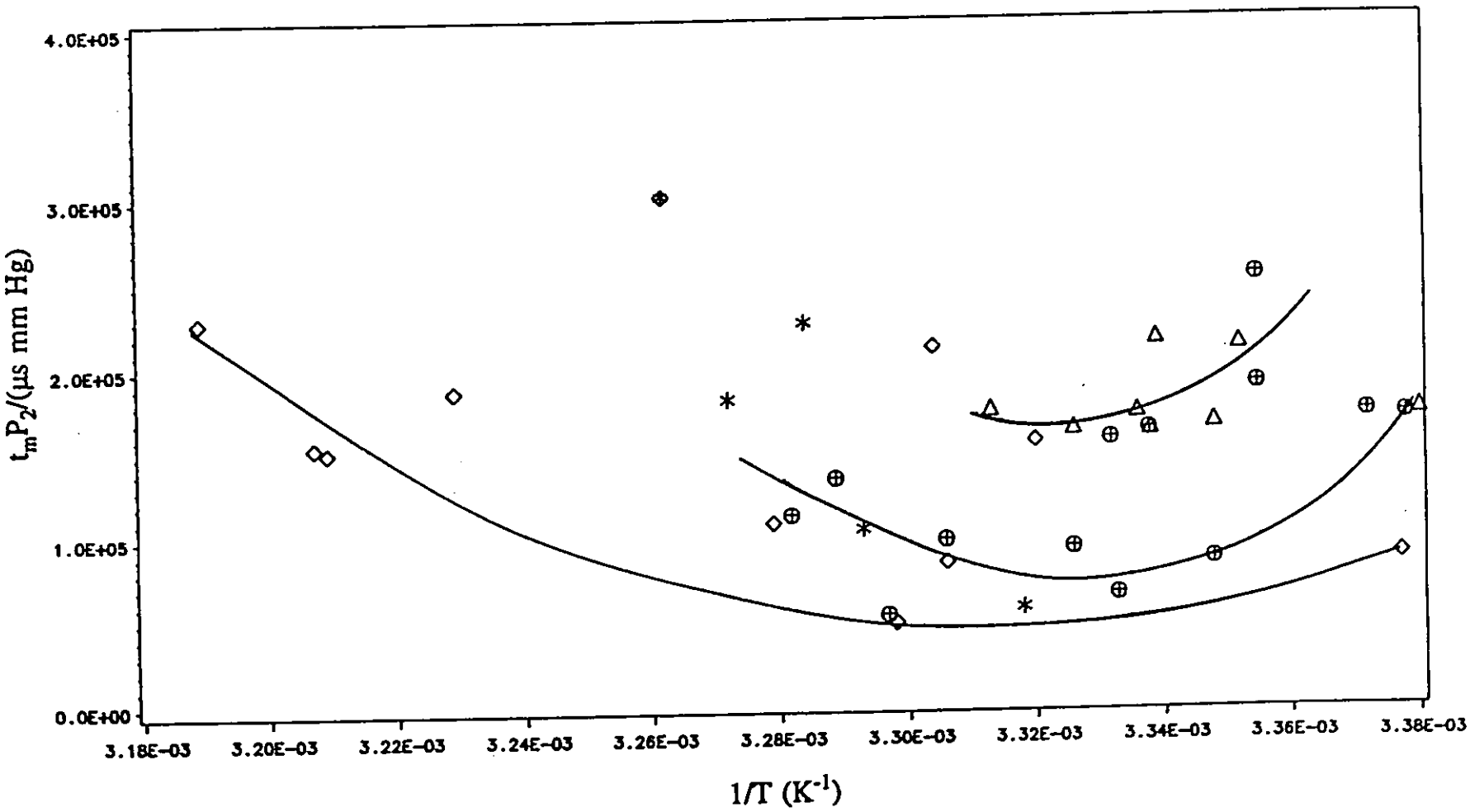

Fig. 3.1.6a t_mP_2 vs 1/T. △ (P_{vap}-P_2)= 32 ±7 mm Hg, ⊕ 50 ±4 mm Hg, * 77 ±7 mm Hg, ◊ 125 ±13 mm Hg.

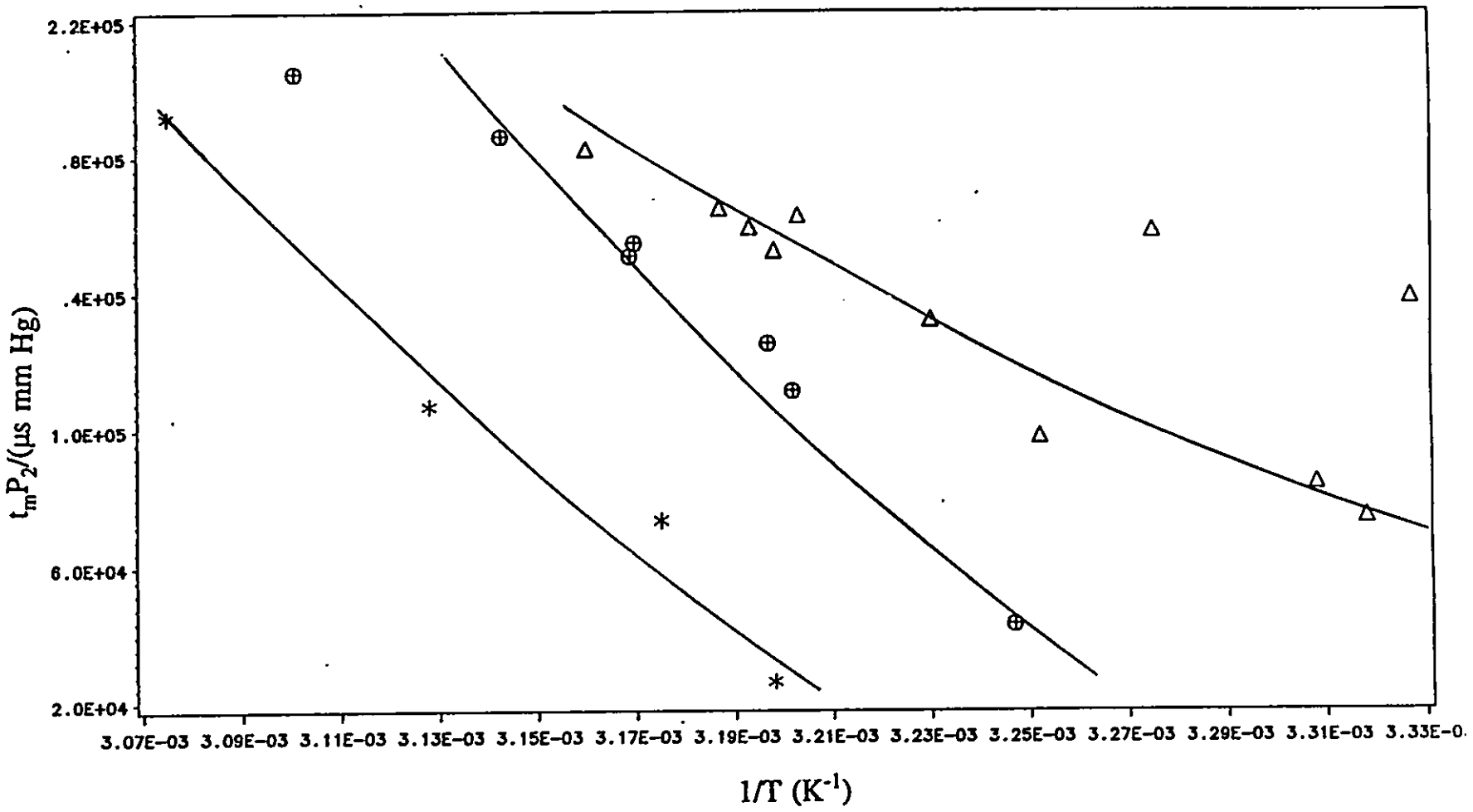

Fig. 3.1.6b t_mP_2 vs 1/T. ▵ (P_{vap}-P_2)= 174 ±14 mm Hg, ⊕ 335 ±15 mm Hg, * 760 ±35 mm Hg.

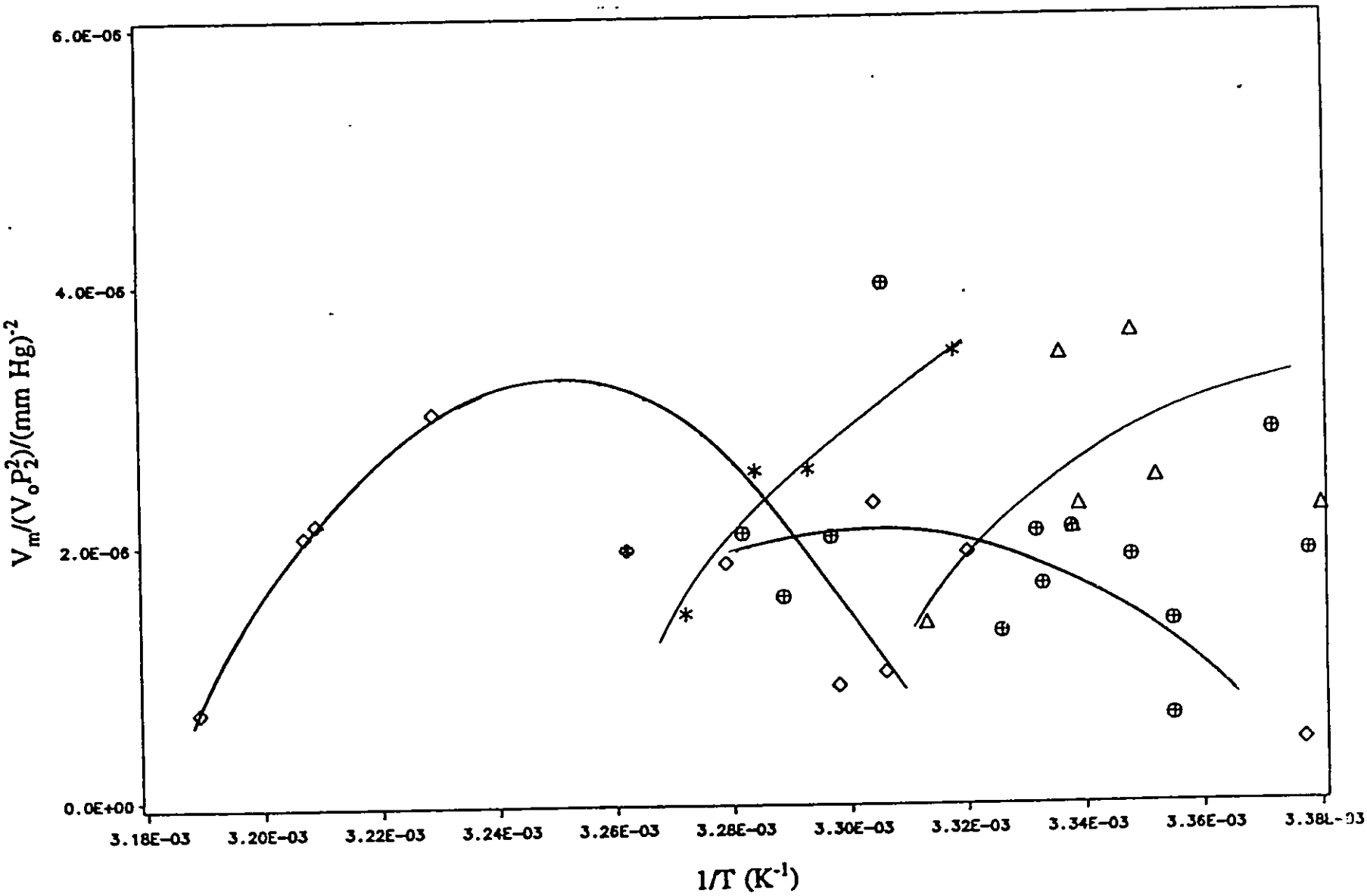

Fig. 3.1.7a $V_m/(V_oP_2^2)$ vs 1/T. △ $(P_{vap}-P_2)$= 32 ±7 mm Hg, ⊕ 50 ±4 mm Hg, * 77 ±7 mm Hg, ◊ 125 ±13 mm Hg.

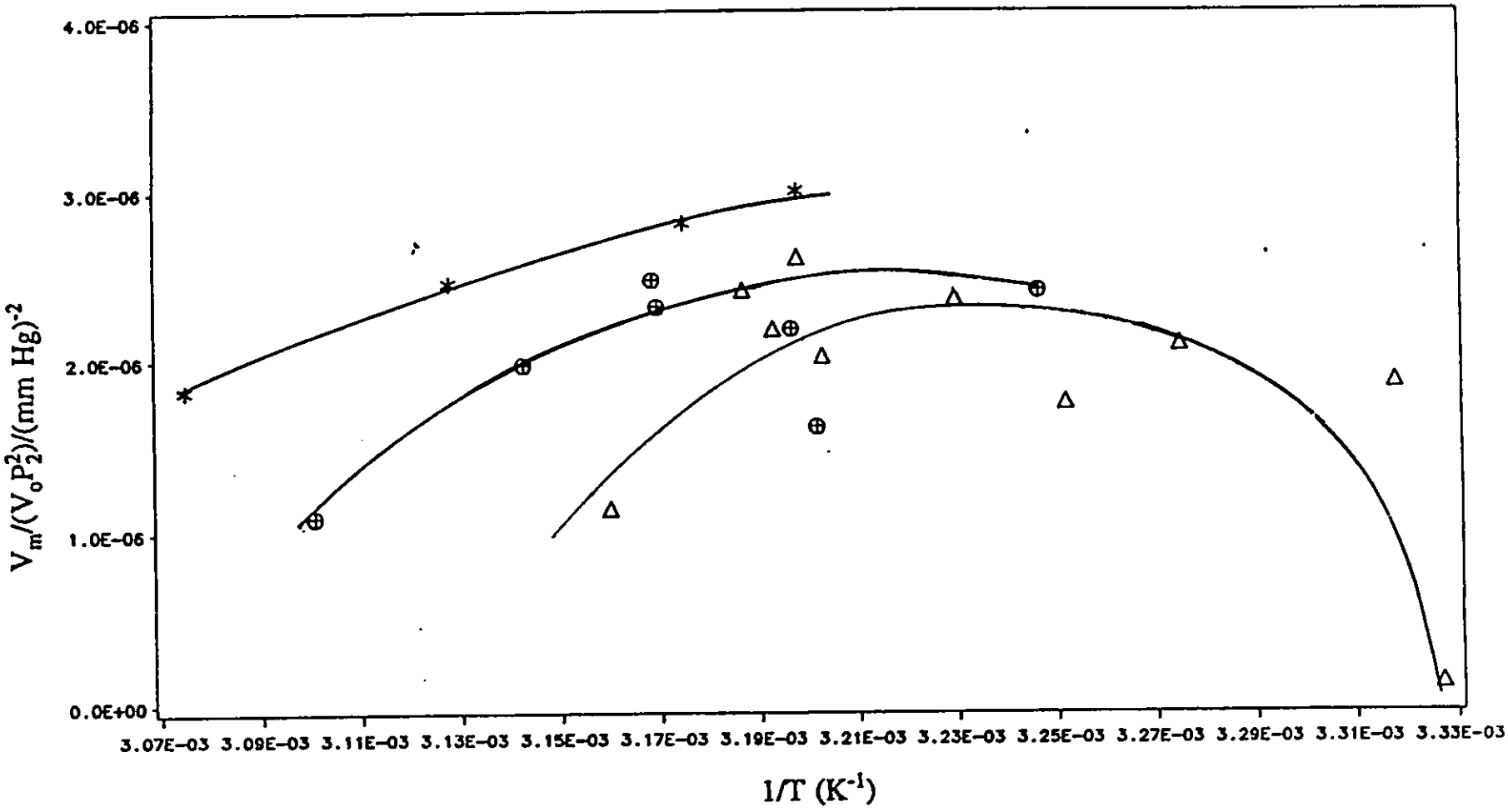

Fig. 3.1.7b $V_m/(V_oP_2^2)$ vs 1/T. Δ $(P_{vap}-P_2)$= 174 ±14 mm Hg, ⊕ 335 ±15 mm Hg, * 760 ±35 mm Hg.

Although we shall discuss the observations below, it is worth noting at this point that the time scales are shortest and the maximum |V| are largest (i.e. the rate "coefficients" of condensation/nucleation are largest) at the lowest temperatures. This is very similar to what one observes for recombination/association of radicals, indicating that the process we are observing is akin to bond formation and lending support to our conclusion that we are observing nucleation of clusters. What is curious and entirely novel in this study is the observation that "rate coefficients" are largest when the initial perturbation ($P_{vap}(T_2)$ - P_2) is largest, i.e. when the gas is least saturated.

3.2 FOURIER ANALYSIS

We have done 190 shock tube experiments at different initial pressures and different shock strengths with different samples. Oscillatory behaviour was observed in these schlieren signals. We surmised in the last chapter that these oscillations are caused by cluster formation, stabilization or dissociation processes. There are still many questions which need to be answered. Do these signals have some common characteristics? Do they have perfectly well defined periods? How many fundamental frequencies does each signal have? What is the difference in the fundamental frequencies from signal to signal? What do these oscillations mean? In order to quantify this oscillation, we must use an "objective" method of analysis such as the Fourier transform.

The Fourier transform has found many applications in almost all areas of science. In

chemistry infrared Fourier transform spectroscopy, fast Fourier transform nuclear magnetic resonance spectroscopy[123], fast Fourier transform mass spectroscopy[124] and fast Fourier transform atomic spectroscopy[125] are common. Fourier transforms also find use in the study of chaotic behaviour, as one of the ways to identify and to characterize a dynamical regime[126,127]. In these areas the procedure for doing Fourier transforms has developed rapidly. In this section first the Fourier transform will be discussed in general, then the method which we used to do the Fourier transform will be discussed. In the third part of this section the spectrum of the schlieren signal will be discussed and the relation of the fundamental frequency of the oscillation signal with other physical parameters will be given.

3.2.1 The Discrete Fourier Transform

There are two equivalent ways of describing the evolution of a process. One way treats the process as a series of events, one following another, either in time or in space. The other way is to represent it as a spectrum, where the amplitude is a function of frequency. The properties of the Fourier transform allow one to examine a function or waveform from the perspective of both the time and frequency domains. There are many studies concerning the properties and applications of Fourier transforms[128,129,130]. The following is a brief discussion of the relationship and difference between the continuous and the discrete Fourier transform. The correct way of doing the Fourier transform is then considered on this basis.

The basic idea of the Fourier transform[128] is that any periodic function can be expressed as the sum of a series of sines and cosines of the same period. For functions defined over an infinite interval, and with no periodicity, the summation of the harmonic series must be replaced by an integral of a continuum of trigonometric functions. The Fourier transform is defined as

$$H(f) = \int_{-\infty}^{\infty} h(t)\, e^{-j2\pi ft} dt \tag{3.2}$$

where $j=\sqrt{(-1)}$. If the integral exists for every value of the frequency, f, the above equation defines H(f), the Fourier transform of h(t). Typically h(t) is termed a function of the variable time, and H(f) is termed a function of the variable frequency. In general, the Fourier transform is a complex quantity:

$$H(f) = R(f) + jI(f) = |H(f)|\, e^{j\theta(f)} \tag{3.3}$$

where R(f) is the real part of the Fourier transform, and I(f) is the imaginary part of the Fourier transform. |H(f)| is the amplitude of the Fourier spectrum of h(t) and is given by $(R^2(f)+I^2(f))^{1/2}$; θ(f) is the phase angle of the Fourier transform and is given by $\tan^{-1}$ [I(f)/R(f)].

The inverse Fourier transform is defined as

$$h(t) = \int_{-\infty}^{\infty} H(f)\, e^{j2\pi ft} df \quad . \tag{3.4}$$

The inverse transform allows the determination of the function of time from its transform. Unfortunately, the process of Fourier transformation is tedious and very limited applications exist. The advent of the digital computer and the invention of the Fast Fourier transform (FFT) algorithm (which reduces the computational labour significantly) have made the FT easily accessible. Since computers are finite machines, any desired computation can only use a finite number of operations. No computer can deal with real value functions of real numbers. Any such function must be sampled in order to be represented in a computer. Instead of having h(t) at all t, we have only the value of h at a finite number of points $h(t_1)$, $h(t_2)$, $h(t_3)$,……, $h(t_n)$. This means the function must first be sampled and truncated into a finitely sampled function. We shall see that the difference between the discrete FT and the continuous FT arises from sampling and truncation.

The discrete Fourier transform is defined as

$$G\left(\frac{n}{NT}\right) = \sum_{k=0}^{N-1} g(kT)\, e^{-j2\pi nk/N} \qquad n=0,1,\cdots,N-1 \tag{3.5}$$

in which N is the number of data points sampled in the original signal, and represented by N discrete values. T is the sampling interval. The equation is the desired discrete Fourier transform which relates N samples of time and N samples of frequency by means of the continuous Fourier transform. One important difference between the continuous and discrete Fourier transform is that the discrete Fourier transform requires both the time and frequency domain function to be periodic. That the period of G(n/NT) is defined by

N samples can be seen from

$$G\left(\frac{n+N}{NT}\right)=\sum_{k=0}^{N-1} g(kT)\, e^{-j2\pi (n+N)\, k/N}$$
$$=\sum_{k=0}^{N-1} g(kT)\, e^{-j\pi nk/N} e^{j2\pi k}$$

$$=\sum_{k=0}^{N-1} g(kT)\, e^{-j2\pi nk/N} \qquad (3.6)$$
$$=G\left(\frac{n}{NT}\right)$$

where $e^{-j2\pi k}=\cos(2\pi k)-j\sin(2\pi k)=1$ has been used.

The discrete inverse Fourier transform is given by

$$g(kt)=\frac{1}{N}\sum_{n=0}^{N-1} G\left(\frac{n}{NT}\right) e^{j2\pi nk/N} \qquad (3.7)$$

Similar to the discrete Fourier transform the discrete inverse Fourier transform exhibits periodicity. The period is defined by N samples of g(kt). This property results from the periodic nature of $e^{j2\pi nk/N}$.

$$g((N+k)\,t)=\frac{1}{N}\sum_{n=0}^{N-1} G\left(\frac{n}{NT}\right) e^{j2\pi n(N+k)/N}$$
$$=\frac{1}{N}\sum_{n=0}^{N-1} G\left(\frac{n}{NT}\right) e^{j2\pi nk/N} \qquad (3.8)$$
$$=g(kt)$$

Both the forward and reverse Fourier transforms take N samples of the time and frequency functions as the periods of periodic functions.

Now we briefly consider the errors caused by both sampling and truncation in the discrete Fourier transform. First, we consider the error caused by sampling. For a band-limited signal, (where the signal is zero for $f > f_c$), the sampling frequency must satisfy the Nyquist theorem, which states that a signal must be sampled at a rate that is at least twice the highest frequency component, f_c, in that signal in order for the sample values to exactly describe the original signal. If the signal is under-sampled, then the higher frequencies will fold over into the lower frequency region. This is termed aliasing. The result of aliasing is that the information on higher frequencies is missed. If the signal is not band-limited, in which case aliasing always exists, aliasing error can be reduced to an acceptable level only by increasing the sampling frequency. The frequency function G(n/NT) is a periodic function in the discrete Fourier transform. If the sampling frequency is less than $2f_c$, two neighbouring periods of frequency function will overlap each other, and then aliasing takes place in the discrete Fourier transform.

Second, we discuss the error caused by truncation. If a periodic function is truncated exactly at the end of a period or a multiple of the period then there is no error caused by truncation. The effect of truncation at a point other than a multiple of the period is to create a periodic function with sharp discontinuities. This is because the discrete Fourier transform requires both the time- and frequency-domain function to be periodic, and the N-sample data input to the discrete Fourier transform algorithm is assumed to span one period. Intuitively, we expect the introduction of these sharp changes in the time domain to result in additional frequency components in the frequency domain. If the extent of a

periodic signal in the time domain were infinite the frequency function would be a series of impulses. After truncation in the time domain the impulses in the frequency domain are replaced by a continuous function of frequency with local maxima centred at the original impulses and a series of other peaks that are termed sidelobes. These side lobes are responsible for the additional frequency components. This effect is termed leakage and is inherent in the discrete Fourier transform because of the necessary truncation in the time domain. To reduce leakage, for those cases where it is impossible to choose NT sufficiently large or where the period of a periodic function is not known, it is necessary to employ a data weighting function or data window function that is associated with a smaller magnitude of side lobes. If we simply truncate a signal then that is the same as using a rectangular window function[129]. It is given by

$$\begin{aligned} w_R(t) &= 1 \qquad |t| \le \frac{T_o}{2} \\ &= 0 \qquad |t| > \frac{T_o}{2} \end{aligned} \tag{3.9}$$

and its Fourier transform is given by

$$w_R(f) = \frac{T_o \sin(\pi f T_o)}{\pi f T_o} \tag{3.10}$$

The amplitudes of the side lobes of a rectangular window function in the frequency domain are large. A catalog and comparison of FFT window functions has been given by E. O. Brigham[128]. The one often used is called the Hanning window function[128]. It is given by

$$
\begin{aligned}
w_H(t) &= \cos^2\left(\frac{\pi t}{T_o}\right) \\
&= \frac{1}{2}\left(1+\cos\left(\frac{2\pi t}{T_o}\right)\right) \qquad |t| \le \frac{T_o}{2} \\
&= 0 \qquad\qquad\qquad\qquad\qquad |t| > \frac{T_o}{2}
\end{aligned}
\tag{3.11}
$$

Its Fourier transform is given by

$$
w_H(f) = \frac{T_o}{2}\frac{\sin(\pi f T_o)}{\pi f T_o[1-(fT_o)^2]} \tag{3.12}
$$

When the Hanning function is applied before an FFT is performed, the two ends of the signal are suppressed (multiplied by a small number). The discontinuity of h(t) in the time domain otherwise caused by a rectangular truncation is thus decreased. The highest side lobe level is -32 dB compared with -13 dB for the highest side lobe associated with a rectangular truncation[129]. The reduced side lobes or reduced leakage is achieved at the expense of main-lobe bandwidth i.e. with an artificial broadening, or decreased spectral resolution.

The Fourier transform is usually represented graphically by means of spectra. There are two methods of representing a transform: the cos-sin method (in which the cosine transform and the sine transform are plotted), and the amplitude-phase method (in which the amplitude and phase are plotted). An alternative to the amplitude spectrum is the power spectrum which is the graph representing $|H(f)|^2$ as a function of the frequency.

The appearance of the power spectrum depends on the way in which the signal, x(t), evolves over time. The power of the Fourier transform lies in the fact that it can reveal properties of the signal which would otherwise remain undetected. For a simple periodic signal the power spectrum is only composed of a sharp peak at a certain frequency and some peaks at its overtones. For a quasi-periodic signal the power spectrum gives fundamental frequencies and their overtones and combinations. For an aperiodic signal the power spectrum is continuous. A continuous spectrum cannot be attributed automatically to an aperiodic signal, however, because this is also the appearance of the spectrum of a quasi-periodic signal containing a very large number of frequencies. It is more complicated since coloured noise also has a continuous power spectrum. The power spectrum of white noise (which is a mixture of signals of all frequencies with random amplitude and phase angle) is independent of frequency.

To sum up, the important concept that the discrete Fourier transform implies is periodicity in both the time and frequency domains. The difference between the discrete and the continuous Fourier transform arises because the discrete Fourier transform requires sampling and truncation. Therefore, great care must be taken in both of these steps. For equivalence of the discrete and continuous transforms we require that (1) the time function h(t) must be periodic, (2) h(t) must be band-limited, (3) the sampling rate must satisfy the Nyquist Theorem, and (4) the truncation function x(t) must be non-zero over exactly one period (or integral multiple of periods) of h(t). Otherwise, the discrete Fourier transform only approximates the continuous Fourier transform. For a signal which is not

band-limited aliasing errors can be reduced to an acceptable range by choosing a sample interval, T, sufficiently small. To reduce the leakage a data window function should be used. The validity of this approximation is strictly a function of the waveform being analyzed.

3.2.2 The Fourier Transform of the Schlieren Signal

In this part the method of performing a Fourier transform on the oscillatory schlieren signal is discussed. The following Fourier transforms were performed using the IMSL routine FFTRC and some results are checked using the commercially available FOURIER PERSPECTIVE II software .

A typical schlieren signal is shown in fig. 3.2.1 after truncation with a rectangular window essentially chopping off the part associated with the passage of the uninteresting shock front. In the schlieren signal the quasi-periodic oscillation is superimposed on the exponentially (or double exponentially) decaying curve. Since the Fourier transform is a linear transform[129], i.e. the transform of [f(x) +g(x)] equals the sum of the Fourier transform of f(x) and the Fourier transform of g(x), the amplitude of the power spectrum of this signal must be the sum of the transform of the oscillatory signal and the transform of the exponentially decaying curve. The aim of performing the transform is to find the fundamental frequencies and the corresponding amplitudes of the oscillatory signal. The existence of the exponentially decaying signal prevents us from finding the true

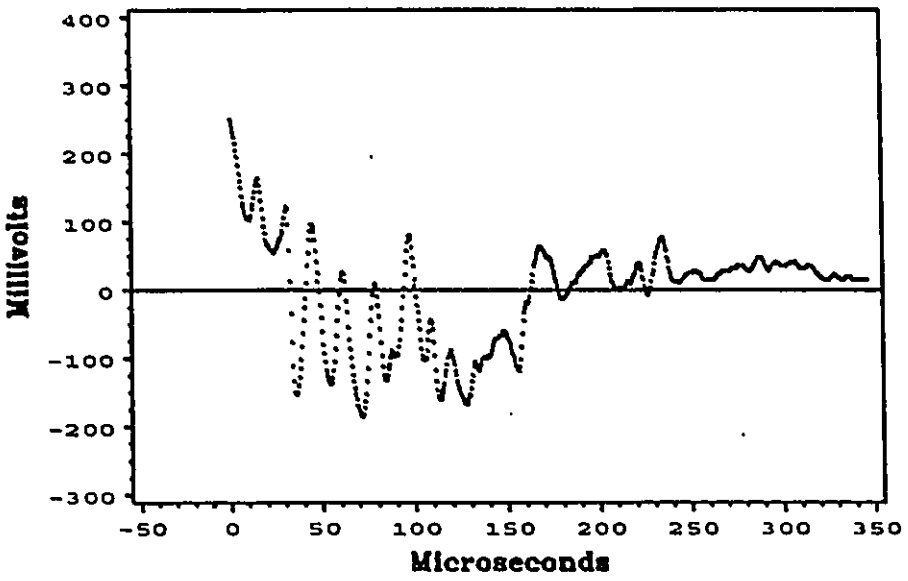

Fig. 3.2.1 The schlieren signal for EXP. 122 (see fig. 2.3.2 for experimental conditions).

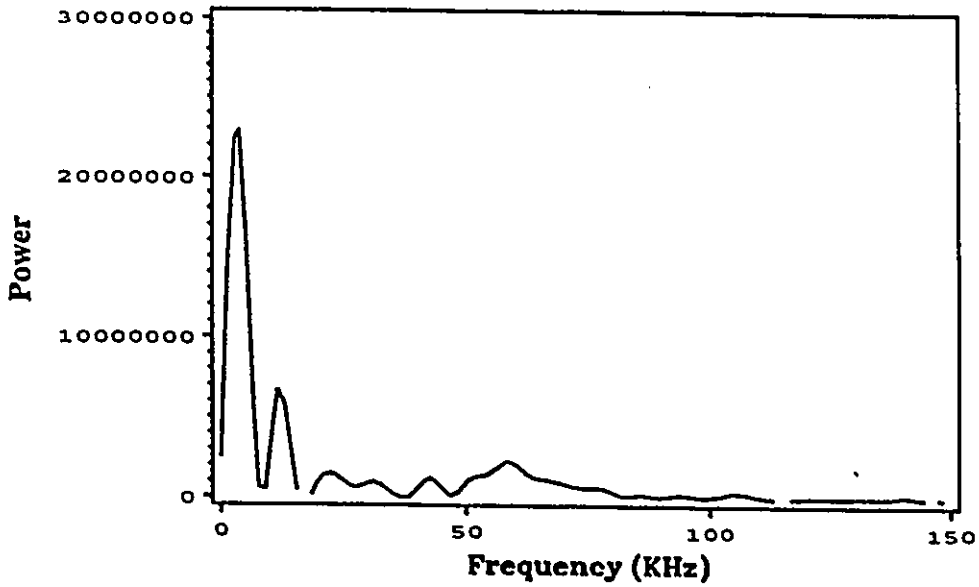

Fig. 3.2.1a The power spectrum for signal in fig. 3.2.1.

magnitude of each frequency component[130]. This is shown in fig. 3.2.1a. The power spectrum was calculated with the data of the signal shown in fig. 3.2.1. The 5 kHz frequency component has the largest amplitude, the 8 kHz one the second largest, and the 55 kHz one the third largest. This result is meaningless however, because it is the combination of the waveform transforms.

Fig. 3.2.1b shows the signal of fig.3.2.1 after the application of a Hanning window. We see that the two ends are reduced to zero. Its Fourier transform is shown in fig. 3.2.1c. Comparing with 3.2.1a we find that number of peaks in fig. 3.2.1c has decreased. The side lobes caused by truncation in fig 3.2.1a are reduced in fig. 3.2.1c. The problem in fig. 3.2.1c is that the amplitude of the zero frequency component is too high. We shall solve this problem later.

Figure 3.2.2 shows the same signal after truncating the first 24 data points. This means that the weight of the exponential decay is reduced in the signal. Its spectrum is shown in figure 3.2.2a. The relative magnitude of the frequency components is quite different than in figure 3.2.1c. The relative height of the 55 kHz component is increased compared with the height of the 19 kHz one. Nevertheless, because the amplitude of the zero frequency, i.e. the D.C. component, is too large, other frequencies cannot be seen in the spectrum. (This is the same problem as in fig. 3.2.1c). The next step is to decrease the D.C. component. The simple way is to shift the whole signal until the base line passes through the middle of the signal. This operation is based on the linearity of the Fourier

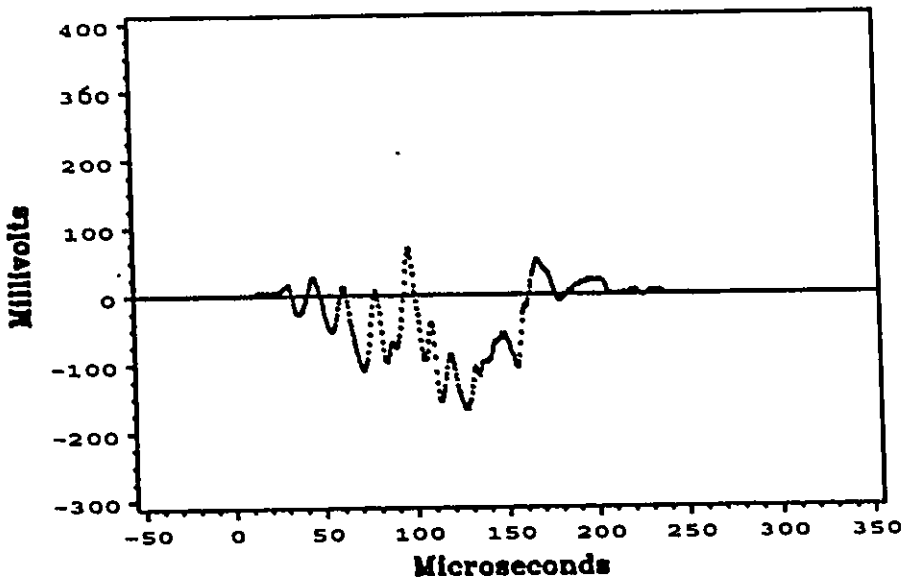

Fig. 3.2.1b The signal shown in fig 3.2.1 after the application of the Hanning window.

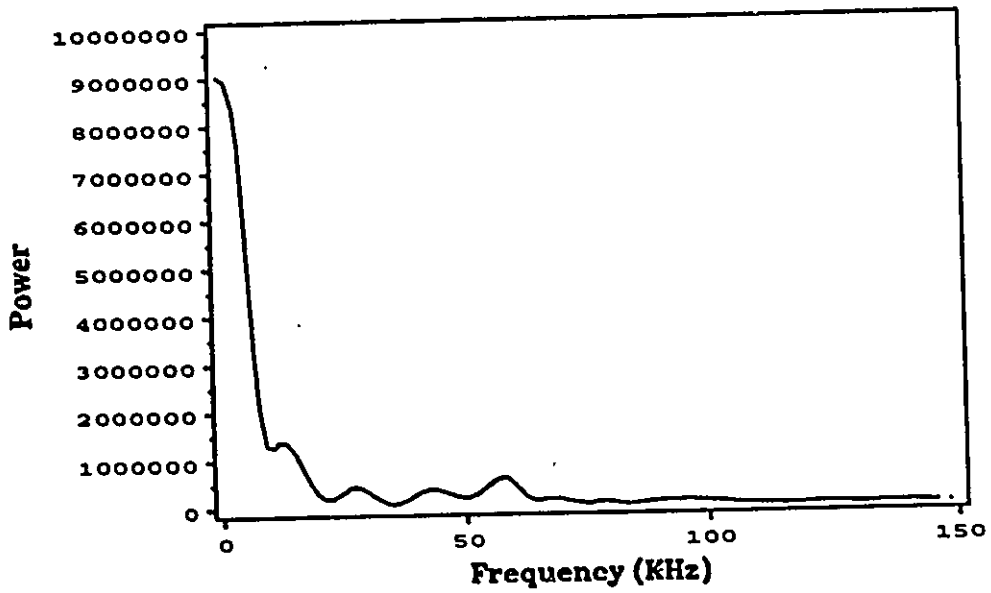

Fig. 3.2.1c The power spectrum for the signal in fig. 3.2.1b.

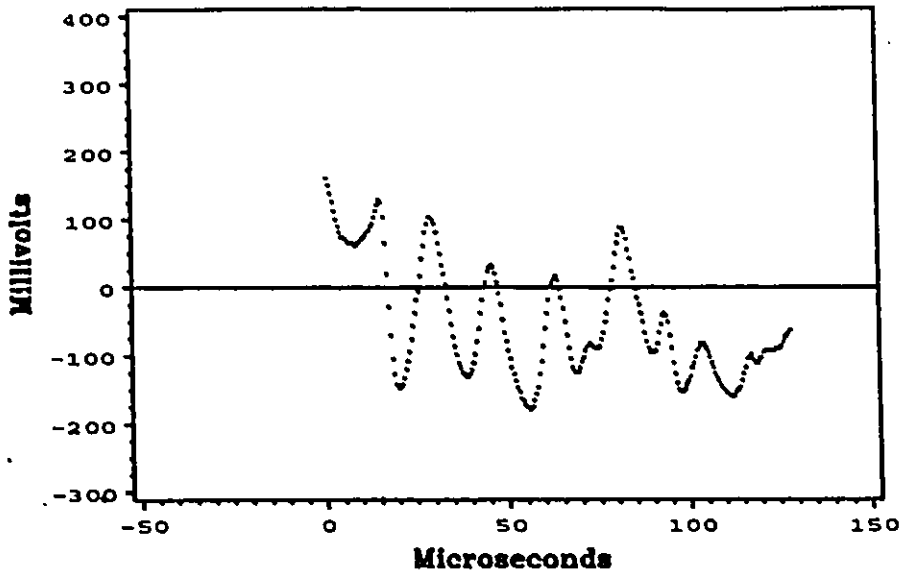

Fig. 3.2.2 Part of the shlieren signal of EXP.122.

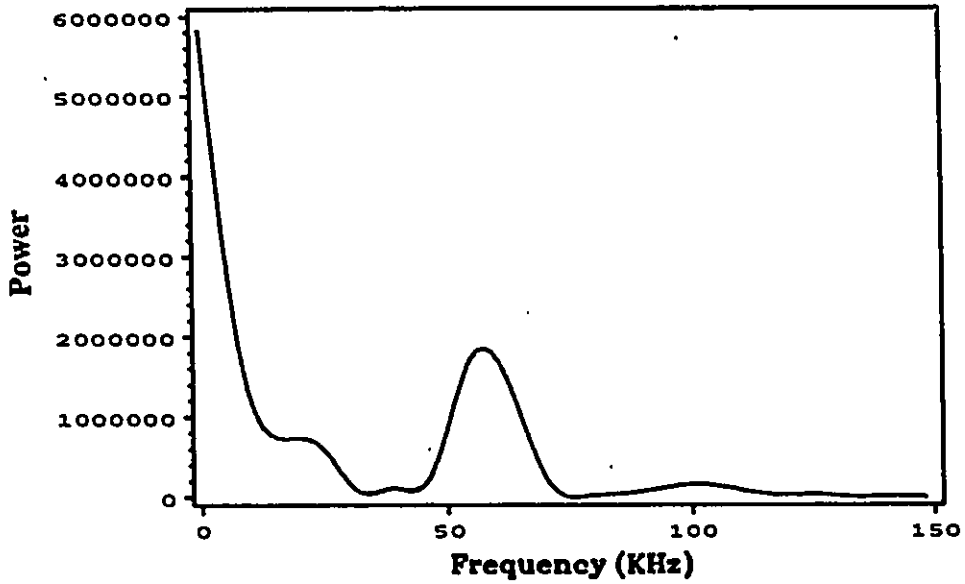

Fig. 3.2.2a The power spectrum for fig. 3.2.2 after the application of the Hanning weighting function.

transform. Figure 3.2.3 shows the signal after shifting. Its power spectrum is shown in figure 3.2.3a in which the D.C component is dramatically reduced. The largest peak is now at 19 kHz. The second largest is at 53 kHz. There are other peaks at 40, 80, 104 and 142 kHz. We do not know if these are side lobes or true frequency components or harmonics of 19 and 53 kHz. The effect of the exponentially decaying curve still exists in figure 3.2.3. The fundamental frequencies still cannot be assigned.

The Hanning window function was employed to suppress end effects and decrease the effect of the exponentially decaying curve. The signal after application of the Hanning weighting is shown in figure 3.2.3b. The two ends are decreased to zero. The exponential decay is also suppressed. The power spectrum of the signal after the Hanning weighting is shown in figure 3.2.3c. There is a large change in the relative amplitudes for each frequency compared with figure 3.2.3a. The frequency component at 53 kHz now has the largest amplitude. The frequency at 19 kHz becomes the second most important one. There are four small components at 40 , 80, 104 and 123 kHz. Comparing the amplitudes of these frequency components in both figures 3.2.3a and 3.2.3c, we can see that as the amplitude of the 53 kHz peak becomes the most pronounced one the peaks at 104 and 123 kHz also increase relative to the other peaks. As the peak at 19 kHz decreases relative to the peak at 53 kHz the peaks at 40 and 80 kHz in figure 3.2.3c also decrease. The peak at 142 kHz disappears. From these observations we can conclude that the peaks at 19 and 53 kHz represent two fundamental frequencies, f_1 and f_2. The component at 104 kHz is an overtone of the fundamental frequency, f_2, while frequencies 40, 80 and 142

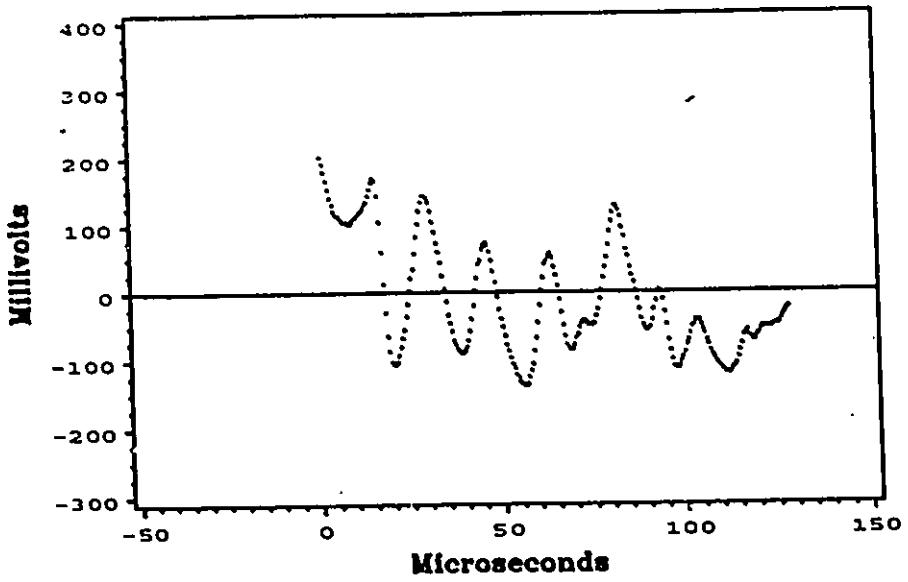

Fig. 3.2.3 Part of the schlieren signal of EXP.122

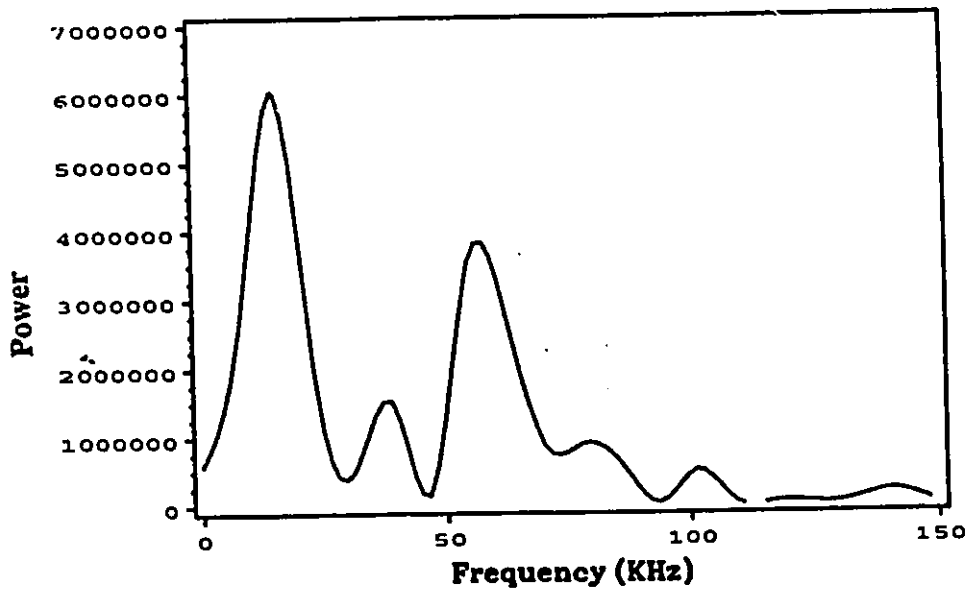

Fig. 3.2.3a The power spectrum for fig. 3.2.3.

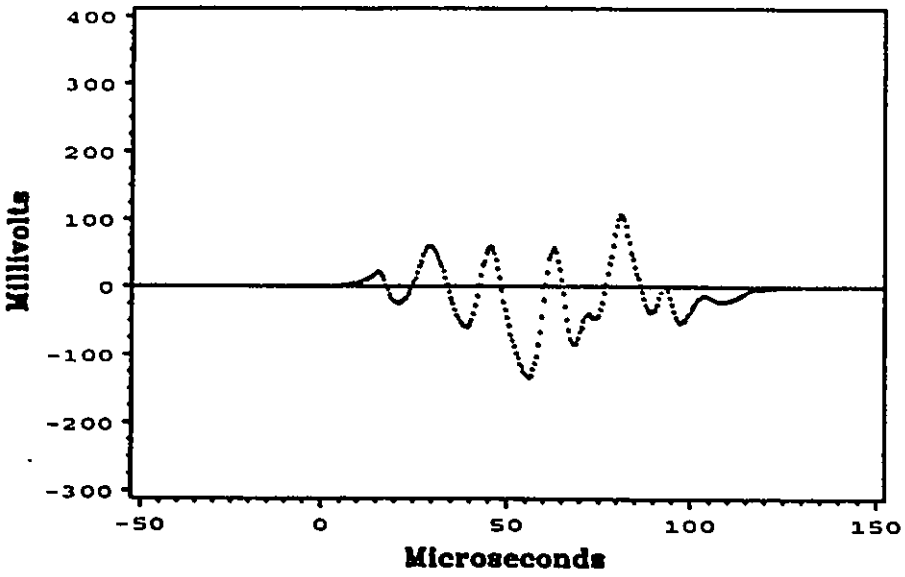

Fig. 3.2.3b The signal shown in fig.3.2.3 after the application of the Hanning weighting function.

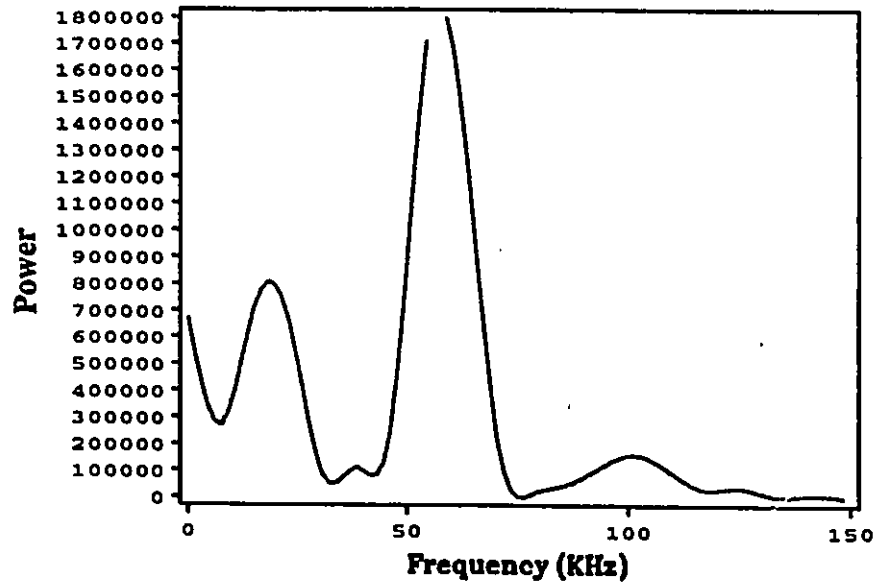

Fig. 3.2.3c The power spectrum for Fig. 3.2.3b.

kHz are overtones of the fundamental frequency, f_1. The peak at 123 kHz is the combination, $2f_2+f_1$, since it increases as the peak at 53 kHz increases.

The first half of the signal of figure 3.2.3 is shown in figure 3.2.4. Its power spectrum is shown in figure 3.2.4a. The signal after the Hanning weighting and its power spectrum are shown in figures 3.2.4b and 3.2.4c respectively. It is interesting to compare the ratios of the amplitudes of the two fundamental frequencies evident in figure 3.2.4c and 3.2.3c. In figure 3.2.3c A_{53kHz}/A_{19kHz} is 19/9=2.1, while in figure 3.2.4c $A_{53kHz}/A_{19kHz} = 7$. This means that the weighting of the first fundamental frequency is increased in the second half of the signal shown in figure 3.2.3. The resolution of the power spectrum is given by the full width at half height (FWHH). The FWHH of the second fundamental frequency increases to 22 kHz in figure 3.2.4c from 15 kHz in figure 3.2.3c because the total time duration (NT) of the signal in figure 3.2.4 is half of that in figure 3.2.3c. In figure 3.2.4c the peaks at 40, 80, 123, and 140 kHz are lost as a result of the dramatic decrease of the importance of f_1. The peak at 104 kHz, the overtone of f_2, is still present. The resolution of the power spectrum is dependent on the time duration of the signal. The longer the signal lasts in the time domain, the higher the resolution in the frequency domain. Comparing the FWHH of the first fundamental frequency in figure 3.2.4a with that in figure 3.2.4c it can be seen that the FWHH in figure 3.2.4c is greater than that in figure 3.2.4a. This is caused by the Hanning weight function since NTs are the same in figs.3.2.4 and 3.2.4b.

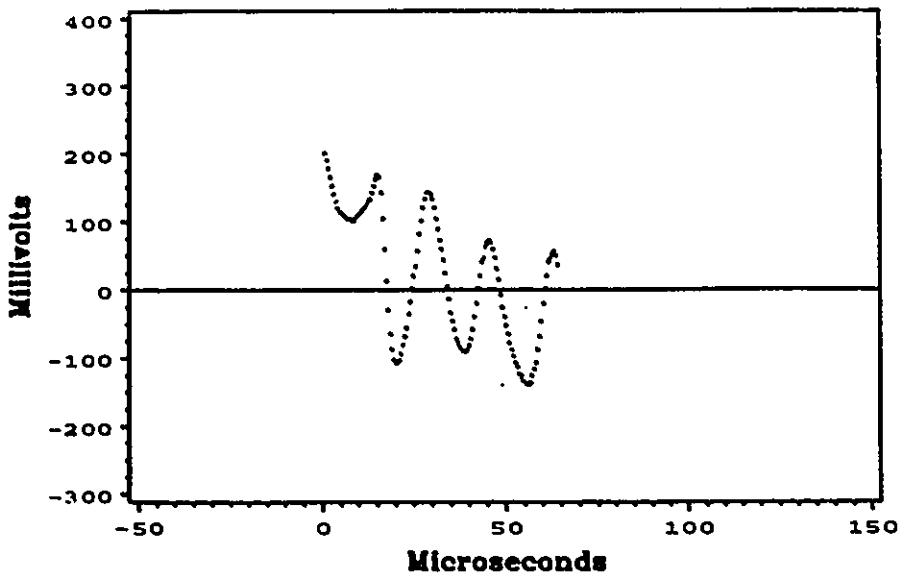

Fig. 3.2.4 Part of the schlieren signal for EXP. 122.

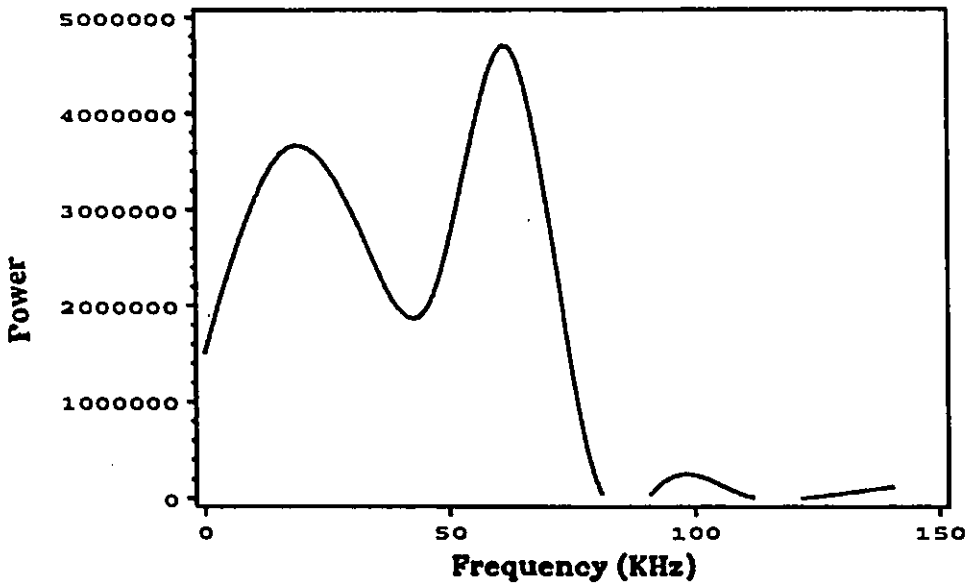

Fig. 3.2.4a The power spectrum for the signal in fig. 3.2.4.

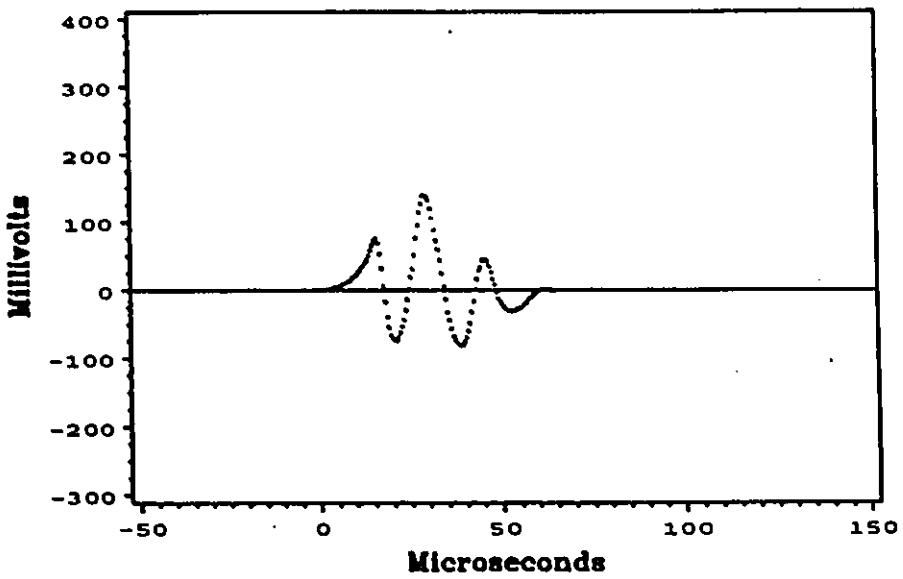

Fig. 3.2.4b The signal shown in fig. 3.2.4 after the application of the Hanning function.

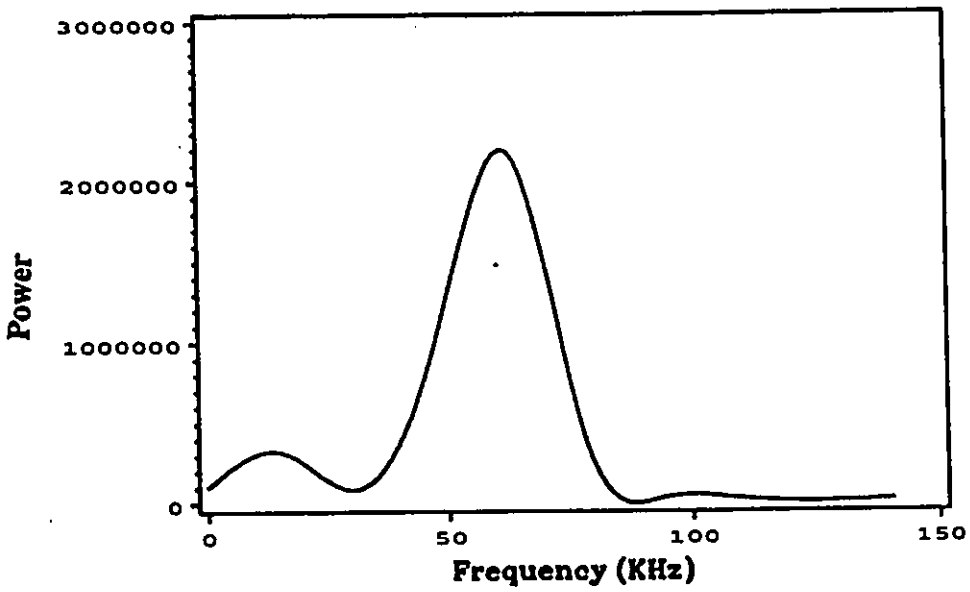

Fig. 3.2.4c The power spectrum for the signal shown in Fig.3.2.4b.

The aliasing error is not serious in the above spectra, because the power spectra show that the amplitudes of the peaks decrease very rapidly as the frequency increases[131].

Summarizing, the power spectrum of the shock tube schlieren signal is meaningless unless the effect of the exponentially decaying curve is removed or its effect is decreased to an acceptable level. Hanning weighting can be used to suppress the effect of an exponentially decaying curve. In some cases decreasing the D.C. component is important. This can be achieved by shifting the signal up or down. The leakage can be decreased by using the window function at the expense of resolution. The resolution of the power spectrum can be increased only by increasing the time duration of the signal. In the next section we shall discuss the power spectrum of some of our schlieren signals obtained using the same method we used for the schlieren signal of exp. 122, that is first to shift the signal to reduce DC component, and then to apply the Hanning window function.

3.2.3 Discussion of the Power Spectrum

In this section we shall use the method of the last section to perform the Fourier transform to some for our experimental signals. The schlieren signal of experiment no. 123 is shown in fig 3.2.5. This is a typical schlieren signal which we obtained in CCl_3F experiments. Since the signal changed from oscillatory to chaotic we divided the whole signal into four regions, A, B, C and D, as shown in fig.3.2.5 after ignoring the portion due to the shock front. The power spectrum for parts A, B and C is given in figs. 3.2.6,

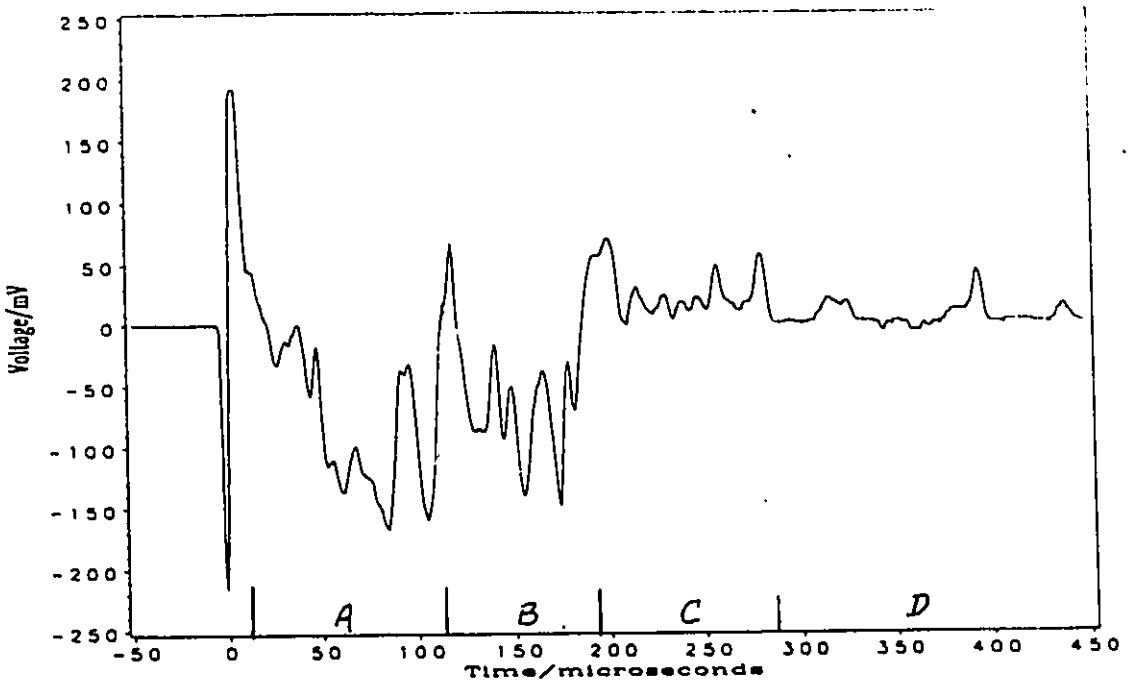

Fig. 3.2.5. Schlieren signal for CCl_2F. Experiment No. 123
T_1 = 292.8 K, P_1 = 441.8 Torr, shock velocity = 230.80 m/s
MACH No. = 1.5794, T_s = 331.5 K, P_s = 1103.0 Torr.

3.2.7 and 3.2.8 respectively, along with the power spectrum for A+B, shown in fig. 3.2.9.

With these graphs we want to show that in different regions of the signal different frequency components dominate. In fig 3.2.6, i.e. in regime A the two highest peaks appear at 25 kHz and 82 kHz respectively, while in fig. 3.2.7, i.e. in region B, the three dominant components are at 90, 160, and 218 kHz. In region C, i.e. in fig 3.2.8, the three largest peaks occur at frequencies 32, 150 and 220 kHz. Because only 64 data points are used in both figs 3.2.7 and 3.2.8, the FWHH of the peaks of both spectra are large; the peaks cannot be separated completely from each other, i.e. the resolution is low. Even though 128 data points are used in fig 3.2.6, resolution is still low. We see that the peak around 25 kHz is not symmetrical. This means that there is another peak that cannot be resolved. Comparing with fig. 3.2.9. we can see that at about 6 kHz there is a peak. So from these figures we can deduce that the dominant frequency components change in different regions of the time domain; we cannot determine fundamental frequencies for each region.

Fig. 3.2.9 shows the spectrum of region A+B. The total length of time is longer, and the resolution of the signal improves greatly. All of the peaks in this spectrum are the overtones or combinations of two fundamental frequencies, f_1=6 kHz and f_2 = 25 kHz. The peak around 56 kHz is the combination of $f_1 + 2 f_2$, the peak at 82 kHz is $f_1 + 3f_2$; the peak at 93 kHz is the combination of $3 f_1 + 2 f_2$. (Although this peak is not separated from the peak at 82 kHz, we know of it from the asymmetry of the peak at 82 kHz and

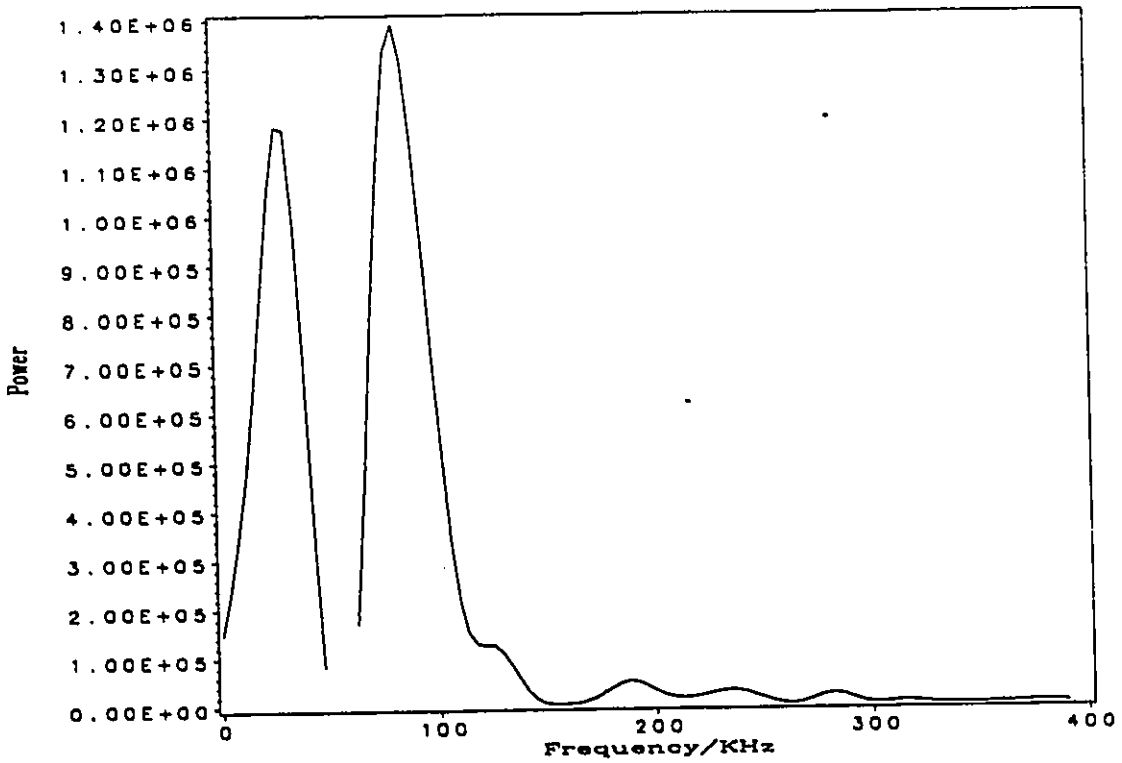

Fig.3.2.6 Power spectrum for part A of the signal of experiment No. 123 . The experimental conditions are as in Fig. 3.2.5.

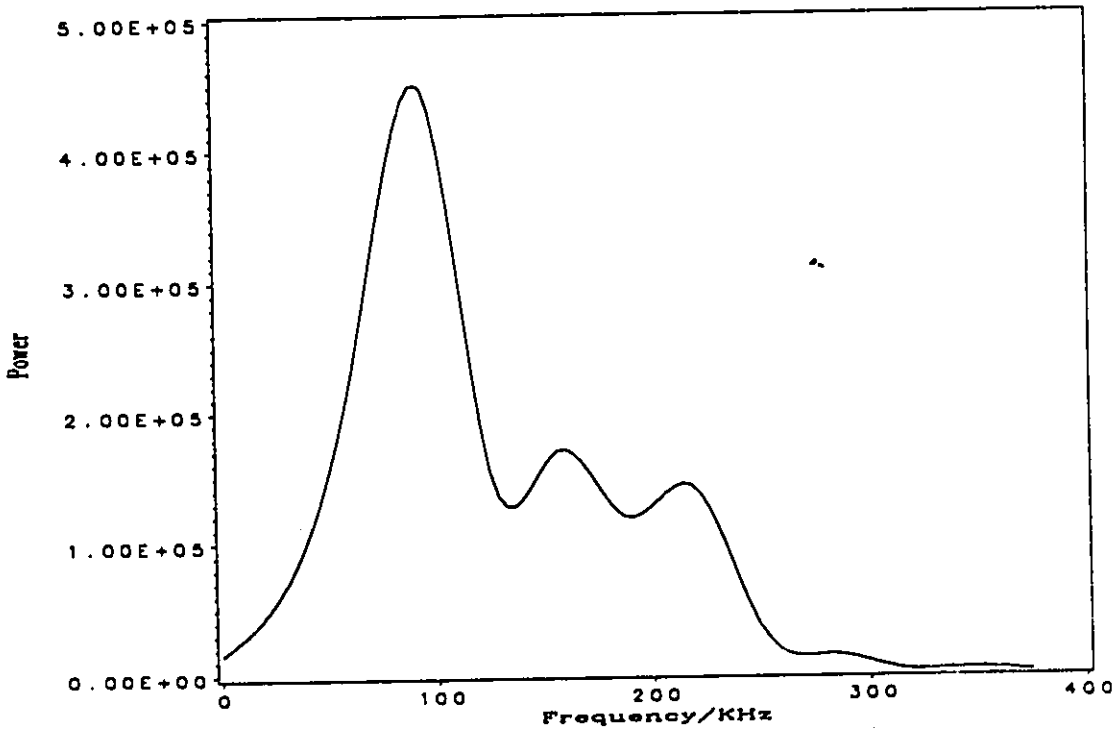

Fig.3.2.7 Power spectrum for part B of the signal of experiment No. 123 . The experimental conditions are as in Fig. 3.2.5.

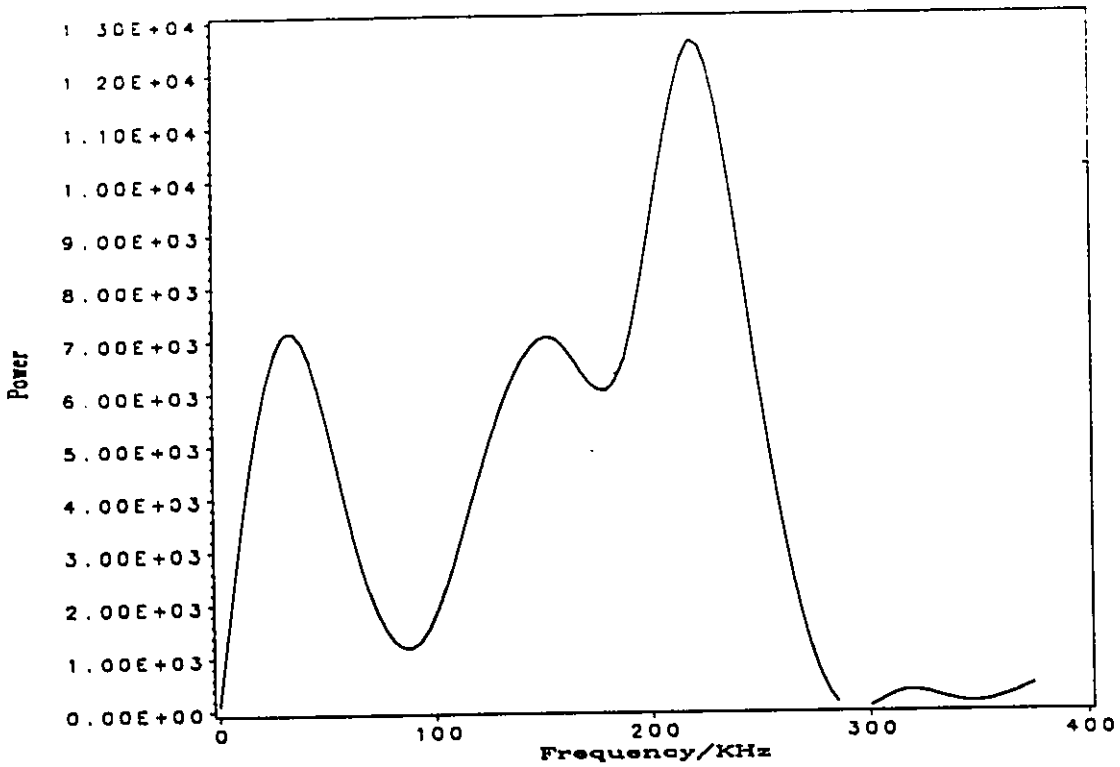

Fig.3.2.8 Power spectrum for part C of the signal of experiment No. &NUM . The experimental conditions are as in Fig. 3.2.5.

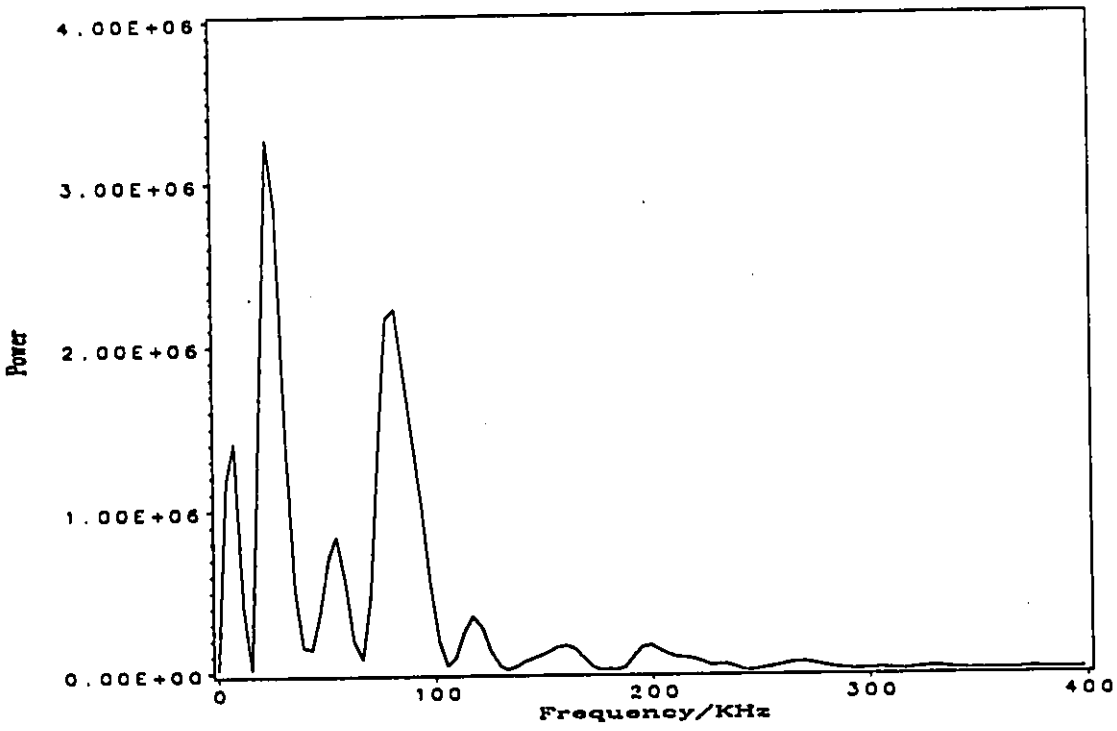

Fig.3.2.9 Power spectrum for part A+B the signal of experiment No. 123 . The experimental conditions are as in Fig. 3.2.5.

from comparison with fig 3.2.7 where a big peak at around 92 kHz. is evident). At 118 kHz we see the combination $3f_1+ 4f_2$; at 160 kHz we see $10f_1+ 4f_2$; $8f_2$ is seen at 200 kHz. From this we can conclude that the first part of the schlieren signal including region A, B, C is quasi-periodic. After about 275 μs the signal enters a chaotic regime. This characteristic is shared by other oscillatory signals we have observed. Some of our examples are shown in table 3.2.1. The spectra for experiments No. 64, 68 and 173 are shown in figs. 3.2.10, 3.2.11 and 3.2.12 respectively.

From the Fourier analysis of the oscillatory schlieren signals three important conclusions were drawn. The first one is that the oscillatory signal can be divided into two regions: the first part is a quasi-periodic region; the second part is chaotic. Secondly, there are two fundamental frequency components in the quasi-periodic regime, one of which can be considered the perturbation frequency. From these two considerations we can deduce that our chemical system is in an oscillation dynamical regime[126,127,132]. The last conclusion is that the ratio of the amplitudes of the two fundamental frequency components is a function of time; in different regions of the signal the dominant frequencies change. This is similar to birhythmicity, i.e. to the bistability between a high-frequency and a low-frequency oscillatory state as demonstrated in several chemical oscillators such as the BZ reaction and the bromate-chlorite-iodide oscillator[133] when the flow rate of reactants (perturbation frequency) is changed. Unfortunately, because the resolution is too low here we cannot test whether the fundamental frequencies change or not in the different signal regions.

Exp. No.	D (mm)	P_1 (torr)	T_1 (K)	u_1 (M/s)	P_2 (torr)	T_2 (K)	ΔP	f_s (Hz)	f_L (kHz)	f_1 (kHz)	f_2 (kHz)
38	0.002	672.8	295.2	143.9	734.3	298.1	59.6	48.83	90	8	32
54	0.002	747.0	296.8	145.9	838.2	300.7	31.0	50.79	91	8	32
55	0.002	664.7	294.3	151.0	804.5	300.7	64.7	56.29	94.51	.15	73
63	0.002	668.8	293.5	150.5	807.2	299.8	35	55.96	94.06	20	90
190 (CCl_4)	0.1	85.6	291.35	548.05	1515.7	529	22668.8	1187.6	342.0	10	32
64	0.013	697.9	294.1	153.4	875.9	301.8	26.8	59.11	95.87	83	120
68	0.013	656.6	293.3	160.8	909.6	304.4	76.0	67.77	100.5	25	65
76	0.013	628.6	292.5	161.1	875.1	303.7	87.0	68.195	100.7	25	70
123	0.1	441.8	292.8	222.9	1103.0	331.5	988.9	169.2	139.31	25	80
122	0.1	537.0	294.2	2062.2	1229.8	324.8	630.1	136.48	128.9	19	60
173	0.1	508.7	292.5	168.2	767.5	306.5	289.4	76.47	105.1	25	85

Table 3.2.1 Summary of Fourier Analysis of Selected Experiments.
in which $\Delta P=P_2-P_{vap}$ (in mm Hg), D is the thickness of diaghram , T_1 and P_1 are the initial temperature and pressure respectively, T_2 and P_2 are post shock temperature and pressure respectively, u_1 is shock velocity, f_s is the reciprocal of the time during which molecules stay in the shock wave, f_L equals $u/1.6\times10^{-3}$ where 1.6×10^{-3} m is the diameter of the laser beam, and f_1 and f_2 are the two fundamental frequencies in the obseved signals as deduced by the analysis.

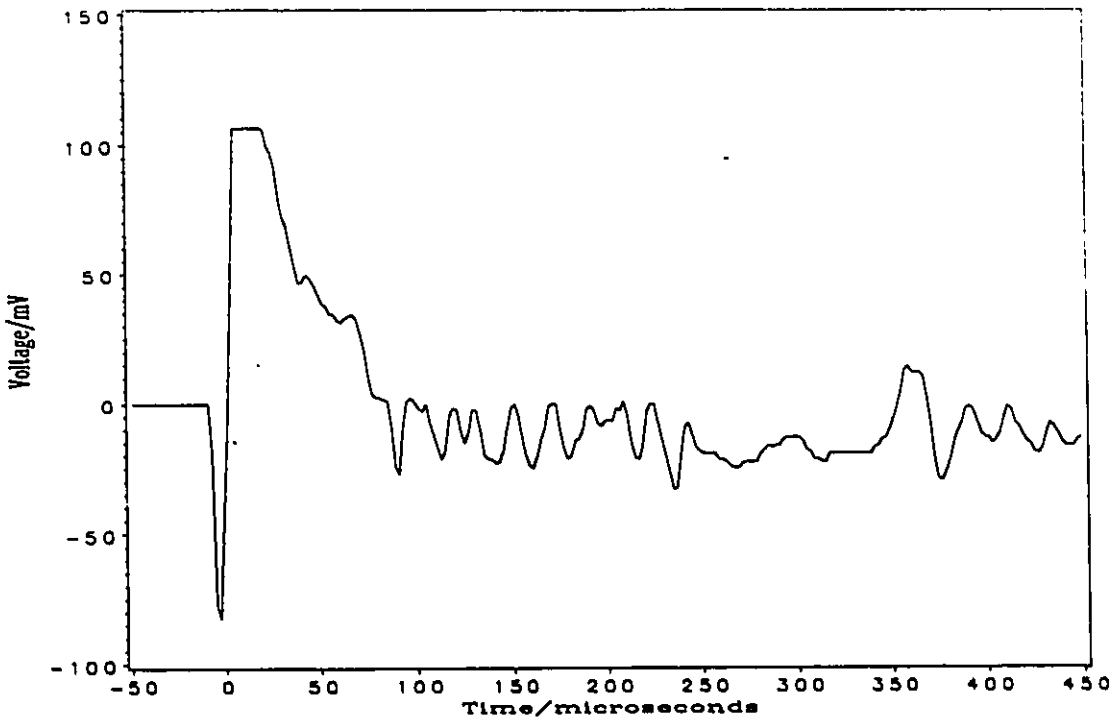

Fig.3.2.10a Schlieren signal for CCl_3F Experiment No. 64 .
T_1=294.1 K, P_1 =697.9 Torr. shock velocity = 153.40 m/s
MACH No. = 1.0816, T_2=301.8 K, P_2 =875.9 Torr.

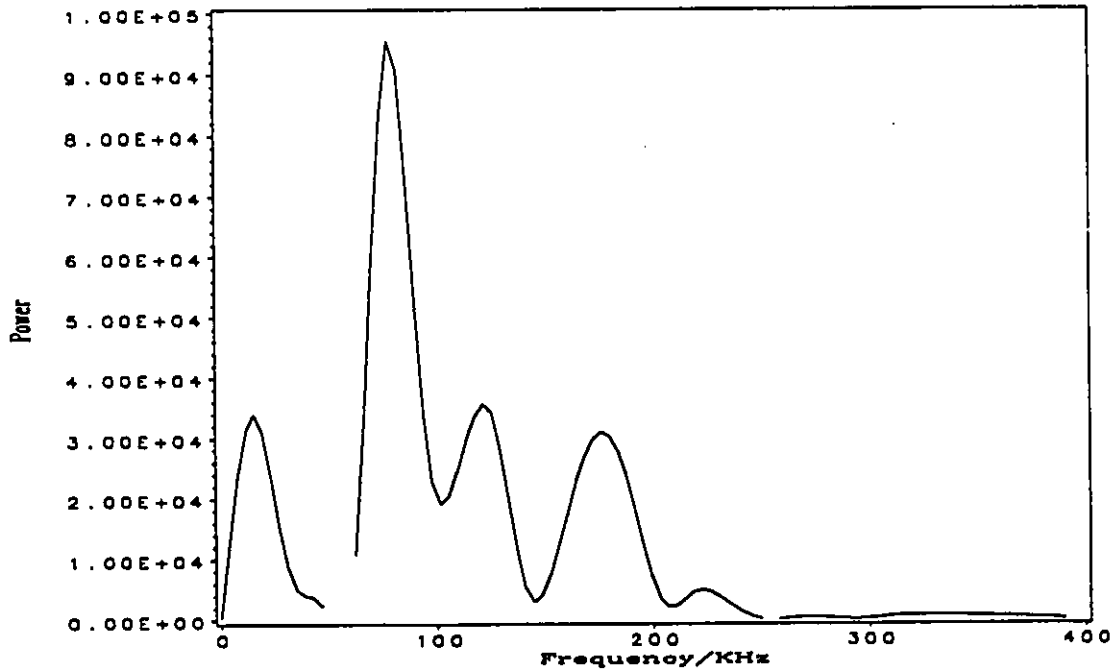

Fig.3.2.10b Power spectrum for experiment No. 64 . The experimental conditions are as in fig.3.2.10a.

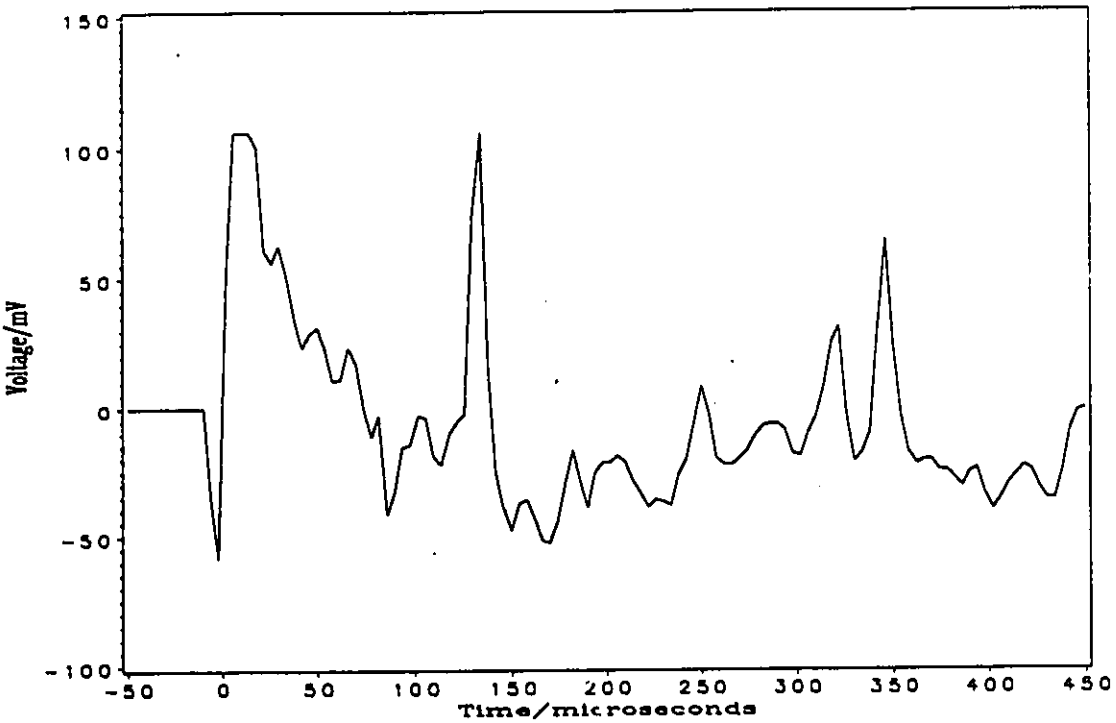

Fig.3.2.11a Schlieren signal for CCl_3F Experiment No. 68 .
T_1=293.3 K. P_1 =656.6 Torr. shock velocity = 160.80 m/s
MACH No. = 1.0903. T_2=304.4 K. P_2 =909.6 Torr.

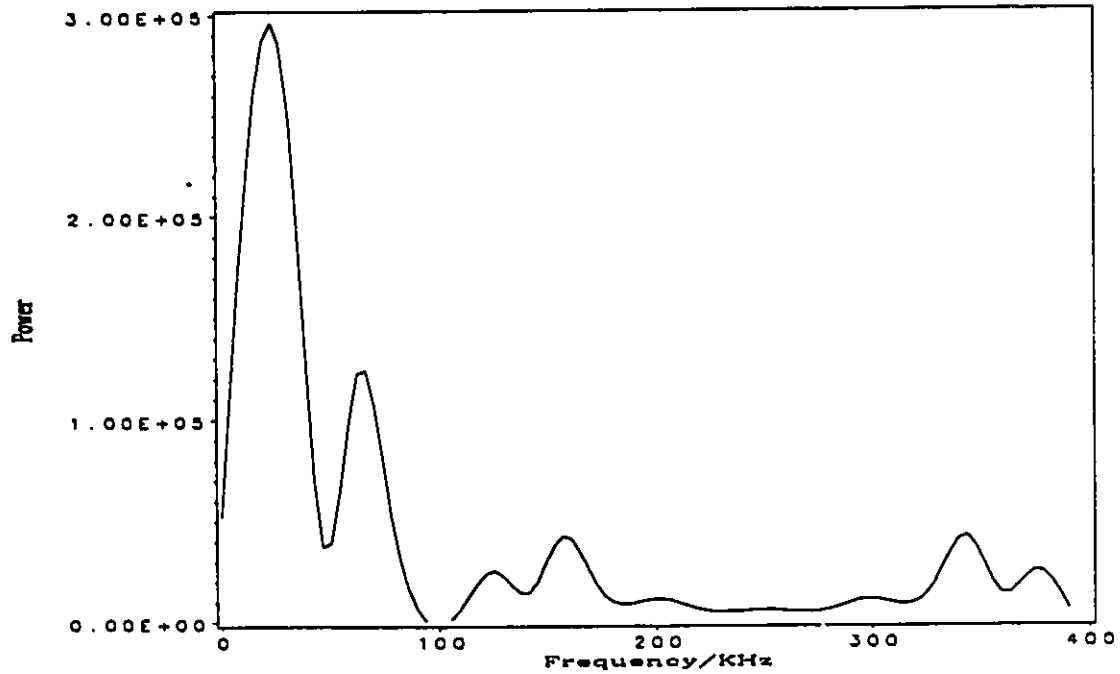

Fig.3.2.11b Power spectrum for experiment No. 68 . The experimental conditions are as in fig.3.2.11a.

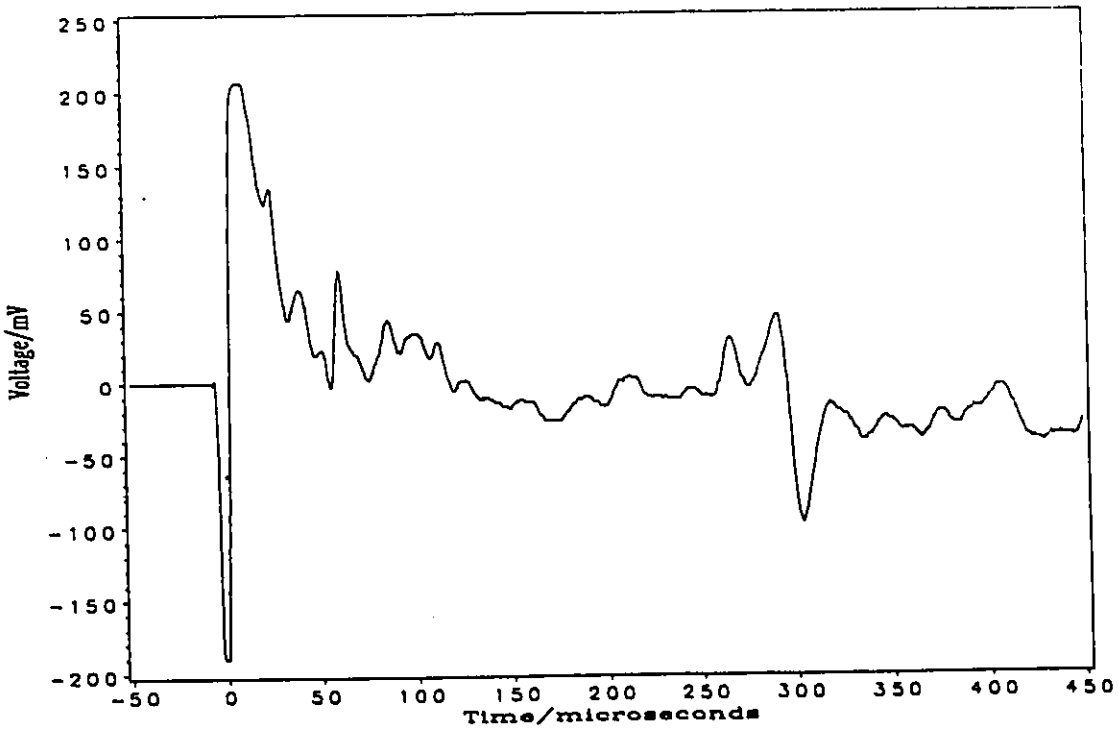

Fig.3.2.12a Schlieren signal for CCl_3F Experiment No. 173 .
T_1=292.5 K, P_1 =508.7 Torr. shock velocity = 166.20 m/s
MACH No. = 1.1950, T_2=306.5 K, P_2 =767.5 Torr.

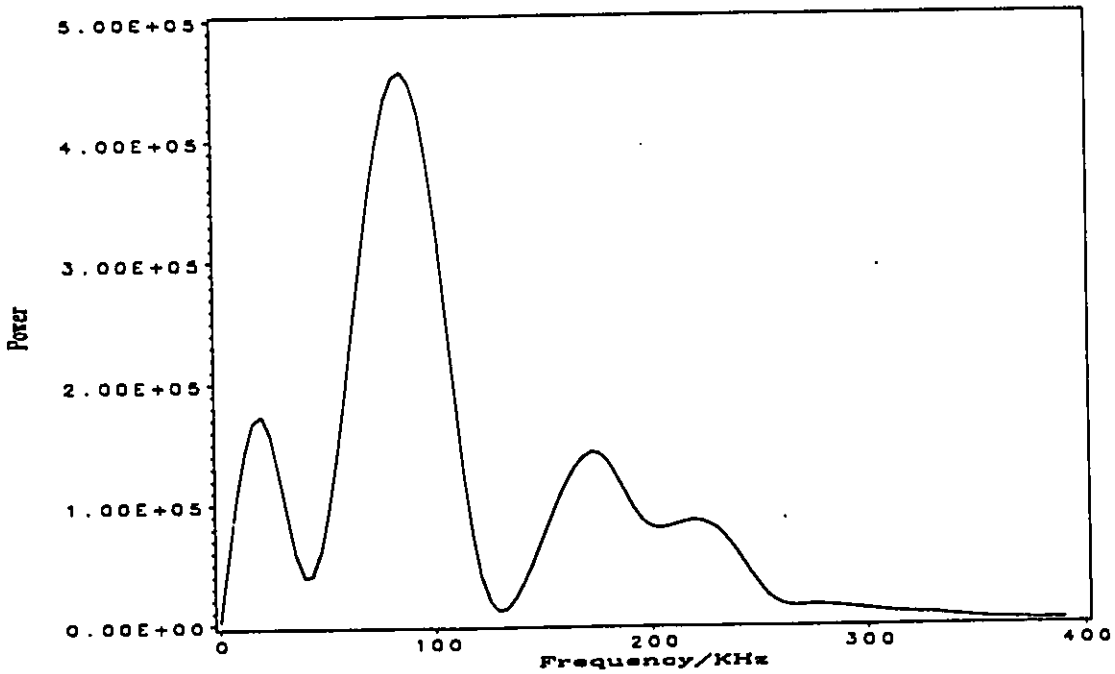

Fig.3.2.12b Power spectrum for experiment No. 173 . The experimental conditions are as in fig.3.2.12a.

3.3 Discussion of the Experimental Results

In Chapter 2 the mechanism of generating oscillatory negative schlieren signals was discussed. It was pointed out that the first cross-point in the schlieren signal, t_o, (at which the signal becomes negative) marks the start of the process of the formation of clusters. (In Chapter 4 our simulations show that it is the stabilization of excited clusters which most affect t_o) Therefore, by measuring t_o, the incubation time for cluster formation can be determined experimentally. Our experimental results showed that the incubation time, t_o, is a function of both temperature and pressure. Figs. 3.1.5a and 3.1.5b show that $P_2 t_o$ increases with temperature. It is worth noting that the order of magnitude of the incubation time measured from our experiments agrees with Hess' result[91] for $(CS)_n$ cluster formation. In contrast to our observations for small clusters under subsaturated conditions CNT predicts that the incubation time for steady state critical cluster formation (Eq. 1.2.39) decreases as the temperature and pressure increase, according to ref. 25.

$$\tau = \frac{-2\pi kT}{\frac{\alpha P}{\sqrt{2\pi mkT}} 4\pi r^{*2} \left(\frac{\partial^2 \Delta G_n^o}{\partial n^2}\right)_{n=n^*}} \qquad (1.2.39)$$

in which

$$\left(\frac{\partial^2 \Delta G_n^o}{\partial n^2}\right)_{n=n^*} = -\frac{2}{9}\beta \left[\frac{3kT}{2\beta} \ln S^*\right]^4$$

where r* is the critical cluster radius, P is the monomer pressure, n* is the critical cluster

size, m is the mass of a monomer, k is boltzmann's constant, T is temperature, $\beta=4\pi\sigma r_o^2$, σ is the surface tension, and r_o is the radius of a monomer. At a supersaturation degree of 4.65 and a temperature of 240 K for Freon-11 $r^* = 1.41\times10^{-9}$ m, and the incubation time, $\tau= 9.68\times10^{-3}$ s. This is longer, as expected, than our subcritical incubation time. Our experiments show also that the incubation time decreases with increasing | extent from equilibrium | i.e. increases with increasing pressure (see fig. 3.1.2a and 3.1.2b). According to CNT, extent from equilibrium is expressed as S or P/P_{vap}. The larger P , the smaller $P\tau$, and this is the opposite of our observations in the subcritical subsaturated regime., as an examination of figs. 3.1.2a and 3.1.2b reveals. In conclusion subcritical and critical cluster formation rates behave dramatically differently.

The power spectrum of the oscillatory part of the schlieren signal that can be decomposed into two fundamental frequencies is similar to one obtained from a periodically perturbed oscillatory system[134]. After a periodic perturbation is applied the response of a chemical oscillator with a natural frequency, f_o, can approach a periodic, quasi-periodic or chaotic trajectory determined by the amplitude(A) and frequency (f_p) of perturbation and the initial conditions of the unperturbed system. If the amplitude of perturbation, A, is large, the perturbation overwhelms the system, no matter what the perturbation frequency is. The response is entrained[134], that is, the response induces a period with frequency, $f_p=nf$, where n is an integer. If the amplitude of the periodic perturbation is small for nearly all of the frequencies the response is quasi-periodic[134]. The power spectrum is composed of several fundamental frequencies, their overtones and combinations. If the number of

fundamental frequencies is two, i.e. f_p and f_o, the response is called biperiodic. Chaos may occur through a period doubling mechanism, when the amplitude of perturbation is not small and not too large. We have examined our system carefully. Although our oscillatory schlieren signals are biperiodic, we are unable to identify the perturbation frequency or to associate it with any physically realistic characteristic time. We have unsuccessfully tried to relate one of the fundamental frequencies to an obvious perturbation, namely to the time required to break the diaphragm. (Because we do not measure this time we try to correlate, in table 3.2.1, the thickness of the diaphragm with the two fundamental frequencies). Alternatively the time (t_s) for molecules to pass through the shock wave or (t_{ls}) through the laser beam are possible bases for comparison. In the previous chapter we found that there was no correlation with acoustic forcing frequencies, either. From the Table 3.2.1 we can see that these frequencies calculated from time periods, t_s and t_{ls}, do not equal to any of the fundamental frequencies. It is difficult to draw any conclusion about the relation of the thickness of the diaphragm and any of the fundamental frequencies, since the time required to break the diaphragm can vary even if the thickness of diaphragms is constant. In the absence of a physical source for the oscillations we consider a chemical source. Our chemical system is complicated. There are several chemical reactions involved, for example the formation of excited dimer, trimer, etc and their subsequent collisional stabilization. Therefore, there is a possibility that f_o and f_p find their origin in the rate constants of two or more oscillatory chemical reactions of the system.

For the purpose of analyzing the oscillations in chemical terms it suffices to choose an average frequency, f, as determined by counting peaks in a given time interval. The results, shown in figs. 3.2.13 to 3.2.16, show scatter similar to that observed for P_2t_o, P_2t_m and $V_{min}/(V_oP_2^2)$, which is related to the technical instability to keep ΔP or T_2 absolutely constant, as the case may be.

Table 3.3.1 shows the activation energies, $E_{a,to}$, $E_{a,tm}$, $E_{a,v}$ and $E_{a,f}$, obtained from log plots of $(P_2t_o)^{-1}$, $(P_2t_m)^{-1}$, V_{min}/P_2^2 and f/P_2 vs 1/T for each fixed ΔP respectively. In all of these cases the ordinates are proportional to effective second order rate coefficients. From this table several conclusion can be drawn. First, we see that activation energy does not depend on ΔP within experimental uncertainty. Second, the negative activation energy implies that some kind of bond is formed in the system. This is consistent with the negative schlieren signal which is proof of an exothermic process (bond formation). Third, the value of the activation energy is about -32 kJ/mol. This is close, in magnitude, to the enthalpy of condensation, 25 kJ/mol. This is proof not only of Van der Waals' bond formation but also of very strong competition with energy transfer (stabilization). This can be understood by analogy with the much stronger chemical processes of atom-atom or radical-radical combinations. Such non-equilibrium process are associated with a pileup of population in super-excited vibration/rotation states. The finite rate of stabilization leads to activation energies depressed (from the expected value zero) by amounts corresponding to those states affected . In the case of clusters where there are few vibration/rotation levels altogether associated with the weak bond and almost all are hard

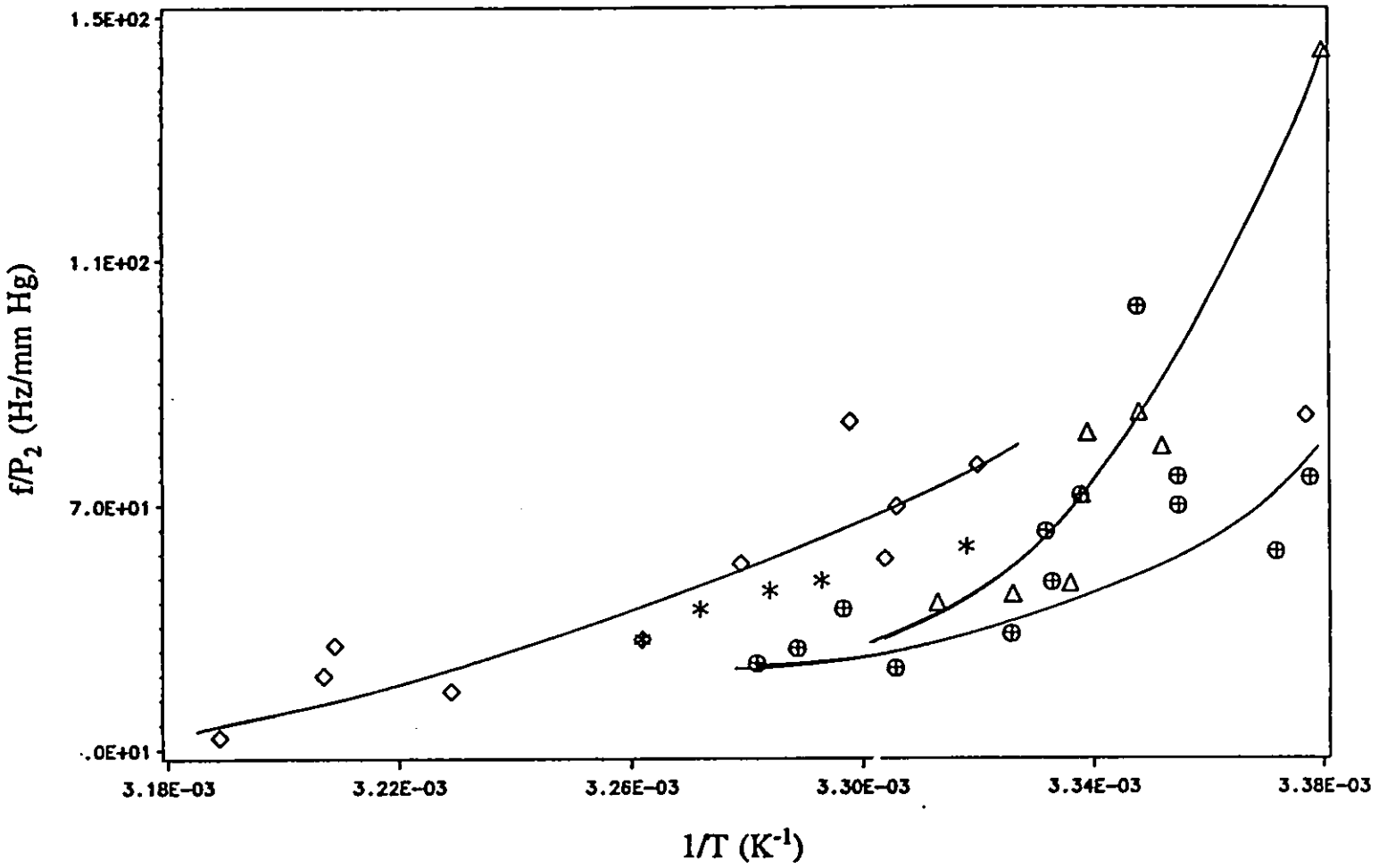

Fig. 3.2.13 f/P_2 vs 1/T. ▵ for $(P_{vap}-P_2)$= 32 ±7 mm Hg, ⊕ 50 ±4 mm Hg, * 77 ±7 mm Hg , ◊ 125 ±13 mm Hg.

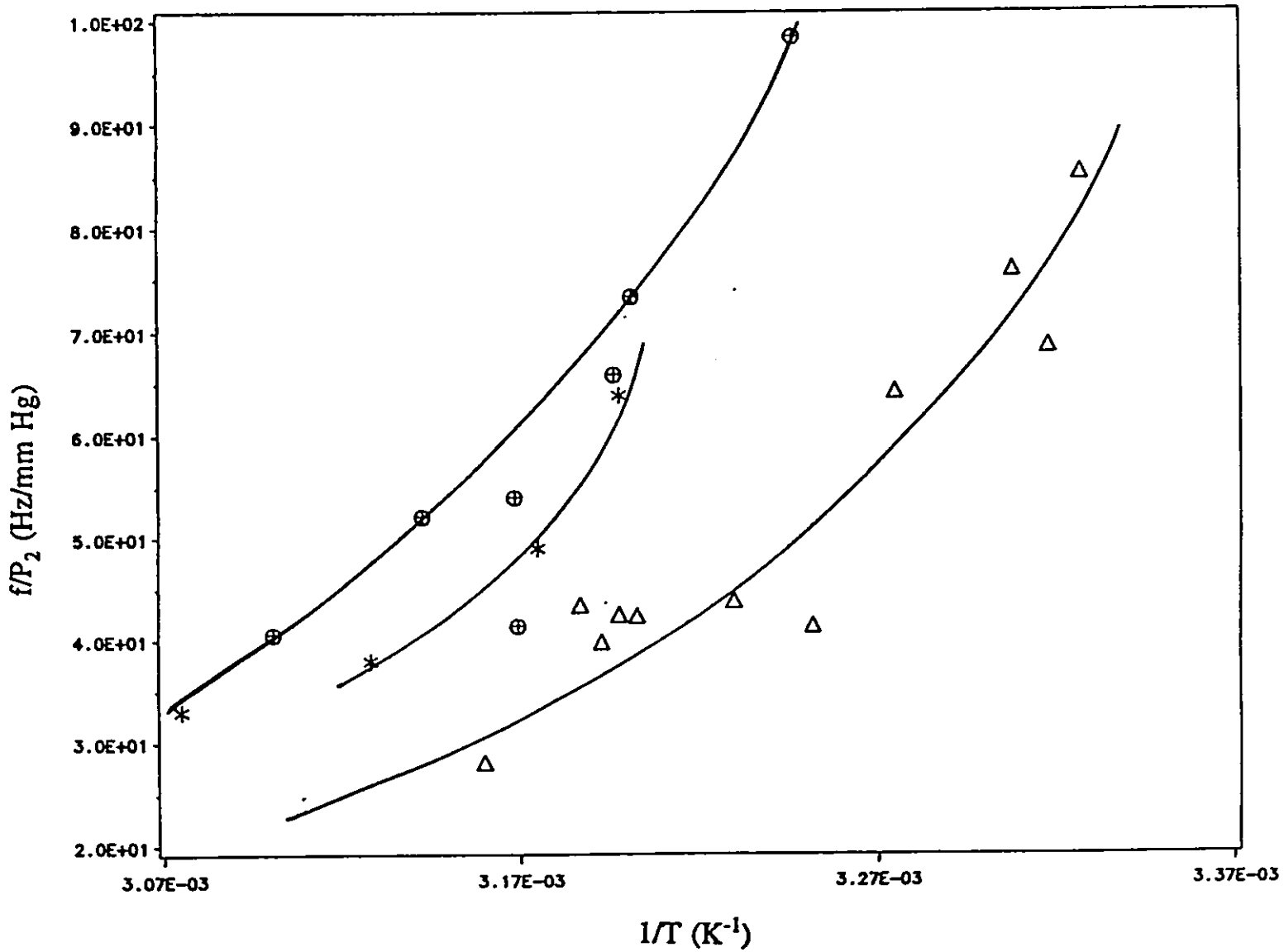

Fig. 3.1.14 f/P_2 vs 1/T. △ $(P_{vap}-P_2)$= 174 ±14 mm Hg, ⊕ 335 ±15 mm Hg, * 760 ±35 mm Hg.

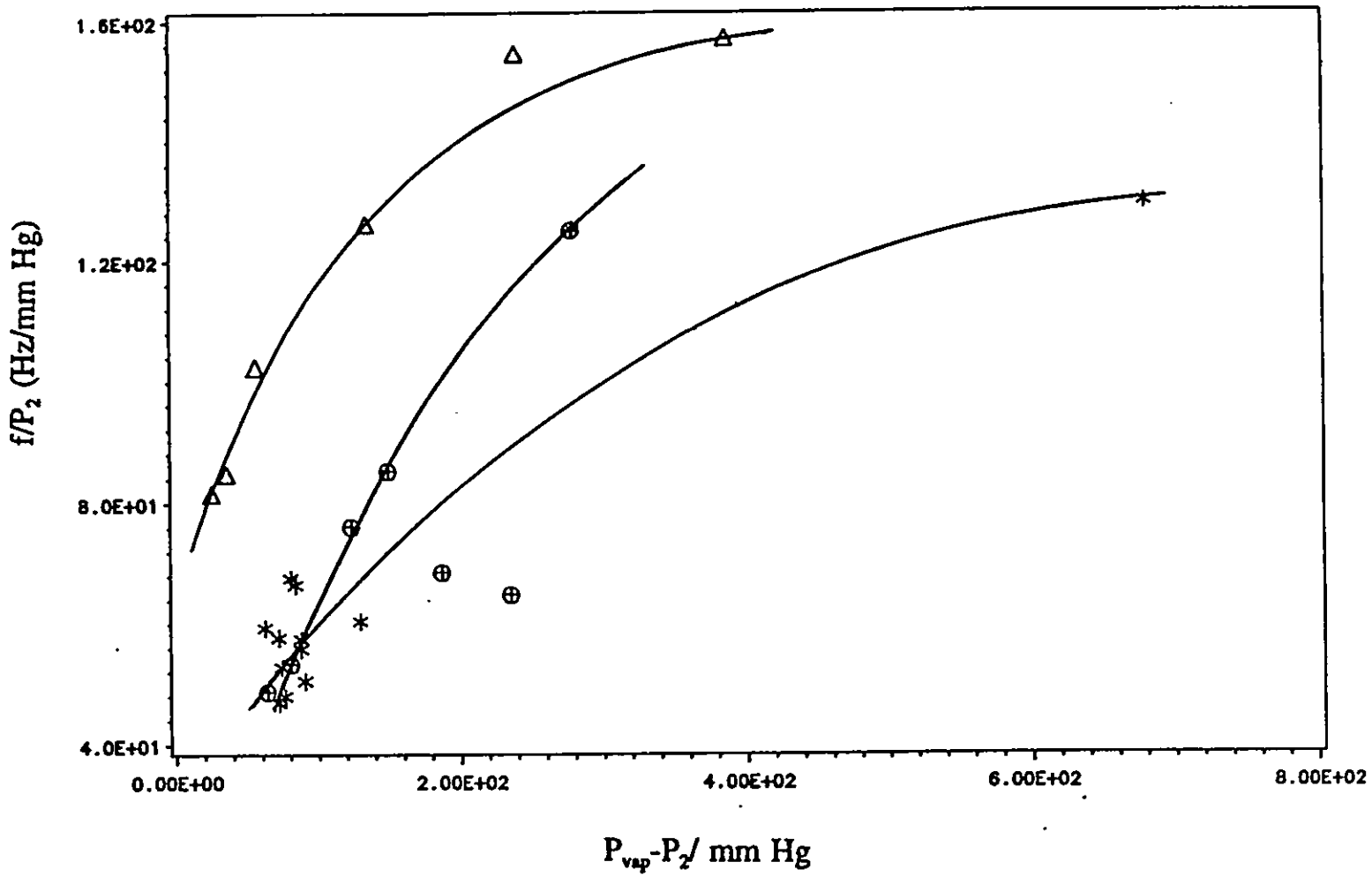

Fig. 3.2.15 f/P_2 vs $(P_{vap}-P_2)$. △ T=298 ±0.5 K, ⊕ T=301±1 K, and * T=304 ±1 K.

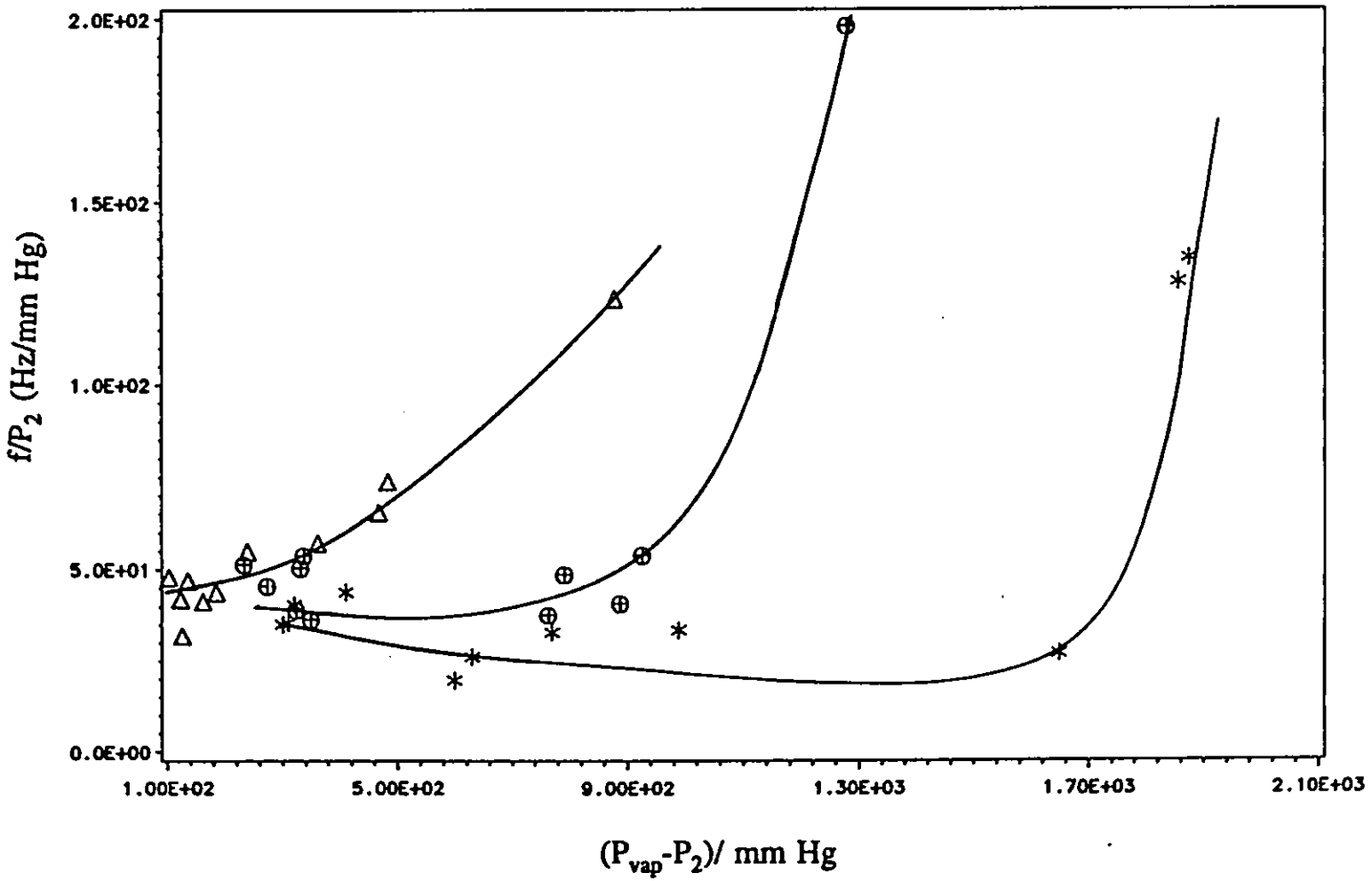

Fig. 3.2.16 f/P_2 vs $(P_{vap}-P_2)$. △ T=308 ±2 K, ⊕ T=315±2 K, and * T=327±6 K.

to stabilize we can expect the maximum depression ~ $\Delta H_n \approx \Delta H_{vap}$ (true for large clusters). Hence in our case, we can expect a depression ~24 kJ/mol.

Table 3.3.1 Activation energies measured from schlieren signals for CCl_3F.

ΔP(mm Hg)	$E_{a,f}$ (kJ/mol)	$E_{a,to}$ (kJ/mol)	$E_{a,tm}$ (kJ/mol)	$E_{a,v}$ (kJ/mol)
32±7	-52±4	-38±2	–	-29±5
50±4	-24.8±0.5	–	–	-43±2
77±7	-17±2	-80±4	-108±5	-36.6±0.2
125±13	-20.1±0.5	-31±2	-27±2	-22.6±0.5
174±14	-23.2±0.5	-24±2	-21.0±0.5	-38±5
335±15	-24.5±0.5	-27±2	-41±2	-
760±35	-34±4	-66.8±0.5	-39±5	-16.6±0.5
Average	-27±9	-37±12[a]	-32±8[b]	-31±8

(a: -80±4 is not counted in the average; b -108±5 is not counted in the average).

Cluster formation can be described by the following set of nonlinear reactions

$$A_{n-1}+A=A_n^*$$
$$A_n^*+M=A_n+M$$

We assume that in the first step a monomer simply sticks onto a (n-1)-mer. Energy is

released in the second step. Also, this is a self-heating process. Furthermore, we used a shock tube as a tool to get the CCl_3F vapour system far from equilibrium. Consequently our system fulfils the requirements for a thermokinetically oscillating system, as described in chapter 1. We expect a process to occur which is similar to the Salnikov-Gray mechanism for the oxidation of organic compounds, which we described in the introduction. There are two differences, however, between cluster formation and hydrocarbon oxidation. First, the heat released by clustering is much smaller than in an oxidation reaction of organic compounds, generally speaking; second, the shock wave is an adiabatic system. No heat can diffuse from the system to the surroundings in the short time available. However, there is an endothermic process which can play the role of spoiler, that is the vibrational relaxation of monomers. Endothermic reactions such as relaxations as well as the evaporation of cluster can produce a negative feedback, i.e. self-cooling, and all the ingredients are present for oscillation. Since in our system the heat effect is much smaller than that observed already in other thermokinetic oscillators, we cannot expect large amplitude oscillations. It is the high sensitivity of the schlieren technique which is crucial for detecting small oscillatory signals (gradients) in homogeneous nucleation experiments. Because a shock wave is a closed system, we also cannot expect that the oscillatory behaviour of CCl_3F vapour can be sustained for a long time. A new equilibrium distribution is achieved in a short time. Therefore, a fast response detection system was crucial in this study. The time response of the laser schlieren detection system is good to 0.01μs. Hence the schlieren technique played a very important role in our study to detect this temporal phenomenon which only lasts about

a hundred microseconds.

In summary, in this chapter we examined our experimental results. We found a process whose time scale depended on temperature much like radical recombination, implying bond (possibly weak bond) formation. The activation energy was around -24 kJ/mol. We also performed Fourier transforms on our schlieren signals, showing biperiodic behaviour, and having frequencies that also displayed a negative temperature dependence. The schlieren technique was capable of recording this temporal phenomenon. From our analysis we know that the cluster formation process for CCl_3F (and CCl_4) vapour is accompanied by self-heating. Together with the non-linear relationship between the temperature and the rate constant, and with very rapid shock-displacement far-from equilibrium, this satisfies the kinetic requirements for a thermokinetic oscillator. In the next chapter we shall build a model with nonlinear dynamic-kinetic laws based on the cluster formation mechanism mentioned above, and show that it leads to the observed behaviour.

CHAPTER 4

COMPUTER SIMULATION

4.1 INTRODUCTION

The computational analogue of our proposed chemical system is used to simulate the experimental results. In this chapter a mathematical model of the process of cluster formation, stabilization and dissociation during shock compression will be described, and the numerical method of simulation and the result of the simulation will be discussed.

The computer simulation can be divided into six steps[136]. 1. Formulation of a physical model. In this study the model is the formation, stabilization and dissociation of small clusters by a pseudo-chemical reaction mechanism. 2. Making some assumptions to simplify the model. 3. Formulation of the mathematical problem. In this step the mathematical equations are derived to represent the relevant mechanism of the model. These mathematical equations are based on basic chemical and physical laws, such as mass balance and energy balance and equilibrium principles. 4. Solving the mathematical equations. 5. Interpreting the solution. 6. Checking the model by comparing the solution with the real model. If unsuccessful we must modify the assumption. The limits of the

mathematical model are determined completely by the assumptions used in its derivation. Steps 2 to 6 are repeated until a satisfactory result is obtained.

4.2 THE BASIC MODEL FOR CLUSTER NUCLEATION

4.2.1 The Physical Model

In the previous chapters we concluded that the exothermic schlieren signal in our experiments is produced by the formation of clusters. The oscillatory behaviour of the schlieren signal is related to the competition of the processes of formation, stabilization and dissociation of small clusters. The arguments can be summarized as follows:

1. 190 experiments were done in two different size shock tubes. Comparing experiments with similar experimental parameters (pressure and temperature) but for different tube dimensions, we found that the oscillations and exothermicity were independent of the dimension of the shock tube.

2. In the same experiment where the main schlieren signal showed oscillation and exothermicity the total signal showed no oscillatory behaviour. This indicates that oscillatory behaviour of the schlieren signal is really caused by laser beam deflection on the detector, and is not caused by faulty response of the electronic circuit of the detector or of the waveform recorder. It is a spatially extended rather than temporally based.

3. Oscillatory behaviour was observed only after the shock front had passed. Before

shock front arrival at the observation window there were no oscillations. This means that oscillations took place in the gas column after shock compression.

4. For pure argon there is neither oscillation nor an endothermic nor an exothermic process; only a signal due to the passage of the shock front, as expected. This means that the oscillatory and exothermic signals which we observed in Freon-11 experiments were not caused by other physical process such as shock tube recoil or the vibration of the observation windows.

5. The temperature range that the experiments were carried out is about 293 to 500 K. No dissociation of CCl_3F takes place in this temperature range. Thus the observed signal is not the result of an overall endothermic pyrolysis of CCl_3F.

6. Comparing experimental results we found oscillations could be observed if the initial pressure was close to the vapour pressure and the speed of shock wave was not larger than 3.0. The lower the postshock temperature, the earlier (in time) the oscillatory behaviour started, when the initial pressures were equal to or close to the vapour pressure. The higher the initial pressure of vapour, the earlier the oscillation began at constant temperature. In general, the deviation of gases from ideality increases the closer to the liquefaction point. This is partially due to an increased number of clusters. The higher the pressure and the lower the temperature of the vapour, the easier it is to form clusters. Therefore, our experimental observation implies that oscillation is related to cluster formation.

7. For CCl_4 at initial pressures close to its vapour pressure (89.55 mm Hg at 293 K) similar oscillatory and exothermic signals were observed.

8. For CH_4 at initial pressures of 604 mm Hg and T=295 K the temperature is too far above the critical temperature (190 K), and molecules have too much kinetic energy. Therefore, no clustering is expected at the temperature that the experiment was carried out. The critical temperature of SF_6 is 318.5 K. With weak shocks the signal showed that exothermic reaction took place, but there was no oscillatory behaviour because after shock arrival the temperature was higher than the critical temperature . After relaxation the temperature decreased and an exothermic process took place. This strongly suggests that oscillatory behaviour and an exothermic schlieren signal are related to the processes of clustering and vibrational relaxation of both monomer and cluster (stabilization of cluster).

9. Some very weak shock experiments (exp. 154 and 157) were done in which the temperature change was less than 2 degrees. These signals showed no oscillation and no exothermic behaviour, rather only the relaxation processes for both clusters and monomers. This suggests that here the temperature change was too small to cause an observable change in the cluster distribution. But this small temperature change nevertheless permitted the process of cluster vibrational relaxation to be observable.

10. The frequency of oscillation is a function of temperature and pressure.

11. In Bauer[23] et al's experiments only one process, that is cluster formation, took place. Their signals were not oscillatory. In their experiments the metal vapour was highly diluted in Ar guaranteeing nearly isothermal conditions and eliminating any thermal feedback. Also, the metal clusters do not have vibrationally excited states. Thus the energy released by the metal clusters was taken up by the atomic gas, Ar. On the other

hand the Freon-11 system is complicated in that the heat released by cluster formation is fed back to the system and there are basically four processes happening: monomer excitation, and cluster formation, stabilization and dissociation. As the temperature changes the rate constants of these processes change nonlinearly. The signal is the result of these four coupled processes.

12. Hess[91] et.al. who observed cluster formation using a variety of techniques also used the technique of photothermal probe beam deflection (PTPD) in studying $(CS)_n$ cluster formation. This is similar to our laser-schlieren technique. In their study if the probe beam passes through the cluster formation region, a negative signal is detected. This confirm that our negative signal is generated by cluster formation.

Based on the above arguments we conclude that cluster formation is the cause of the exothermic signal. Oscillatory behaviour is related to the competing processes of cluster formation , stabilization and dissociation and vibrational relaxation of monomers and clusters. The proposed physical model is that after a shock wave arrival, CCl_3F is compressed suddenly. Both the temperature and the pressure increase dramatically. Then rotational and vibrational relaxation of both monomers and clusters take place. These are endothermic processes. Because of the temperature and pressure jump, the equilibrium cluster distribution of the CCl_3F vapour must also change. Note that cluster formation does not require supersaturation[2] More clusters will tend to form and stabilize. This is an exothermic process. The heat released at each stabilization step affects the equilibrium cluster distribution nonlinearly, and each rate constant depends nonlinearly on the

temperature, T. The Arrhenius representation for the rate constant is $k= Ae^{-E/RT}$, where (assuming an adiabatic process) T changes according to

$$\sum_{i=1}^{n} C_i [A_i] \frac{dT}{dt} = \sum_{i=1}^{n} \Delta \overline{H_i} \frac{d[A_i]}{dt}$$

where C_i is the molar heat capacity of the cluster of size i; $[A_i]$ is the molar concentration of i-mer, and ΔH_i is the heat change occurring upon the loss or gain of a mole of cluster i. Thus the mechanism is present for self-catalysis of dissociation and self-inhibition of association[119]. Both the monomer vibrational excitation (endothermic) and the cluster stabilization processes (exothermic) interfere with each other. It is these coupled processes that give rise to the oscillating and exothermic signal.

This is our physical model. Based on it and the following assumptions we shall build a mathematical model to simulate the processes occurring in our experiments.

4.2.2 The Assumptions

In this study the major assumptions are

(1) The concentration of the collider , [M] , is constant.

(2) A cluster is formed by the addition of a relaxed monomer to a smaller cluster.

(3) A cluster dissociates by losing a monomer.

(4) A monomer has only two effective vibrational levels.

(5) The largest cluster considered is a pentamer.

Since there are no thermodynamic and kinetic data for the formation and dissociation of small clusters, some assumptions are made to derive these data.

(6)The molecular motions are adequately described by classical mechanics with interactions described by a pairwise additive square well potential function. This type of potential, though inexact, should suffice for the present purpose.

(7) The vibrational frequencies of a molecule are not affected by clustering .

(8) The density within a cluster is the same as the density of the liquid phase.

(9) A cluster is spherical in shape.

4.2.3 Derivation of the ODEs

Monomers can be vibrationally excited or unexcited by collision

$$A_1 + M = A^*_1 + M$$

where A_1 is the monomer of CCl_3F, M is the collider, A_1^* is excited monomer, k^s_{-1} is the rate coefficient for the formation of excited monomer, and k_1^s is the rate coefficient for the backward reaction. Two vibrationally relaxed monomers can form an excited dimer, A_2^*

$$A^*_1 + A^*_1 = A^*_2$$

k_2^f is the rate coefficient for the formation of dimer; and k^f_{-2} is the rate coefficient for the reverse dimer dissociation reaction. Dimers can be stabilized by the process

$$A^*_2 + M = M + A_2$$

where A_2 is the stable, unexcited dimer, k^s_2 is the rate coefficient for the stabilization process, and k^s_{-2} is the rate coefficient for the excitation of dimer. The general reaction for the formation of an excited n-mer and its reverse is represented by

$$A_{n-1} + A^*_1 \rightleftharpoons A^*_n$$

where A^*_n is the excited n-mer. k^f_n is the rate coefficient for the formation of n-mer. k^f_{-n} is the rate coefficient for the reverse process.

The general stabilization reaction and the vibrational relaxation of clusters is represented by

$$A^*_n + M = M + A_n$$

where A_n is the stable unexcited n-mer, k^s_n is the rate coefficient for the stabilization process, and k^s_{-n} is the rate coefficient for the reverse process. The rate of change of the concentration of each component is given below by

$$\frac{d[A_1]}{dt} = -k^s_{-1}[A_1][M] + k^s_1[M][A^*_1] \tag{4.1}$$

and

$$\frac{d[A^*_1]}{dt} = k^s_{-1}[A_1][M] - k^s_1[M][A^*_1] + 2k^f_{-2}[A^*_2] - 2k^f_2[A^*_1][A^*_1] + \sum_{n=3}^{N}\left(-k^f_n[A_{n-1}][A^*_1] + k^f_{-n}[A^*_n]\right) \tag{4.2}$$

For cluster sizes n=2 to n<N, where N is the largest cluster size in system.

$$\frac{d[A_n]}{dt} = k_n^s [A_n^*]\,[M] - k_{-n}^s [A_n]\,[M] + k_{-(n+1)}^f [A_{n+1}^*] - k_n^f [A_n]\,[A_1^*] \quad (4.3)$$

and

$$\frac{d[A_n^*]}{dt} = k_n^f [A_{n-1}]\,[A_1^*] - k_{-n}^f [A_n^*] - k_n^s [A_n^*]\,[M] + k_{-n}^s [A_n]\,[M] \quad (4.4)$$

For cluster size n=N

$$\frac{d[A_N]}{dt} = k_N^s [A_N^*]\,[M] - k_{-N}^s [A_N^*]\,[M] \quad (4.5)$$

and

$$\frac{d[A_N^*]}{dt} = k_N^f [A_{N-1}]\,[A_1^*] - k_{-N}^f [A_N^*] - k_N^s [A_N^*]\,[M] + k_{-N}^s [A_N]\,[M] \quad (4.6)$$

We divided the above equations (4.1 to 4.6) by ($k_2^f\,[A_1^*]_o C$). Here $k_2^f\,[A_1^*]_o$ is the initial concentration of excited monomers; and C is the total concentration of clusters .

$$C = \sum_{i=1}^{N} ([A_i] + [A_i^*]) \quad (4.7)$$

Let

$$t' = t k_{2,e}^f [A_1^*]_o$$

here t' is a dimensionless time scale; and $k_{2,e}^f$ is the rate constant of the formation of dimer at the equilibrium temperature. We define the following parameters in order to simplify the differential equations:

$$s=\frac{[A_1^*]_0}{[A_1^*]_{eq}} \tag{4.8}$$

$$g_n=\frac{[A_n^*]_{eq}}{[A_{n-1}^*]_{eq}} \tag{4.9}$$

$$y_i=\frac{[A_i]}{C} \tag{4.10}$$

Then

$$\frac{[A_1^*]}{[A_1^*]_0}=y_1^*\frac{C}{[A_1^*]_0}=\frac{y_1^*C}{y_{1,0}^*C_0} \tag{4.11}$$

in which $y^*_{1,0} = [A_1^*]_0/C_0$ and C_0 is the sum of the total concentrations of all clusters, including monomer, at time zero. The stabilization term

$$\begin{aligned} k_n^s\frac{[M]}{[A_1^*]_0} &= \frac{k_n^sC+k_n^{s,Ar}[Ar]}{[A_1^*]_0} \\ &= k_n^s\left(\frac{C}{C_0y_{1,0}^*}+\frac{k_n^{s,Ar}}{k_n^s}\frac{[Ar]}{[A_1^*]_0}\right) \\ &= k_n^s\left(\frac{C}{C_0y_{1,0}^*}+\beta Z_0\right) \end{aligned} \tag{4.12}$$

in which $Z_0 = [Ar]/[A_1^*]_0$, [Ar] is the concentration of a diluent, argon, $k_n^{s,Ar}$ is the stabilization rate coefficient of argon, and $\beta = k_n^{s,Ar}/k_n^s$ is the relative efficiency of stabilization by Ar compared with CCl_3F itself. Using the above relations the working

differential equations can be derived.

$$\frac{dy_1}{dt'}+\frac{y_1 dC'}{C'dt'}=\frac{k_1^s}{k_{2,e}^f}\left(\frac{C'}{y_{1,0}^*}+\beta z_0\right)(y_1^*-f_1 y_1) \tag{4.13}$$

$$\begin{aligned}\frac{dy_1^*}{dt'}+\frac{y_1^* dC'}{C'dt'}=&-\frac{k_1^s}{k_{2,e}^f}\left(\frac{C'}{y_{1,0}^*}+\beta z_0\right)(y_1^*-f_1 y_1)-2\left(\frac{k_2^f}{k_{2,e}^f}\right)\left(y_1^*\frac{y_1^* C'}{y_{1,0}^*}-\frac{y_2^*}{sg_2}\right)\\ &-\sum_3^N \frac{k_n^f}{k_{2,e}^f}\left(y_{n-1}\frac{y_1^* C'}{y_{1,0}^*}-\frac{y_n^*}{sg_n f_{n-1}}\right)\end{aligned} \tag{4.14}$$

$$\frac{dy_2}{dt'}+\frac{y_2 dC'}{C'dt'}=\frac{k_2^s}{k_{2,e}^f}\left(\frac{C'}{y_{1,0}^*}+\beta z_0\right)(y_2^*-f_2 y_2)-\frac{k_3^f}{k_{2,e}^f}\left(y_2\frac{y_1^* C'}{y_{1,0}^*}-\frac{y_3^*}{sg_3 f_2}\right) \tag{4.15}$$

$$\frac{dy_2^*}{dt'}+\frac{y_2^* dC'}{C'dt'}=-\frac{k_2^s}{k_{2,e}^f}\left(\frac{C'}{y_{1,0}^*}+\beta z_0\right)(y_2^*-f_2 y_2)+\frac{k_2^f}{k_{2,e}^f}\left(y_1^*\frac{y_1^* C'}{y_{1,0}^*}-\frac{y_2^*}{sg_2}\right) \tag{4.16}$$

$$\frac{dy_3}{dt'}+\frac{y_3 dC'}{C'dt'}=\frac{k_3^s}{k_{2,e}^f}\left(\frac{C'}{y_{1,0}^*}+\beta z_0\right)\left(y_3^*-f_3 y_3\right)-\frac{k_4^f}{k_{2,e}^f}\left(y_3\frac{y_1^* C'}{y_{1,0}^*}-\frac{y_4^*}{sg_4 f_3}\right) \tag{4.17}$$

$$\frac{dy_3^*}{dt'}+\frac{y_3^* dC'}{C'dt'}=-\frac{k_3^s}{k_{2,e}^f}\left(\frac{C'}{y_{1,0}^*}+\beta z_0\right)\left(y_3^*-f_3 y_3\right)+\frac{k_3^f}{k_{2,e}^f}\left(y_2\frac{y_1^* C'}{y_{1,0}^*}-\frac{y_3^*}{sg_3 f_3}\right) \tag{4.18}$$

$$\frac{dy_4}{dt'}+\frac{y_4 dC'}{C'dt'}=\frac{k_4^s}{k_{2,e}^f}\left(\frac{C'}{y_{1,0}^*}+\beta z_0\right)\left(y_4^*-f_4 y_4\right)-\frac{k_5^f}{k_{2,e}^f}\left(y_4\frac{y_1^* C'}{y_{1,0}^*}-\frac{y_5^*}{sg_5 f_4}\right) \tag{4.19}$$

$$\frac{dy_4^*}{dt'}+\frac{y_4^* dC'}{C'dt'}=-\frac{k_4^s}{k_{2,e}^f}\left(\frac{C'}{y_{1,0}^*}+\beta z_0\right)\left(y_4^*-f_4 y_4\right)+\frac{k_4^f}{k_{2,e}^f}\left(y_3\frac{y_1^* C'}{y_{1,0}^*}-\frac{y_4^*}{sg_4 f_3}\right) \tag{4.20}$$

$$\frac{dy_5}{dt'}+\frac{y_5 dC'}{C'dt'}=\frac{k_5^s}{k_{2,e}^f}\left(\frac{C'}{y_{1,0}^*}+\beta z_0\right)\left(y_5^*-f_5 y_5\right) \tag{4.21}$$

$$\frac{dy_5^*}{dt'}+\frac{y_5^* dC'}{C'dt'}=-\frac{k_5^s}{k_{2,e}^f}\left(\frac{C'}{y_{1,0}^*}+\beta z_0\right)\left(y_5^*-f_5 y_5\right)+\frac{k_5^f}{k_{2,e}^f}\left(y_4\frac{y_1^* C'}{y_{1,0}^*}-\frac{y_5^*}{sg_5 f_4}\right) \tag{4.22}$$

where C′ equals C/C_o . Using mass balance ,

$$\Sigma\, d([A_i] + [A_i^*]) = 0$$

the following equation can be derived

$$\frac{dC'}{dt'} = -\frac{k_2^f}{k_{2,e}^f}\left(y_1^* \frac{y_1^* C'}{y_{1,0}^*} - \frac{y_2^*}{sg_2}\right) - \sum_3 \frac{k_n^f}{k_{2,e}^f}\left(y_{n-1} \frac{y_1^* C'}{y_{1,0}^*} - \frac{y_n^*}{sg_n f_{n-1}}\right) \tag{4.23}$$

By substituting the above expressions for dy_i/dt' into the expression for the conservation of energy,

$$\Sigma\,(H_i\, d[A_i] + H_i^*\, d[A_i^*]) = \Sigma(C_{p,i}[A_i] + C_{p,i^*}[A_i^*])dT$$

in which H_i and H_i^* are the molar enthalpies of Ar, unexcited and excited i-mer respectively, $C_{p,i}$ and C_{p,i^*} are the molar heat capacities of Ar, unexcited and excited i-mer respectively, and T is the temperature, the rate of change of temperature is given by

$$\frac{dT}{dt'} = \left[\frac{C'}{y_{1,0}^*} + \beta z_0\right]\left[\sum \frac{k_i^s}{k_{2,e}^f}(H_i^* - H_i)(y_i^* - f_i y_i) + \frac{k_2^f}{k_{2,e}^f}(2H_1^* - H_2^*)\left(y_1^* \frac{y_1^* C'}{y_{1,0}^*} - \frac{y_2^*}{sg_2}\right)\right.$$
$$\left. + \sum_2 (H_n + H_1^* - H_{n+1}^*)\frac{k_n^f}{k_{2,e}^f}\left(y_{n-1} \frac{y_1^* C'}{y_{1,0}^*} - \frac{y_n^*}{sg_n f_{n-1}}\right)\right] / \left(\sum_1 (C_{p,i} y_i + C_{p,i^*} y_i^*) + z_0 y_{1,0}^* \frac{C_{p,Ar}}{C'}\right) \tag{4.24}$$

The rate constants are all unknown. To minimize the number of parameters without loss of generality we express the stabilization rate constants for monomer and dimer in Arrhenius form,

$$\frac{k_1^s}{k_{2,e}^f} = \frac{k_{1,e}^s}{k_{2,e}^f} e^{-\frac{E_1}{RT}} \tag{4.25}$$

and

$$\frac{k_2^s}{k_{2,e}^f} = \frac{k_{2,e}^s}{k_{2,e}^f} e^{-\frac{E_2}{RT}} \tag{4.26}$$

while for large clusters (n>2),

$$\frac{k_n^s}{k_{2,e}^f} = \frac{k_{n,e}^s}{k_{2,e}^f} e^{A(n-2)} \tag{4.27}$$

where the scaling constant, A, can be positive or negative. A similar scaling factor, B, is used to express the dependence of the formation rate constant on n. Here k_n^f is based on a barrierless hard sphere collision model and is proportional to the effective collision area and the square of the reduced mass,

$$\frac{k_n^f}{k_{2,e}^f} = \left(\frac{1+n^{1/3}}{1+2^{1/2}}\right)\sqrt{\frac{2}{3}\left(\frac{n+1}{n}\right)}\, e^{B(n-2)} \tag{4.28}$$

The schlieren signal in the experiments is essentially dρ/dy vs t. In the ideal gas law, ρ=pμ/RT, we take pμ as approximately constant in time during the shock wave[117], and we obtain the following relation :

Therefore, for the purpose of simulating the experimental observable, dρ/dy, it is

$$-\frac{d\rho}{dt'}\frac{dt'}{dy}=\frac{p\mu}{R}\frac{dT}{T^2dt'}\frac{dt'}{dy} \qquad (4.29)$$

sufficient to calculate $dT/(T^2\,dt')$.

4.2.4 The Equilibrium Distribution

In the above system of differential equations there are two kinds of coefficients. One consists of constants like $y^*_{1,0}$ and z_o . The others are coefficients that change with temperature during the integration, such as f_n, g_n , k^s_n , k^s_{-n} , k^f_{-n} and k^f_n . The cluster mole fractions, y_n and y^*_n , together with C' , T and t' are variables. In order to numerically integrate this system of equations the coefficients and the initial values of the variables must be given. In this section we discuss how to derive the equilibrium distribution at a given temperature, because it relates to the initial values of y and to the reverse rate coefficients through the appropriate equilibrium constants.

The initial distribution of clusters is calculated using the equilibrium constant, K_p, of the reaction, $A_n \rightleftharpoons A_{n-1} + A$. All clusters are considered to be in the gas phase. If P_n , P_{n-1} and P_1 are the equilibrium partial pressures of A_n , A_{n-1} and A_1 respectively. Then

$$K_p=\frac{P_{n-1}P_1}{P_n} \qquad (4.30)$$

From thermodynamics

$$K_{p,n}=e^{-\frac{\Delta G_n^o}{RT}} \tag{4.31}$$

where ΔG_n^o is the standard Gibbs free energy change for the above process, and R is the universal gas constant. From Eqns. 4.30 and 4.31 the following equation can be derived

$$\frac{y_{n-1,o}y_{1,o}}{y_{n,o}}=\frac{e^{-\frac{\Delta G_{n,T_o}^o}{RT_o}}}{\sum p_{i,o}} \tag{4.32}$$

where the subscript o is used to indicate the initial condition. $\Sigma p_{i,0}$ is given by

$$\begin{aligned}\sum p_{i,o}&=\frac{p_o}{p_{vap,T_o}}p_{vap,T_o}\\&=s_o e^{-\frac{\Delta H_{vap}}{R}(\frac{1}{T_o}-\frac{1}{T_b})}\end{aligned} \tag{4.33}$$

Here P_o is the total pressure of the vapour phase at the initial condition. $P_{vap,To}$ is the saturated vapour pressure at the initial temperature T_o. s_o is the degree of supersaturation of CCl_3F at the initial temperature. T_b is the normal boiling point of CCl_3F.

Let

$$X_{n,T_o}=\frac{y_1 y_{n-1}}{y_n} \tag{4.34}$$

Using the mass conservation condition,

$$\sum y_{n,T_o}=1, \tag{4.35}$$

a polynomial equation is obtained:

$$\sum_{n=2}^{N} \frac{y_1^n}{\prod_{i=2}^{n} X_{i,T_o}} + y_1 - 1 = 0 \tag{4.36}$$

Once y_i is determined, the mole fraction of excited i-mer can be determined from y_i and from the partition function that is given below

$$f_{i,T_o}=e^{-\frac{\Delta H_i^o+\frac{3}{2}RT}{RT}}=\frac{y_i^*}{y_i} \tag{4.37}$$

where ΔH_i^o is the enthalpy change for the process $A_n = A_{n-1} + A$. In other words the excited cluster is considered to be the same as its two components barely holding together like a rotating double star with rotational energy 3/2RT. Hence the cluster distribution at the initial temperature can be calculated.

This procedure is , however, not acceptable for monomers, which contain a significant population in a large number of stable states. In order to keep the problem tractable we proceeded as follows:

The equilibrium mole fraction of monomer, y_p, directly obtained by solving the polynomial equations was partitioned in the following way. First, the degeneracy, g(e(v)), the number of ways a given amount of vibration energy, e(v) , can be distributed among the quantized vibrational modes of CCl_3F molecule, was calculated with the algorithm proposed by Beyer and Swinharts[137,138]. The fundamental frequency[139] of each mode of CCl_3F was used in the calculation. Then, a graph of $g(e(v))e^{-e(v)/RT}$ against e(v) was made. For simplicity, the molecule of CCl_3F was assumed to have only two energy states in the model, which we called ground and excited states. Choosing the maximum point on the curve, we found the corresponding vibrational energy, e(v,max). Then, the partition factor, P_q, was determined by

$$P_q = \frac{\sum_{e(v)=0}^{e(v,max)} g(e(v))e^{-\frac{e(v)}{RT}}}{\sum_{e(v)=0}^{e(v)=\infty} g(e(v))e^{-\frac{e(v)}{RT}}} \qquad (4.38)$$

The total monomer mole fraction, y_p, obtained by solving the polynomial equations was then partitioned, according to $y_1 = y_p P_q$ and $y_1^* = y_p(1-P_q)$. This procedure was repeated for other temperatures.

The values of P_q, the partition factor, and the thermodynamic data for CCl_3F, such as

vapour pressure, entropy and enthalpy of vaporization and the density of the liquid state at the vapour pressure, and the corresponding temperature were read into the program. They served as the data base for the Eqcalcu Fortran program. In the program the data base was built up by calling subroutine Splifit in which cubic spline fitting was implemented. The data at any temperature below 600 K could be interpolated from the data base.

The equilibrium distribution of clusters after passage of the shock can be calculated in the following way. From the equilibrium constant for the process $A_n = A_{n-1} + A$ the following equation is obtained as in Eq. 4.32,

$$\frac{y_{n-1}y_1}{y_n} = \frac{e^{-\frac{\Delta G_n^\circ}{RT}} \Sigma i p_{i,2}}{\Sigma i p_{i,2} \Sigma p_{i,2}} \tag{4.39}$$

Here the number 2 indicates the postshock pressure. $\Sigma i p_{i,2}$ is given by

$$\begin{aligned} \sum i p_{i,2} &= \sum i p_{i,o} \frac{p_2}{p_o} \\ &= p_2 \sum i y_{i,o} \\ &= \frac{p_2 p_o}{p_o p_{vap,T_o}} p_{vap,T_o} \sum i y_{i,o} \\ &= \frac{p_2}{p_o} s_o e^{-\frac{\Delta H_{vap}}{R}\left(\frac{1}{T_o} - \frac{1}{T_b}\right)} \sum i y_{i,o} \end{aligned} \tag{4.40}$$

where p_2/p_o is the compression factor determined by the shock wave conditions, p_2 is

the pressure behind the shock wave, and p_o is the pressure ahead of the shock wave. s_o is the degree of supersaturation at the initial temperature. ΔH_{vap} is the enthalpy of vaporization. $y_{i,o}$ is the equilibrium cluster mole fraction at the initial temperature.

Letting

$$X_i=\frac{e^{-\frac{\Delta G^o_{i,T}}{RT}}}{\frac{p_2}{p_o}s_o e^{\frac{-\Delta H_{vap}}{R}(\frac{1}{T_o}-\frac{1}{T_b})\sum i y_{i,o}}} \tag{4.41}$$

then

$$X_n=\frac{y_1 y_{n-1}}{y_n \sum i y_i} \tag{4.42}$$

and

$$\sum y_i=1 \tag{4.43}$$

Starting with y_1 and y_2 as a basis, application of the above recursion relation leads to two simultaneous polynomial equations in y_1 and y_2:

$$\frac{\sum_{n=1}^{N-2} y_2^{n+1}(\frac{X_2}{y_1})^n}{\prod_{i=3}^{n+2} X_i}+y_2+y_1-1=0 \tag{4.44}$$

and

$$\sum_{n=1}^{N-2} \frac{(n+2)y_2^{n+1}(\frac{X_2}{y_1})^n}{\prod_{i=3}^{n+2} X_i} + 2y_2 + y_1 - \frac{y_1^2}{y_2 X_2} = 0 \qquad (4.45)$$

From these two equations y_1 and y_2 can be found. The remaining y_i can be easily calculated from the recursion relation. y_i can be partitioned into excited y_i^* and y_i using the partition equation (4.33), and all y_i and y_i^* renormalized using $\Sigma(y_i+y_i^*)=1$. From the equilibrium distribution, g_n, f_n and s can be calculated.

4.2.5 Thermodynamic Data for Clusters

In order to solve the polynomial equations and derive the equilibrium distribution the standard free energy change and the standard enthalpy change for the process

$$A_n \rightleftharpoons A_{n-1} + A \qquad (4.46)$$

must be known. In this section the formulae for calculating the internal energy change, the standard enthalpy change , the standard entropy change and the standard Gibbs free energy change are discussed.

1. **Energy change.** In this model the potential interactions between CCl_3F molecules in a cluster are represented by a pairwise additive square potential function. The cluster is defined as a group of CCl_3F molecules bound together by their intermolecular interactions. The distance between molecules in a cluster is comparable in magnitude

with the intermolecular distance in the liquid phase. The total interaction energy of i-mers can be derived from the following consideration. First, supposing all molecules are interacting with each other, the total interaction energy, U_n, is

$$-\frac{\varepsilon n(n-1)}{2} \tag{4.47}$$

where ε is the depth of the square well potential function i.e. the decrease in energy when two separate molecules form a stable dimer. n is the number of molecules in the cluster. If the radius of the cluster, R , is larger than the range of the molecular force (η) not all of the molecule interact with all of the other (n-1) molecules; rather only with $[(\eta/R)^3 n-1]$ molecules, providing that the cluster has uniform density. The total interaction energy is equal to

$$-\frac{\varepsilon n}{2}[(\frac{\eta}{R})^3 n-1] \tag{4.48}$$

If a molecule is situated on or close to the surface of the cluster it interacts with fewer molecules than $[(\eta/R)^3 n-1]$. Therefore, the above calculation overestimates the total interaction energy. After correcting this problem[27] the total interaction energy is given by

$$U_n=-\frac{\varepsilon}{2}[(\frac{\eta}{r_o})^3(n-\frac{9\eta}{16r_o}n^{\frac{2}{3}}+\frac{1}{32}(\frac{\eta}{r_o})^3)-n] \tag{4.49}$$

The total interaction energy of the cluster calculated using eq.4.49 is based on the assumption that monomers do not have any intrinsic energy of their own which depends on its neighbours. The energy *per molecule*, U_n , has is given by

$$\overline{U_n}=-\frac{\epsilon}{2}((\frac{\eta}{r_o})^3[1-\frac{9\eta}{16r_o}n^{-\frac{1}{3}}+\frac{1}{32}(\frac{\eta}{r_0})^3\frac{1}{n}]-1) \tag{4.50}$$

As the cluster size, n, goes to infinity the liquid phase is obtained. At this condition the average interaction energy per molecule is

$$\overline{U}_{liquid}=-\frac{\epsilon}{2}((\frac{\eta}{r_O})^3-1) \tag{4.51}$$

according to this model. This is the interaction energy of one average molecule of CCl_3F in the liquid phase. Since it is assumed that there is no interaction between monomers this is simply the energy difference between a molecule in the liquid and in the vapour. Shifting the energy scale to let the energy of a monomer in the liquid phase be zero, adds the term

$$\overline{U}=\frac{\epsilon}{2}((\frac{\eta}{r_O})^3-1) \tag{4.52}$$

to the energy of a monomer in the gas phase.

Now the total interaction energy of the n-mer is given by

$$U_n'=\frac{\epsilon}{64}(\frac{\eta}{r_o})^4[18n^{\frac{2}{3}}-(\frac{\eta}{r_o})^2] \tag{4.53}$$

for n≥2. For the monomer

$$\overline{U_1}=\frac{\epsilon}{2}\left(\left(\frac{\eta}{r_o}\right)^3-1\right) \tag{4.54}$$

The total energy of the n-mer should include the translational, vibrational, and rotational energy as well as the interaction energy with other molecules. The total energy of the n-mer cluster is then given by

$$\overline{E_n}=U_n'+(12n-3)kT \tag{4.55}$$

The term (12n-3)kT is the result of treating the energy of every degree of freedom of translation , rotation and vibration classically. Within each cluster there are 3n free rotations and 3n free translations. Accounting for 3 translations and 3 rotations of the cluster as a unit, leaves (9n-6) vibrations. Similarly for the monomer

$$\overline{E_1}=12kT+U_1' \tag{4.56}$$

The energy change for the process $A_n = A_{n-1} + A$ is given by

$$\Delta\overline{E_n}=\frac{\epsilon}{2}\left[\left(\frac{\eta}{r_o}\right)^3\left(1-\frac{9\eta}{16r_o}\left(n^{\frac{2}{3}}-(n-1)^{\frac{2}{3}}\right)-1\right]\right. \tag{4.57}$$

The value of ϵ/k is 399 K for CCl_3F (see ref.140). Replacing k by R gives molar units instead of molecular units.

2. **Entropy change.** In equilibrium statistical mechanics[141] entropy is given by

$$S=k\ln Q+kT\left(\frac{\partial \ln Q}{\partial T}\right)_{v,N} \tag{4.58}$$

where k is Boltzmann's constant, N is the number of particles in the system, and Q is the partition function of the system given by

$$Q=\left[\frac{1}{N!}q_{tr}^{N}\right]q_{rot}^{N}q_{vib}^{N}q_{ele}^{N} \tag{4.59}$$

for an assembly of any species of weakly coupled units. q_{tr}, q_{rot}, q_{vib} and q_{ele} are the molecular partition functions for translation, rotation, vibration and electronic motions respectively .

For monomers

$$q_{tr}=\left(\frac{2\pi mkT}{h^2}\right)^{\frac{3}{2}}V \tag{4.60}$$

and

$$q_{rot}=\frac{\pi^{\frac{1}{2}}}{\sigma}\left(\frac{T^3}{\theta_A\theta_B\theta_C}\right)^{\frac{1}{2}} \tag{4.61}$$

where

$$\theta_i=\frac{h^2}{8\pi^2 I_i k} \tag{4.62}$$

σ is the symmetry number, and $I_i = \sum m_i r_i^2$ is the moment of inertia where r_i symbolizes the distance of each atom (of mass m_i) from the axis of rotation. The product of the moments of inertia of CCl_3F, $I_A I_B I_c$, is 5.7360×10^{-113} g^3 cm^6 (see ref 139). h is Planck 's constant = 6.6262×10^{-34} Js. At high enough temperatures q_{vib} is given by

$$q_{vib}=\prod_{i=1}^{9}\frac{kT}{h\nu_i} \tag{4.63}$$

The entropy of the monomer is given by

$$\frac{S_{monomer}}{k}=-NlnN+NlnV+\frac{3}{2}Nlnm+\frac{3}{2}NlnI+\frac{3}{2}NlnT+\frac{3}{2}NlnT$$
$$+\sum_{i=1}^{9}[NlnT+Nln(\frac{ke}{h\nu_i})]+Nlne^4+Nln(\frac{2\pi k}{h^2})^{\frac{3}{2}}+Nln(\frac{8\pi^2(2\pi k)^{\frac{3}{2}}}{\sigma h^3}) \tag{4.64}$$

After forming a cluster a given molecule's vibrational and electronic energy do not change according the model. Only the translational movement changes since a molecule in a cluster can only move in a very small volume, v_o, and this movement is limited by the interaction forces between molecules for the restricted motion. The translational partition function under such circumstance can be shown to be given approximately by

$$q_{tr}^{/}=(\frac{2\pi mkT}{h^2})^{\frac{3}{2}}v_o e^{-\frac{U_*}{kT}} \tag{4.65}$$

q'_{tr} is the molecular translational partition function for motion within an n-mer. v_o is the free volume in which molecule can move around within the n-mer. U_n is the interaction energy that a molecule possesses in the n-mer. Let

$$q_{tr,u}=e^{-\frac{U_n}{kT}} \tag{4.66}$$

and let $S_{tr,u}$ be the contribution of $q_{tr,u}$ to the entropy of the n-mer. $S_{tr,u}$ is equal to

$$\begin{aligned} S_{tr,u} &= Nk(lnq_{tr,\epsilon}+T(\frac{\partial lnq_{tr,\epsilon}}{\partial T})_{N,v}] \\ &= Nk(-\frac{U_n}{kT}+T\frac{\partial(-\frac{U_n}{kT})}{\partial T}) \\ &= 0 \end{aligned} \tag{4.67}$$

The above shows that $q_{tr,u}$ does not contribute to the entropy of an n-mer. The partition functions for rotation and vibration are the same as those for the monomer . Now the entropy of the (n-1)-mer is given by

where N is the number of (n-1)-mers in the system, and (n-1) is the number of molecules in the cluster. The first line of the equation is the contribution of the cluster as a unit; the

$$\frac{S_{(n-1)-mer}}{k}=-NlnN+NlnV+3NlnT+\frac{3}{2}N\ln[(n-1)m]+\frac{3}{2}N\ln[(n-1)^{\frac{5}{3}}I]+const_1$$
$$-N(n-1)\ln(n-1)+N(n-1)\ln[(n-1)v_0]+3N(n-1)lnT+\frac{3}{2}N(n-1)lnm$$
$$+\frac{3}{2}N(n-1)lnI+const_2 \qquad (4.68)$$

second line is the contribution of (n-1) molecules within each cluster to the entropy of the (n-1)-mer. Since we assume that the cluster is a sphere the moments of inertia of the (n-1)-mer, I_A, I_B and I_C are equal to $I_i=2Mr^2/5$, where M is the mass of the cluster (proportional to n), and r is the radius of the cluster (proportional to $n^{1/3}$). Therefore, the moment of inertia of an (n-1)-mer is $Cn^{5/3}$ times that of the monomer, wherein C is a constant. In the same way, the entropy of the n-mer is given by

$$\frac{S_{(n-mer)}}{k}=-NlnN+NlnV+3NlnT+\frac{3}{2}Nln(nm)+\frac{3}{2}Nln(n^{\frac{5}{3}}I)+const_{1'} \qquad (4.69)$$
$$-NnlnN+Nnln(nv_o)+3NnlnT+\frac{3}{2}NnlnI+\frac{3}{2}nNlnI+const_{2'}$$

Then, for $A_n \rightleftharpoons A_{n-1} + A$

$$\frac{\Delta S}{k}=\frac{S_{monomer}}{k}+\frac{S_{(n-1)-mer}}{k}-\frac{S_{n-mer}}{k} \qquad (4.70)$$
$$=Nln(\frac{V}{Nv_o})+Nln(\frac{n-1}{n})^4$$

As $n \to \infty$, $\Delta S / k$ become

$$\frac{\Delta S_{\infty}}{k} = N \ln\left(\frac{V_{gas}}{N v_o}\right) \tag{4.71}$$

This is the entropy change for the process of transformation from pure liquid to vapour . The entropy change for the process $A_n \rightleftharpoons A_{n-1} + A$ can be written as

$$\frac{\Delta S}{k} = \frac{\Delta S_{\infty}}{k} + N \ln\left(\frac{n-1}{n}\right)^4 \tag{4.72}$$

If we consider the process $A_n \rightarrow nA$ the entropy change is given by

$$\frac{\Delta S_n}{Nk} = \ln \frac{V_{gas}}{N v_o} - \frac{1}{n}\left[4 \ln n + \ln\left(\frac{T^3 m^{\frac{3}{2}} I^3 e^4 \pi^5 64 k^3}{\sigma v_o h^6}\right)\right] \tag{4.73}$$

As $n \to \infty$ the same limiting values are obtained whether the process is $A_n \rightarrow A_{n-1} + A$ or $A_n \rightarrow nA$.

In the above derivation the classical approximation was made for the vibrational partition function

$$q_{vib} = \frac{e^{-\frac{h\nu}{2kT}}}{1 - e^{-\frac{h\nu}{kT}}} \approx \frac{kT}{h\nu} \tag{4.74}$$

where the frequencies, ν, are not affected by clustering.

Now we discuss the effect of this approximation. The cluster $(CCl_3F)_n$ has a total of 5n atoms and thus have a total of 15n degrees of freedom. Taking the cluster as a unit it has three degrees of freedom of translational movement and three degrees of freedom of rotational movement. Every molecule in the cluster has three degrees of (restricted) translational freedom and three degrees of rotational freedom . Therefore, the total degrees of vibrational freedom within the cluster is 15n -6n -6 =9n -6 . Each monomer has three translational degrees of freedom and three rotational degrees of freedom, for a remainder of 15-6=9 vibrational degrees of freedom. The contribution of the vibrational motion to the entropy change of $A_n \rightarrow A_{n-1} + A$ is thus given by

$$\begin{aligned}\frac{\Delta S_{vib}}{k} &= \frac{S_{(n-1)-mer,vib}}{k} + \frac{S_{mono,vib}}{k} - \frac{S_{n-mer,vib}}{k} \\ &= (9n-15+9-9n+6)[k[lnq_v + T(\frac{\partial \ln q_v}{\partial T})_{N,V}] \\ &= 0\end{aligned} \tag{4.75}$$

where each oscillator is treated on the same footing whether it is inside or outside of the cluster. Had we partitioned the energy differently, e.g. had we ascribed the internal restricted translations and rotations to vibrations, then there would have been a loss of 6 oscillators. With our procedure there is no net change in the number of oscillators and there is no need to assign frequencies in calculating ΔS_{vib}. As it stands vibration contributes nothing to the entropy change of the process.

Another approximation that has been made is Stirling's formula ln N! ≈ NlnN-N. When considering the number of monomers or the number of clusters this approximation is valid because N is a large number. However, when considering the number of molecules in an n-mer this approximation as applied to ln n! is not valid because n is a small number in our work. Let us find the effect of using the Stirling's approximation for the process $A_n = A_{n-1} + A$. The difference is given by

$$\begin{aligned}
&[\ln n! - (n\ln n - n)] - [\ln(n-1)! - (n-1)\ln(n-1) + (n-1)\ln e] \\
&= \ln\frac{n!}{(n-1)!} - n\ln n + (n-1)\ln(n-1) + \ln e \\
&= \ln n - n\ln n + (n-1)\ln(n-1) + \ln e \\
&= -(n-1)\ln n + (n-1)\ln(n-1) + \ln e \\
&= (n-1)\ln\frac{n-1}{n} + \ln e
\end{aligned} \tag{4.76}$$

So we must add this difference to our formula for entropy change, ΔS,

$$\begin{aligned}
\frac{\Delta S}{k} &= \frac{\Delta S_m}{k} + 4\ln\frac{n-1}{n} + (n-1)\ln\frac{n-1}{n} + \ln e \\
&= \frac{\Delta S'_{vap}}{k} + (n+3)\ln\frac{n-1}{n}
\end{aligned} \tag{4.77}$$

in which

$$\frac{\Delta S'_{vap}}{k} = \ln\frac{V_{gas}}{N v_o} + 1 \tag{4.78}$$

v_o is the average free volume in which a molecule can move around within a cluster. If the vapour phase can be treated as an ideal gas then $\Delta S'_{vap}$ at pressure, P, and temperature, T, can be written as

in which V_{gas} is replaced by the molar volume, V_{gas} at the saturated vapour pressure.

$$\Delta\overline{S'_{vap}} = R(\ln\frac{V_{gas}}{\overline{v_o}} + 1)$$

$$= R[\ln\frac{\overline{V}(T,P_{vap})\frac{P_{vap}}{P}}{\overline{v_o}(T,P_{vap})} + 1] \qquad (4.79)$$

$$= \Delta\overline{S_{vap}}(T,P_{vap}) - R\ln s_o$$

Nv_o is replaced by the free molar volume, v_o, in which a molecule can move around in the liquid phase at the saturated vapour pressure. ΔS_{vap} is the molar entropy change for liquid → vapour, and s_o is the degree of supersaturation defined by P/P_{vap} .

For $A_n \rightleftharpoons A_{n-1} + A$ the entropy change is given by

$$\frac{\Delta\overline{S_n}}{k} = \frac{\Delta\overline{S_{vap}}(T,P_{vap})}{k} + \ln(\frac{n-1}{n})^{(3+n)} - R\ln s_o \qquad (4.80)$$

Here ΔS_{vap} (T,P_{vap}) is the molar entropy change at the temperature, T, and the vapour pressure, P_{vap}, for liquid → vapour. The standard entropy change can be calculated by replacing P with 1atm.

3. Enthalpy change. From H = U + PV , the molar enthalpy of n-mers can be written as

$$H_n = (12n-3)RT + U_n + PV_{liq} \qquad (4.81)$$

For monomers the molar enthalpy is given by

$$H_1 = 12RT + U_1 + RT \tag{4.82}$$

For the process $A_n = A_{n-1} + A$

$$\begin{aligned}\Delta H_n &= RT + \overline{U_{n-1}} + \overline{U_1} - \overline{U_n} + \overline{PV_{liq}} \\ &= RT - \overline{PV_{liq}} + \frac{\varepsilon}{2}\left[\left(\frac{\eta}{r_o}\right)^3\left(1 - \frac{9}{16}\left(\frac{\eta}{r_o}\right)\left(n^{\frac{2}{3}} - (n-1)^{\frac{2}{3}}\right) - 1\right]\end{aligned} \tag{4.83}$$

For dimer evaporation

$$\Delta H_2 = 4kT + \varepsilon\left[\left(\frac{\eta}{r_o}\right)^3 - 1\right] - \frac{\varepsilon}{64}\left(\frac{\eta}{r_o}\right)^4\left[18 * 2^{\frac{2}{3}} - \left(\frac{\eta}{r_o}\right)^2\right] \tag{4.84}$$

As $n \to \infty$ A_n becomes a bulk liquid, and ΔH_n becomes the enthalpy of evaporation

$$\overline{\Delta H_{vap}}(T, P_{vap}) = RT + \frac{\varepsilon}{2}\left[\left(\frac{\eta}{r_o}\right)^3 - 1\right] - P_{vap}\overline{V_{liq}} \tag{4.85}$$

The known value of ΔH_{vap} allows us to determine the value of the parameter (η/r_o). ΔH_n for the process $A_n = A_{n-1} + A$ is a function of pressure .

4. Free energy change. Since the enthalpy change and the entropy change of the process have been derived the free energy change can be readily derived, using the equation $\Delta G = \Delta H - T\Delta S$. The free energy change as a function of temperature , cluster size and pressure is given by

$$\Delta G_n = RT + \frac{\varepsilon}{2}\left[\left(\frac{\eta}{r_o}\right)^3 - 1\right] + \frac{9\varepsilon}{32}\left(\frac{\eta}{r_o}\right)^4\left[(n-1)^{\frac{2}{3}} - n^{\frac{2}{3}}\right] - RT\left[\ln\frac{V}{Nv_o} + 1 + \ln\left(\frac{n-1}{n}\right)^{(3+n)}\right] \quad (4.86)$$

For the calculation of the distribution cluster the standard free energy change, ΔG^o, for the process $A_n = A_{n-1} + A$ is required. The standard free energy change refers to that the reactants in their standard states transforming to the products in their standard states. The standard states for gas phase n-mers , (n-1)-mers and monomers are pure substances at unit pressure, P. In order to get ΔG^o, V in the equation for ΔG is replaced by NkT/P, and we set $P = P^o$.

$$\Delta G_n^o = RT + \frac{\varepsilon}{2}\left[\left(\frac{\eta}{r_o}\right)^3 - 1\right] + \frac{9\varepsilon}{32}\left(\frac{\eta}{r_o}\right)^4\left[(n-1)^{\frac{2}{3}} - n^{\frac{2}{3}}\right] - RT\left[\ln\frac{kT}{P^o v_o} + 1 + \ln\left(\frac{n-1}{n}\right)^{(3+n)}\right]$$

(4.87)

The difference between 4.87 and 4.86 is simply

$$\Delta G - \Delta G^o = RT\ln\frac{P}{P^o} \quad (4.88)$$

Then

$$\Delta G_n^o = RT + \frac{\varepsilon}{2}\left[\left(\frac{\eta}{r_o}\right)^3 - 1\right] + \frac{9\varepsilon}{32}\left(\frac{\eta}{r_o}\right)^4\left[(n-1)^{\frac{2}{3}} - n^{\frac{2}{3}}\right] - RT\left[\ln\frac{kT}{P^o v_o} + 1 + \ln\left(\frac{n-1}{n}\right)^{3+n}\right] + RT\ln\frac{P}{P^o}$$

(4.89)

As $n \to \infty$, and when the pressure equals to the equilibrium vapour pressure evaporation takes place and ΔG equals to zero, that is $\Delta H_{vap} = T\,\Delta S_{vap}$. Using this relation and

the equation for ΔH_{vap} and ΔS_{vap} the following is obtained

$$RT+\frac{\varepsilon}{2}[(\frac{\eta}{r_o})^3-1]-RT[\ln\frac{kT}{P_{vap}v_o}]=PV_{liq} \qquad (4.90)$$

so the standard free energy change for the process can be simplified to

$$\Delta G_n^o=PV_{liq}+RT\ln\frac{P^o}{P_{vap,T}}+\frac{9\varepsilon}{32}(\frac{\eta}{r_o})^4[(n-1)^{\frac{2}{3}}-n^{\frac{2}{3}}]-RT\ln(\frac{n-1}{n})^{(3+n)}] \qquad (4.91)$$

in which V_{liq} is the molar volume of the liquid phase. P^o is equal to 1 atm if the unit of the vapour pressure, P_{vap}, is atmosphere. This equation is for n-mers with n larger than 2. For dimers

$$\Delta G_2^o=3RT+PV_{liq}+RT\ln\frac{P^o}{P_{vap,T}}+\frac{\epsilon}{2}[(\frac{\eta}{r_o})^3-1]+\frac{\epsilon}{64}(\frac{\eta}{r_o})^4[18*2^{\frac{2}{3}}-(\frac{\eta}{r_o})^2]-RT\ln(\frac{n-1}{n})^{(3+n)}] \qquad (4.92)$$

Now all of the thermodynamic data for cluster formation can be calculated from the equation that is based on our cluster model and from thermodynamic data for bulk liquid and vapour . In the next section the mathematical procedure for solving the system of ODEs will be discussed.

4.3 Discussion of the Numerical Method

A mathematical model has been constructed based on the proposed physical model of the

last section. It is composed of 12 coupled nonlinear first order differential equations. The initial cluster distribution is known, that is the value of the dependent variable is known at the starting point. There is no analytical solution of our nonlinear coupled system of differential equations. We have to use a numerical method to solve them. In this section we shall first examine our equations for a unique solution , Then we shall discuss the basic idea of the numerical method and finally we shall discuss stiff[142] equations and Gear's method[143].

4.3.1 Properties of the ODEs

Some initial-value differential equations can have more than one solution for given initial values[144]. Many numerical methods will return some numbers, but it is obvious that they do not have any meaning if the problem has no unique solution. Before attempting to solve our initial-value problem, we must know whether a unique solution exists.

To discover if an equation has a unique solution first we must discuss the Lipschitz condition[145]: If $y'=f(t,y)$ is a differential equation $f(t,y)$ is said to satisfy a Lipschitz condition in the variable, y, on a set $D=\{(t,y)| 0\leq t \leq b, -\infty<y<+\infty\}$, provided that a constant $L>0$ exists with the property that

$$|f(y,t)-f(y^*,t)| \leq L |y-y^*|$$

whenever $(t,y), (t,y^*) \in D$. The constant, L, is called a Lipschitz constant for f. The theorem states that f(t,y) is continuous and differentiable on D. If f satisfies a Lipshitz

condition on D in the variable y, then the initial-value problem

$$y'=f(t,y), \quad a \le t \le b, \quad y(a)= \alpha$$

has a unique solution, y(t), for $a \le t \le b$.

Our system of differential equations was examined with this theorem. We found all of our equations are continuous and differentiable on the region $0 \le t' \le b$ (b is sufficiently large). The first ten ODEs can be written as

$$f(y_i,t')=A_i^{\circ}y_i^2+A_iy_i+f(y_j,t') \qquad (j=1,2,3.... \text{ and } \neq i)$$

in which $A_i^{\circ}$and A_i are not functions of y_i, and the finite numbers, j are not equal to i. The above equation is continuous. Since $df(y_i,t)/dy_i = 2\ A_i^{\circ}\ y_i + C$, and the maximum of y_i is 1.0, $2\ A_i^{\circ}\ y_i + C < L$ (L is sufficiently large). Therefore, these ten ODEs satisfy the Lipschitz condition. They a have unique solution in a specified region ($0 \le t$). The 11th equation can be written as

$$g(C',t')=BC'^2 + B_2C'$$

Here $C'=C/C_o=y_{11}$ and $0 \le C' < 1$, while B and B_2 are the bounded functions of y_i. $dg(C',t')/dt'$ is continuous and differentiable on the region $0 \le t' \le b$. B and y_{11} are finite numbers in this region. It satisfies the above theorem. The 12th equation can be written as

$$h(T,t')=\sum_i \frac{Dh_{1,i}(T)e^{-\frac{E}{RT}}+Kh_{2,i}(T)}{Gh_3(T)}$$

where D, K, G and E are not functions of T, but rather finite numbers. $h_1(T)$, $h_2(T)$ and $h_3(T)$ are functions of temperature. As long as T is larger than zero, $h_3(T)$ is not equal to

zero. Therefore, dh(T,t')/dT is bounded on the region $0 \leq t' \leq b$. The 12th equation, therefore, also satisfies the Lipschitz condition. We can conclude that there is exactly one solution of our system of ODEs for a set of initial values.

The second question is whether these ODEs are well posed or not. Well-posedness means that small perturbations in the stated problem will lead to only small changes in the solutions[143]. This is obviously a useful condition, because a numerical approximation to the solution may well introduce perturbations such that a different problem would be solved. It is desirable that the solution can be made as accurate as needed by keeping these perturbations small. Unless the original problem is well-posed, though, there is little reason to expect that the numerical solution to a perturbed problem will even approximate the solution to the original problem. Fortunately, the Lipschitz condition is a sufficient condition for an ordinary initial-value problem to be well posed. The theorem[145] states that

if f(y,t) is continuous and satisfies the Lipschitz condition in the variable y on the set D, then the initial-value problem $y'=f(y,t)$, $a \leq t \leq b$, $y(a)=\alpha$ is well posed.

The third question asks whether our system of equations is stiff or not. If some variables are known to change on a time scale very different from that of the others, and if the physical problem is well-posed the governing equations are likely to be stiff[142]. We know that a set of stiff differential equations arises in almost all chemical kinetics studies due to the existence of a set of greatly differing time constants. All of our equations are

characterized by a transient stage at the beginning followed by a relatively slow variation. We can conclude that our system of differential equations is stiff. More detail will be given in section 4.3.3.

4.3.2 The numerical method

The numerical method which we used for the initial-value system of differential equations is a difference method[143]. The solution is approximated by the values of y_i at sequences of discrete points called the mesh points. The space between these points can be either constant or varying. The space between two mesh points is called the step size, h.

The underlying idea of the difference method is to rewrite dy and dt as finite steps Δy and Δt. Multiplying the differential equations by Δt we get $\Delta y = f(t)\Delta t$. Replacing Δy by $y_i - y_{i-1}$, where y_i and y_{i-1} are two values of y at neighbouring mesh points, t_i and t_{i-1}, and where Δt is the step size, h, then we get $y_i = y_{i-1} + hf(t_{i-1})$. This is the difference equation. It give us algebraic formulae for the change in the function when the independent variable, t, is stepped up by the size "h". In the limit of very small step size, $h \to 0$, the value of y at the mesh point, t_i, is obtained. For the initial-value problem the value of y_o at t=0 is known. Using the difference equation the initial value differential equation can be solved.

What we have discussed above is the so-called Euler method[145]. In Euler method we use

the slope, y_1', at the beginning of the interval to determine the increment to the function. But this is not perfect because the slope is not necessarily a constant. Euler method merely illustrates the basic idea of the difference method. It cannot be used in practice. Euler's method is called a one-step method because the approximation for the mesh point, t_i, involves information from only one of the previous mesh points, t_{i-1}. The error[145] in Euler's method behaves as $O(h^1)$ as $h \to 0$. For this reason it is called a first order method. The most common method is the multi-step method, which uses more than one previous mesh point to determine an approximation at the next point.

A multistep method[143] for solving the initial value problem $y'=f(y,t)$,$a \leq t \leq b$,$y(a)=\alpha$ is one whose difference equation for finding the approximation, w_{i+1}, at the mesh point, t_{i+1}, can be represented by the following equation, where m is an integer greater than 1.

$$w_{i+1}=a_{m-1}w_i+a_{m-2}w_{i-1}+\cdots\cdots+a_o w_{i+1-m}+h[b_m f(w_{i+1}, t_{i+1})+b_{m-1}f(w_i, t_i)+\cdots\cdots+b_o f(w_{i+1-m}, t_{i+1-m})]$$

for i=m-1, m,$\cdots$ N-1 where the starting values are $w_o=\alpha$, $w_1=\alpha_1$, $w_2=\alpha_2$,$\cdots$ $w_{m-1}=\alpha_{m-1}$, and h=(b-a)/N. When $b_m=0$ the method is called explicit; when $b_m \neq 0$ the method is called implicit. In practice the combination of explicit and implicit techniques is used. It is called the predictor-corrector method. The explicit method predicts an approximation, and the implicit method corrects this prediction. The Adams-Bashforth-Moulton method[143] is one multistep predictor-corrector method in which the first step is to calculate the starting values, w_0, w_1, w_2, and w_3 for the four step method. To do this, a fourth-order one-step method, the Runge-Kutta method[143], is used. The next step is to calculate an

approximation, w_4^o, to $y(t_4)$ using the Adams-Bashforth four-step method as the predictor

$$w_4^o=w_3+h[55f(t_3,w_3)-59f(t_2,w_2)+37f(t_1,w_1)-9f(t_o,w_o)]/24$$

This approximation is improved by use of the three-step Adams-Moulton implicit method as the corrector,

$$w_4^1= w_3+h[9f(t_4,w_4^o)+19f(t_3,w_3)-5f(t_2,w_2)+f(t_1,w_1)]/24$$

The value, w_4^1, is then used as the approximation to $y(t_4)$, and the technique of using the Adams-Bashforth method as a predictor followed by the Adams -Moulton method as a corrector is repeated to find w_5^o and w_5^1, the initial and final approximation to $y(t_5)$ etc. In theory, improved approximations to $y(t_{i+1})$ can be obtained by iterating the Adams-Moulton formula,

$$w_{i+1}^{k+1}= w_i+h[9f(t_{i+1},w_{i+1}^k)+19f(t_i,w_i)-5f(t_{i-1},w_{i-1})+f(t_{i-2},w_{i-2})]/24$$

k+1 times. In practice, since $\{w_{i+1}^{k+1}\}$ converges to the approximation given by the implicit formula, rather than to the solution, $y(t_{i+1})$, it is usually more efficient to use a reduction in the step size if improved accuracy is needed. The derivation of both the Adams-Bashforth and Adams-moulton method can be found in Gear'work (reference 143).

One of the important concepts in the difference equation method is numerical stability. This refers to those errors which do not grow in subsequent steps. We say that the mathematical problem itself is well-posed if the effects of error build up are bounded regarding the problem itself. We also need to know that small changes in the initial values produce only a bounded change in the numerical approximation provided by the method. If there exists an $h_o>0$ for each differential equation such that a change in the starting

values by a fixed amount produces a bounded change in the numerical solution for all $h \le h_o$, then the method is numerically stable[142]. A stable method is one that depends continuously on the initial data. Well-posedness is related to the mathematical problem while numerical stability is related to the method. Generally speaking, the higher order the method the smaller the stability region is. Implicit methods usually have larger stability regions than those of the corresponding explicit method.

There is a rule for determining whether the method is stable or not. For multistep methods it is given below[145].

The multistep difference equation method is written as

$$w_{i+1} = a_{m-1}w_i + a_{m-2}w_{i-1} + \cdots\cdots + a_o w_{i+1-m} + hF(t_i, h, w_{i+1}, w_i, \cdots\cdots, w_{i+1-m}).$$

and $$w_o = \alpha, \quad w_1 = \alpha_1, \cdots\cdots w_{m-1} = \alpha_{m-1},$$

The characteristic polynomial equation associated with the multistep method is given by

$$P(\lambda) = \lambda^m - a_{m-1}\lambda^{m-1} - \cdots\cdots - a_1\lambda - a_o$$

Let $\lambda_1, \lambda_2 \cdots\cdots \lambda_m$ denote the roots (not necessary distinct) of the characteristic polynomial equation. If $|\lambda_i| \le 1$ for each i =1, 2, ..., m, and all roots with absolute value 1 are simple roots, then the difference method is said to satisfy the root condition.

(1) Methods that satisfy the root condition and have $\lambda = 1$ as the only root of the characteristic equation of magnitude one are called strongly stable.

(2) Methods that satisfy the root condition and have more than one distinct root with magnitude one are called weakly stable

(3) Methods that do not satisfy the root condition are called unstable.

The magnitude of the roots of the characteristic polynomial of multistep methods is associated with the round-off stability of the method. If the $|\lambda_i|>1$, the round-off error will be amplified at each step, and the method is unstable. If a method satisfies the root condition the round-off error is damped, and the multistep method is stable. The characteristic polynomial for the Adams-Bashforth method is $P(\lambda)=\lambda^3(\lambda-1)$, which has roots $\lambda_1=1$, $\lambda_2=0$, $\lambda_3=0$, and $\lambda_4=0$. It is strongly stable. The Adams-Moulton method is strongly stable also.

4.3.3 Stiff ODEs and Gear's Method

Curtiss and Hirschfelder[146] first identified "stiffness" as an important property of differential equations in their chemical kinetics studies. A characteristic of virtually all chemical kinetics systems is the widely disparate time scales involved. This range of times gives rise to a number of computational problems, the best known of which is "stiffness". We can use the simple example given by Kee et al[154] to describe stiffness. Consider the following simple linear first order ODE.

$$y'=-A(y-(t^2-1))+2t \qquad 0\leq t\leq b \qquad y(t=0)=y_o$$

where A is a large positive constant. The general solution of this equation is

$$y=[y_o-1]\, e^{-At} + (t^2+1)\,.$$

For the initial condition $y_o=1$, the solution has only the slowly varying component, $y=t^2+1$. For all other initial conditions, the solution approaches the particular solution

$y=t^2+1$ very rapidly. The larger the value of A the more rapidly the solution approaches $y=t^2+1$. This is the two time-scale problem. The integration curve is composed of two parts: the initial transient part corresponding to the fast process with time constant, 1/A; and the slowly varying part corresponding to $y=t^2+1$.

There is no problem if the above equation is solved analytically. When it is solved numerically, the stiffness problem become evident. If an explicit method is used to solve the above equation in the initial transient part a small step size, h, must be taken for reasons of accuracy, because y changes very fast. In the slowly changing part the step size is restricted to be of the order of h=1/A, i.e. the smallest step size, in order to preserve numerical stability, not accuracy. Stiffness arises only when accuracy would allow us to take a relatively large step size, but stability dictates a much smaller one. It is a remarkable property of the implicit method that it does not suffer such severe stability restrictions. For both linear and nonlinear problems implicit methods are far superior to explicit methods[143].

In our mathematical model the change of mole fraction of monomer and the temperature change are similar to the above example. The integration curve is composed of two processes: a fast transient and a slowly varying part.

The most widely used class of linear multistep methods for stiff problems consists of the implicit "backward differentiation formulae", or Gear's method. As the name suggests,

the derivative at the current point, f_{n+k}, is approximated using the previous (k+1) values, y_{n+j} ($0 \le j \le k$), leading to linear multistep methods of the form

$$\sum_{j=0}^{k} \alpha_j y_{n+j} - h\eta_{n+k} f_{n+k} = 0, \qquad \alpha_k = 1$$

For k=1, the Euler backward difference method is obtained. As noted above, Curtiss and Hirschfelder, who first recognized stiffness problems in ODEs were also the first to propose solving stiff problems using backward differentiation formulae (BDF). Gear[143] showed that the BDF method for k=1,2, ⋯ ,6 satisfied his definition of stiff stability, and outlined a sophisticated implementation of the method as an algorithm with automatic step size and order-changing that provided for careful error control. The mathematical formula of the method is similar to the Adams-Bashforth-Moulton method. It uses a pth order predictor formula of the form

$$w_n^o = \alpha_1 w_{n-1} + \alpha_2 w_{n-2} + \cdots + \alpha_p w_{n-p} + \eta_1 h f(w_{n-1}, t_{n-1})$$

and a p-th order corrector

$$w_n^{m+1} = \beta_1 w_{n-1} + \beta_2 w_{n-2} + \cdots + \beta_p w_{n-p} + \eta_0 h f(w_n^m, t_n).$$

The details of the derivation and the constants α_i, β_i, η_1 and η_0 are given by Gear[143]. This method has been implemented into a very robust, user friendly computer subroutine called IMPAG by IMSL.

Enright and Hull[147] tested different numerical methods for the solution of stiff systems of ODEs arising from chemical kinetics. They tested Gear's method, the method based on the trapezoidal rule proposed by Dahlquist[148], the implicit Runge-Kutta methods

suitable for stiff equations based on the formulae of Butcher[149], methods based on the use of preliminary mathematical transformations to remove stiffness, and methods based on second derivative multistep formulae on standard kinetics problems, kinetics problems with oscillatory solutions, and on reactor problems. They concluded that among the five methods they had tested, Gear's method was suitable as a general purpose method for stiff ordinary differential equations that arise in chemical kinetics studies.

In this section we have examined our ODEs and discussed numerical methods, stiff equations and Gear's method. Now that we have concluded that our stiff ODEs are well-posed, they can be solved using Gear's numerical method. Gear[150] pointed out that for a nonlinear system, when it reaches or closes to chaotic, numerical methods are going to yield very different solutions for different error controls. In our calculation we decrease the parameter, tol, in intregrator, DIVPAG, until integration result does not change. The parameter, tol, controls local error in DIVPAG.

4.4 COMPUTER PROGRAM

The calculation is carried out using two computer programs, Eqcalcu Fortran (Appendix 8) and Integral Fortran (Appendix 9). Eqcalcu Fortran was used for calculating the equilibrium cluster distribution and f_i, g_i and s at different temperatures. Integral Fortran was used to simulate cluster formation, stabilization and dissociation processes as the temperature was changing behind the shock. In order to get higher accuracy, double

precision was used in both computer programs. Both programs were debugged with WATFOR-77 and the results were checked by manual calculations.

The flow chart of the computer program Eqcalcu Fortran is shown in Fig. 4.4.1. First the initial conditions such as the temperature, the degree of supersaturation, and the equilibrium condition were read in. Subroutine Splifit was called to build up the database. Then, the initial cluster distribution was calculated by calling the Yzero routine in which the coefficients of the y_i polynomial equation were calculated. The Therm routine was called to calculate x_i. y_p at the initial condition was calculated by solving the polynomial equation with the IMSL routine DZPORC. Then y_p was partitioned, and the other clusters' mole fractions were calculated, and renormalized. Next we calculated the equilibrium distribution at the post shock temperature. In subroutine Solve the set of simultaneous polynomial equations was solved to get y_P and y_2. The flow chart for this part of EQCALCU is shown in figure 4.4.2. Before entering a loop a trial value of y_p was chosen . Then, in the loop the coefficients of the two simultaneous polynomial equations were calculated. In this calculation subroutine Thermo was called to calculate the value of x_i. After this the IMSL routine DZPORC was called to solve each polynomial. Two values of y_2 were obtained, called y_2 and y_{21}. After comparing them , y_p was decreased or increased depending on whether the value of y_2-y_{21} was positive or negative. This procedure was repeated until the value of $|y_2-y_{21}|$ was less than 10^{-9}. Using the values of y_p and y_2, the cluster distribution was calculated by calling the subroutine Distri. Then g_i and s could be calculated.

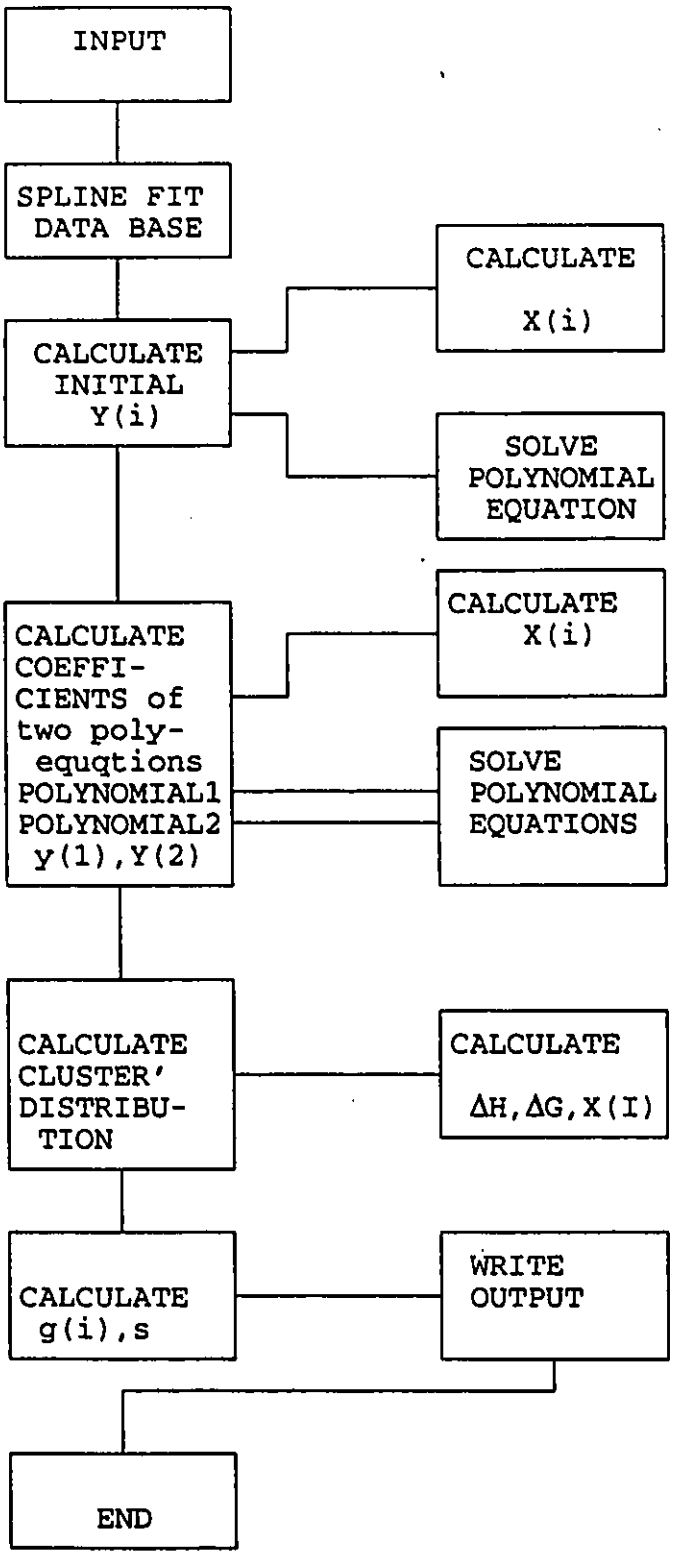

Fig. 4.4.1 The flow chart of computer program Eqcalcu Fortran

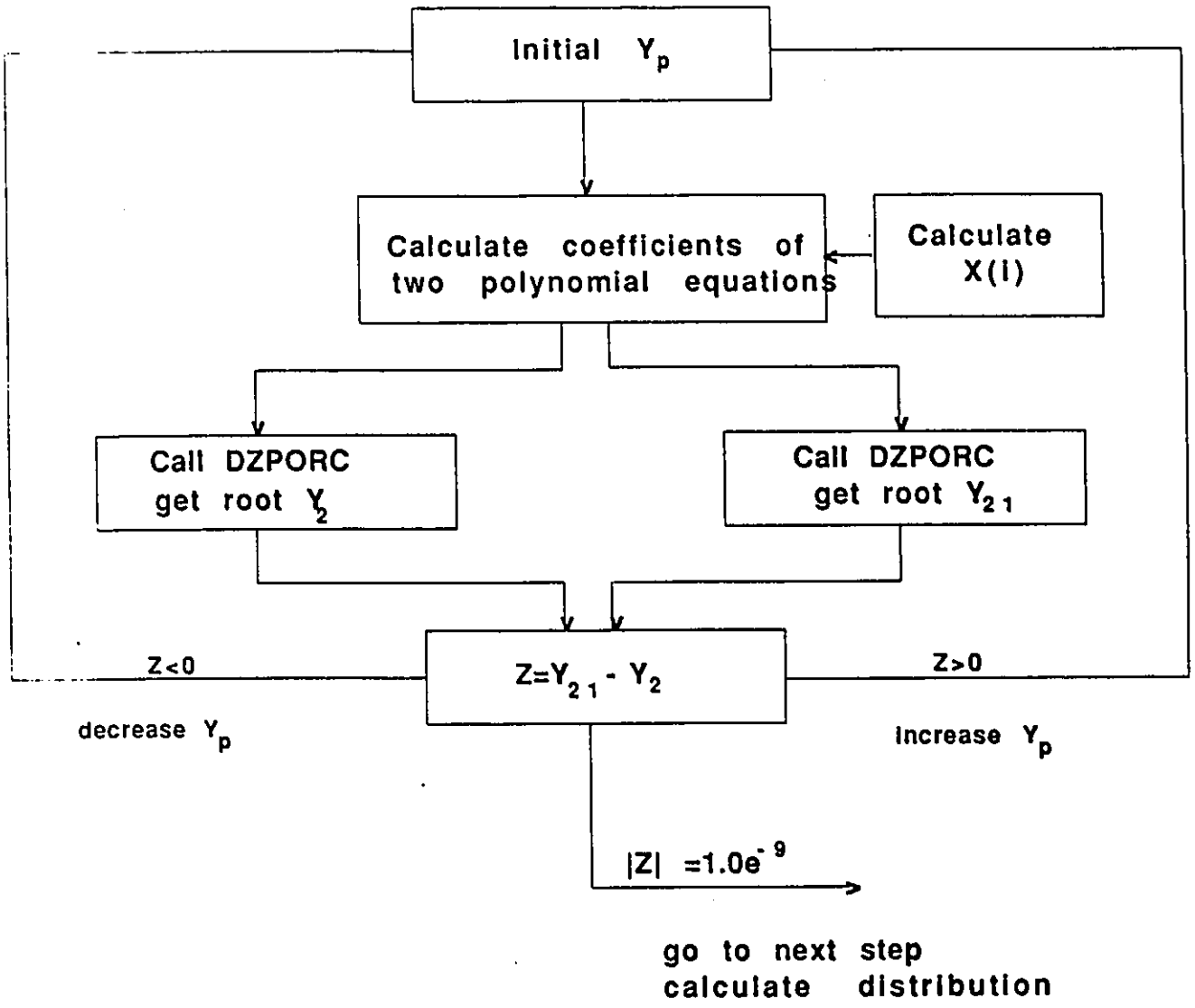

Fig. 4.4.2 The flow chart of subroutine SOLV for solving the two simultaneous polynomial equations in EQCALCU FORTRAN

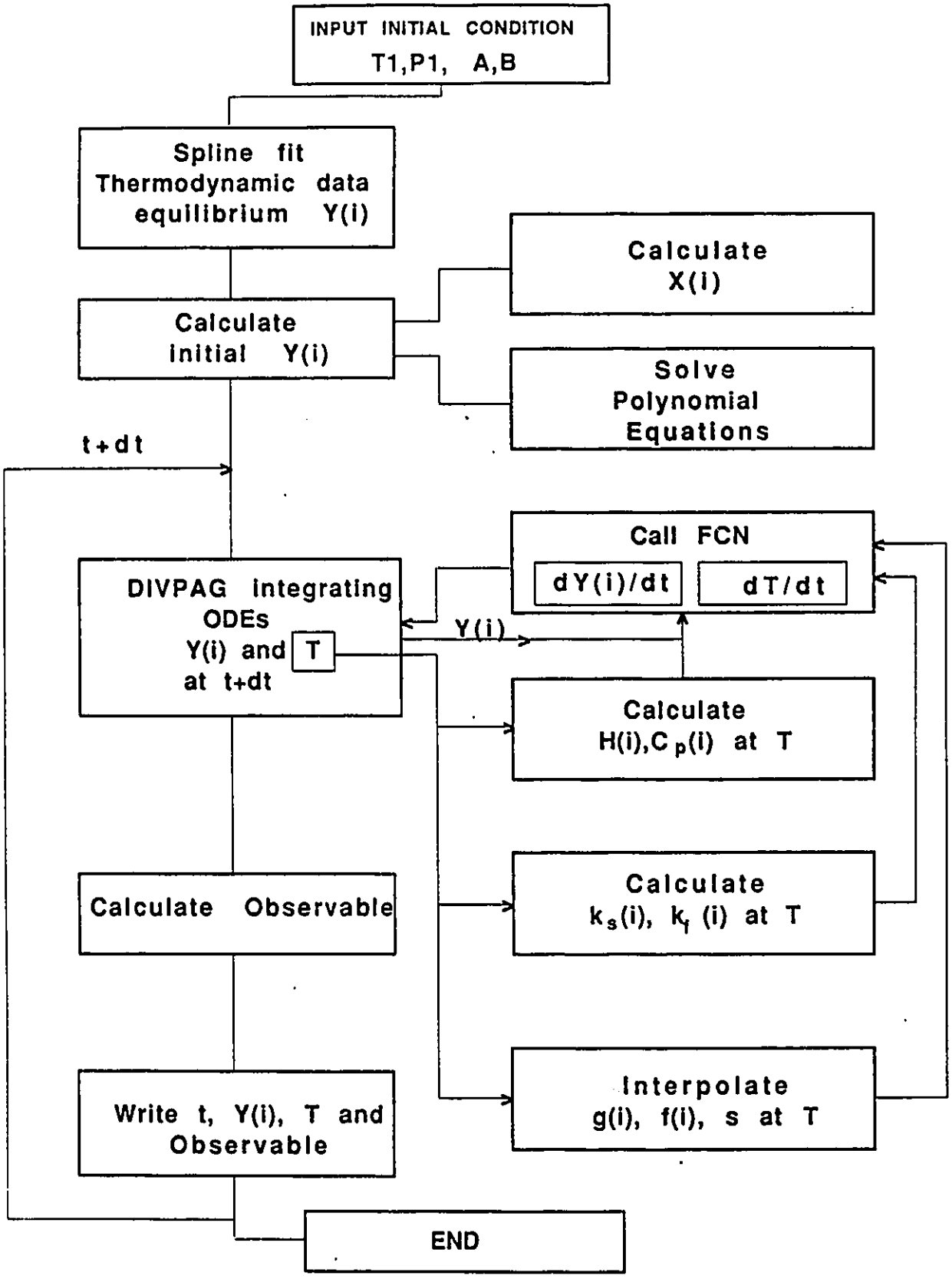

Fig. 4.4.3 The flowchart of Integral Fortran.

The flow chart of Integral Fortran is shown in fig 4.4.3. The input data for this program are the post shock temperature, T_2, the initial temperature, T_1, the supersaturation ratio, S_o, the tolerance for controlling the local error of the integration subroutine, Divpag, (about 1.0×10^{-12}), the parameters for calculating k_n^s and k_n^f, and the values of $k_{1,e}^s$ and $k_{2,e}^s$. The initial fractional cluster population was provided by subroutine Yzero. The data base for this program included the thermodynamic data for CCl_3F and f_n, g_n and s. After the initial distribution was calculated at t'=0 the IMSL routine Divpag was used to solve the initial value system of differential equations. The parameter METH in Divpag was set to 2 in order to use Gear's method. The rate of change of all y_n were evaluated in subroutine FCN in which first the values of f_n, g_n and s at temperature T were interpolated by calling the cubic spline subroutine Parafg. Then the subroutine Parakf was called to calculate the rate coefficients, k_n^s and k_n^f at temperature T. The heat capacity, $C_{p,n}$, and enthalpy, H_n, were calculated by calling the subroutine DTdt. At each integration step a new temperature was obtained permitting all of the parameters to be recalculated at the new temperature. The result was output at the desired time points.

4.5 Result

The equilibrium cluster distributions are shown in fig 4.5.1, 4.5.2 and 4.5.3 as a function of temperature for supersaturation degree 0.7, 1.0 and 1.5 respectively. These were calculated by solving the polynomial equations, discussed in section 4.2.4, using computer

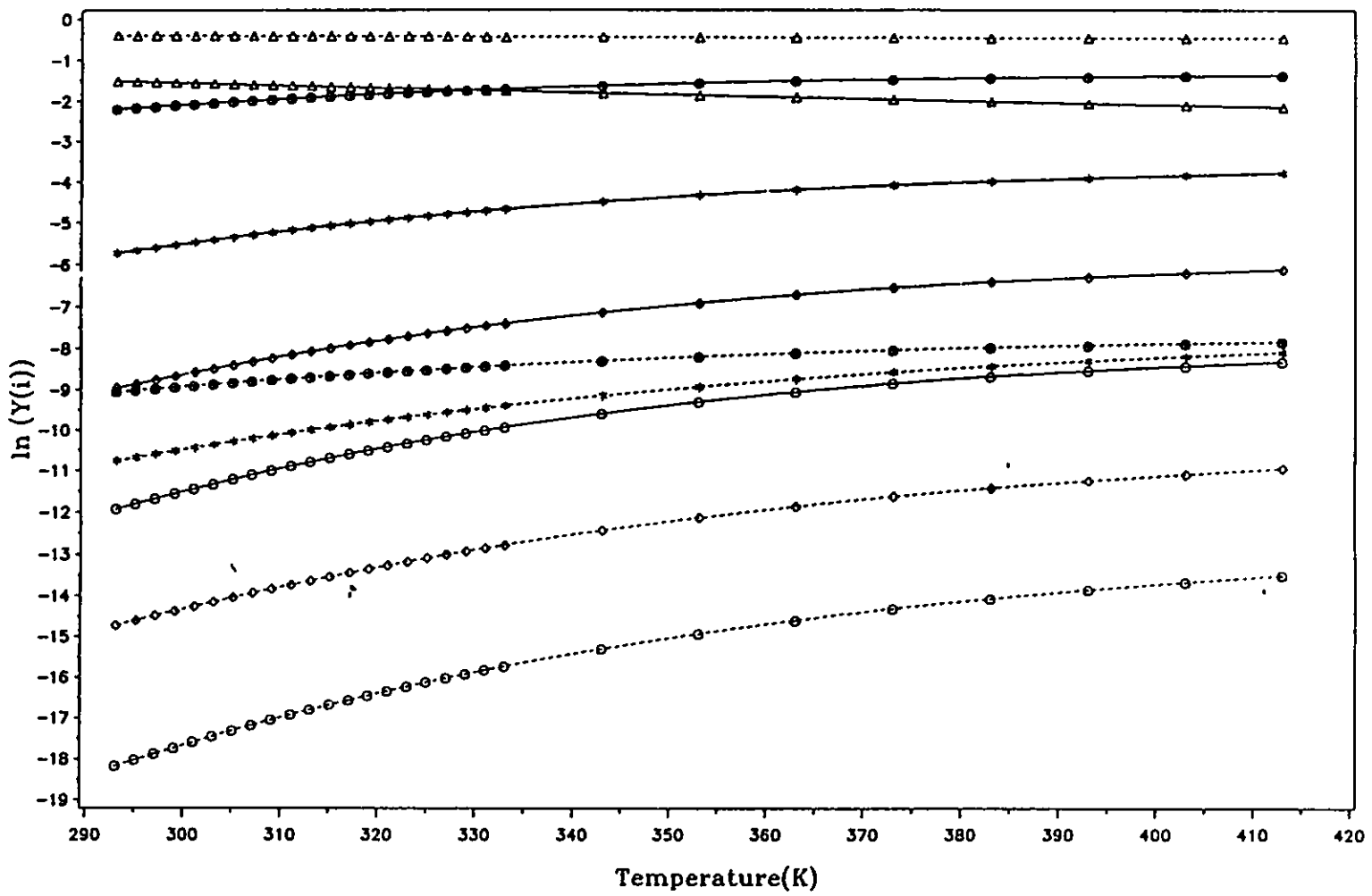

Fig. 4.5.1 Distribution of clusters vs temperature for a degree of supersaturation=0.7. Solid lines are for the stable cluster, broken lines are for the excited clusters. Δ monomer , ⊕ dimers, * trimer, ◊ tetramer, ⊙ pentamer.

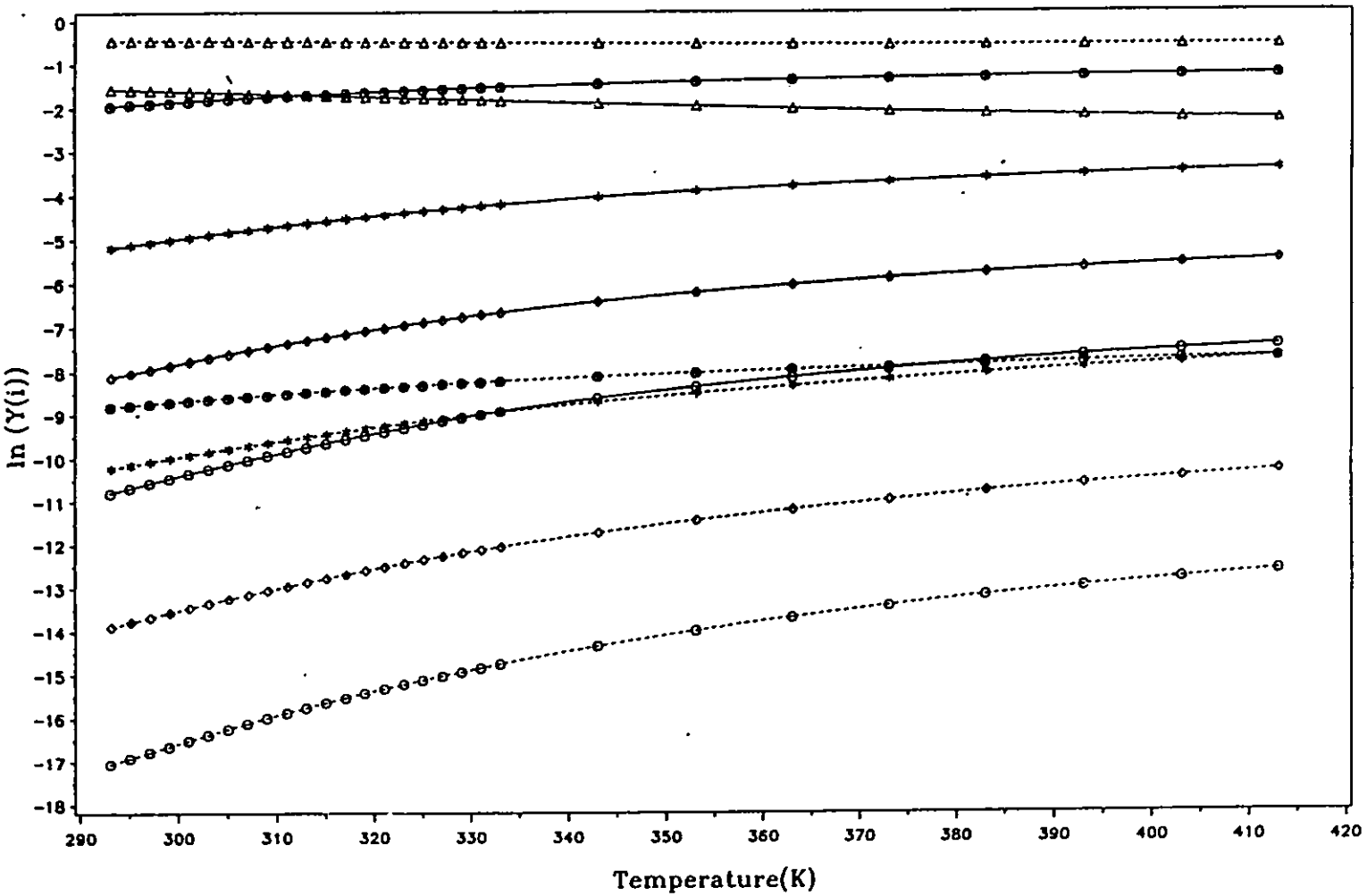

Fig. 4.5.2 Distribution of clusters vs temperature for a degree of supersaturation=1.0. Solid lines are for the stable cluster, broken lines are for the excited clusters. Δ monomer , ⊕ dimers, * trimer, ◊ tetramer, ⊙ pentamer.

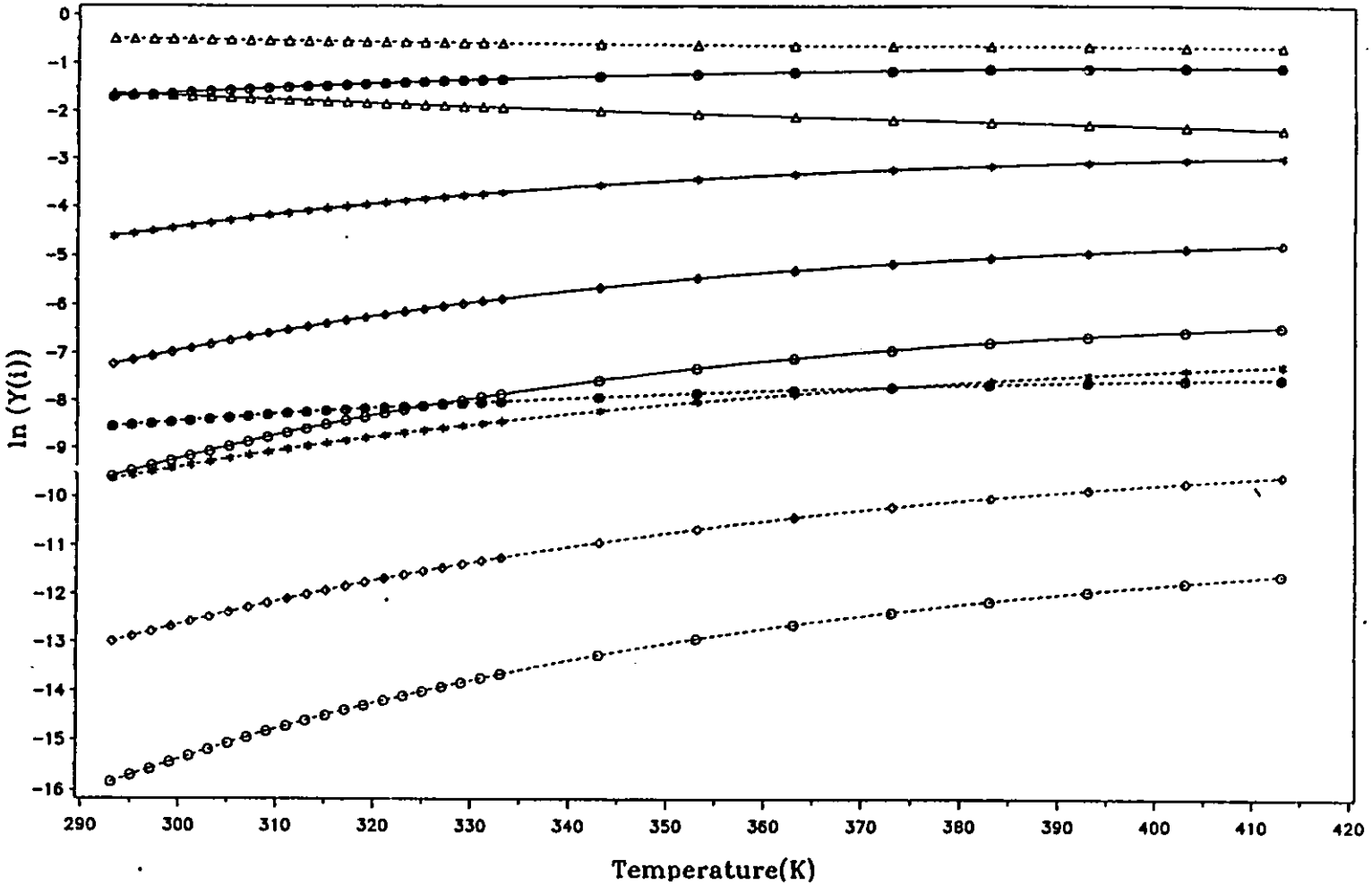

Fig. 4.5.3 Distribution of clusters vs temperature for a degree of supersaturation=1.5. Solid lines are for the stable cluster, broken lines are for the excited clusters. Δ monomer , ⊕ dimers, * trimer, ◊ tetramer, ⊙ pentamer.

program EQCALCU FORTRAN (see appendix8). In these graphs three points are worthy of note. First, as the temperature increases the mole fraction of the monomer (both vibrationally relaxed and unrelaxed) decreases, while the mole fractions of the clusters increase when the degree of supersaturation is constant. Although this may seem counter intuitive, the favouring of clusters has less to do with the increasing temperature than with the increasing pressure which occurs simultaneously in a shock compression. Second, the mole fraction of the vibrationally relaxed monomer has the largest value. This can be understood by realizing that CCl_3F vapour has a large enthalpy. Only a small fraction of this enthalpy originates from the zero-point energy of the vibrational mode (socalled unrelaxed monomers). Our method of partitioning monomers into two sorts (unrelaxed and relaxed) naturally ascribes the largest fraction to relaxed monomers. Third, as supersaturation increases the mole fractions of clusters increase and the mole fraction of monomers decreases. This is expected because the free energy of cluster formation is a decreasing function of supersaturation. For a degree of supersaturation of 1.5 the mole fraction of dimer is larger than that for monomer. However, for a degree of supersaturation of 0.7 the mole fraction of dimer is larger than that for monomer only when temperature is higher than 326 K.

The negligible mole fractions for tetramers and penta-mers justifies the truncation of our model at N=5. Figs 4.5.4 to 4.5.15 show the results of the simulation. Fig. 4.5.4 shows the observable which is proportional to $d\rho/dy$ as we discussed in Section 4.2.3. Fig. 4.5.5 shows the temperature as a function of time. Fig. 4.5.6 to 4.5.15 show the time

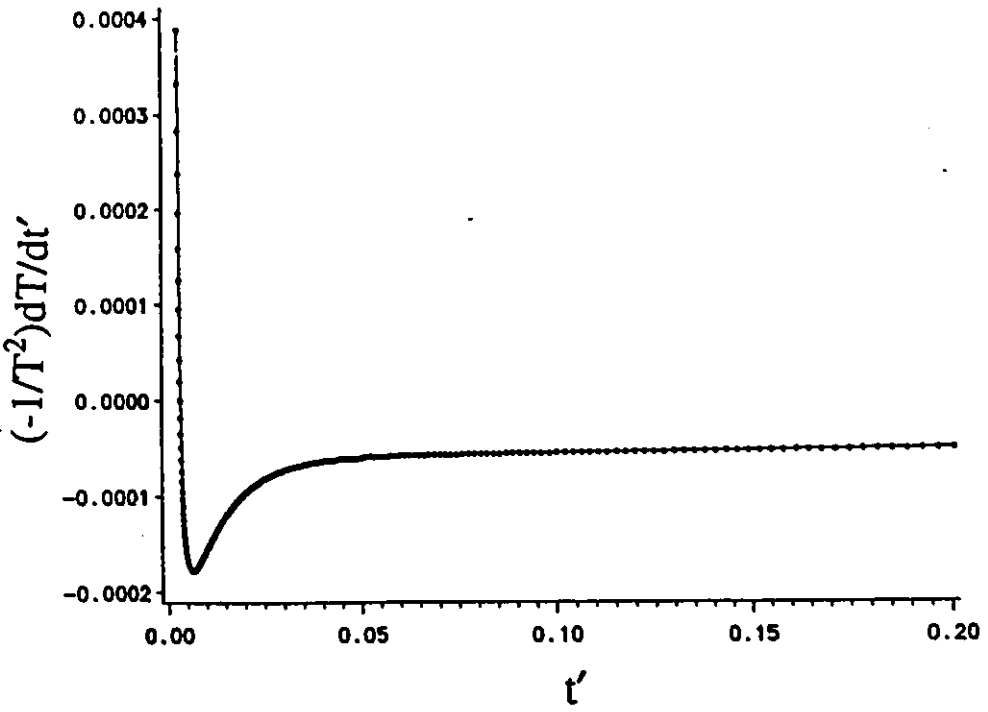

Fig. 4.5.4 -1/TdT/dt′ vs t′. The parameters used in the integration are given in Table 4.5.1.

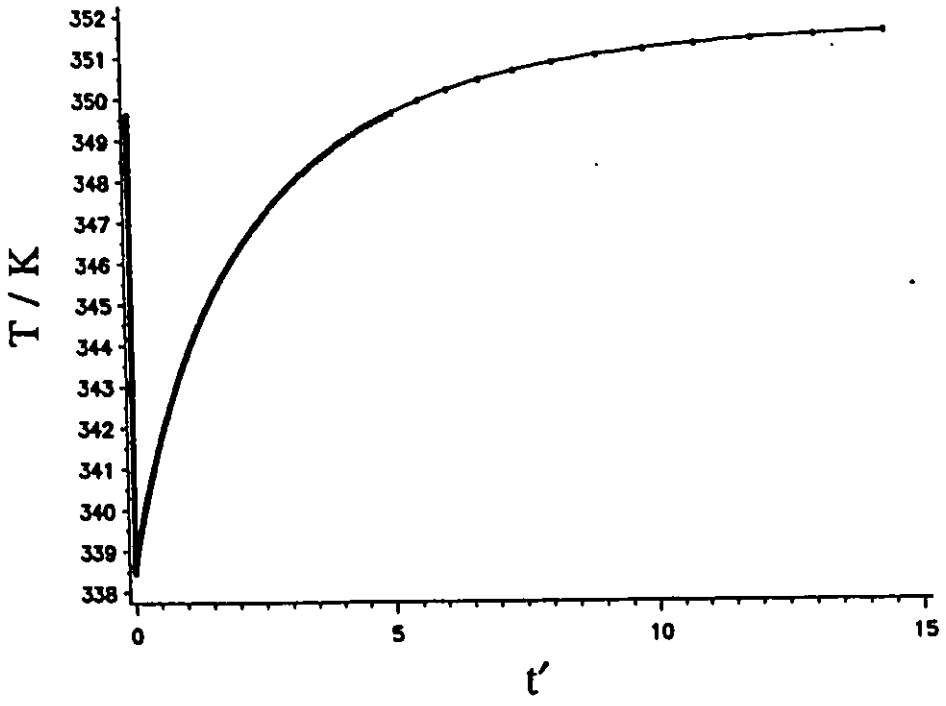

Fig. 4.5.5 Temperature vs t′. The parameters used in the integration are given in Table 4.5.1.

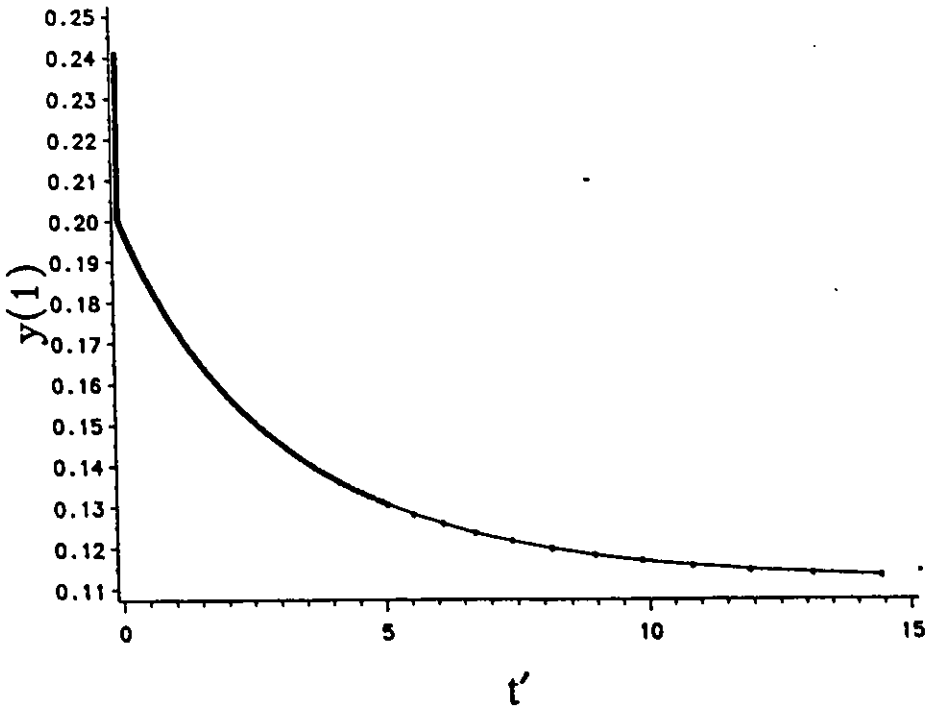

Fig. 4.5.6 y(1) vs t'. The parameters used in the integration are given in Table 4.5.1.

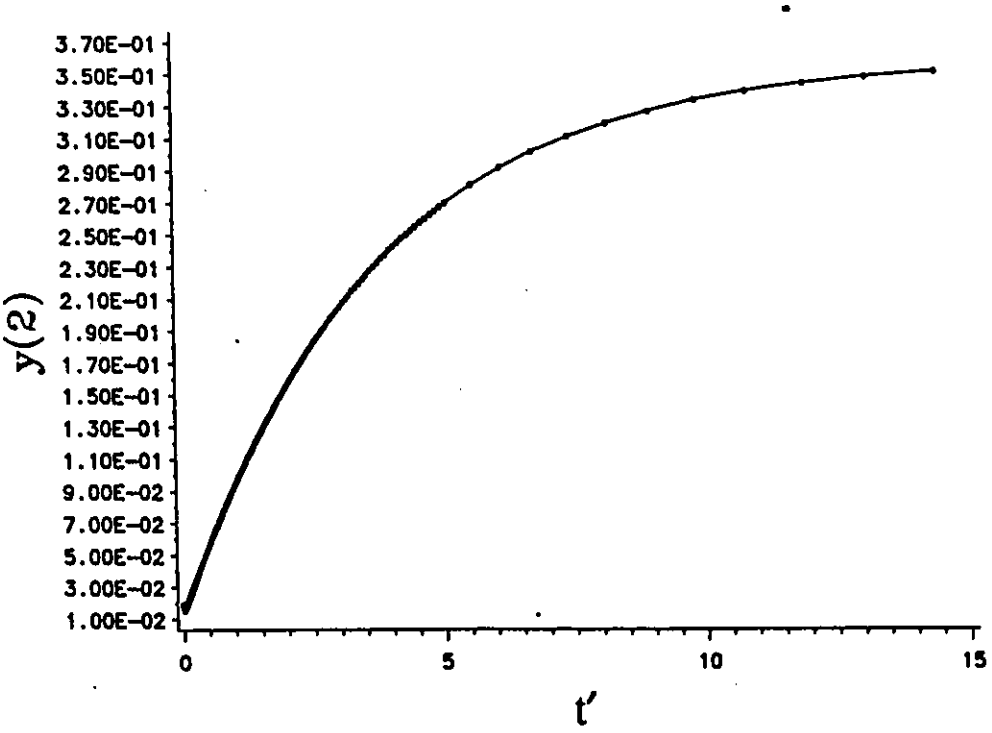

Fig. 4.5.7 y(2) vs t'. The parameters used in the integration are given in Table 4.5.1.

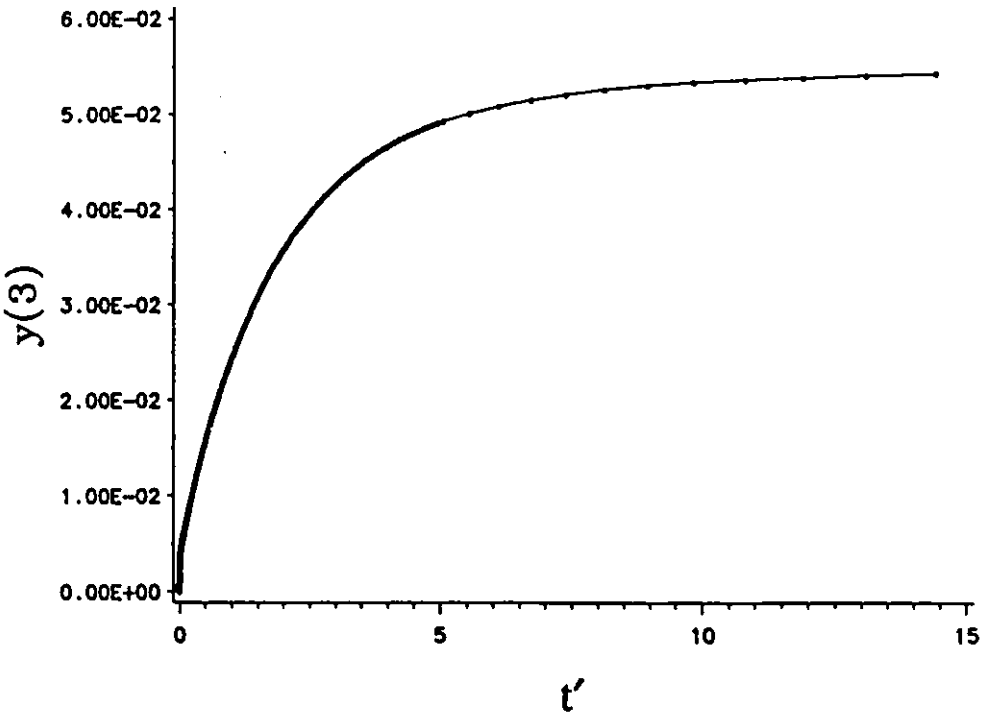

Fig. 4.5.8 y(3) vs t'. The parameters used in the integration are given in Table 4.5.1.

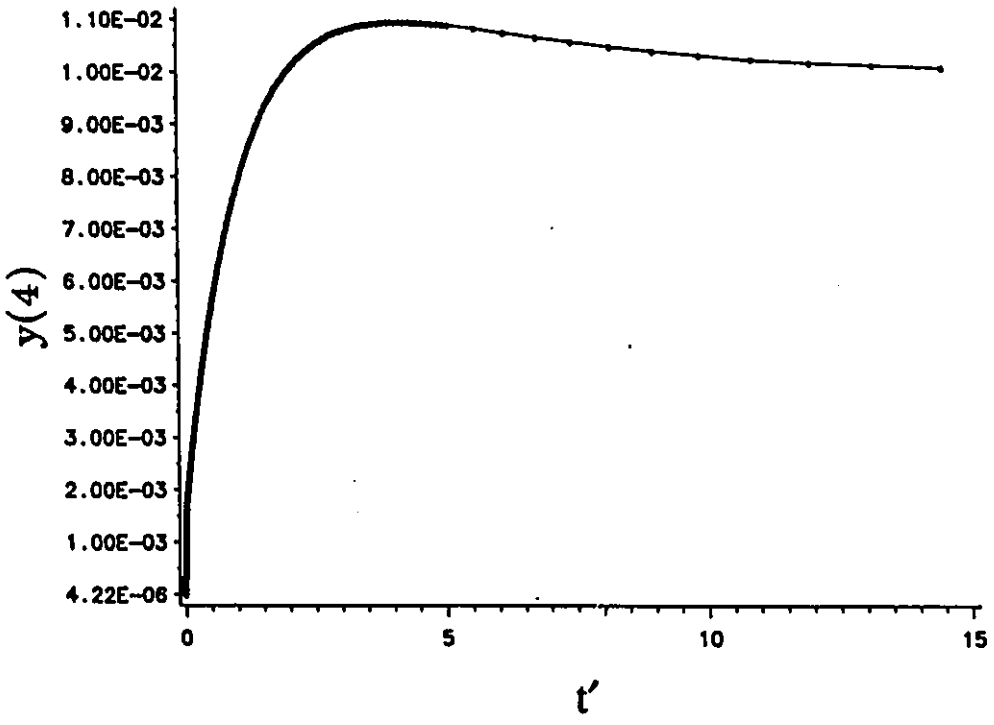

Fig. 4.5.9 y(4) vs t'. The parameters used in the integration are given in Table 4.5.1.

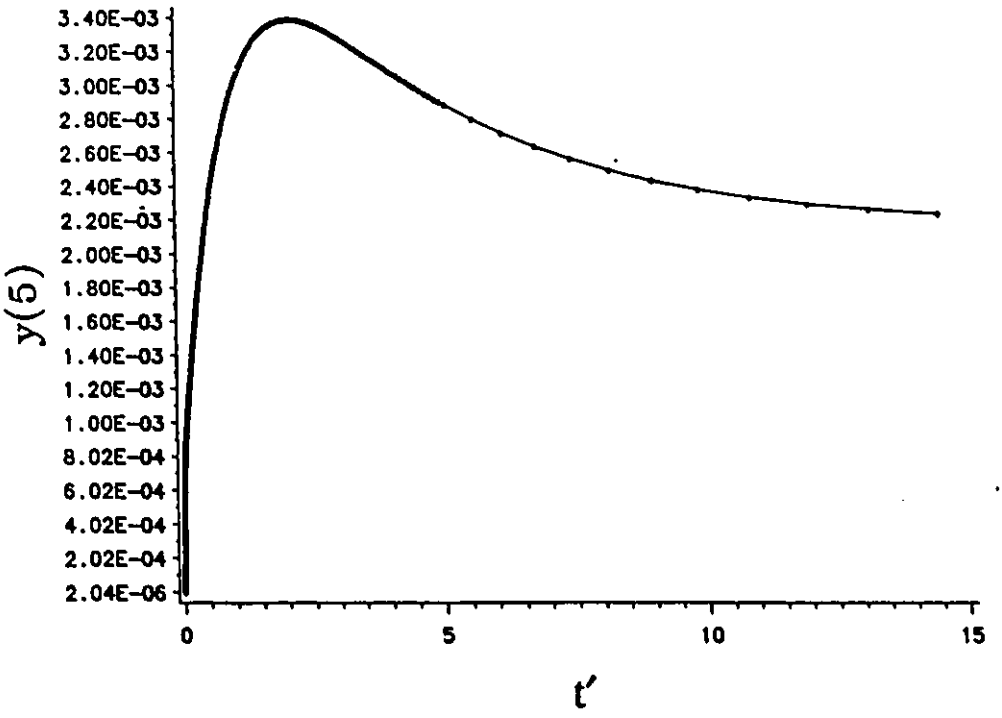

Fig. 4.5.10 y(5) vs t′. The parameters used in the integration are given in Table 4.5.1.

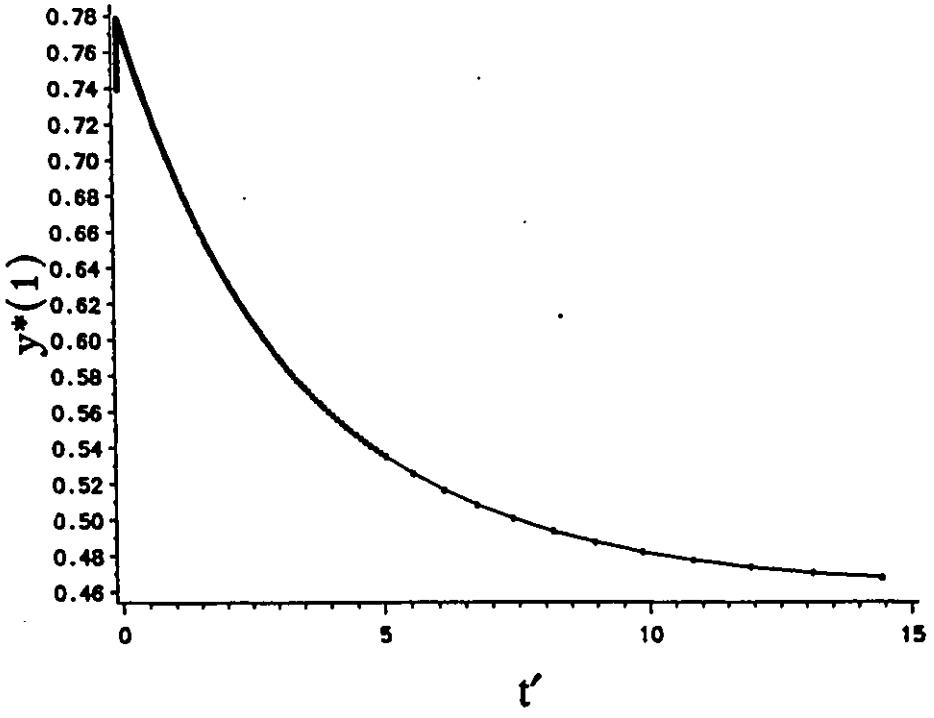

Fig. 4.5.11 y*(1) vs t′. The parameters used in the integration are given in Table 4.5.1.

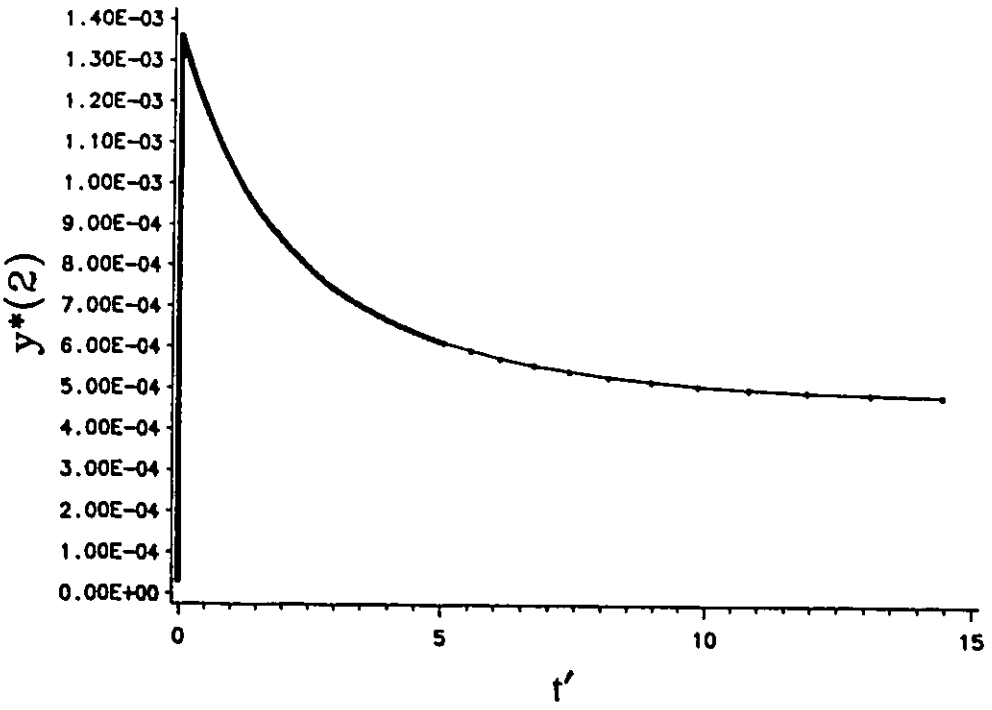

Fig. 4.5.12 y*(2) vs t'. The parameters used in the integration are given in Table 4.5.1.

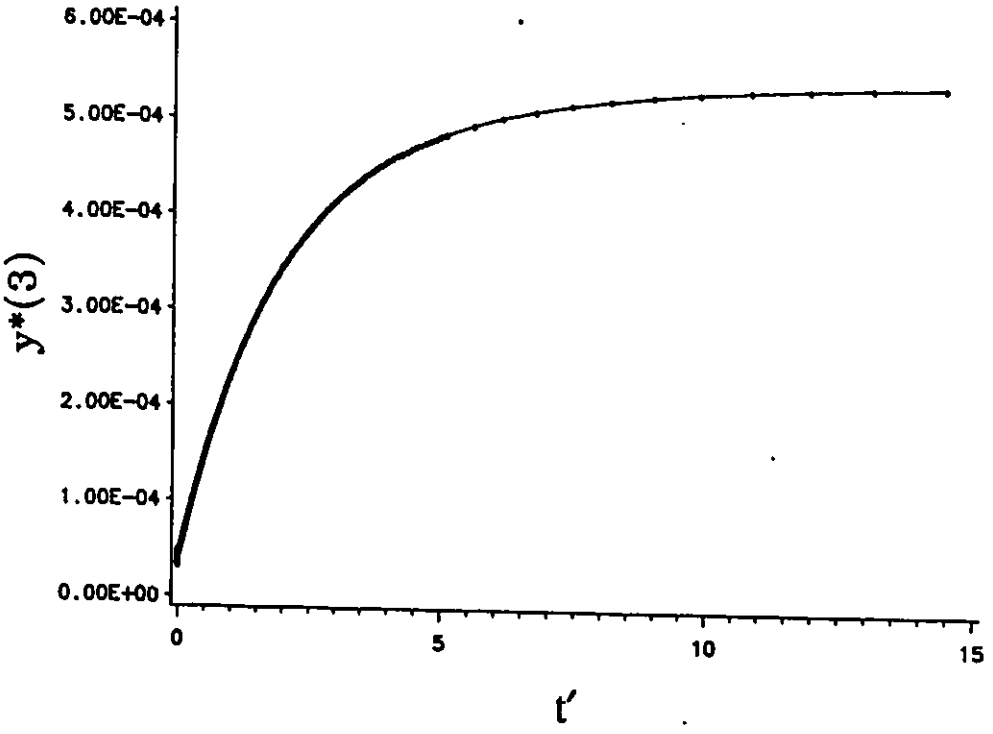

Fig. 4.5.13 y*(3) vs t'. The parameters used in the integration are given in Table 4.5.1.

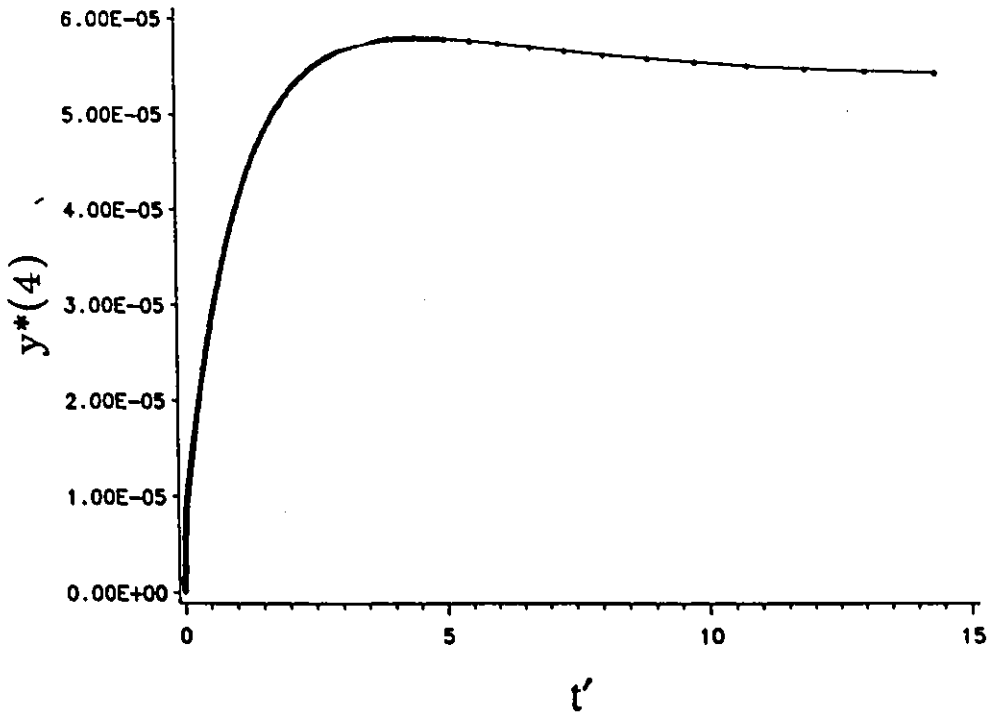

Fig. 4.5.14 y*(4) vs t'. The parameters used in the integration are given in Table 4.5.1.

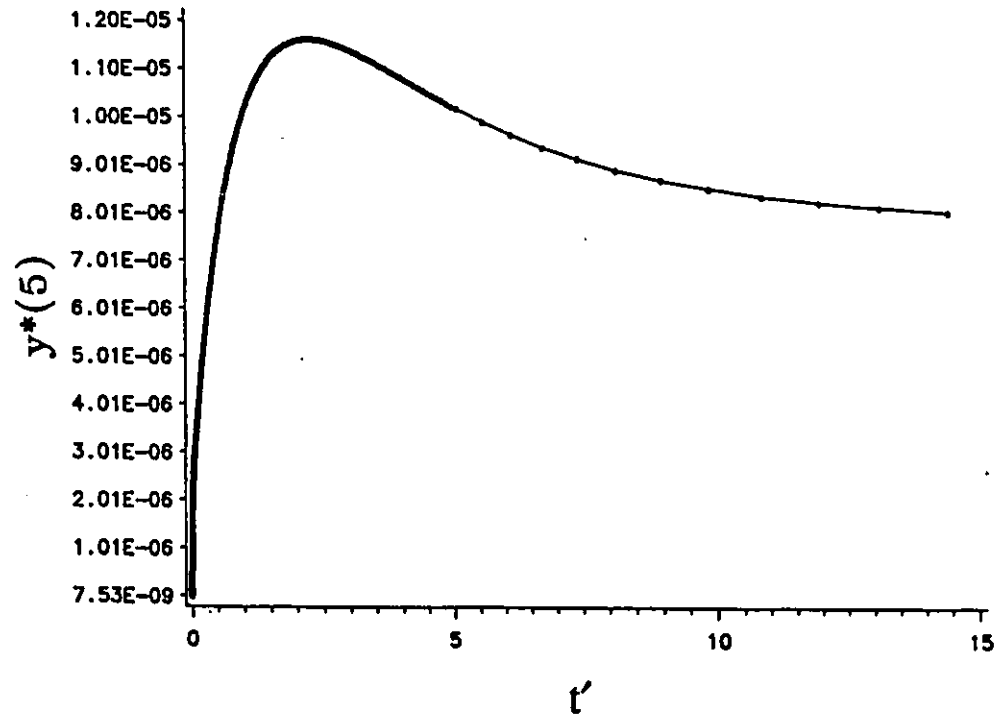

Fig. 4.5.15 y*(5) vs t'. The parameters used in the integration are given in Table 4.5.1.

dependence of cluster mole fractions.

The parameters which we used in this calculation are given in table 4.5.1. S is the degree of supersaturation, T is the integration temperature, A and B are the exponential scaling factors for stabilization and formation of clusters respectively, which together with the activation energies, E_1, and E_2, and the pre-exponential factors, $k^s_{1,e}/k^f_{2,e}$ and $k^s_{2,e}/k^f_{2,e}$, define the cluster formation and stabilization rate constants.

Table 4.5.1 The parameters used for integration showed in Figs 4.5.4 to 4.5.15.

S	T/ K	A	B	$k^s_{1,e}/k^f_{2,e}$	$k^s_{2,e}/k^f_{2,e}$	E_1 /kJ/mol	E_2 /kJ/mol	T_{ini}/K
2.0	350.15	5	5	3546	1000	7100	7500	291.2

The observable is a steeply decaying positive signal followed by a negative signal, as we observed in the experimental schlieren signals. At beginning the temperature drops from 350 K to 338.5 K in the first 3.6×10^{-3} dimensionless time units and then rises to 351.8 K. The temperature drop is caused by the vibrational relaxation of the monomer as can be seen in figs 4.5.6 and 4.5.11. During the same time period that the temperature drops the concentration of vibrationally relaxed monomer increases by 0.0386 C_o, in which C_o is the initial total concentration of clusters and monomers. While the unrelaxed monomer concentration decreases by 0.0435 C_o there are 0.0049 C_o vibrationally relaxed

monomers which form clusters. The overshoot is caused by a relatively larger rate of vibrational relaxation than that of cluster formation. When we decrease the relaxation rate constant, k_1^s, either by decreasing $k_{1,e}^s$ from 3541 to 3.541 or by increasing E_1 from 7100 to 71000, this overshoot disappears. In that case the temperature increases monotonically. For times larger than 3.9×10^{-3}, the net result is the formation of clusters. Both relaxed and unrelaxed monomer mole fractions are decrease, while those for n-mers increase. This is an exothermic process, so the temperature increases. The overshoot for excited dimers depends on the value of k_2^s. We increased k_2^s from 1000.0 to 1500, and the overshoot for excited dimers decreased. A decrease in k_2^f had a similar effect. The overshoot for tetramers and pentamers could be removed by choosing negative B. That means that the rate constant for the formation of pentamers is smaller than that for tetramers, which is in turn smaller than that for trimer, which is then smaller than that for dimer. For the most part, though we kept B positive.

The depth of the well in the observable is controlled by the process of cluster formation. A decrease in supersaturation results in a decrease of the depth of the well. As $k_{2,e}^s$ increases so too does the depth of well. Similarly parameters A and B magnify the exothermicity. However, an increase in E_2 decreases the depth of the well because it means a slower stabilization. $k_{1,e}^s$ has no effect on the depth of the well, since k_1^s deals with the prior vibrational relaxation of monomers.

Fig 4.5.16 shows an example of a simulation of the experimental signal. As a first

approximation we calculate the envelope of the experimental schlieren signal. By adjusting the different parameters, such as A, B, E_1, E_2, $k^s_{1,e}$ and $k^s_{2,e}$, the best fitting envelope can be obtained. There may be more than one set of these parameters which can give the best envelope. We need other independent methods to determine them. However, at present no other reliable methods exist. Therefore, the method we used in the following description does not guarantee that the rate constants of formation and stabilization are correct. The best fit envelope was obtained by first choosing the different parameters to make the simulated observable (in real time units) of the match the experimental signal (in particle time) approximately. Second, we change one of the parameters at a time by a small amount, make a plot, and measure the changes in t_o, the point in time at which the simulation curve first goes negative, in t_m, the point in time at which the signal reaches a minimum, in V_m, the depth of the well, in S_o, the slope of curve at time t_o and in S_1, the slope of the curve after passing the minimum point. When we change A by ΔA we get a new simulation curve from which we can calculate the linear sensitivity factors $(\Delta t_o/\Delta A)$, $(\Delta t_m/\Delta A)$, $(\Delta V_m/\Delta A)$, $(\Delta S_o/\Delta A)$ and $(\Delta t_1/\Delta A)$ keeping the other parameters constant. In the same way changing B by ΔB and leads to $(\Delta t_o/\Delta B)$, $(\Delta t_m/\Delta B)$, $(\Delta V_m/\Delta B)$, $(\Delta S_o/\Delta B)$ and $(\Delta S_1/\Delta B)$. The same procedure applies to the other parameters. Third, we can construct the cumulative effect, e.g.

$$\Delta t_o = \frac{\partial t_o}{\partial A}\Delta A + \frac{\partial t_o}{\partial B}\Delta B + \frac{\partial t_o}{\partial (k^s_{1,e}/k^f_{2,e})}\Delta (k^s_{1,e}/k^f_{2,e}) + \frac{\partial t_o}{\partial (k^s_{2,e}/k^f_{2,e})}\Delta (k^s_{2,e}/k^f_{2,e}) + \frac{\partial t_o}{\partial (k^f_{2,e})}\Delta (k^f_{2,e})$$

We obtain similar equations for Δt_m, ΔV_m, ΔS_o and ΔS_1:

$$\Delta t_o = \frac{\Delta t_o}{\Delta A}\Delta A + \frac{\Delta t_o}{\Delta B}\Delta B + \frac{\Delta t_o}{\Delta (k_{1,e}^s / k_{2,e}^f)}\Delta (k_{1,e}^s / k_{2,e}^f) + \frac{\Delta t_o}{\Delta (k_{2,e}^s / k_{2,e}^f)}\Delta (k_{2,e}^s / k_{2,e}^f) + \frac{\Delta t_o}{\Delta (k_{2,e}^f)}\Delta (k_{2,e}^f)$$

$$\Delta t_m = \frac{\Delta t_m}{\Delta A}\Delta A + \frac{\Delta t_m}{\Delta B}\Delta B + \frac{\Delta t_m}{\Delta (k_{1,e}^s / k_{2,e}^f)}\Delta (k_{1,e}^s / k_{2,e}^f) + \frac{\Delta t_m}{\Delta (k_{2,e}^s / k_{2,e}^f)}\Delta (k_{2,e}^s / k_{2,e}^f) + \frac{\Delta t_m}{\Delta (k_{2,e}^f)}\Delta (k_{2,e}^f)$$

$$\Delta V_m = \frac{\Delta V_m}{\Delta A}\Delta A + \frac{\Delta V_m}{\Delta B}\Delta B + \frac{\Delta V_m}{\Delta (k_{1,e}^s / k_{2,e}^f)}\Delta (k_{1,e}^s / k_{2,e}^f) + \frac{\Delta V_m}{\Delta (k_{2,e}^s / k_{2,e}^f)}\Delta (k_{2,e}^s / k_{2,e}^f) + \frac{\Delta V_m}{\Delta (k_{2,e}^f)}\Delta (k_{2,e}^f)$$

$$\Delta S_o = \frac{\Delta S_o}{\Delta A}\Delta A + \frac{\Delta S_o}{\Delta B}\Delta B + \frac{\Delta S_o}{\Delta (k_{1,e}^s / k_{2,e}^f)}\Delta (k_{1,e}^s / k_{2,e}^f) + \frac{\Delta S_o}{\Delta (k_{2,e}^s / k_{2,e}^f)}\Delta (k_{2,e}^s / k_{2,e}^f) + \frac{\Delta S_o}{\Delta (k_{2,e}^f)}\Delta (k_{2,e}^f)$$

$$\Delta S_1 = \frac{\Delta S_1}{\Delta A}\Delta A + \frac{\Delta S_1}{\Delta B}\Delta B + \frac{\Delta S_1}{\Delta(k_{1,e}^s/k_{2,e}^f)}\Delta(k_{1,e}^s/k_{2,e}^f)$$
$$+ \frac{\Delta S_1}{\Delta(k_{2,e}^s/k_{2,e}^f)}\Delta(k_{2,e}^s/k_{2,e}^f) + \frac{\Delta S_1}{\Delta(k_{2,e}^f)}\Delta(k_{2,e}^f)$$

These 5 linear equations include five unknowns. They can be solved easily. We determine Δt_o, Δt_m, ΔV_m, ΔS_o and ΔS_1, by comparing the simulation curve obtained in the first step with the experimental signal. For experiment No. 74 these values are given in Table 4.5.2. The sensitivity factor in the above equations obtained in the second step for the same experiment are given in table 4.5.3.

Table 4.5.2

Observed differences from simulated curve when A=7.5, B=1.0, $k_{1,e}^s/k_{2,e}^f$=0.1431, $k_{2,e}^s/k_{2,e}^f$=0.130, E_1=9800 J/mol, E_2=0.9800 J/mol, and $k_{2,e}^f$=6810.00 L/(mol s)

Δt_o	Δt_m	ΔV_m	ΔS_o	ΔS_1
2.0	2.3	0.5×10^{-5}	9.05×10^{-6}	2.03×10^{-9}

Fourth, solving this set of equations we obtain the group of parameters $x_j = \Delta A, \Delta B, \Delta k_{1,e}^s/k_{2,e}^f, \Delta k_{2,e}^s/k_{2,e}^f$ and $\Delta k_{2,e}^f$. Fifth, we change the simulation parameters used in step one and recalculate the simulation curve. In the last step, we compare with the experimental signal again, if the agreement is not satisfactory we repeat the above procedure.

Table 4.5.3

The sensitivity factors $a_{i,j}$ for $b_i = \Delta t_o$, Δt_m, ΔV_m, ΔS_o, and ΔS_1 in $b_i = a_{i1}x_{11} + a_{i2}x_{21} + a_{i3}x_{31} + a_{i4}x_{41} + a_{i5}x_{51}$

i	a_{i1}	a_{i2}	a_{i3}	a_{i4}	a_{i5}
1	-6.333	-0.5	-50	-50	1.235×10^{-3}
2	-3.333	-5.5	-100.0	-75.0	1.235×10^{-3}
3	1.566×10^{-4}	-1.3×10^{-3}	9.0×10^{-4}	-1.10×10^{-3}	6.173×10^{-9}
4	-4.02×10^{-5}	-1.7×10^{-5}	-7.69×10^{-4}	-6.01×10^{-5}	8.08×10^{-9}
5	1.832×10^{-7}	7.23×10^{-7}	6.54	3.765×10^{-5}	-7.22×10^{-11}

The results obtained for experiment 74 are given in Table 4.5.4.

In this simulation there is no oscillatory signal appeared even though all of the ingredients are present for nonlinear kinetics. Therefore simple thermal feedback to the rate coefficients was insufficient for any combination of parameters to lead to instability. The one "parameter" which we have not yet considered is the choice of initial concentrations and the associated temperature dependence. To some extent we are not free to choose equilibrium conditions, because we are constrained by our model and by thermodynamics. On the other hand, our model is weakest in its treatment of excited species (monomers are artificially divided into 2 species only —— unrelaxed and relaxed; —— whereas excited n-mers are treated as rotating double stars). Our consequence of this is figs. 4.5.1

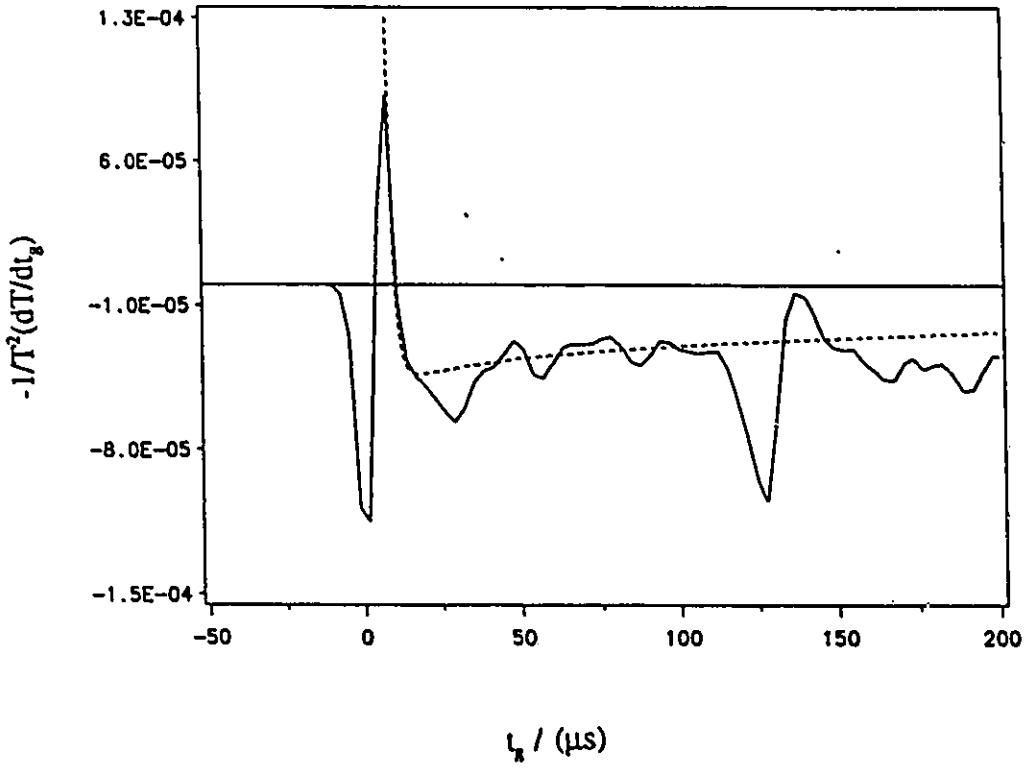

Fig. 4.5.16 Comparision of the simulation signal with experimental signal for experiment No. 74. The broken line is the computer simulation; the solid line is the signal of experiment No. 74. The experimental conditions are T_1=293.3 K, P_1=412.1 torr, u_1=174.2 m/s, T_2=309.6 K and P_2=663.4 torr. The simulation parameters are $k^f_{2,e}$=6810 L/(mol s), E_1=9800 J/mol, E_2=9.8 J/mol, A=7.5, B=1.0, $k^s_1/ k^f_{2,e}$=0.1341 and $k^s_2/ k^f_{2,e}$= 0.1300.

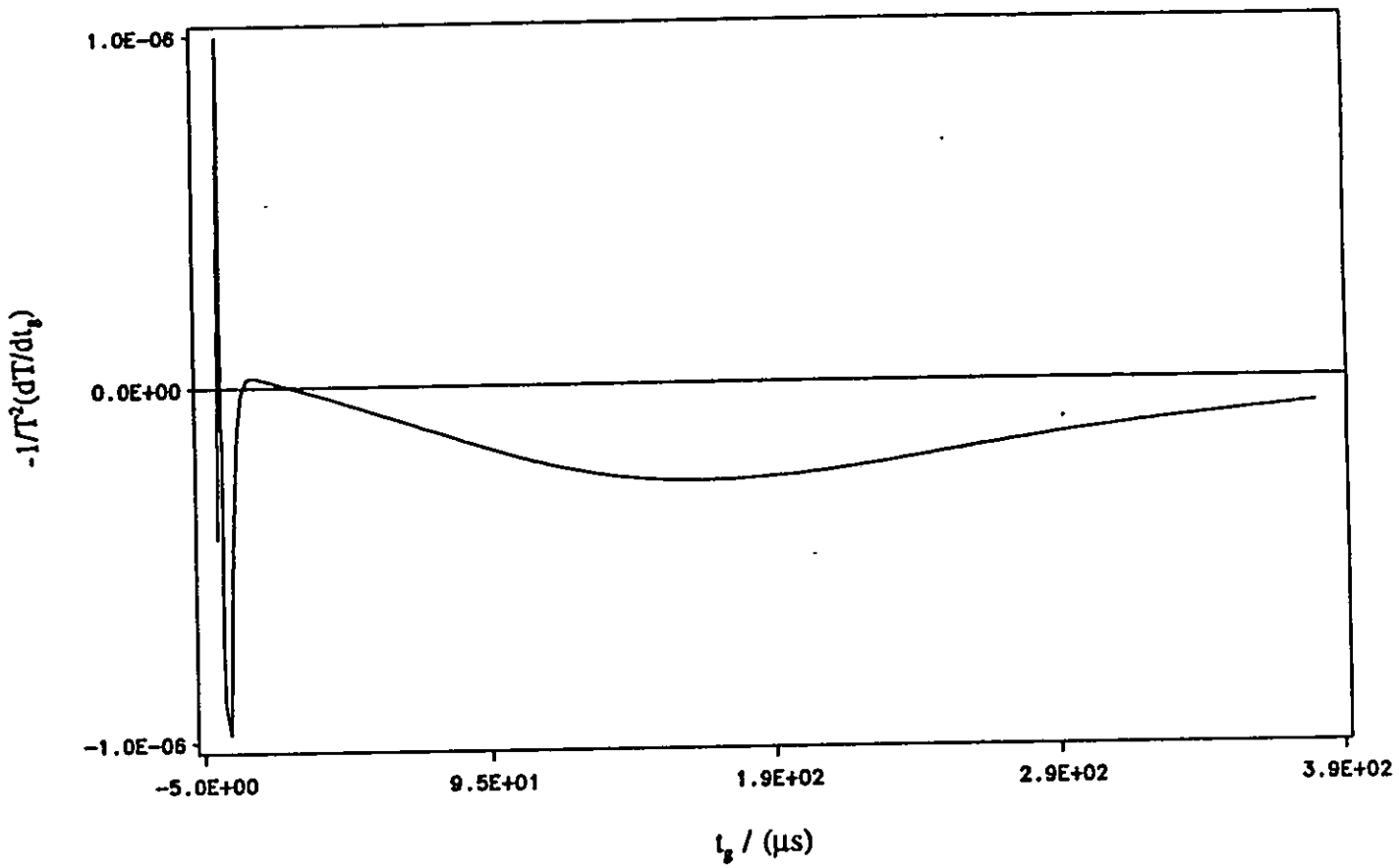

Fig. 4.5.17 Simulation for case when y_2^{eq} decreases with increasing temperature. $k_{2,e}^f$=6810 L/(mol s), E_1=9800 J/mol, E_2=9.8 J/mol, A=5.0, B=1.0, $k_1^s/\ k_{2,e}^f$=1.341 and $k_2^s/\ k_{2,e}^f$= 0.01300.

to 4.5.3, where y_1^e decrease with T while y_2^e increases with T. Close examination reveals interesting behaviour: If there are too few dimers to start, condensation results leading to heat release and a temperature increase. Figs 4.5.1 to 4.5.3 show that y_2^e also increases as a consequence, so that y_2 always lags behind y_2^e. Similarly, even if there are too many dimers to start monotonic behaviour results. In that case evaporation leads to a temperature drop, so that the initially low y_2^e become even lower, and y_2 could undershoot/ overshoot y_2^e depending on the value of the appropriate rate constants. As a test of this concept we ignored Figs 4.5.1-4.5.3 and chose an arbitrary equilibrium cluster distribution for which y_2^e decrease with T. The distribution is shown in Table 4.5.5. Using this data we simulated an experiment shown in fig. 4.5.17. Without having to adjust parameters much we could obtain a signal containing 3 oscillations. This proves that the origin of the instability lies in thermal feedback to equilibrium cluster distributions rather than to rate coefficients.

Table 4.5.4 Parameters used in computer simulation of experiment No.74.

$k_{2,e}^f$ $Lmol^{-1}s^{-1}$	E_1 J/mol	E_2 J/mol	A	A	$k_{1,e}^s/k_{2,e}^f$	$k_{2,e}^s/k_{2,e}^f$
6810	9800	0.98	7.5124	1.0006	0.1341	0.1300

Table 4.5.5 Modified equilibrium cluster distributions.

	300 K	350 K	400 K
y_1	0.1763	0.1786	0.1561
y_2	0.1763	0.0510	0.0184
y_3	0.04406	0.1276×10^{-1}	4.596×10^{-3}
y_4	0.03085	0.8929×10^{-2}	3.213×10^{-3}
y_5	0.1322×10^{-1}	0.3827×10^{-2}	1.377×10^{-3}
y_1^*	0.5587	0.7746	0.8163
y_2^*	1.904×10^{-4}	6.735×10^{-5}	2.791×10^{-5}
y_3^*	3.023×10^{-4}	1.276×10^{-4}	5.967×10^{-5}
y_4^*	1.036×10^{-4}	4.885×10^{-5}	2.462×10^{-5}
y_5^*	2.750×10^{-5}	1.393×10^{-5}	7.381×10^{-6}

CHAPTER 5

SUMMARY AND CONCLUSION

Classical nucleation theory assumes that a cluster is a spherical object with the characteristics of a liquid. The macroscopic properties of a liquid are used in calculating the rate of nucleation and the equilibrium cluster distribution. Therefore, this theory is only good for large clusters. Experimental studies of nucleation are also limited by the inability of the light scattering method used to detect clusters before they grow to macroscopic size (about 20 μm). There is also a gap between the theory and reality. — namely how do vapour molecules form into small clusters? In this dissertation the rate of formation of small clusters has been studied using the shock tube method and computer simulation. From this study the following conclusions can be drawn.

1. By detailed examination of both the experimental signals obtained from different shock tubes, and from different experimental conditions we verified that the oscillatory signal is the result of a process which occurs in the shock wave. Then by examining the schlieren signal obtained from carefully chosen gases, such as argon, methane, carbon tetrachloride, sulphur hexafluoride and Freon-11, and by comparing the thermodynamic properties of these gases, such as second viral coefficients, B, dB/dT, the Van der Waals' empirical constant, a, critical temperature, and the heat of vaporization, and by checking

the mass spectrum of Freon-11 before and after shock wave passage, we conclude that oscillatory signals only happened when the vapour was at a temperature below its critical temperature, and when the vapour has a large B and dB/dT. It is the result of a competition between vibrational relaxation (endothermic) and cluster formation (exothermic). The mechanism is given as follows: When the shock wave arrives the translational energy of the molecule increases suddenly and dramatically. Originally existing clusters are dissociated. After that, rotational and vibrational relaxation processes take place first. This causes a temperature drop, and cluster formation starts. Heat is released and temperature increases. The energy is fed back and affects the rate constants and the equilibrium cluster distribution. Concurrently monomer and clusters are undergoing vibrational relaxation. Repetitive overshoots and undershoots are related to the inability of the competing processes to stay in phase. The temperature changes cause a density change along the shock axis, which shows up as an oscillatory schlieren signal.

2. By measuring the characteristic time in the schlieren signal the activation energy, E_a, of the net process could be determined. We found E_a = -25 kJ/mol.

3. For small cluster formation in our subsaturated system, P_2t_o increases with temperature and decreases with $(P_{vap}-P_2)$. This is different from the dependence of incubation time on temperature and pressure in saturated vapours given by the classic nucleation theory for the formation of critical clusters.

4. Using the Fourier transform technique, it was found that although the overall shape of the oscillatory schlieren signals varied as the experimental conditions changed, there were some common features. All of these oscillatory signals started as biperiodic ones, degenerating to chaotic signals. Dominant frequencies changed with time. The amplitudes of the high frequency components increased with time. The experimental signals show that the formation of small clusters in shock waves is a nonlinear kinetic process which satisfies the requirements of a thermokinetic oscillator.

5. A mathematical model for cluster formation and vibrational relaxation was built on the basis of thermodynamics and nonlinear kinetics. Using this model the envelope of the schlieren signal could be simulated. It is confirmed by simulation that cluster formation processes are responsible for the negative schlieren signals. Furthermore, the model can give rise to the oscillatory signals if we assume that the cluster distribution is far away from equilibrium distribution and if the equilibrium cluster mole fractions decrease with increasing temperature.

6. From the above conclusions we can conclude that the shock tube coupled with the schlieren technique together with computer simulation is a useful method for studying the formation of small clusters.

Future work

1. Most of the experiments in CCl_3F which we have performed are with high initial pressures and with weak shock waves (Mach numbers were less than 2). It is under these conditions that oscillatory signals were observed. For low initial pressures and relatively high shock speeds the oscillation appeared after the signal became negative. We only performed one experiment with CCl_4 at an initial pressure close to its vapour pressure with much higher shock wave (Mach number was larger than 4). Oscillation was observed. The vapour pressure of CCl_4 is much lower than that of CCl_3F at the same temperature. It is only 89.55 mm Hg at 20°C for CCl_4 while it is 666.83 mm Hg for CCl_3F. Some experiments should be performed for CCl_4 close to its vapour pressure using a weak shock wave (making the Mach number less than 2), and for CCl_3F at its vapour pressure using a strong shock wave (letting the Mach number be larger than 5). Additional experiments should also be performed with other refrigerant gases, with a variety of diluents, and with various degrees of dilution in order to study the effects of varying the thermal feedback.

2. Our numerical model suffers from a lack of knowledge of the rate constants for cluster formation, evaporation and stabilization, and from insufficient knowledge of the equilibrium distribution. Advances in molecular dynamics would allow us to determine some of these rate constants and would allow us to pin down the others using our experiments.

3. Spectroscopy of jet-cooled clusters would identify spectral features which we could exploit for distinguishing between different size clusters.

Appendix 1. Table of Shock Wave Parameters

In the following table the initial pressure ($P_{ini.}$) and the pressure behind the shock front (P_2) are given in mm Hg. The initial temperature ($T_{ini.}$) and the temperature behind the shock front (T_2) are given in K. The shock wave velocity (u) is in mm per micro-second. x is the ratio of pre-shock to post shock densities.

No.	$P_{ini.}$	$T_{ini.}$	P_2	T_2	x	u
3	556.3	294.0	2003.7	348.5	0.3185	0.2571
7	551.2	293.2	961.5	312.8	0.6044	0.1804
8	551.0	293.2	948.7	312.3	0.6116	0.1793
10	405.4	294.0	834.9	319.7	0.5221	0.1966
15	303.7	292.0	1570.4	370.3	0.2401	0.3088
16	305.0	292.2	593.7	315.0	0.5496	0.1913
17	305.3	293.2	616.7	317.7	0.5322	0.1952
18	207.9	293.3	573.4	331.1	0.4066	0.2277
20	109.3	293.2	339.0	342.5	0.3776	0.2427
21	59.8	292.0	701.6	453.4	0.1332	0.4641
25	26.2	293.0	114.3	358.5	0.2783	0.2889
26	79.7	293.2	149.2	316.0	0.5767	0.1901
27	153.5	292.0	254.4	308.6	0.6363	0.1779
28	221.5	292.2	278.7	299.5	0.8131	0.1555
29	306.8	292.2	563.6	312.7	0.5786	0.1860
30	505.4	294.5	755.6	308.2	0.6949	0.1681
31	30.0	295.2	95.4	339.8	0.3707	0.2435
32	33.5	295.2	91.6	332.5	0.4167	0.2285
33	98.1	295.2	216.0	328.6	0.5071	0.2071
34	117.3	295.2	200.4	318.3	0.6317	0.1842
36	408.2	294.5	589.4	306.5	0.7170	0.1656
37	607.0	295.2	715.8	300.6	0.8606	0.1495
38	672.8	295.2	734.4	298.1	0.9233	0.1439
39	682.7	295.2	1159.3	313.6	0.6170	0.1777

No.	$P_{ini.}$	$T_{ini.}$	P_2	T_2	x	u
40	631.0	294.2	930.3	307.5	0.7026	0.1661
51	690.5	294.3	1201.5	313.6	0.6033	0.1794
52	692.5	295.3	801.3	300.2	0.8756	0.1479
53	617.5	295.8	751.4	302.3	0.8364	0.1519
54	747.0	296.8	838.2	300.7	0.9004	0.1459
55	664.7	294.3	804.5	300.7	0.8405	0.1510
56	697.0	295.1	797.0	299.6	0.8850	0.1470
58	633.4	295.3	785.8	302.5	0.8219	0.1532
59	664.0	293.8	801.5	300.1	0.8425	0.1506
60	660.6	293.5	802.3	300.0	0.8379	0.1510
61	703.1	294.8	808.6	299.5	0.8804	0.1473
63	668.8	293.5	807.2	299.8	0.8426	0.1505
64	697.9	294.1	875.9	301.8	0.8131	0.1534
65	672.8	294.3	1177.1	313.8	0.6006	0.1800
66	688.6	295.1	871.6	303.1	0.8069	0.1544
67	704.6	295.3	952.0	305.6	0.7602	0.1592
68	656.6	293.3	909.6	304.4	0.7434	0.1608
69	634.0	292.8	882.1	304.0	0.7405	0.1611
70	658.6	292.8	933.3	304.7	0.7281	0.1624
71	646.8	293.3	869.1	303.3	0.7643	0.1585
72	662.6	293.3	869.6	302.5	0.7808	0.1567
73	662.6	293.0	915.2	304.0	0.7453	0.1605
74	412.1	293.0	663.4	309.0	0.6503	0.1742
75	637.1	292.0	889.1	303.3	0.7384	0.1611
76	628.6	292.5	875.1	303.7	0.7402	0.1611
77	622.8	293.1	828.9	302.7	0.7710	0.1578
78	642.9	293.0	901.5	304.5	0.7353	0.1617
79	618.5	293.0	795.8	301.4	0.7950	0.1553

No.	$P_{ini.}$	$T_{ini.}$	P_2	T_2	x	u
80	649.0	292.8	775.2	298.7	0.8507	0.1497
81	631.2	292.3	851.8	302.4	0.7613	0.1586
82	642.3	292.1	774.4	298.3	0.8434	0.1502
83	633.0	293.0	827.6	302.0	0.7836	0.1564
84	672.6	293.8	1131.5	311.8	0.6224	0.1765
85	630.8	292.3	846.5	302.2	0.7652	0.1582
86	625.4	292.8	702.8	296.6	0.8991	0.1454
87	638.3	292.8	1040.6	309.7	0.6411	0.1738
88	632.8	293.0	1129.7	313.2	0.5901	0.1816
89	616.7	291.8	1108.1	312.2	0.5869	0.1819
90	627.2	292.3	875.8	303.6	0.7381	0.1613
91	631.2	292.8	754.7	298.7	0.8499	0.1498
92	564.2	293.2	1056.3	315.5	0.5668	0.1865
93	586.4	291.5	984.4	309.6	0.6252	0.1763
94	590.4	292.8	1044.9	312.9	0.5959	0.1812
95	620.4	293.3	876.0	305.0	0.7307	0.1625
96	503.2	293.2	624.0	300.4	0.8231	0.1534
97	599.6	293.2	760.2	301.2	0.8062	0.1545
98	653.0	293.2	1110.8	311.6	0.6163	0.1774
99	616.4	293.2	716.1	298.1	0.8723	0.1479
100	562.7	293.3	775.3	304.2	0.7479	0.1610
101	586.7	293.3	833.1	305.3	0.7276	0.1632
102	576.1	293.5	1073.5	315.6	0.5690	0.1861
104	572.1	293.8	849.0	307.4	0.6992	0.1670
105	510.2	293.8	773.3	308.0	0.6863	0.1690
106	564.0	294.0	702.3	301.4	0.8198	0.1536
107	616.2	293.2	1114.9	312.7	0.6001	0.1801
108	609.5	293.2	1058.0	312.4	0.6059	0.1794
109	603.5	293.4	1022.1	311.7	0.6197	0.1775

No.	$P_{ini.}$	$T_{ini.}$	P_2	T_2	x	u
111	602.2	293.2	812.0	303.2	0.7619	0.1590
112	600.0	293.7	1081.3	314.3	0.5857	0.1829
113	633.2	293.7	1186.2	315.8	0.5650	0.1861
114	594.1	293.7	1178.3	318.2	0.5374	0.1917
115	643.3	293.8	1222.9	316.5	0.5574	0.1874
116	649.2	294.0	1378.0	321.3	0.5046	0.1978
117	623.2	294.2	1396.0	323.8	0.4812	0.2033
118	657.2	294.0	1439.2	322.7	0.4906	0.2008
119	682.8	294.2	1283.1	316.5	0.5627	0.1863
120	637.6	293.2	1418.6	322.5	0.4839	0.2022
122	537.0	294.2	1229.8	324.8	0.4734	0.2062
123	441.8	292.8	1103.2	331.5	0.4128	0.2308
124	399.0	294.2	1174.8	336.4	0.3814	0.2342
125	338.5	294.2	1102.7	341.7	0.3508	0.2465
126	472.5	293.6	1111.5	325.2	0.4631	0.2091
127	559.8	293.7	1336.7	326.2	0.4558	0.2101
147	606.5	293.2	2269.4	349.8	0.3070	0.2611
148	607.0	294.4	2238.6	350.2	0.3108	0.2598
149	606.5	294.7	741.6	302.8	0.7588	0.1598
150	424.8	294.0	4135.8	447.8	0.1518	0.4236
151	666.7	295.0	687.5	296.0	0.9724	0.1399
152	500.7	294.7	678.4	304.9	0.7596	0.1604
153	700.8	295.1	702.9	295.2	0.9973	0.1382
154	590.8	294.0	627.2	296.1	0.9476	0.1427
155	678.3	294.2	714.3	295.9	0.9540	0.1411
156	434.6	295.0	2418.3	380.7	0.2246	0.3207
158	514.6	294.4	599.7	299.6	0.8710	0.1494
159	662.0	293.6	669.2	294.0	0.9903	0.1383
160	482.5	293.7	552.8	298.0	0.8837	0.1476

No.	$P_{inj.}$	$T_{ini.}$	P_2	T_2	x	u
161	679.0	293.6	679.4	293.7	0.9995	0.1374
162	375.0	294.7	425.5	298.8	0.8921	0.1479
163	696.5	295.8	746.8	298.1	0.9384	0.1427
164	502.0	293.8	618.2	300.8	0.8283	0.1531
165	692.5	295.5	956.7	306.6	0.7451	0.1611
166	398.5	293.2	721.6	313.6	0.5854	0.1845
167	710.5	295.7	928.4	304.8	0.7837	0.1568
168	309.5	295.0	604.7	318.3	0.5482	0.1926
169	153.0	295.2	413.9	332.2	0.4150	0.2266
170	111.8	295.7	144.1	308.5	0.8091	0.1640
171	510.5	293.6	700.0	304.2	0.7514	0.1610
172	249.7	295.7	336.1	305.3	0.7652	0.1614
173	508.7	292.5	767.5	306.5	0.6892	0.1682
174	118.0	292.7	376.2	342.8	0.3678	0.2456
175	126.4	293.2	402.7	342.3	0.3666	0.2455
221	54.8	293.0	382.1	381.0	0.1881	0.3577

Appendix 2. Table of the Characteristic Time Scale and the Maximum Rate of Heat Release

In this table P_2(mm Hg) and T_2(K) are the pressure and temperature behind the shock front in each experiment. $\Delta P(T_1)$(mm Hg) is the difference from the vapour presssure at T_1 and P_1 . $\Delta P(T_2)$(mm Hg) is the difference from the vapour pressure at T_2 and P_2.

No.	P_2	T_2	$\Delta P(T_1)$	$\Delta P(T_2)$	$t_0 * P_2$	$t_{min.} * P_2$	V_{min} / P_2^2
3	2003.7	348.50	0.1297E+03	0.1500E+04	0.4718E+05	0.8493E+05	0.5033E-06
7	961.5	312.80	0.1151E+03	0.3333E+03	0.6363E+05	0.1257E+06	0.2186E-05
8	948.7	312.30	0.1153E+03	0.3258E+03	0.6205E+05	0.1117E+06	0.1610E-05
10	834.9	319.70	0.2806E+03	0.7656E+03	0.1919E+05	0.1071E+06	0.2461E-05
15	1570.4	370.30	0.3339E+03	0.4225E+04	0.3270E+05	0.4448E+06	0.6493E-06
16	593.7	315.00	0.3373E+03	0.7931E+03	0.7562E+04	0.7346E+05	0.5625E-05
17	616.7	317.70	0.3610E+03	0.8900E+03	0.5794E+04	0.7996E+05	0.4812E-05
18	573.4	331.10	0.4608E+03	0.1650E+04	0.7051E+04	0.1058E+06	0.4986E-05
20	339.0	342.50	0.5570E+03	0.2674E+04	0.2693E+04	0.6464E+05	0.9290E-05
21	701.6	453.40	0.5778E+03	0.2365E+05	0.1686E+06	0.3160E+06	0.1954E-05
25	114.3	358.50	0.6352E+03	0.4336E+04	0.3286E+04	0.1396E+05	0.5994E-04
26	149.2	316.00	0.5866E+03	0.1281E+04	0.1552E+04	0.8796E+04	0.3703E-04
27	254.4	308.60	0.4841E+03	0.8776E+03	0.1599E+04	0.9196E+04	0.2474E-04

28	278.7	299.50	0.4208E+03	0.5551E+03	0.1714E+04	0.1371E+05	0.4422E-05
29	563.6	312.70	0.3355E+03	0.7271E+03	0.4870E+04	0.2630E+05	0.3001E-05
30	755.6	308.20	0.1931E+03	0.3618E+03	0.2501E+05	0.3480E+05	0.3252E-06
31	95.4	339.80	0.6863E+03	0.2857E+04	0.1866E+04	0.8795E+04	0.2038E-04
32	91.6	332.50	0.6828E+03	0.2238E+04	0.1144E+01	0.4118E+01	0.1878E-04
33	216.0	328.60	0.6182E+03	0.1857E+04	0.2556E+04	0.2982E+05	0.1976E-04
34	200.4	318.30	0.5990E+03	0.1334E+04	0.1903E+04	0.1047E+05	0.9579E-05
36	589.4	306.50	0.2903E+03	0.4675E+03	0.7398E+04	0.2302E+05	0.3054E-05
37	715.8	300.60	0.1093E+03	0.1504E+03	0.3743E+05	0.6654E+05	0.8154E-06
38	734.4	298.10	0.4351E+02	0.5960E+02	0.1193E+06	0.2529E+06	0.6148E-06
39	1159.3	313.60	0.3361E+02	0.1684E+03	0.5073E+05	0.2010E+06	0.1224E-05
40	930.3	307.50	0.5994E+02	0.1619E+03	0.5958E+05	0.9798E+05	0.1747E-05
51	1201.5	313.60	0.2946E+01	0.1262E+03	0.7568E+05	0.2290E+06	0.2356E-05
52	801.3	300.20	0.2639E+02	0.5310E+02	0.6040E+05	0.1716E+06	0.1878E-04
53	751.4	302.30	0.1144E+03	0.1668E+03	0.1348E+05	0.8445E+05	0.7569E-05
54	838.2	300.70	0.1142E+02	0.3100E+02	0.7727E+05	0.1629E+06	0.1487E-04
55	804.5	300.70	0.2875E+02	0.6470E+02	0.8806E+05	0.9285E+05	0.1290E-05

56	797.0	299.60	0.1674E+02	0.3970E+02	0.9006E+05	0.1621E+06	0.2101E-05
58	785.8	302.50	0.8549E+02	0.1386E+03	0.7840E+05	0.8413E+05	0.9665E-06
59	801.5	300.10	0.1699E+02	0.4990E+02	0.6184E+05	0.1570E+06	0.2077E-05
60	802.3	300.00	0.1300E+02	0.4620E+02	0.2394E+05	0.6415E+05	0.1659E-05
61	808.6	299.50	0.2977E+01	0.2520E+02	0.7990E+05	0.2158E+06	0.2274E-05
63	807.2	299.80	0.4803E+01	0.3540E+02	0.6514E+05	0.1724E+06	0.3425E-05
64	875.9	301.80	-0.9456E+01	0.2680E+02	0.8833E+05	0.1745E+06	0.1358E-05
65	1177.1	313.80	0.2065E+02	0.1590E+03	0.7839E+05	0.1646E+06	0.2416E-05
66	871.6	303.10	0.2514E+02	0.7180E+02	0.6481E+05	0.2160E+06	0.2448E-05
67	952.0	305.60	0.1429E+02	0.7380E+02	0.8140E+05	0.1816E+06	0.1436E-05
68	909.6	304.40	0.1211E+02	0.7600E+02	0.6730E+05	0.2080E+06	0.2412E-05
69	882.1	304.00	0.2261E+02	0.9030E+02	0.8577E+05	0.1370E+06	0.2904E-05
70	933.3	304.70	-0.1989E+01	0.6220E+02	0.9870E+05	0.1128E+06	0.2075E-05
71	869.1	303.30	0.2191E+02	0.8070E+02	0.9666E+05	0.1706E+06	0.2493E-05
72	869.6	302.50	0.6114E+01	0.5490E+02	0.6682E+05	0.9801E+05	0.3991E-05
73	915.2	304.00	-0.1170E+01	0.5720E+02	0.4543E+05	0.2947E+06	0.2608E-05
74	663.4	309.00	0.2493E+03	0.4834E+03	0.7141E+04	0.2040E+05	0.1850E-05

75	889.1	303.30	0.5054E+00	0.6070E+02	0.2167E+05	0.5298E+05	0.2048E-05
76	875.1	303.70	0.2083E+02	0.8760E+02	0.5557E+05	0.1040E+06	0.2557E-05
77	828.9	302.70	0.4105E+02	0.1018E+03	0.8923E+05	0.2118E+06	0.2302E-05
78	901.5	304.50	0.1853E+02	0.8740E+02	0.6498E+05	0.2268E+06	0.2548E-05
79	795.8	301.40	0.4293E+02	0.9460E+02	0.4705E+05	0.5606E+05	0.3449E-05
80	775.2	298.70	0.7611E+01	0.3580E+02	0.6014E+05	0.1658E+06	0.3590E-05
81	851.8	302.40	0.1348E+02	0.6950E+02	0.8280E+05	0.1734E+06	0.2666E-05
82	774.4	298.30	-0.2341E+01	0.2530E+02	0.4866E+05	0.2121E+06	0.2481E-05
83	827.6	302.00	0.2843E+02	0.8120E+02	0.8027E+05	0.2155E+06	0.2146E-05
84	1131.5	311.80	0.8392E+01	0.1230E+03	0.7817E+05	0.1545E+06	0.2067E-05
85	846.5	302.20	0.1388E+02	0.6850E+02	0.8850E+05	0.1217E+06	0.2257E-05
86	702.8	296.60	0.3121E+02	0.5030E+02	0.5315E+05	0.1712E+06	0.2827E-05
87	1040.6	309.70	0.1831E+02	0.1325E+03	0.1250E+06	0.1331E+06	0.3979E-05
88	1129.7	313.20	0.2863E+02	0.1814E+03	0.1187E+06	0.1589E+06	0.2181E-05
89	1108.1	312.20	0.1622E+02	0.1624E+03	0.9063E+05	0.1624E+06	0.2018E-05
90	875.8	303.60	0.1748E+02	0.8370E+02	0.9255E+05	0.1768E+06	0.1591E-05
91	754.7	298.70	0.2541E+02	0.5620E+02	0.7104E+05	0.8525E+05	0.1874E-05

92	1056.3	315.50	0.1021E+03	0.3522E+03	0.7827E+05	0.1547E+06	0.2324E-05
93	984.4	309.60	0.3955E+02	0.1849E+03	0.8975E+05	0.1323E+06	0.2361E-05
94	1044.9	312.90	0.6621E+02	0.2540E+03	0.7540E+05	0.1455E+06	0.2444E-05
95	876.0	305.00	0.4831E+02	0.1296E+03	0.9111E+05	0.1079E+06	0.1838E-05
96	624.0	300.40	0.1631E+03	0.2363E+03	0.1744E+05	0.7050E+05	0.2448E-05
97	760.2	301.20	0.6668E+02	0.1241E+03	0.8204E+05	0.1556E+06	0.1913E-05
98	1110.8	311.60	0.1328E+02	0.1357E+03	0.7209E+05	0.1514E+06	0.2163E-05
99	716.1	298.10	0.4988E+02	0.7790E+02	0.7717E+05	0.1765E+06	0.1487E-05
100	775.3	304.20	0.1060E+03	0.2038E+03	0.4976E+05	0.1545E+06	0.1903E-05
101	833.1	305.30	0.8201E+02	0.1826E+03	0.7671E+05	0.1580E+06	0.2087E-05
102	1073.5	315.60	0.9750E+02	0.3394E+03	0.7358E+05	0.1509E+06	0.2481E-05
104	849.0	307.40	0.1089E+03	0.2396E+03	0.3036E+05	0.9714E+05	0.1620E-05
105	773.3	308.00	0.1708E+03	0.3369E+03	0.1408E+05	0.4338E+05	0.2412E-05
106	702.3	301.40	0.1220E+03	0.1881E+03	0.3769E+05	0.7453E+05	0.1866E-05
107	1114.9	312.70	0.3008E+02	0.1758E+03	0.9661E+05	0.1523E+06	0.2607E-05
108	1058.0	312.40	0.5678E+02	0.2206E+03	0.9080E+05	0.1467E+06	0.2691E-05
109	1022.1	311.70	0.6765E+02	0.2284E+03	0.8577E+05	0.1352E+06	0.2409E-05

111	812.0	303.20	0.6408E+02	0.1346E+03	0.2345E+05	0.4796E+05	0.8674E-06
112	1081.3	314.30	0.7852E+02	0.2758E+03	0.9231E+05	0.1532E+06	0.3163E-05
113	1186.2	315.80	0.4532E+02	0.2354E+03	0.1848E+06	0.3527E+06	0.4606E-05
114	1178.3	318.20	0.8442E+02	0.3514E+03	0.6578E+05	0.1864E+06	0.1977E-05
115	1222.9	316.50	0.3769E+02	0.2296E+03	0.3905E+05	0.9105E+05	0.1785E-05
116	1378.0	321.30	0.3675E+02	0.3007E+03	0.7373E+05	0.2321E+06	0.1035E-05
117	1396.0	323.80	0.6774E+02	0.4106E+03	0.6963E+05	0.2263E+06	0.1685E-05
118	1439.2	322.70	0.2875E+02	0.3102E+03	0.9681E+05	0.2494E+06	0.6803E-06
119	1283.1	316.50	0.8138E+01	0.1694E+03	0.8665E+05	0.1824E+06	0.1138E-05
120	1418.6	322.50	0.2868E+02	0.3206E+03	0.8795E+05	0.2052E+06	0.1092E-05
122	1229.8	324.80	0.1539E+03	0.6301E+03	0.1091E+06	0.2078E+06	0.1817E-05
123	1103.0	331.50	0.2148E+03	0.9889E+03	0.6316E+05	0.2440E+06	0.1705E-05
124	1174.8	336.40	0.2919E+03	0.1393E+04	0.2156E+05	0.2403E+06	0.2144E-05
125	1102.7	341.70	0.3524E+03	0.1849E+04	0.2200E+05	0.5658E+05	0.2955E-05
126	1111.5	325.20	0.2036E+03	0.7699E+03	0.4800E+05	0.1920E+06	0.1825E-05
127	1336.7	326.20	0.1187E+03	0.5997E+03	0.5865E+05	0.2346E+06	0.1630E-05
147	2269.4	349.80	0.5978E+02	0.1349E+04	0.9684E+06	0.1818E+07	0.1160E-06

148	2238.6	350.20	0.8895E+02	0.1415E+04	0.4826E+06	0.9760E+06	0.5091E-06
149	821.5	304.90	0.9703E+02	0.1807E+03	0.7795E+05	0.1375E+06	0.9416E-06
150	4135.8	447.80	0.2612E+03	0.1838E+05	0.7084E+06	0.6811E+06	0.1238E-07
151	687.5	296.00	0.4448E+02	0.4970E+02	0.8838E+05	0.1697E+06	0.2373E-05
152	678.4	304.90	0.2028E+03	0.3238E+03	0.3126E+05	0.3572E+05	0.4873E-06
153	702.9	295.20	0.1294E+02	0.1340E+02	0.5991E+05	0.6696E+05	0.6952E-06
154	627.2	296.10	0.9515E+02	0.1126E+03	0.4832E+05	0.7943E+05	0.4109E-06
155	714.3	295.90	0.1264E+02	0.2020E+02	0.6963E+05	0.1722E+06	0.2242E-05
156	2418.3	380.70	0.2766E+03	0.4786E+04	0.3015E+06	0.3316E+07	0.3518E-06
158	599.7	299.60	0.1814E+03	0.2371E+03	0.2479E+05	0.3167E+05	0.1131E-05
159	669.2	294.00	0.1406E+02	0.1000E+01	0.6758E+05	0.1960E+06	0.1383E-05
160	552.8	298.00	0.1960E+03	0.2396E+03	0.2189E+05	0.3003E+05	0.7595E-06
161	679.4	293.70	-0.2939E+01	-0.1600E+01	0.5098E+05	0.5438E+05	0.1268E-05
162	425.5	298.80	0.3285E+03	0.3871E+03	0.6678E+04	0.2194E+05	0.2645E-05
163	746.8	298.10	0.3538E+02	0.4780E+02	0.8595E+05	0.1886E+06	0.1359E-05
164	618.2	300.80	0.1790E+03	0.2534E+03	0.2612E+05	0.2761E+05	0.3966E-06
165	956.7	306.60	0.3156E+02	0.1029E+03	0.1374E+06	0.3017E+06	0.1946E-05

166	721.6	313.60	0.2678E+03	0.6061E+03	0.4931E+05	0.1664E+06	0.4366E-06
167	928.4	304.80	0.1877E+02	0.7180E+02	0.1185E+06	0.1718E+06	0.2263E-05
168	604.7	318.30	0.4017E+03	0.9279E+03	0.4412E+04	0.2206E+05	0.1874E-05
169	413.9	332.20	0.5633E+03	0.1875E+04	0.9973E+04	0.2194E+05	0.4731E-05
170	144.1	308.50	0.6175E+03	0.9828E+03	0.8905E+04	0.2743E+05	0.1419E-04
171	700.0	304.20	0.1656E+03	0.2797E+03	0.1211E+05	0.1584E+05	0.2461E-06
172	336.1	305.30	0.4796E+03	0.6795E+03	0.1098E+05	0.1933E+05	0.3489E-05
173	767.5	306.50	0.1407E+03	0.2894E+03	0.6125E+05	0.1927E+06	0.4967E-06
174	376.2	342.80	0.5362E+03	0.2660E+04	0.2046E+04	0.1125E+05	0.4961E-05
175	402.7	342.30	0.5399E+03	0.2595E+04	0.5492E+04	0.1208E+05	0.3271E-05
221	382.1	381.00	0.6066E+03	0.6866E+04	0.1016E+05	0.1422E+06	0.3917E-04

Appendix 3 Thermodynamic Data for Freon-11

The thermodynamic data of saturated trichloromonofluoromethane. The specific volume (V) in m^3/kg, enthalpy (ΔH) in kJ/kg, entropy (S) in kJ/(kg K) of both vapour (g) and liquid (l) heat of vaorization (ΔH_{vap}) and the vapour pressure (P) in bar, as a function of temperature (T) in degree celsius.

T	P	$V_l \times 10^3$	V_g	ΔH_l	ΔH_g	ΔH_{vap}	S_l	S_g
0	0.4030	0.6517	0.4037	500.00	690.34	190.34	1.0000	1.6968
2	0.4388	0.6536	0.3730	501.75	691.38	189.63	1.0064	1.6956
4	0.4771	0.6556	0.4351	503.50	692.43	188.93	1.0127	1.6944
6	0.5181	0.6576	0.3197	505.26	693.47	188.22	1.0190	1.6944
8	0.5617	0.6596	0.2966	507.02	694.52	187.50	1.0253	1.6922
10	0.6083	0.6616	0.2755	508.77	695.56	186.79	1.0315	1.6912
12	0.6579	0.6637	0.2561	510.54	696.61	186.07	1.0377	1.6902
14	0.7106	0.6657	0.2384	512.30	697.65	185.35	1.0438	1.6893
16	0.7666	0.6678	0.2222	514.07	698.70	184.63	1.0499	1.6885
18	0.8261	0.6700	0.2073	515.84	699.74	183.90	1.0560	1.6871
20	0.8891	0.6721	0.1936	517.61	700.78	183.17	1.0621	1.6869
22	0.9558	0.6743	0.1810	519.39	701.82	182.43	1.0681	1.6862
24	1.026	0.6765	0.1964	521.17	702.86	181.69	1.0741	1.6855
26	1.101	0.6787	0.1587	522.95	703.90	180.95	1.0800	1.6849
28	1.180	0.6809	0.1488	524.73	704.93	180.20	1.0859	1.6843
30	1.263	0.6832	0.1397	526.52	705.97	179.45	1.0918	1.6838
32	1.350	0.6855	0.1312	528.31	707.00	178.69	1.0977	1.6833
34	1.442	0.6878	0.1233	530.10	708.03	177.93	1.1035	1.6828
36	1.539	0.6901	0.1161	531.9	709.05	177.16	1.1093	1.6824
38	1.641	0.6925	0.1093	533.70	710.08	176.38	1.1151	1.6820
40	1.748	0.6949	0.1030	535.50	711.10	175.60	1.1208	1.6816
42	1.860	0.6973	0.09719	537.31	712.12	174.81	1.1266	1.6812

T	P	$V_l \times 10^3$	V_g	ΔH_l	ΔH_g	ΔH_{vap}	S_l	S_g
44	1.978	0.6998	0.09174	539.12	713.13	174.01	1.1323	1.6809
46	2.102	0.7023	0.08667	540.93	714.14	173.21	1.1380	1.6806
48	2.231	0.7048	0.08194	542.75	715.15	172.40	1.1436	1.6804
50	2.366	0.7073	0.07752	544.57	716.15	171.58	1.1492	1.6802
52	2.508	0.7099	0.07338	546.40	717.15	170.75	1.1548	1.6799
54	2.655	0.7125	0.06952	548.23	718.15	169.91	1.1604	1.6797
56	2.810	0.7151	0.06590	550.07	719.14	169.07	1.1659	1.6796
58	2.971	0.7178	0.06251	551.91	720.12	168.21	1.1715	1.6794
60	3.138	0.7205	0.05932	553.76	721.11	167.35	1.1770	1.6793
70	4.088	0.7346	0.04608	563.06	725.93	162.87	1.2042	1.6788
80	5.240	0.7497	0.03626	572.52	730.61	158.09	1.2310	1.6787
90	6.6190	0.7660	0.02884	582.13	735.10	152.97	1.2574	1.6787
100	8.253	0.7838	0.02315	591.93	739.39	147.46	1.2835	1.6786
110	10.168	0.8034	0.01872	601.93	743.43	141.50	1.3092	1.6785
120	12.393	0.8252	0.01523	612.16	747.19	135.03	1.3346	1.6780
130	14.959	0.8499	0.01242	622.63	750.60	127.97	1.3596	1.6771
140	17.896	0.8785	0.01014	633.38	753.60	120.22	1.3843	1.6753

Appendix 4 Comparision of Calculated Thermodynamic Data with Reference Data

Comparison of calculated enthalpy and pressure from the fitted equation with the data from reference 108. In the table enthalpy (H) is units of kJ/kg, pressure (P) is in mm Hg, temperature (T) is in degree celsius, the specific volume (V) of gas is in m^3/kg, and error is the percentage difference between calculated and reference data. Subscripts c and r means calculated and reference values respectively.

T	V	H_r	H_c	Error	P_c	Error
75.0 mm Hg						
0.0	1.6470	690.87	690.86	0.0012	75.25	-0.3327
10.0	1.7080	696.42	696.42	-0.0006	74.65	0.4686
20.0	1.7690	702.06	702.07	-0.0011	74.26	0.9909
30.0	1.8290	707.78	707.79	-0.0016	74.12	1.1796
40.0	1.8900	713.59	713.59	-0.0004	74.14	1.1453
50.0	1.9510	719.47	719.47	-0.0001	74.38	0.8317
60.0	2.0120	725.43	725.42	0.0008	74.82	0.2386
70.0	2.0730	731.46	731.45	0.0012	75.48	-0.6338
80.0	2.1330	737.55	737.55	-0.0001	77.79	-3.7264
90.0	2.1940	743.71	743.72	-0.0016	76.66	-2.2111
150.0 mm Hg						
10.0	0.8507	696.25	696.17	0.0110	149.66	0.2260
20.0	0.8814	701.90	701.89	0.0017	149.25	0.4973
30.0	0.9119	707.63	707.67	-0.0055	149.09	0.6082
40.0	0.9425	713.44	713.51	-0.0105	149.11	0.5923
50.0	0.9731	719.33	719.42	-0.0130	149.34	0.4383
60.0	1.0040	725.29	725.39	-0.0144	149.74	0.1756
70.0	1.0340	731.33	731.43	-0.0131	150.47	-0.3139
80.0	1.0650	737.43	737.52	-0.0118	152.69	-1.7939
90.0	1.0950	743.59	743.67	-0.0103	151.64	-1.0926
100.0	1.1260	749.82	749.87	-0.0071	150.82	-0.5493
110.0	1.1560	756.10	756.14	-0.0049	150.52	-0.3437
120.0	1.1870	762.44	762.46	-0.0020	150.45	-0.3013
130.0	1.2170	768.84	768.83	0.0015	150.57	-0.3791
140.0	1.2470	775.29	775.25	0.0045	150.52	-0.3468
150.0	1.2780	781.78	781.73	0.0059	150.36	-0.2427
160.0	1.3080	788.33	788.27	0.0082	150.34	-0.2250
170.0	1.3390	794.92	794.85	0.0092	150.21	-0.1394
180.0	1.3700	801.55	801.48	0.0088	150.10	-0.0639
190.0	1.4000	808.23	808.16	0.0085	150.10	-0.0695
200.0	1.4300	814.95	814.89	0.0071	150.12	-0.0820
210.0	1.4600	821.70	821.67	0.0036	150.15	-0.1015

T	V	H_r	H_c	Error	P_c	Error
220.0	1.4910	828.50	828.50	0.0004	150.09	-0.0610
230.0	1.5210	835.33	835.37	-0.0048	150.14	-0.0960
240.0	1.5520	842.19	842.29	-0.0118	150.11	-0.0739
250.0	1.5820	849.09	849.25	-0.0193	150.19	-0.1247
300.0 mm Hg						
10.0	0.4222	695.92	695.86	0.0088	299.68	0.1051
20.0	0.4377	701.58	701.59	-0.0010	299.26	0.2473
30.0	0.4532	707.33	707.38	-0.0072	299.03	0.3231
40.0	0.4686	713.15	713.24	-0.0125	299.07	0.3110
50.0	0.4841	719.05	719.16	-0.0154	299.24	0.2535
60.0	0.4995	725.02	725.14	-0.0170	299.67	0.1090
70.0	0.5149	731.07	731.19	-0.0158	300.31	-0.1021
80.0	0.5302	737.18	737.29	-0.0146	302.63	-0.8764
90.0	0.5456	743.35	743.45	-0.0132	301.51	-0.5048
100.0	0.5610	749.58	749.66	-0.0113	300.76	-0.2543
110.0	0.5763	755.88	755.94	-0.0076	300.43	-0.1423
120.0	0.5916	762.23	762.27	-0.0046	300.45	-0.1512
130.0	0.6069	768.63	768.65	-0.0022	300.53	-0.1765
140.0	0.6222	775.09	775.08	0.0011	300.44	-0.1463
150.0	0.6376	781.59	781.57	0.0027	300.31	-0.1033
160.0	0.6528	788.14	788.11	0.0041	300.28	-0.0946
170.0	0.6681	794.74	794.70	0.0055	300.22	-0.0733
180.0	0.6834	801.38	801.34	0.0056	300.17	-0.0551
190.0	0.6987	808.06	808.02	0.0045	300.12	-0.0402
200.0	0.7140	814.78	814.76	0.0024	300.09	-0.0286
210.0	0.7292	821.55	821.54	0.0007	300.10	-0.0341
220.0	0.7445	828.34	828.38	-0.0043	300.09	-0.0290
230.0	0.7597	835.18	835.25	-0.0088	300.12	-0.0406
240.0	0.7750	842.05	842.18	-0.0151	300.13	-0.0423
250.0	0.7902	848.95	849.15	-0.0230	300.18	-0.0603
450.0 mm Hg						
10.0	0.2794	695.58	695.51	0.0099	449.69	0.0691
20.0	0.2898	701.26	701.26	0.0001	449.30	0.1561
30.0	0.3003	707.02	707.07	-0.0073	448.94	0.2358
40.0	0.3107	712.85	712.95	-0.0137	448.92	0.2409
50.0	0.3211	718.77	718.89	-0.0161	449.08	0.2049
60.0	0.3314	724.75	724.88	-0.0186	449.56	0.0974
70.0	0.3418	730.80	730.94	-0.0196	450.10	-0.0217
80.0	0.3521	736.92	737.06	-0.0190	452.40	-0.5338
90.0	0.3624	743.11	743.23	-0.0168	451.38	-0.3059
100.0	0.3727	749.35	749.46	-0.0153	450.69	-0.1538
110.0	0.3830	755.65	755.75	-0.0133	450.35	-0.0782
120.0	0.3933	762.01	762.09	-0.0105	450.36	-0.0795
130.0	0.4036	768.42	768.48	-0.0083	450.41	-0.0908
140.0	0.4139	774.88	774.93	-0.0063	450.29	-0.0640
150.0	0.4241	781.40	781.43	-0.0033	450.28	-0.0617

T_c	V	H_r	H_c	Error	P_c	Error
160.0	0.4344	787.95	787.97	-0.0030	450.17	-0.0368
170.0	0.4446	794.56	794.57	-0.0014	450.16	-0.0357
180.0	0.4548	801.20	801.22	-0.0023	450.16	-0.0351
190.0	0.4651	807.89	807.91	-0.0029	450 06	-0.0138
200.0	0.4753	814.62	814.66	-0.0045	450.07	-0.0152
210.0	0.4855	821.39	821.45	-0.0069	450.08	-0.0175
220.0	0.4957	828.19	828.28	-0.0113	450.09	-0.0208
230.0	0.5059	835.03	835.17	-0.0163	450.11	-0.0253
240.0	0.5161	841.90	842.09	-0.0230	450.14	-0.0311
250.0	0.5263	848.81	849.07	-0.0301	450.17	-0.0383
600.0 mm Hg						
20.0	0.2159	700.93	700.81	0.0166	599.24	0.1272
30.0	0.2238	706.70	706.65	0.0070	598.94	0.1762
40.0	0.2317	712.55	712.55	0.0000	598.82	0.1974
50.0	0.2395	718.48	718.51	-0.0041	599.10	0.1494
60.0	0.2474	724.48	724.53	-0.0066	599.31	0.1144
70.0	0.2552	730.54	730.60	-0.0088	599.93	0.0115
80.0	0.2630	736.67	736.74	-0.0092	602.19	-0.3653
90.0	0.2708	742.86	742.93	-0.0090	601.20	-0.1995
100.0	0.2786	749.12	749.17	-0.0067	600.52	-0.0864
110.0	0.2864	755.43	755.47	-0.0049	600.16	-0.0267
120.0	0.2942	761.79	761.82	-0.0035	600.13	-0.0212
130.0	0.3019	768.21	768.22	-0.0011	600.33	-0.0547
140.0	0.3097	774.68	774.67	0.0012	600.15	-0.0252
150.0	0.3174	781.20	781.17	0.0035	600.16	-0.0270
160.0	0.3251	787.77	787.72	0.0058	600.17	-0.0278
170.0	0.3328	794.38	794.32	0.0071	600.17	-0.0277
180.0	0.3406	801.03	800.97	0.0073	599.99	0.0023
190.0	0.3483	807.72	807.67	0.0067	599.98	0.0030
200.0	0.3560	814.46	814.41	0.0066	599.98	0.0040
210.0	0.3637	821.23	821.19	0.0045	599.97	0.0052
220.0	0.3713	828.04	828.02	0.0019	600.12	-0.0203
230.0	0.3796	834.88	834.90	-0.0023	599.17	0.1388
240.0	0.3867	841.76	841.82	-0.0070	600.10	-0.0170
250.0	0.3944	848.67	848.73	-0.0131	600.10	-0.0158
750.0 mm Hg						
30.0	0.1779	706.39	706.29	0.0141	748.98	0.1363
40.0	0.1842	712.25	712.21	0.0055	749.10	0.1201
50.0	0.1906	718.19	718.19	0.0000	748.96	0.1381
60.0	0.1969	724.20	724.23	-0.0038	749.36	0.0855
70.0	0.2033	730.28	730.32	-0.0057	749.53	0.0622
80.0	0.2096	736.42	736.47	-0.0069	751.73	-0.2309
90.0	0.2159	742.62	742.67	-0.0074	750.77	-0.1030
100.0	0.2221	748.88	748.93	-0.0070	750.43	-0.0571
110.0	0.2284	755.20	755.24	-0.0056	750.03	-0.0045
120.0	0.2347	761.58	761.60	-0.0031	749.94	0.0084
130.0	0.2409	768.00	768.02	-0.0020	750.18	-0.0237

T	V	H_r	H_c	Error	P_c	Error
140.0	0.2471	774.48	774.48	0.0004	750.22	-0.0293
150.0	0.2533	781.01	780.99	0.0029	750.24	-0.0325
160.0	0.2596	787.58	787.55	0.0044	749.97	0.0045
170.0	0.2658	794.19	794.15	0.0049	749.97	0.0043
180.0	0.2720	800.85	800.80	0.0058	749.96	0.0058
190.0	0.2782	807.55	807.50	0.0060	749.93	0.0087
200.0	0.2844	814.29	814.24	0.0055	749.90	0.0129
210.0	0.2905	821.07	821.03	0.0045	750.12	-0.0161
220.0	0.2967	827.88	827.86	0.0019	750.07	-0.0094
230.0	0.3029	834.73	834.74	-0.0011	750.01	-0.0020
240.0	0.3091	841.61	841.66	-0.0056	749.96	0.0060
250.0	0.3152	848.53	848.62	-0.0102	750.13	-0.0172
1125.0 mm Hg						
40.0	0.1210	711.49	711.41	0.0119	1124.26	0.0657
50.0	0.1254	717.46	717.42	0.0055	1123.50	0.1337
60.0	0.1297	723.50	723.49	0.0010	1123.67	0.1183
70.0	0.1340	729.61	729.62	-0.0013	1123.90	0.0973
80.0	0.1383	735.77	735.80	-0.0042	1125.83	-0.0740
90.0	0.1426	742.00	742.03	-0.0046	1124.94	0.0053
100.0	0.1468	748.29	748.32	-0.0040	1124.97	0.0029
110.0	0.1511	754.63	754.66	-0.0034	1124.42	0.0516
120.0	0.1553	761.03	761.04	-0.0016	1124.78	0.0192
130.0	0.1595	767.43	767.48	-0.0062	1125.12	-0.0105
140.0	0.1638	773.97	773.96	0.0012	1124.54	0.0409
150.0	0.1680	780.52	780.49	0.0037	1124.60	0.0355
160.0	0.1720	787.10	787.07	0.0040	1125.90	-0.0801
170.0	0.1764	793.74	793.69	0.0061	1124.59	0.0368
180.0	0.1805	800.41	800.36	0.0063	1125.13	-0.0118
190.0	0.1847	807.12	807.07	0.0059	1125.02	-0.0014
200.0	0.1889	813.88	813.83	0.0064	1124.87	0.0119
210.0	0.1931	820.67	820.63	0.0052	1124.69	0.0277
220.0	0.1972	827.49	827.47	0.0025	1125.05	-0.0043
230.0	0.2014	834.36	834.35	0.0009	1124.81	0.0171
240.0	0.2055	841.25	841.28	-0.0032	1125.09	-0.0078
250.0	0.2097	848.18	848.24	-0.0074	1124.80	0.0182
1500.0 mm Hg						
50.0	0.0927	716.71	716.68	0.0046	1499.54	0.0306
60.0	0.0960	722.79	722.78	0.0009	1498.87	0.0755
70.0	0.0993	728.92	728.94	-0.0032	1498.47	0.1021
80.0	0.1026	735.12	735.16	-0.0048	1500.39	-0.0258
90.0	0.1059	741.38	741.42	-0.0051	1499.53	0.0312
100.0	0.1092	747.69	747.73	-0.0054	1498.70	0.0866
110.0	0.1124	754.06	754.09	-0.0042	1499.21	0.0526
120.0	0.1156	760.48	760.50	-0.0027	1499.73	0.0180
130.0	0.1189	766.94	766.96	-0.0022	1498.93	0.0712
140.0	0.1221	773.46	773.46	0.0001	1499.10	0.0602
150.0	0.1253	780.02	780.01	0.0016	1499.17	0.0556

T	V	H_r	H_c	Error	P_c	Error
160.0	0.1285	786.63	786.60	0.0038	1499.15	0.0568
170.0	0.1316	793.28	793.24	0.0054	1500.16	-0.0110
180.0	0.1348	799.97	799.92	0.0066	1499.96	0.0024
190.0	0.1380	806.70	806.64	0.0075	1499.70	0.0203
200.0	0.1412	813.46	813.40	0.0069	1499.36	0.0425
210.0	0.1443	820.27	820.21	0.0074	1500.00	0.0002
220.0	0.1475	827.11	827.06	0.0066	1499.53	0.0313
230.0	0.1506	833.98	833.94	0.0046	1500.00	0.0000
240.0	0.1537	840.89	840.87	0.0026	1500.38	-0.0256
250.0	0.1569	847.83	847.83	-0.0003	1499.74	0.0171
2250.0 mm Hg						
60.0	0.0623	721.31	721.34	-0.0036	2251.16	-0.0515
70.0	0.0647	727.52	727.56	-0.0054	2245.80	0.1866
80.0	0.0669	733.79	733.83	-0.0056	2249.18	0.0364
90.0	0.0692	740.10	740.15	-0.0069	2248.97	0.0458
100.0	0.0715	746.47	746.52	-0.0064	2248.92	0.0482
110.0	0.0737	752.89	752.93	-0.0053	2249.04	0.0427
120.0	0.0759	759.35	759.39	-0.0049	2249.07	0.0413
130.0	0.0782	765.86	765.89	-0.0037	2249.16	0.0372
140.0	0.0804	772.42	772.43	-0.0017	2249.37	0.0278
150.0	0.0826	779.02	779.02	0.0000	2249.37	0.0281
160.0	0.0847	785.67	785.65	0.0027	2249.41	0.0261
170.0	0.0869	792.35	792.32	0.0039	2249.51	0.0217
180.0	0.0891	799.07	799.03	0.0051	2249.66	0.0151
190.0	0.0913	805.83	805.78	0.0063	2249.86	0.0064
200.0	0.0934	812.63	812.57	0.0076	2250.10	-0.0043
210.0	0.0956	819.46	819.40	0.0078	2250.15	-0.0066
220.0	0.0977	826.35	826.26	0.0107	2250.02	-0.0011
230.0	0.0998	833.23	833.16	0.0079	2249.96	0.0019
240.0	0.1020	840.16	840.10	0.0067	2249.29	0.0314
250.0	0.1041	847.12	847.08	0.0047	2249.77	0.0101
3000.0 mm Hg						
70.0	0.0472	726.06	726.16	-0.0143	3003.86	-0.1286
80.0	0.0490	732.40	732.50	-0.0137	3001.34	-0.0446
90.0	0.0508	738.79	738.88	-0.0123	3000.92	-0.0307
100.0	0.0526	745.21	745.30	-0.0127	3001.07	-0.0358
110.0	0.0543	751.69	751.77	-0.0107	3000.75	-0.0249
120.0	0.0561	758.21	758.28	-0.0090	3000.51	-0.0170
130.0	0.0577	764.77	764.83	-0.0075	3001.83	-0.0609
140.0	0.0595	771.37	771.42	-0.0059	3000.06	-0.0021
150.0	0.0612	778.01	778.04	-0.0043	2999.88	0.0040
160.0	0.0629	784.69	784.71	-0.0026	3000.25	-0.0084
170.0	0.0645	791.41	791.41	-0.0006	3000.25	-0.0083
180.0	0.0662	798.17	798.16	0.0018	3000.33	-0.0111
190.0	0.0679	804.96	804.93	0.0032	3000.50	-0.0166
200.0	0.0695	811.79	811.75	0.0051	3000.74	-0.0248
210.0	0.0712	818.65	818.60	0.0063	3000.65	-0.0217

T	V	H_r	H_c	Error	P_c	Error
220.0	0.0728	825.55	825.48	0.0082	3000.65	-0.0216
230.0	0.0745	832.47	832.40	0.0082	3000.33	-0.0111
240.0	0.0761	839.43	839.35	0.0090	3000.11	-0.0037
250.0	0.0777	846.41	846.34	0.0082	2999.98	0.0007

Appendix 5 Frequency Characteristics of the Apparatus.

Summary of the results of the frequency of schlieren signals disscused in chapter 2.In the table a_l is velocity of plane longitudinal wave in bulk material, a_s is velocity of plane transverse (shear) wave, a_{ext} is velocity of longitudinal wave (extensional wave) in thin rods.

No	$a_l/(2f)$ (steel) (mm)	$a_s/(2f)$ (steel) (mm)	$a_{ext}/(2f)$ (steel) (mm)	$a_l/(2f)$ (quartz) (mm)	$a_s/(2f)$ (quartz) (mm)	$a_{ext}/(2f)$ (quartz) (mm)
3	0.2627E-01	0.1407E-01	0.2269E-01	0.2708E-01	0.1708E-01	0.2613E-01
7	0.4566E-01	0.2445E-01	0.3943E-01	0.4707E-01	0.2968E-01	0.4542E-01
8	0.4152E-01	0.2223E-01	0.3586E-01	0.4280E-01	0.2699E-01	0.4131E-01
10	0.9133E-01	0.4890E-01	0.7887E-01	0.9414E-01	0.5938E-01	0.9086E-01
15	0.2610E+00	0.1397E+00	0.2254E+00	0.2690E+00	0.1697E+00	0.2596E+00
16	0.9971E-01	0.5338E-01	0.8610E-01	0.1028E+00	0.6482E-01	0.9919E-01
17	0.1143E+00	0.6119E-01	0.9869E-01	0.1178E+00	0.7429E-01	0.1137E+00
18	0.1859E+00	0.9953E-01	0.1605E+00	0.1916E+00	0.1209E+00	0.1849E+00
20	0.1812E+00	0.9704E-01	0.1565E+00	0.1868E+00	0.1178E+00	0.1803E+00
25	0.2254E+00	0.1207E+00	0.1947E+00	0.2323E+00	0.1465E+00	0.2242E+00
26	0.9789E-01	0.5241E-01	0.8454E-01	0.1009E+00	0.6364E-01	0.9739E-01
27	0.9208E-01	0.4930E-01	0.7952E-01	0.9491E-01	0.5986E-01	0.9160E-01
29	0.8039E-01	0.4304E-01	0.6942E-01	0.8286E-01	0.5226E-01	0.7997E-01
30	0.6694E-01	0.3584E-01	0.5780E-01	0.6899E-01	0.4351E-01	0.6659E-01
32	0.2537E-03	0.1358E-03	0.2191E-03	0.2615E-03	0.1649E-03	0.2524E-03
33	0.1047E+00	0.5604E-01	0.9039E-01	0.1079E+00	0.6805E-01	0.1041E+00
36	0.7498E-01	0.4014E-01	0.6475E-01	0.7728E-01	0.4874E-01	0.7459E-01
37	0.4733E-01	0.2534E-01	0.4087E-01	0.4879E-01	0.3077E-01	0.4709E-01
38	0.5643E-01	0.3022E-01	0.4873E-01	0.5817E-01	0.3669E-01	0.5614E-01
39	0.6256E-01	0.3350E-01	0.5402E-01	0.6448E-01	0.4067E-01	0.6224E-01

40	0.7516E-01	0.4024E-01	0.6491E-01	0.7747E-01	0.4886E-01	0.7477E-01
51	0.7540E-01	0.4037E-01	0.6511E-01	0.7772E-01	0.4902E-01	0.7501E-01
52	0.1127E+00	0.6036E-01	0.9735E-01	0.1162E+00	0.7328E-01	0.1121E+00
53	0.5068E-01	0.2714E-01	0.4377E-01	0.5224E-01	0.3295E-01	0.5042E-01
54	0.6252E-01	0.3347E-01	0.5399E-01	0.6444E-01	0.4064E-01	0.6219E-01
55	0.7358E-01	0.3940E-01	0.6354E-01	0.7584E-01	0.4783E-01	0.7320E-01
56	0.5081E-01	0.2720E-01	0.4388E-01	0.5237E-01	0.3303E-01	0.5055E-01
58	0.5283E-01	0.2829E-01	0.4562E-01	0.5446E-01	0.3435E-01	0.5256E-01
59	0.5498E-01	0.2944E-01	0.4748E-01	0.5667E-01	0.3574E-01	0.5469E-01
60	0.6299E-01	0.3373E-01	0.5440E-01	0.6493E-01	0.4095E-01	0.6266E-01
61	0.4384E-01	0.2347E-01	0.3786E-01	0.4519E-01	0.2850E-01	0.4362E-01
63	0.6298E-01	0.3372E-01	0.5439E-01	0.6492E-01	0.4095E-01	0.6266E-01
64	0.6134E-01	0.3284E-01	0.5297E-01	0.6323E-01	0.3988E-01	0.6103E-01
65	0.5664E-01	0.3033E-01	0.4891E-01	0.5838E-01	0.3682E-01	0.5635E-01
66	0.7070E-01	0.3785E-01	0.6105E-01	0.7287E-01	0.4596E-01	0.7033E-01
67	0.5750E-01	0.3079E-01	0.4965E-01	0.5927E-01	0.3738E-01	0.5720E-01
68	0.6621E-01	0.3545E-01	0.5717E-01	0.6824E-01	0.4304E-01	0.6586E-01
69	0.6490E-01	0.3475E-01	0.5604E-01	0.6689E-01	0.4219E-01	0.6456E-01
70	0.5226E-01	0.2798E-01	0.4513E-01	0.5386E-01	0.3397E-01	0.5198E-01
71	0.4924E-01	0.2637E-01	0.4252E-01	0.5076E-01	0.3201E-01	0.4899E-01
72	0.7694E-01	0.4119E-01	0.6644E-01	0.7931E-01	0.5002E-01	0.7654E-01
73	0.6798E-01	0.3640E-01	0.5870E-01	0.7007E-01	0.4419E-01	0.6763E-01
74	0.5904E-01	0.3161E-01	0.5099E-01	0.6086E-01	0.3838E-01	0.5874E-01
75	0.6142E-01	0.3289E-01	0.5304E-01	0.6331E-01	0.3993E-01	0.6110E-01
76	0.5749E-01	0.3078E-01	0.4965E-01	0.5926E-01	0.3737E-01	0.5719E-01
77	0.5706E-01	0.3055E-01	0.4928E-01	0.5882E-01	0.3710E-01	0.5677E-01
78	0.5749E-01	0.3078E-01	0.4964E-01	0.5925E-01	0.3737E-01	0.5719E-01
79	0.5766E-01	0.3087E-01	0.4979E-01	0.5943E-01	0.3748E-01	0.5736E-01
80	0.4397E-01	0.2354E-01	0.3797E-01	0.4532E-01	0.2858E-01	0.4374E-01
81	0.5070E-01	0.2715E-01	0.4378E-01	0.5226E-01	0.3296E-01	0.5044E-01
82	0.4702E-01	0.2518E-01	0.4061E-01	0.4847E-01	0.3057E-01	0.4678E-01
83	0.6539E-01	0.3501E-01	0.5647E-01	0.6740E-01	0.4251E-01	0.6505E-01
84	0.6091E-01	0.3261E-01	0.5260E-01	0.6279E-01	0.3960E-01	0.6060E-01
85	0.5171E-01	0.2768E-01	0.4465E-01	0.5330E-01	0.3361E-01	0.5144E-01

86	0.6598E-01	0.3533E-01	0.5698E-01	0.6801E-01	0.4289E-01	0.6564E-01
87	0.7056E-01	0.3778E-01	0.6093E-01	0.7273E-01	0.4587E-01	0.7019E-01
88	0.6438E-01	0.3447E-01	0.5560E-01	0.6636E-01	0.4185E-01	0.6405E-01
89	0.6166E-01	0.3301E-01	0.5325E-01	0.6355E-01	0.4008E-01	0.6134E-01
90	0.4971E-01	0.2662E-01	0.4293E-01	0.5124E-01	0.3232E-01	0.4945E-01
91	0.3747E-01	0.2006E-01	0.3236E-01	0.3862E-01	0.2436E-01	0.3728E-01
92	0.7456E-01	0.3992E-01	0.6439E-01	0.7686E-01	0.4847E-01	0.7418E-01
93	0.6714E-01	0.3595E-01	0.5798E-01	0.6920E-01	0.4365E-01	0.6679E-01
94	0.5345E-01	0.2862E-01	0.4615E-01	0.5509E-01	0.3474E-01	0.5317E-01
95	0.5468E-01	0.2927E-01	0.4722E-01	0.5636E-01	0.3555E-01	0.5439E-01
96	0.7149E-01	0.3827E-01	0.6173E-01	0.7369E-01	0.4647E-01	0.7112E-01
97	0.4987E-01	0.2670E-01	0.4307E-01	0.5141E-01	0.3242E-01	0.4962E-01
98	0.5546E-01	0.2969E-01	0.4789E-01	0.5716E-01	0.3605E-01	0.5517E-01
99	0.4028E-01	0.2156E-01	0.3478E-01	0.4152E-01	0.2618E-01	0.4007E-01
100	0.5884E-01	0.3150E-01	0.5081E-01	0.6065E-01	0.3825E-01	0.5853E-01
101	0.4675E-01	0.2503E-01	0.4038E-01	0.4819E-01	0.3039E-01	0.4651E-01
102	0.4988E-01	0.2671E-01	0.4308E-01	0.5141E-01	0.3243E-01	0.4962E-01
104	0.6208E-01	0.3324E-01	0.5361E-01	0.6398E-01	0.4035E-01	0.6175E-01
105	0.3800E-01	0.2035E-01	0.3282E-01	0.3917E-01	0.2470E-01	0.3781E-01
106	0.6006E-01	0.3215E-01	0.5186E-01	0.6190E-01	0.3904E-01	0.5975E-01
107	0.6110E-01	0.3272E-01	0.5277E-01	0.6298E-01	0.3972E-01	0.6079E-01
108	0.6371E-01	0.3411E-01	0.5501E-01	0.6567E-01	0.4142E-01	0.6338E-01
109	0.4205E-01	0.2251E-01	0.3631E-01	0.4334E-01	0.2734E-01	0.4183E-01
111	0.2823E-01	0.1511E-01	0.2438E-01	0.2910E-01	0.1835E-01	0.2808E-01
112	0.5849E-01	0.3132E-01	0.5051E-01	0.6029E-01	0.3803E-01	0.5819E-01
113	0.4731E-01	0.2533E-01	0.4086E-01	0.4877E-01	0.3076E-01	0.4707E-01
114	0.4713E-01	0.2523E-01	0.4070E-01	0.4858E-01	0.3064E-01	0.4689E-01
115	0.1082E+00	0.5793E-01	0.9344E-01	0.1115E+00	0.7034E-01	0.1076E+00
116	0.5967E-01	0.3195E-01	0.5153E-01	0.6150E-01	0.3879E-01	0.5936E-01
117	0.4711E-01	0.2522E-01	0.4068E-01	0.4856E-01	0.3063E-01	0.4687E-01
118	0.5647E-01	0.3023E-01	0.4876E-01	0.5820E-01	0.3671E-01	0.5618E-01
119	0.8026E-01	0.4297E-01	0.6931E-01	0.8273E-01	0.5218E-01	0.7985E-01
120	0.5023E-01	0.2689E-01	0.4338E-01	0.5178E-01	0.3266E-01	0.4997E-01
122	0.8967E-01	0.4801E-01	0.7743E-01	0.9242E-01	0.5829E-01	0.8920E-01

123	0.7275E-01	0.3895E-01	0.6282E-01	0.7499E-01	0.4729E-01	0.7237E-01
124	0.7320E-01	0.3919E-01	0.6321E-01	0.7545E-01	0.4758E-01	0.7282E-01
125	0.7066E-01	0.3783E-01	0.6102E-01	0.7283E-01	0.4593E-01	0.7029E-01
126	0.7886E-01	0.4222E-01	0.6810E-01	0.8129E-01	0.5127E-01	0.7845E-01
127	0.1100E+00	0.5887E-01	0.9496E-01	0.1133E+00	0.7149E-01	0.1094E+00
147	0.1203E+00	0.6440E-01	0.1039E+00	0.1240E+00	0.7819E-01	0.1197E+00
149	0.4687E-01	0.2509E-01	0.4048E-01	0.4831E-01	0.3047E-01	0.4663E-01
151	0.5657E-01	0.3029E-01	0.4885E-01	0.5831E-01	0.3677E-01	0.5627E-01
153	0.5661E-01	0.3031E-01	0.4888E-01	0.5835E-01	0.3680E-01	0.5631E-01
154	0.5461E-01	0.2924E-01	0.4716E-01	0.5629E-01	0.3550E-01	0.5433E-01
155	0.2805E-01	0.1502E-01	0.2422E-01	0.2891E-01	0.1823E-01	0.2790E-01
158	0.3190E-01	0.1708E-01	0.2755E-01	0.3288E-01	0.2074E-01	0.3173E-01
159	0.1492E+00	0.7986E-01	0.1288E+00	0.1537E+00	0.9696E-01	0.1484E+00
160	0.3384E-01	0.1812E-01	0.2923E-01	0.3488E-01	0.2200E-01	0.3367E-01
161	0.3186E-01	0.1706E-01	0.2751E-01	0.3284E-01	0.2071E-01	0.3170E-01
162	0.4327E-01	0.2317E-01	0.3737E-01	0.4460E-01	0.2813E-01	0.4304E-01
163	0.5202E-01	0.2785E-01	0.4493E-01	0.5362E-01	0.3382E-01	0.5175E-01
164	0.3088E-01	0.1653E-01	0.2666E-01	0.3182E-01	0.2007E-01	0.3072E-01
165	0.6314E-01	0.3380E-01	0.5452E-01	0.6508E-01	0.4104E-01	0.6281E-01
166	0.1031E+00	0.5520E-01	0.8903E-01	0.1063E+00	0.6702E-01	0.1026E+00
167	0.5401E-01	0.2892E-01	0.4664E-01	0.5567E-01	0.3511E-01	0.5373E-01
168	0.8846E-01	0.4736E-01	0.7639E-01	0.9118E-01	0.5751E-01	0.8800E-01
169	0.5202E-01	0.2785E-01	0.4492E-01	0.5362E-01	0.3382E-01	0.5175E-01
170	0.4247E-01	0.2274E-01	0.3667E-01	0.4378E-01	0.2761E-01	0.4225E-01
171	0.3302E-01	0.1768E-01	0.2851E-01	0.3403E-01	0.2146E-01	0.3285E-01
172	0.6639E-01	0.3554E-01	0.5733E-01	0.6843E-01	0.4316E-01	0.6604E-01
173	0.7449E-01	0.3988E-01	0.6433E-01	0.7678E-01	0.4843E-01	0.7410E-01
174	0.4518E-01	0.2419E-01	0.3902E-01	0.4657E-01	0.2937E-01	0.4495E-01
175	0.5075E-01	0.2717E-01	0.4383E-01	0.5231E-01	0.3299E-01	0.5049E-01
221	0.1411E+00	0.7553E-01	0.1218E+00	0.1454E+00	0.9171E-01	0.1403E+00

Appendix 6 Table of Observed Frequencies in the Schlieren Signals

The average frequency (f) and the value of f divided by P_2 for each experimental schlieren signal, together with P_2 and T_2.

No	P_2 mm Hg	T_2 K	F kHz	f/p_2 kHz/mm Hg
3	2003.700	348.50	0.1102E+06	0.5500E+02
7	961.500	312.80	0.6340E+05	0.6594E+02
8	948.700	312.30	0.6972E+05	0.7349E+02
10	834.900	319.70	0.3170E+05	0.3796E+02
15	1570.400	370.30	0.1109E+05	0.7064E+01
16	593.700	315.00	0.2904E+05	0.4891E+02
17	616.700	317.70	0.2533E+05	0.4108E+02
18	573.400	331.10	0.1557E+05	0.2716E+02
20	339.000	342.50	0.1597E+05	0.4712E+02
25	114.300	358.50	0.1284E+05	0.1124E+03
26	149.200	316.00	0.2957E+05	0.1982E+03
27	254.400	308.60	0.3144E+05	0.1236E+03
29	563.600	312.70	0.3601E+05	0.6390E+02
30	755.600	308.20	0.4325E+05	0.5724E+02
32	91.600	332.50	0.1141E+08	0.1246E+06
33	216.000	328.60	0.2766E+05	0.1280E+03
36	589.400	306.50	0.3861E+05	0.6551E+02
37	715.800	300.60	0.6116E+05	0.8545E+02
38	734.400	298.10	0.5130E+05	0.6985E+02
39	1159.300	313.60	0.4627E+05	0.3992E+02
40	930.300	307.50	0.3852E+05	0.4140E+02
51	1201.500	313.60	0.3839E+05	0.3196E+02
52	801.300	300.20	0.2568E+05	0.3205E+02
53	751.400	302.30	0.5712E+05	0.7602E+02
54	838.200	300.70	0.4631E+05	0.5525E+02
55	804.500	300.70	0.3934E+05	0.4890E+02
56	797.000	299.60	0.5698E+05	0.7149E+02
58	785.800	302.50	0.5480E+05	0.6973E+02
59	801.500	300.10	0.5266E+05	0.6570E+02
60	802.300	300.00	0.4596E+05	0.5728E+02
61	808.600	299.50	0.6603E+05	0.8166E+02
63	807.200	299.80	0.4596E+05	0.5694E+02
64	875.900	301.80	0.4719E+05	0.5388E+02
65	1177.100	313.80	0.5111E+05	0.4342E+02
66	871.600	303.10	0.4095E+05	0.4698E+02

67	952.000	305.60	0.5035E+05	0.5289E+02
68	909.600	304.40	0.4373E+05	0.4807E+02
69	882.100	304.00	0.4461E+05	0.5057E+02
70	933.300	304.70	0.5540E+05	0.5936E+02
71	869.100	303.30	0.5879E+05	0.6764E+02
72	869.600	302.50	0.3763E+05	0.4327E+02
73	915.200	304.00	0.4259E+05	0.4653E+02
74	663.400	309.00	0.4903E+05	0.7391E+02
75	889.100	303.30	0.4713E+05	0.5301E+02
76	875.100	303.70	0.5036E+05	0.5754E+02
77	828.900	302.70	0.5073E+05	0.6120E+02
78	901.500	304.50	0.5036E+05	0.5586E+02
79	795.800	301.40	0.5021E+05	0.6310E+02
80	775.200	298.70	0.6584E+05	0.8494E+02
81	851.800	302.40	0.5710E+05	0.6703E+02
82	774.400	298.30	0.6157E+05	0.7950E+02
83	827.600	302.00	0.4427E+05	0.5350E+02
84	1131.500	311.80	0.4753E+05	0.4200E+02
85	846.500	302.20	0.5599E+05	0.6614E+02
86	702.800	296.60	0.4388E+05	0.6243E+02
87	1040.600	309.70	0.4103E+05	0.3943E+02
88	1129.700	313.20	0.4497E+05	0.3980E+02
89	1108.100	312.20	0.4695E+05	0.4237E+02
90	875.800	303.60	0.5824E+05	0.6649E+02
91	754.700	298.70	0.7726E+05	0.1024E+03
92	1056.300	315.50	0.3883E+05	0.3676E+02
93	984.400	309.60	0.4312E+05	0.4380E+02
94	1044.900	312.90	0.5417E+05	0.5184E+02
95	876.000	305.00	0.5295E+05	0.6044E+02
96	624.000	300.40	0.4050E+05	0.6490E+02
97	760.200	301.20	0.5805E+05	0.7636E+02
98	1110.800	311.60	0.5220E+05	0.4699E+02
99	716.100	298.10	0.7188E+05	0.1004E+03
100	775.300	304.20	0.4920E+05	0.6346E+02
101	833.100	305.30	0.6192E+05	0.7432E+02
102	1073.500	315.60	0.5804E+05	0.5406E+02
104	849.000	307.40	0.4664E+05	0.5493E+02
105	773.300	308.00	0.7618E+05	0.9851E+02
106	702.300	301.40	0.4820E+05	0.6864E+02
107	1114.900	312.70	0.4738E+05	0.4250E+02
108	1058.000	312.40	0.4544E+05	0.4295E+02
109	1022.100	311.70	0.6885E+05	0.6736E+02
111	812.000	303.20	0.1026E+06	0.1263E+03
112	1081.300	314.30	0.4949E+05	0.4577E+02
113	1186.200	315.80	0.6119E+05	0.5158E+02
114	1178.300	318.20	0.6142E+05	0.5213E+02
115	1222.900	316.50	0.2676E+05	0.2188E+02
116	1378.000	321.30	0.4852E+05	0.3521E+02
117	1396.000	323.80	0.6145E+05	0.4402E+02
118	1439.200	322.70	0.5127E+05	0.3562E+02
119	1283.100	316.50	0.3607E+05	0.2811E+02
120	1418.600	322.50	0.5763E+05	0.4063E+02

122	1229.800	324.80	0.3229E+05	0.2625E+02
123	1103.000	331.50	0.3979E+05	0.3358E+02
124	1174.800	336.40	0.3955E+05	0.3367E+02
125	1102.700	341.70	0.4097E+05	0.3716E+02
126	1111.500	325.20	0.3671E+05	0.3303E+02
127	1336.700	326.20	0.2633E+05	0.1970E+02
147	2269.400	349.80	0.2407E+05	0.1061E+02
149	821.500	304.90	0.6177E+05	0.7519E+02
151	687.500	296.00	0.5118E+05	0.7444E+02
153	702.900	295.20	0.5114E+05	0.7276E+02
154	627.200	296.10	0.5301E+05	0.8452E+02
155	714.300	295.90	0.1032E+06	0.1445E+03
158	599.700	299.60	0.9076E+05	0.1513E+03
159	669.200	294.00	0.1941E+05	0.2900E+02
160	552.800	298.00	0.8554E+05	0.1547E+03
161	679.400	293.70	0.9086E+05	0.1337E+03
162	425.500	298.80	0.6691E+05	0.1572E+03
163	746.800	298.10	0.5565E+05	0.7451E+02
164	618.200	300.80	0.9376E+05	0.1517E+03
165	956.700	306.60	0.4585E+05	0.4793E+02
166	721.600	313.60	0.2808E+05	0.3892E+02
167	928.400	304.80	0.5361E+05	0.5774E+02
168	604.700	318.30	0.3273E+05	0.5412E+02
169	413.900	332.20	0.5565E+05	0.1345E+03
170	144.100	308.50	0.6817E+05	0.4731E+03
171	700.000	304.20	0.8768E+05	0.1253E+03
172	336.100	305.30	0.4361E+05	0.1297E+03
173	767.500	306.50	0.3886E+05	0.5064E+02
174	376.200	342.80	0.6407E+05	0.1703E+03
175	402.700	342.30	0.5704E+05	0.1417E+03
221	382.100	381.00	0.2052E+05	0.5371E+02

Appendix 7. Computer Code SHOCK FORTRAN

```
C*********************************************************************
C  N is the experiment number.
C  P0 is the initial pressure.
C  T0 is the initial temperiture.
C  Pe is the pressure after shock.
C  Pv s the vapor pressure.
C  dp is the Pv-Pe.
C  Te is the Temperiture after shock.
C  U0 is the velocity of shock wave.
C  X is parameter in shockwave calulation.
C  tz is the time interval between the points the zero point and the
C  dense0 is the initial density.
C     signal cross the zero line in schlieren signal.
C  tm is the time interval between the points the zero point and the
C     signal minimum point.
C  Vm is the depth of the minimum point in schlieren signal.
C  V0  is the voltage of laser signal when it is on a quadrant.
C  vi is the the voltage input range on the Biomation wave recorder
C  dense is the density after shock.
C  H0 is enthalpy at initial condition in kj/kg
C  He is the enthalpy at equilibrium temperature in kl/kg
C
*********************************************************************
      CHARACTER *1 LINE(113)
      INTEGER K,N
      REAL *8 T0,P0,TE,PE,U0,DENSE,DENS0,X,Z,PV,DP,TZ,TM,VM,VI,V0
     + ,U
C P0,T0 AND U0 ARE THE INITIAL PRESSURE,TEMPERATURE AND SHOCK VELOCITY
      READ(3,200) LINE
      WRITE(6,200) LINE
      READ(3,200) LINE
      WRITE(6,200) LINE
      READ(3,200)LINE
      WRITE(6,200)LINE
      CALL SPLFIT
      DO 80 K=1,2
      READ(3,*)N,P0,T0,PE,TE,PV,DP,X,U0,TZ,TM,VM,VI,V0
 800  FORMAT('INITIAL PRESSURE = ', F10.4, '  MM HG')
      CALL SHOCK(T0,P0,U0,DENS0,TE,PE,DENSE,U,X,PV,DP,Z)
      WRITE(6,100)N, P0,T0,PE,TE,DENSE,PV,DP,X,U,TZ,TM,VM,VI,V0,Z
 80   CONTINUE
 700  FORMAT(F5.2)
 100  FORMAT(I4,4F10.4,F8.4,2F11.4,2F8.4,2F6.1,F7.2,F4.1,F5.1,F8.4)
 200  FORMAT(113A1)
      STOP
      END
C-------------------------------------------------------------
       SUBROUTINE SPLFIT
C        THIS PROGRAM FITS DATA WITH A CUBIC INTERPOLATING SPLINE.
C        USING PARABOLIC END CONDITION: S(0)=S(1),S(N-1)=S(N).
      INTEGER N,I,K,N0
      REAL*8 X(17),Y(17),A(17),B(17),C(17),S(17),Y1(17),Y2(17)
     + ,A1(17),B1(17),C1(17),S1(17),A2(17),B2(17),C2(17),S2(17)
     + , X0(26),Y0(26),A0(26),B0(26),C0(26),S0(26)
```

```
      COMMON /ENTH/ X,Y,A,B,C,S,Y1,A1,B1,C1,S1,Y2,A2,B2,C2,S2,N
      COMMON /PVT/X0,Y0,A0,B0,C0,N0
C
      N=17
      N0=26
      READ(5,*)
      READ(5,*)
      READ(5,*)
      DO 8 K=1,N
    8 READ(5,200)Y(K),Y1(K),Y2(K),X(K)
      READ(5,*)
      READ(5,*)
      READ(5,*)
      DO 9 I=1,N0
    9 READ(5,300) Y0(I),X0(I)
C
      CALL CUBSPL(X,Y,N,A,B,C,S)
C
      CALL CUBSPL(X,Y1,N,A1,B1,C1,S1)
C
      CALL CUBSPL(X,Y2,N,A2,B2,C2,S2)
C
      CALL CUBSPL(X0,Y0,N0,A0,B0,C0,S0)
C
  100 FORMAT(3E13.4)
  200 FORMAT(E16.7,E16.7,E16.8,E12.1)
  300 FORMAT(E17.10,E12.2)
      RETURN
      END

C-------------------------------------------------------

      SUBROUTINE SHOCK(T0,P0,U0,DENS0,TE,PE,DENSE,U1,X,PVA,DIFP,Z)
C INPUT: T0,P0,U0; OUTPUT:PE,DENSE,U1,HE,H0; PRESSURE IN MM HG
      REAL *8
R,P0,T0,TE,PE,WM,P2,Z,H0,HE,B1,BE1,DENS0,DENSE,X,Y,BE,B0,
     + C0,CE,T01,AA,BB,CC,U00,U1,Z1,Y1,DIFP,VAP,PVA,U0
      R=8.314510D-00
C WM IS MOLECULAR WEIGHT OF FREON11 IN KG/MOL
      WM=1.3739D-01
C HERE THE PE AND TE ARE THE INITIAL TRIAL VALUE FOR CALCULATION NOT
C TRUE VALUE.
      PE=P0+200.0D0
      TE=T0+10.0D0
C     WRITE (8,*)P0,T0,U0,PE,TE
      Y1=1.0D00
   70 IF (ABS(Y1) .LE. 2.0D-04) GOTO 10
      IF(Y1.LT.0.0) THEN
        TE=TE-0.05D0
      ELSE
        TE=TE+0.05D0
      ENDIF
      P2=PE
      Z=2.0D02
      Z1=3.5D02
   30 IF(ABS(Z) .LE. 1.0D-05  ) GO TO 20
```

```
      Z1=Z
      CALL ENTHAL (P0,T0,H0)

      CALL ENTHAL (P2,TE,HE)
C     WRITE(8,100)TE,H0,HE
      CALL STATE (T0,P0,TE,DENS0,B1,BE1)
C HE-H0 IS THE ENTHALPY DIFF. BETWEEN THE INITIAL AND FINAL
CONDITIONS.
      Y=(HE-H0)*WM*1.0D+03/R
      B0=B1*1.0D-03
      BE=BE1*1.0D-03
      C0=B0*DENS0/WM
      CE=BE*DENS0/WM
      T01=T0/(1.0D00+C0)
      AA=T01
      BB=(1.00D0+CE)*AA+2.0D0*Y-TE
      CC=(2.0D0*Y+T01)*CE-TE
      X=(-BB+(BB**2-4.0D0*AA*CC)**0.5)/(2.0D0*AA)
      DENSE=DENS0/X
      CALL STATE2(TE,DENSE,PE)
C U00 IS THE VELOCITY OF SHOCK WAVE IN M/SECOND
      U00=(2.0D0*(HE-H0)*1.0D03/(1.0D0-X**2))**0.5
C U1 IS VELOCITY OF SHOCK WAVE IN MM/MICROSECOND
      U1=U00*1.0D-03
C     WRITE(8,*)U1,U00
      Z=PE-P2
C     WRITE(8,8)Z,P2,PE,HE,H0
 8    FORMAT(5E13.4)
C     WRITE(8,100) P0,T0,P2,PE,TE,Z,X,U1,HE,H0
      IF (Z .LT. -1.0D-5 .AND. Z .GE. -1.0D-02) THEN
       P2=P2-0.01D-5
      ELSE IF (Z .LT. -1.00D-02 .AND. Z .GE. -1.0D-01) THEN
       P2=P2-0.1D-2
      ELSE IF (Z .LT. -1.00D-01 .AND. Z .GE. -7.0D-00) THEN
       P2=P2-0.1D-0
      ELSE IF (Z .LT. -7.00D-00 .AND. Z .GE. -7.0D01) THEN
       P2=P2-5.0D00
        ELSE IF (Z .GT. 1.0D-05 .AND. Z .LE.  0.1D-03) THEN
         P2=P2+0.010D-6
        ELSE IF (Z .GT. 1.0D-03 .AND. Z .LE.  1.0D-02) THEN
         P2=P2+0.010D-5
        ELSE IF (Z .GT. 1.0D-02 .AND. Z .LE.  1.0D-01) THEN
         P2=P2+0.010D-01
        ELSE IF (Z .GT. 1.0D-01 .AND. Z .LE.  7.0D00) THEN
        P2=P2+0.10D-0
        ELSE IF (Z .GT. 7.0D-00 .AND. Z .LE.  7.0D01) THEN
         P2=P2+5.00D0
       ELSE
      P2=(P2+PE)/2.0D0
        END IF
      IF (PE .LE. P0 ) GO TO 10
      GO TO 30
 20   CONTINUE
      Y1=U0-U00*0.1D-2
      GOTO 70
 10   CONTINUE
```

```
C VAP IS VAPOR PRESSURE OF FREON11 IN KPA AND PVA IS IN MM HG
      VAP=6.01505D0-1043.6D0/((TE-273.15D0)+236.584D0)
       PVA=(760.0D00/101.325D0)*10**VAP
     DIFP=PVA-PE
  100 FORMAT(3F14.4)
      RETURN

     END

C-------------------------------------------------------------
C CALCULATE THE ENTHALPY (KJ/KG) AT TEMPERATURE (K)
      SUBROUTINE ENTHAL(P,T,H)
      INTEGER N
      REAL*8 X(17),Y(17),A(17),B(17),C(17),S(17),P,Y1(17),Y2(17)
     + ,A1(17),B1(17),C1(17),S1(17),A2(17),B2(17),C2(17),S2(17),T,H
     + ,TEMP,TEMP1,TEMP2
      COMMON /ENTH/ X,Y,A,B,C,S,Y1,A1,B1,C1,S1,Y2,A2,B2,C2,S2,N
      TEMP=SEVAL(N,P,X,Y,A,3,C)
C
      TEMP1=SEVAL(N,P,X,Y1,A1,B1,C1)
C
      TEMP2=SEVAL(N,P,X,Y2,A2,B2,C2)
C
      H=TEMP+TEMP1*T**TEMP2
C     WRITE(8,100)TEMP,TEMP1,TEMP2
  100 FORMAT(3F15.4)
       RETURN
       END
C    -------------------------------------------------------
      SUBROUTINE STATE(T0,P0,TE,DENS0,B1,BE1)
      REAL *8  T0,P0,TE,DENS0,B1,BE1,R,V
    + ,X0(26),Y0(26),A0(26),B0(26),C0(26)
      COMMON /PVT/X0,Y0,A0,B0,C0,N0
      R=8.2058D-02
C
      B1=SEVAL(N0,T0,X0,Y0,A0,B0,C0)
C VOLUME IN LITER/MOL (DM)**3
      V=(R*T0*760.0D0/P0-B1)
C DENSITY  IN G/LITER
       DENS0=137.390D0/V
C     WRITE(8,*)B1,V,DENS0
C
       BE1=SEVAL(N0,TE,X0,Y0,A0,B0,C0)
       RETURN
       END
C-------------------------------------------------------
       SUBROUTINE STATE2(T2,DENS2,P2)
        REAL *8 T2,P2,DENS2,B1,V,R,A0(26),B0(26),C0(26),X0(26),Y0(26)
        COMMON /PVT/X0,Y0,A0,B0,C0,N0
        R=8.2058D-02
       B1=SEVAL(N0,T2,X0,Y0,A0,B0,C0)
C VOLUME IN LITER/MOL (DM)**3
        V=1.3739D+02/DENS2
C PRESSURE IN MM HG
        P2=(R*T2/(V+B1))*760.0D0
        RETURN
```

```
        END
C
C-----------------------------------------------------------------
C
C
       SUBROUTINE CUBSPL(X,Y,N,A,B,C,S)
C  THIS SUBROUTINE COMPUTES THE MATRIX FOR FINDING THE COEFFICIENTS OF
C CUBIC SPLINE THROUGH A SET OF DATA.
      INTEGER N,NM1,NM2,I,J,FIRST,LAST
      REAL *8 X(N),Y(N),S(N),A(N),B(N),C(N),SMATRX(0:26,4)

     +     ,DX1,DY1,DX2,DY2,DXN1,DXN2
      REAL H(26)
C
C  COMPUTER FOR THE N-2 ROWS
C
      NM2=N-2
      NM1=N-1
      DX1=X(2)-X(1)
      DY1=(Y(2)-Y(1))/DX1*6.0D0
      DO 10 I=1,NM2
          DX2=X(I+2)-X(I+1)
          DY2=(Y(I+2)-Y(I+1))/DX2*6.0D0
          SMATRX(I,1)=DX1
         SMATRX(I,2)=2.0D0*(DX1+DX2)
          SMATRX(I,3)=DX2
          SMATRX(I,4)=DY2-DY1
          DX1=DX2
          DY1=DY2
 10     CONTINUE
        FIRST=2
        LAST=NM2
C   FOR END CONDITION=3
  80   DX1=X(2)-X(1)
       DX2=X(3)-X(2)
       SMATRX(1,2)=(DX1+DX2)*(DX1+2.0D0*DX2)/DX2
       SMATRX(1,3)=(DX2*DX2-DX1*DX1)/DX2
       DXN2=X(NM1)-X(NM2)
       DXN1=X(N)-X(NM1)
       SMATRX(NM2,1)=(DXN2*DXN2-DXN1*DXN1)/DXN2
       SMATRX(NM2,2)=(DXN1+DXN2)*(DXN1+2.0D0*DXN2)/DXN2
C
C     PRINT OUT TRIDIAGONAL MATRIX IN COMPACT FORM
C
C      DO 11 I = FIRST-1,LAST
C II    PRINT*,(SMATRX(I,J),J=1,4)

C NOW SOLVE THE TRIDIAGONAL SYSTEM.
       DO 110 I= FIRST,LAST
         SMATRX(I,1)=SMATRX(I,1)/SMATRX(I-1,2)
        SMATRX(I,2)=SMATRX(I,2)-SMATRX(I,1)*SMATRX(I-1,3)
         SMATRX(I,4)=SMATRX(I,4)-SMATRX(I,1)*SMATRX(I-1,4)
 110   CONTINUE
C
C-----------------------------------------------------------------
C
```

```
C NOW WE BACT SUBSTITUTE
      SMATRX(LAST,4)=SMATRX(LAST,4)/SMATRX(LAST,2)
      DO 120 J=LAST-1,FIRST-1,-1
        SMATRX(J,4)=(SMATRX(J,4)-SMATRX(J,3)*SMATRX(J+1,4))
     +       /SMATRX(J,2)
120   CONTINUE
C
C NOW PUT THE VALUES INTO THE S VECTOR
C
      DO 130 I=FIRST-1,LAST
         S(I+1)=SMATRX(I,4)
 130  CONTINUE
C
C-----------------------------------------------


c GET S(1) AND S(N) ACCORDING TO END CONDITIONS
      S(1)=((DX1+DX2)*S(2)-DX1*S(3))/DX2
      S(N)=((DXN2+DXN1)*S(NM1)-DXN1*S(NM2))/DXN2
C
C WRITE OUT COEFFICIENTS OF THE POLYNOMIALS
C
C     PRINT 99
C99   FORMAT(/T2,60('*')//T10,'THE CUBIC POLYNOMIALS, G(X)'
C    +,'DEFINED ON THE INTERVALS',//)
C     PRINT 101
     DO 200 I=1,N-1
        H(I)=X(I+1)-X(I)
        A(I)=(S(I+1)-S(I))/(6.0D0*H(I))
        B(I)=S(I)/2.0D0

       C(I)=((Y(I+1)-Y(I))/H(I))-((2.0D0*H(I)*S(I)+H(I)*S(I+1))/6.0D0)
C
C     PRINT 102,I,A(I),B(I),C(I),Y(I)
C101  FORMAT(T5,'I',T17,'I',T27,'B',T37,'C',T47,'D'/)
C102  FORMAT(T5,I1,T12,F8.4,T22,F8.4,T32,F8.4,T42,F8.4)
 200  CONTINUE
      RETURN
      END
C
C

      REAL FUNCTION SEVAL(N,U,X,Y,A,B,C)
      INTEGER N
      REAL*8 U,X(N),Y(N),B(N),C(N),A(N)
C
c THIS SUBROUTINE EVALUATE THE CUBIC SPLINE FUNCTION
C SEVAL=Y(I)+C(I)*(U-X(I))+B(I)*(U-X(I)**2+A(I)*(U-X(I))**3
C
      INTEGER I,J,K
      REAL*8 DX
      SAVE I
      DATA I/1/
      IF (I.GE.N) THEN
         I=1
      END IF
```

```
      IF (U.GE.X(N)) THEN
        DX=U-X(N-1)
         SEVAL=Y(N-1)+DX*(C(N-1)+DX*(B(N-1)+DX*A(N-1)))
         RETURN
      ENDIF
      IF(U.GE.X(I)) THEN
        IF(U .LE. X(I+1)) THEN
           DX=U-X(I)
           SEVAL=Y(I)+DX*(C(I)+DX*(B(I)+DX*A(I)))
         RETURN
        END IF
      ENDIF
      I=1
      J=N+1
 10   K=(I+J)/2
C     WRITE(8,*)K
      IF(U .LT. X(K)) THEN
         J=K
    ELSE
         I=K
    END IF
      IF (J .GT. I+1) THEN
         GOTO 10
      ELSE
C
C     EVALUATE SPLINE
C
          DX=U-X(I)
           SEVAL=Y(I)+DX*(C(I)+DX*(B(I)+DX*A(I)))
           RETURN
      END IF
C     END
       RETURN
       END
```

Appendix 8. **Computer Code: EQCALCU FORTRAN**

```
C     CLUSTER DISTRIBUTION CALCULATION


      DOUBLE PRECISION X2,XC,YNS,Y1,Y2,Y21,DH,T,CS,S,T0K,
     1  YD(5),YDE(5),YDN(5),YEN(5),YNN(5),YON(5),GN(4), FN(5),YOEN(5),
     1 PV0,VL0,HL,HG,H10,SL0,SG0,PVA,VL,VG,H1,SL,SG,T0,T1,GG(5),FF(5),
     1 DEG,EVB,TA(16),GE(16)
      INTEGER K1,M,K,N,NA
      COMMON /TPP/TA,GE/TPPN/NA
      EXTERNAL YZERO ,THERMO,SOLV,DISTR,BIGS,SPLFIT
C     S=(PRESSURE OF GAS)/(VAPER PRESSURE)
      S=0.777200D-00
C      M IS THE SIZE OF THE LARGEST CLUSTER
      M=5
C WRITE TITLE OF OUTPUT
      WRITE(9,998)
      WRITE(9,996)   S
      WRITE(11,997)
      WRITE(11,996) S
 998 FORMAT(4X,'TEMP',4X,'G(2)',10X,'G(3)',10X,'G(4)',10X,'G(5)',10X,
     &       'S')
 997 FORMAT(4X,'TEMP',4X,'F(1)',10X,'F(2)',10X,'F(3)',10X,'F(4)',10X,
     &       'F(5)')
 996 FORMAT(D14.4, ' IS THE SUPERCSATURATION' )
C READ THE TEMPERATURE, DEGENERACY AND VIBRATIONAL ENERGY AND SPLINE C
C  FIT
      NA= 16
      READ(2,*)
      DO 12 I=1,NA
12    READ(2,*  ) TA(I), GE(I)
       CALL SPLFIT
C  READ THE THERMODYNAMIC DATA.
      READ(5,*)
      READ(5,*)
      READ(5,*)
      READ(5,999) K1
      READ(5,888)  T0,PV0,VL0,VG,HL,HG,H10,SL0,SG0

CALCULATE THE EQUALIBRIUM DISTRIBUTION FOR INITIAL TEMPERATURE
      CALL YZERO(M,T0,PV0,VL0,H10,SL0,SG0,S,YON,YOEN,YNN,GG,FF,CS)
      T0K=T0+273.15D00
      WRITE(9,103)T0K,(GG(I),I=2,5),CS
      WRITE(11,105)T0K,FF
C     T1=DBLE(K1)
C     WRITE(4,*) T1
      WRITE(8,102)T0K,YON,YOEN
C CALCULATE THE DISTRIBUTION AT HIGHER TEMPERATURES
      dO 10 K=1,K1
C     WRITE(4,*) K
      READ(5,888)  T1,PVA,VL,VG,HL,HG,H1,SL,SG
C     WRITE(4,*)  T1,PVA,VL,VG,HL,HG,H1,SL,SG
C     GIVE ENTHALPY(H1) AND ENTROPY(S1) IN J/G AND TEMPERATURE(T) IN C
C     dC     N=2 IS SIZE OF DIMER
```

```
            N=2
            YNS=YNN(2)
            CALL THERMO(N,T1,T0,PVA,VL,H1,H10,SL,SG,S,YNS,XC,DH)
            X2=XC
      C     WRITE(4,*)X2
      C SOLVE TWO POLYNOMIAL EQUATIONS
            CALL SOLV(M,T1,T0,PVA,VL,H1,H10,SL,SG,S, YNN,X2,Y1,Y2,Y21)
     CALCULATE THE CLUSTER DISTRIBUTION
           CALL DISTR(T1,T0,M,S,YNN,H1,H10,SL,SG,PVA,VL,Y1,
          & Y2,X2,YD,YDE,YDN,YEN,FN)
           T=T1+273.15D00

CALCULATION THE FUNCTION GN CS
      CALL BIGS(YON,YOEN,YDN,YEN,GN,CS)
C WRITE OUTPUT
      WRITE(3,100)T,YDN
      WRITE(7,101)T,YEN
      WRITE(9,103)T,GN,CS
      WRITE(10,104)Y1,Y2,Y21
      WRITE(11,105)T,FN
  10  CONTINUE
 100 FORMAT(F8.2,5E15.7)
 101 FORMAT(F8.2,5E15.7)
 102 FORMAT(F8.2,5E23.15/5E23.15)
 103 FORMAT(F8.2,5E23.15)
 104 FORMAT(3E19.9)
 105 FORMAT(F8.2,5E23.15)
 888 FORMAT(D13.4,8D14.5)
 999 FORMAT(I2)
C     WRITE(4,105)YDE
 106  FORMAT(5E17.7)
     STOP
     END
C---------------------------------------
     SUBROUTINE YZERO(M,T1,PVA,V,H1,SL,SG,S,YON,YOEN,YNN,GG,FF,CS)
       COMMON /TPP/TA,GE,/TPPFIT/A,B,C,/TPPN/NA
       INTEGER NDEG,M,N,I,J,K,L,NA
       DOUBLE PRECISION YO(5),YNN(5),YOE(5),FN(5),YON(5),YOEN(5),A0(5),
     +      X,S,ENO,DH,E1,R,T,T1,YT,YOT,YOET,EN,PVA,V,H1,SL,SG,AA(6),F
      +       ,GG(5),FF(5),CS,Q,YOP,SEVAL, TA,GE,A,B,C,DEG,EVB
C     +       ,B(14),C(14),A1(14),B1(14),C1(14),DEG,EVB
      DIMENSION TA(16),GE(16)  ,A(16),B(16)  ,C(16)
      PARAMETER(NDEG=5)
       EXTERNAL DZPORC,THERM
      COMPLEX*16  Z(5)
       N=M+1
       R=8.314D0
       T=T1+273.15D0
C AA(I) IS THE COEFICIENTS OF THE POLYNOMIAL
       AA(1)=-1.0D0
       A0(1)=1.0D0
       DO 10 I=2,M
       CALL THERM(I,T1,PVA,V,H1,SL,SG,S,X,DH)
       A0(I)=A0(I-1)/X
C      WRITE(8,*)X,A0(I)
  10  CONTINUE
```

```
      DO 30 J=2,6
      AA(J)=A0(J-1)
   30 CONTINUE
C SOLVE THE POLYNOMIAL
      CALL DZPORC(NDEG,AA,Z)
      DEG=SEVAL(NA,T,TA,GE,A,B,C)
C       EVB=SEVAL(NA,T,TA,E,A1,B1,C1)
      EVB=9.0D0*8.314D0*T
      Q=1.0D0/(1.0D0+DEG*DEXP(-EVB/(R*T)))
      YOP=REAL(Z(1))
c      YO(1)=YOP*Q
      YO(1)=YOP*DEG
C     CALCULATION OF EXCITED MONOMER
C      EXCITED MONOMER
     YOE(1)=YOP-YO(1)
C      YOE(1)=YOP*DEG*DEXP(-EVB/(R*T))/Q
C      E1=-4560.181846D0+26.078275D0*T+0.033411D0*T**2.0D0
C      FN(1)=DEXP(-E1/(R*T))
C      YOE(1)=YO(1)*FN(1)
C YOET IS THE TOTAL MOLES OF EXCITED CLUSTER; YOT UNEXCITED CLUSTER.
       YOET=YOE(1)
        YOT=YO(1)
  C      EXCITED CLUSTER DISTRIBUTION (DIMER TO M-MER )
       DO 20 K=2,5
       YO(K)=A0(K)*YO(1)**(K)
       YOT=YOT+YO(K)
       CALL THERM(K,T1,PVA,V,H1,SL,SG,S,X,DH)
       ENO=DH/(R*T)
       EN=ENO+(3.0D0/2.0D0)
       FN(K)=DEXP(-EN)
       YOE(K)=YO(K)*FN(K)
       YOET=YOET+YOE(K)
    20 CONTINUE
       YT=YOET+YOT
 C NORMALIZATION
       DO 50 L=1,5
       YON(L)=YO(L)/YT
       YOEN(L)=YOE(L)/YT
    50 CONTINUE
       YNN(1)=(YON(1)+YOEN(1))*1.0D0
       DO 60 N=2,5
       F=DBLE(N)
       YNN(N)=YNN(N-1)+F*(YON(N)+YOEN(N))
   60  CONTINUE
       DO 88 I=1,5
       FF(I)=YOEN(I)/YON(I)
   88  CONTINUE
       GG(1)=0.0D0
       DO 89 I=2,5
       GG(I)=YOEN(I)/YOEN(I-1)
   89  CONTINUE
       CS=1.0D0
       RETURN
       END
```

```
C  ------------------------------------------------
      SUBROUTINE THERM(N, T1, PVA,V, H1,SL,SG,S,X,DH)
C     COMMON /TPP/TA,GE,E,/TPPFIT/A,B,C,A1,B1,C1,/NUM/NA
      INTEGER N,N1,NA
      DOUBLE PRECISION T1,PVA,V,H1,SL,SG,S,X,DH,R,EP,WM,TB,T,PV,P,
     &  VOL,H0,S0,PARA,DS,DG,DNS,DG1,DH1,DN,HE1,HUE,HUE0
C     & TA(14),GE(14),A(14),B(14),C(14),EVB,SEVAL
       R=8.314D00
       EP=R*399.0D0
       WM=137.39D-3
       TB=296.85D00
       T=273.15D0+T1
       PV =PVA*1.0D05
       P=PV
       VOL=V*WM*1.0D-03
       H0=H1*WM*1.0D03
       S0=(SG-SL)*WM*1.0D03
C PARA= a**4; a=eta/r0
       PARA=2.45D0**4
       EVB=SEVAL(NA,T,TA,E,A1,B1,C1)
       EVB=9.0D0*R*T
C HE1 IS THE ENTHALPY OF EXCITED MONOMER
       HE1=DBLE(4)*R*T+(EP/2.0D0)*(PARA**(3.0/4.0)-1.0D0)+EVB
C      PARA=(2.0D0*(H0+P*VOL-R*T)/EP+1.0D0)**(4.0D0/3.0D0)
       IF (N .LE. 2)THEN
C THE FOLLOWING HUE IS THE ENTHALPY OF DIMER.
       HUE=(12.0D0*DBLE(N)-2.0D0)*R*T+(EP/64.0D0)*(18.0D0*DBLE(N)**(
     &     2.0D0/3.0D0)-PARA**(1.0D0/2.0D0))*PARA
       DH=2.0D0*HE1-HUE
C      WRITE(4,*)HE1,HUE,DH,2
       DS=S0+R*5.0D0*DLOG(0.5D0)-R*DLOG(S)
       DG=P*VOL+3.0D0*R*T+(EP/2.0D0)*(PARA**(3.0/4.0)-1.0D0)
     &-(EP/64.D0)*PARA*(18.D0*2.0D0**(2.0D0/3.0D0)-PARA**(0.5D0))
     &-R*T*5.0D0*DLOG(0.5D0)-R*T*DLOG(PVA*0.986842D00)
       ELSE
       N1=N-1
      DN=DBLE(N)**(2.0D0/3.0D0)-DBLE(N1)**(2.0D0/3.0D0)
C HUE IS THE SAME AS THE H(N) IN THE MODE2 FORTRAN
C HUE0 IS THE ENTHALPY OF An-1 ; HUE is the enthalpy of n-mer.
      HUE0=(12.0D0*DBLE(N1)-2.0D0)*R*T+(EP/64.0D0)*(18.0D0*DBLE(N1)**
     &    (2.0D0/3.0D0)-PARA**(1.0D0/2.0D0))*PARA
     HUE=(12.0D0*DBLE(N)-2.0D0)*R*T+(EP/64.0D0)*(18.0D0*DBLE(N)**(
     &     2.0D0/3.0D0)-PARA**(1.0D0/2.0D0))*PARA
C DH is the enthalpy change for process An = An-1 + A*
      DH=HUE0+HE1-HUE
      WRITE(4,*)HUE0,HUE,DH, N
      DNS=(DBLE(N1)/DBLE(N))**(3+N)
      DS=S0+R*DLOG(DNS)-R*DLOG(S)
      DG=P*VOL-R*T*DLOG(PVA*0.986842105D00)-9.0D0/32.D0*EP*PARA*DN
     & -R*T*DLOG(DNS)
      END IF
      DG1=(DG/(R*T))
      DH1=(1.0D0/T-1.0D0/TB)*H0/R
      X=(DEXP(-DG1))/(S*DEXP(-DH1))
      WRITE(4,*)X
      RETURN
```

```
      END
C

      SUBROUTINE SOLV(M,T1,T0,PVA,V,H1,H10,SL,SG,S,YNN,
     &    X2,Y1,Y2,Y21 )
      INTEGER NDEG1,NDEG2,I,L,J
      PARAMETER(NDEG1=4)
      PARAMETER(NDEG2=5)
      DOUBLE PRECISION T1,PVA,V,H1,SL,SG,S,X2,Y1,Y2,Y21,
     & YNS,X,DH,YNN(5),A(5),B(5),T0,H10,B1(6),Z

C     REAL A1(5),B1(6)
      COMPLEX*16  ZA(4) ,ZB(5)
      EXTERNAL THERMO,DZPORC
      Y1=0.200D00
      Z=0.2D00
25    IF (ABS(Z) .LT. 0.5D-07) GO TO 20
      A(1)=Y1-1.0D00
      B1(1)=(-Y1**2.0D00)
      B(1)=X2*Y1
      B(2)=X2*2.0D00
      WRITE(4,*) X2,B(1),B(2)
      A(2)=1.0D00
      DO 10 I=3,M
      YNS=YNN(I)
      CALL THERMO(I,T1,T0,PVA,V,H1,H10,SL,SG,S,YNS,X,DH)
      A(I)=A(I-1)*X2/(Y1*X)
 10   CONTINUE
      DO 40 J=3,M
      YNS=YNN(J)
      CALL THERMO(J,T1,T0,PVA,V,H1,H10,SL,SG,S,YNS,X,DH)
      B(J)=DBLE(J)*B(J-1)*X2/(Y1*X*DBLE(J-1))
 40   CONTINUE
      DO 50 L=1,M
      B1(L+1)=B(L)
 50   CONTINUE
      CALL DZPORC (NDEG1,A,ZA)
      CALL DZPORC (NDEG2,B1,ZB)
      WRITE(4,*)ZA
      Y2=REAL(ZA(1))
      Y21=REAL(ZB(1))
      Z=Y21-Y2
      IF( Z  .EQ. 0.0D-0) GO TO 21
      IF (Z .LT. 0.0D-0 .AND. Z .GE. -2.0D-5) THEN
      Y1=Y1+0.01D-5
      ELSE  IF (Z .LT. -2.0D-5 .AND. Z .GT. -2.0D-3) THEN
      Y1=Y1+0.01D-2
      ELSE IF (Z .LE. -2.0D-3) THEN
      Y1=Y1+0.1D00
      ELSE IF (Z .GT. 0.0D-0 .AND. Z .LE. +2.0D-5) THEN
      Y1=Y1-0.01D-6
      ELSE IF (Z .GT. 2.0D-5 .AND. Z .LE. +2.0D-3) THEN
      Y1=Y1-0.01D-4
      ELSE
      Y1=Y1-0.01D-1
```

```
        END IF
      WRITE(4,100)Y1,Z,Y21,Y2
      GO TO 25
100   FORMAT(4E13.4)
 20   CONTINUE
 21   RETURN
      END

C


C SUBPROGRAM FOR CALCULATION OF THERMODYNAMIC PRAMETER.
      SUBROUTINE THERMO(N, T1,T0, PVA,V, H1,H10,SL,SG,S,YNS,X,DH)
C      COMMON /TPP/TA,GE,E,/TPPFIT/A,B,C,A1,B1,C1,/NUM/NA
      DOUBLE PRECISION T1,PVA,V,H1,SL,SG,S,YNS,X,DH,R,EP,WM,TB,T,PV,P,
     &0,S0,PARA,DS,DG,DN,DNS,DG1,DH1,PEP0,T0,H10,VOL,T0K,H0V,HE1,HUE,
     &  HUE0
     & TA(14),GE(14),E(14),A(14),B(14),C(14),A1(14),B1(14),C1(14),EVB,
      INTEGER N,N1
      R=8.314D00
      EP=R*399.0D0
      WM=137.39D-3
      TB=296.85D00
      T0K=T0+273.15D0
      T=273.15D0+T1
      PV=PVA*1.0D05
      P=PV
      VOL=V*WM*1.0D-03
      H0=H1*WM*1.0D03
      H0V=H10*WM*1.0D03
      S0=(SG-SL)*WM*1.0D03
C     PARA= a**4; a=eta/r0
      PARA=2.45D0**4
      PARA=(2.0D0*(H0+P*VOL-R*T)/EP+1.0D0)**(4.0D0/3.0D0)
      EVB=9.0D0*R*T
c     EVB=SEVAL(NA,T,TA,E,A1,B1,C1)
      HE1=DBLE(4)*R*T+(EP/2.0D0)*(PARA**(3.0/4.0)-1.0D0)+EVB
      IF (N .LE. 2)THEN
      HUE=(12.0D0*DBLE(N)-2.0D0)*R*T+(EP/64.0D0)*(18.0D0*DBLE(N)**(
     &     2.0D0/3.0D0)-PARA**(1.0D0/2.0D0))*PARA
      DH=2.0D0*HE1-HUE
C     WRITE(4,*)HUE,DH,2
      DH=2.D0*(H0+P*VOL+R*T)-EP*PARA*(28.6D0-PARA**0.5D0)/6.4D01
      DS=S0+R*5.0D0*DLOG(0.5D0)-R*DLOG(S)
      DG=P*VOL+3.0D0*R*T+(EP/2.0D0)*(PARA**(3.0/4.0)-1.0D0)
     &-(EP/64.D0)*PARA*(18.D0*2.0D0**(2.0D0/3.0D0)-PARA**(0.5D0))
     &-R*T*5.0D0*DLOG(0.5D0)-R*T*DLOG(PVA*0.9868421D00)
        ELSE
        N1=N-1
        DN=DBLE(N)**(2.0D0/3.0D0)-DBLE(N1)**(2.0D0/3.0D0)
C HUE IS THE SAME AS THE H(N) IN THE MODE2 FORTRAN
      HUE0=(12.0D0*DBLE(N1)-2.0D0)*R*T+(EP/64.0D0)*(18.0D0*DBLE(N1)**
     &     (2.0D0/3.0D0)-PARA**(1.0D0/2.0D0))*PARA
      HUE=(12.0D0*DBLE(N)-2.0D0)*R*T+(EP/64.0D0)*(18.0D0*DBLE(N)**(
     &     2.0D0/3.0D0)-PARA**(1.0D0/2.0D0))*PARA
C
```

```
      DH=HUE0+HE1-HUE

C     WRITE(4,*)HUE0,HUE,DH, N,T
C     DH=H0+P*VOL-9.0D0*EP*PARA*DN/32.0D0
      DNS=(DBLE(N1)/DBLE(N))**(3+N)
      DS=S0+R*DLOG(DNS)-R*DLOG(S)
C     WRITE(4,*)DS
      DG=P*VOL-R*T*DLOG(PVA*0.9868421D00)-9.D0/32.D0*EP*PARA*DN
     & -R*T*DLOG(DNS)
      END IF
      DG1=(DG/(R*T))
      DH1=(1.0D0/T0K-1.0D0/TB)*H0V/R
C PEP0 IS FUNCTION OF THE INITIAL TEMPERATURE.FOLLOWING IS OBTAINED
C AT INITIAL TEMPERATURE 291.15 K
      IF (T .LE. 380.D00) THEN

     PEP0=90.20147742D0-0.84463205D0*T+2.54203D-3*T**2-2.38109D-6*T**3
     ELSE
     PEP0=-73.81008027+0.43332065*T-7.7612D-04*T**2+4.8985D-07*T**3
C     PEP0=-42.77992225D0+0.277140080D0*T-0.007674900D0*T**1.5
     END IF

C DH1=0.82045D0 IS CALCULATED FROM DATA AT INITIAL T=291.15

C     X=(DEXP(-DG1))/(PEP0*YNS*S*0.82045D0)
      X=(DEXP(-DG1))/(PEP0*YNS*S*DEXP(-DH1))
C     WRITE(4,*)X
      RETURN
      END


C


      SUBROUTINE DISTR(T1,T0,M,S,YNN,H1,H10,SL,SG,PVA,V,
     &  Y1,Y2,X2,YD,YDE,YDN,YEN,FN)
      COMMON /TPP/TA,GE,/TPPFIT/A,B,C,/TPPN/NA
      INTEGER M,I,K ,N,NA
      DOUBLE PRECISION T1,S,H1,SL,SG,PVA,V,Y1,Y2,X2,YD,YDE,YDN,YEN,
     & SEVAL,FN,YNN,R,T,YDT,Y,E1,YDET,EN0,EN,YNORM,YNS ,DH,T0,H10,X,
     +    Q,TA,GE,A,B,C,DEG
      DIMENSION YD(M),YDE(M),YDN(M),YEN(M),FN(M),YNN(M),TA(16),GE(16)
      DIMENSION A(16),B(16),C(16)
      EXTERNAL THERMO
C     WRITE(4,*)M
      R=8.314D00
      T=273.15D0+T1
      DEG=SEVAL(NA,T,TA,GE,A,B,C)
      EVB=SEVAL(NA,T,TA,E,A1,B1,C1)
      EVB=9.0D0*R*T
C     Q=1.0D0/(1.0D0+DEG*DEXP(-EVB/(R*T)))
C     YD(1)=Y1*Q
      YD(1)=Y1*DEG
      YD(2)=Y2
      YDT=YD(1)+YD(2)
C     THE CLUSTER DISTRIBUTION (3-MER,4-MER...)
```

```
      DO 10 I=3,M
      YNS=YNN(I)
      CALL THERMO(I,T1,T0,PVA,V,H1,H10,SL,SG,S,YNS,X,DH)
      Y=YD(2)*YD(I-1)*X2
      YD(I)=Y/(YD(1)*X)
      YDT=YDT+YD(I)
 10   CONTINUE
C     EXCITED MONOMER
C     E1=-4560.181846D0+26.078275D0*T+0.033411D0*T**2.0D0
C     FN(1)=DEXP(-E1/(R*T))
      YDE(1)=Y1-YD(1)
      YDET=YDE(1)
C     EXCITED CLUSTER DISTRIBUTION (DIMER TO M-MER )
      DO 20 K=2,M
      YNS=YNN(K)
      CALL THERMO(K,T1,T0,PVA,V,H1,H10,SL,SG,S,YNS,X,DH)
      EN0=DH/(R*T)
      EN=EN0+(3.0D00/2.0D00)
      FN(K)=DEXP(-EN)
      YDE(K)=YD(K)*FN(K)
      YDET=YDET+YDE(K)
  20  CONTINUE
C     NORMALIZATION
      YNORM=YDT+YDET
      DO 40 N=1,M
      YDN(N)=YD(N)/YNORM
      YEN(N)=YDE(N)/YNORM
      FN(N)=YEN(N)/YDN(N)
  40  CONTINUE
      RETURN
      END


C


C CS={(X1*)t=0}/{(X1*)eq.}
      SUBROUTINE BIGS(YON,YOE,YDN,YEN,GN,CS)
       INTEGER I
      DOUBLE PRECISION YON(5),YDN(5),GN(4),SUM0,SUME,CS,YEN(5),YOE(5)
     &                 ,SUM02,SUME2
      DO 80 I=1,4
        GN(I)=YEN(I+1)/YEN(I)
  80  CONTINUE

      SUM0=YON(1)+2.0D0*YON(2)+3.0D0*YON(3)+4.0D0*YON(4)+5.0D0*YON(5)
      SUM02=YOE(1)+2.0D0*YOE(2)+3.0D0*YOE(3)+4.0D0*YOE(4)
     &      +5.0D0*YOE(5)
      SUME=YDN(1)+2.0D0*YDN(2)+3.0D0*YDN(3)+4.0D0*YDN(4)+5.0D0*YDN(5)
        SUME2=YEN(1)+2.0D0*YEN(2)+3.0D0*YEN(3)
     & +4.0D0*YEN(4)+5.0D0*YEN(5)
       CS=(YOE(1)/YEN(1))*((SUME+SUME2)/(SUM0+SUM02))
      RETURN
       END
```

```
C

C

C-----------------------------------------------------------------
C
C
      SUBROUTINE CUBSPL(X,Y,N,A,B,C,S)
C  THIS SUBROUTINE COMPUTES THE MATRIX FOR FINDING THE COEFFICIENTS OF
C CUBIC SPLINE THROUGH A SET OF DATA.
      INTEGER N,NM1,NM2,I,J,FIRST,LAST
      REAL *8 X(N),Y(N),S(N),A(N),B(N),C(N),SMATRX(0:26,4)

     +     ,DX1,DY1,DX2,DY2,DXN1,DXN2
      REAL H(26)
C
C  COMPUTER FOR THE N-2 ROWS
C
      NM2=N-2
      NM1=N-1
      DX1=X(2)-X(1)
      DY1=(Y(2)-Y(1))/DX1*6.0D0
      DO 10 I=1,NM2
          DX2=X(I+2)-X(I+1)
          DY2=(Y(I+2)-Y(I+1))/DX2*6.0D0
          SMATRX(I,1)=DX1
         SMATRX(I,2)=2.0D0*(DX1+DX2)
          SMATRX(I,3)=DX2
          SMATRX(I,4)=DY2-DY1
          DX1=DX2
          DY1=DY2
 10     CONTINUE
        FIRST=2
        LAST=NM2
C   FOR END CONDITION=3
  80   DX1=X(2)-X(1)
       DX2=X(3)-X(2)
       SMATRX(1,2)=(DX1+DX2)*(DX1+2.0D0*DX2)/DX2
       SMATRX(1,3)=(DX2*DX2-DX1*DX1)/DX2
       DXN2=X(NM1)-X(NM2)
       DXN1=X(N)-X(NM1)
       SMATRX(NM2,1)=(DXN2*DXN2-DXN1*DXN1)/DXN2
       SMATRX(NM2,2)=(DXN1+DXN2)*(DXN1+2.0D0*DXN2)/DXN2
C
C     PRINT OUT TRIDIAGONAL MATRIX IN COMPACT FORM
C
C      DO 11 I = FIRST-1,LAST
C II    PRINT*,(SMATRX(I,J),J=1,4)

C NOW SOLVE THE TRIDIAGONAL SYSTEM.
       DO 110 I= FIRST,LAST
         SMATRX(I,1)=SMATRX(I,1)/SMATRX(I-1,2)
        SMATRX(I,2)=SMATRX(I,2)-SMATRX(I,1)*SMATRX(I-1,3)
```

```
        SMATRX(I,4)=SMATRX(I,4)-SMATRX(I,1)*SMATRX(I-1,4)
 110  CONTINUE
C
C-------------------------------------------------------------
C
C NOW WE BACT SUBSTITUTE
      SMATRX(LAST,4)=SMATRX(LAST,4)/SMATRX(LAST,2)
      DO 120 J=LAST-1,FIRST-1,-1
        SMATRX(J,4)=(SMATRX(J,4)-SMATRX(J,3)*SMATRX(J+1,4))
     +       /SMATRX(J,2)
120  CONTINUE
C
C NOW PUT THE VALUES INTO THE S VECTOR
C
      DO 130 I=FIRST-1,LAST
         S(I+1)=SMATRX(I,4)
 130  CONTINUE
C
C-----------------------------------------------


c GET S(1) AND S(N) ACCORDING TO END CONDITIONS
      S(1)=((DX1+DX2)*S(2)-DX1*S(3))/DX2
      S(N)=((DXN2+DXN1)*S(NM1)-DXN1*S(NM2))/DXN2
C
C WRITE OUT COEFFICIENTS OF THE POLYNOMIALS
C
C      PRINT 99
C99    FORMAT(/T2,60('*')//T10,'THE CUBIC POLYNOMIALS, G(X)'
C     +,'DEFINED ON THE INTERVALS',//)
C      PRINT 101
      DO 200 I=1,N-1
         H(I)=X(I+1)-X(I)
         A(I)=(S(I+1)-S(I))/(6.0D0*H(I))
         B(I)=S(I)/2.0D0

        C(I)=((Y(I+1)-Y(I))/H(I))-((2.0D0*H(I)*S(I)+H(I)*S(I+1))/6.0D0)
C
C      PRINT 102,I,A(I),B(I),C(I),Y(I)
C101   FORMAT(T5,'I',T17,'I',T27,'B',T37,'C',T47,'D'/)
C102   FORMAT(T5,I1,T12,F8.4,T22,F8.4,T32,F8.4,T42,F8.4)
 200  CONTINUE
      RETURN
      END
C
C


      REAL FUNCTION SEVAL(N,U,X,Y,A,B,C)
      INTEGER N
      REAL*8 U,X(N),Y(N),B(N),C(N),A(N)
C
c THIS SUBROUTINE EVALUATE THE CUBIC SPLINE FUNCTION
C SEVAL=Y(I)+C(I)*(U-X(I))+B(I)*(U-X(I)**2+A(I)*(U-X(I))**3
C
      INTEGER I,J,K
      REAL*8 DX
```

```
      SAVE I
      DATA I/1/
      IF (I.GE.N) THEN
         I=1
      END IF
      IF (U.GE.X(N)) THEN
        DX=U-X(N-1)
         SEVAL=Y(N-1)+DX*(C(N-1)+DX*(B(N-1)+DX*A(N-1)))
         RETURN
      ENDIF
      IF(U.GE.X(I)) THEN
        IF(U .LE. X(I+1)) THEN
           DX=U-X(I)
           SEVAL=Y(I)+DX*(C(I)+DX*(B(I)+DX*A(I)))
         RETURN
        END IF
      ENDIF
      I=1
      J=N+1
 10   K=(I+J)/2
C     WRITE(8,*)K
      IF(U .LT. X(K)) THEN
         J=K

     ELSE
         I=K
    END IF
      IF (J .GT. I+1) THEN
         GOTO 10
      ELSE
C
C     EVALUATE SPLINE
C
          DX=U-X(I)
           SEVAL=Y(I)+DX*(C(I)+DX*(B(I)+DX*A(I)))
           RETURN
      END IF
C     END
       RETURN
       END
```

Appendix 9. Computer code: INTEGRAL FORTRAN

```
C THIS IS MODIFIED ODE1 FORTRAN. dT/dt' is included as YPRIME(12).
      INTEGER   NEQ, NPARAM
      PARAMETER (NEQ=12, NPARAM=50)
C
      INTEGER  IDO,IEND,IMETH,INORM,IATYPE,MTYPE,MXSTEP
     1       , N,I,NO,MITER,NLIMIT,MAXORD ,NA
      REAL  *8  A(1,1),PARAM(NPARAM),TOL,X,XEND,Y(NEQ),HMAX,
     &          A1,B,Y10,SAT,T,TYPRIM,DLCT,T0(30),Z0,Y12,KS(5),
     &          KF(5) ,  ZND,ZZ,YT,HINT,TINI,KS1E,KS2E,E1S,E2S
     &    ,TIME  ,G5(30),G2(30),G3(30),G4(30),BS(30),F1(30),F2(30),
     &     K2F,  F3(30),F4(30),F5(30) ,TH(30),HV(30),PVA(30),VL(30)
     &    ,CINI  ,VG,HL,HG,SL,SG,S0(30),HTRIAL,WM,SATT,YDOT(12),
     &    PPOST,  ENERG,THH(5),HE(5) ,TA(16),GE(16) ,TOLR,BETA,SIG
        CHARACTER*14 CHECK   /  ' I COME HERE '/
C
C TH IS TEMPERATURE; HV IS THE ENTHALPY OF EVAPORATION DATA
C AT CORRESPONDING T IN J/MOL; NO IS DIMENTION OF ARRAY
C
      COMMON /ENTHA/TH,HV,PVA,VL,NO
C Z0 IS INITIAL MOLE FRACTION OF argon.
      COMMON /MIX/Z0,BETA
C
C T0 IS TEMPERATURE DATA;G2(N),...G5(N) ARE G(2),G(3)... G(5) IN ODES;
C NIS THE ARRAY DIMMENSION OF G2(N),G3(N); F1(N),...ARE
F(1),F(2)...F(5)
C BS CORRESPONDS   TO S IN ODES
C
      COMMON /GNDATA/T0,G2,G3,G4,G5,BS,N
      COMMON /FNDATA/F1,F2,F3,F4,F5
C
C IS KS(1);D IS KS(2); E IS KF(2); TINI IS INITIAL TEMPERATURE
C A1 IS EXPONENTIAL PARAMETER OF KS(I) AT TINI; TE IS EQULIBRIUM TEMP.
C B IS EXPONENTIAL PARAMETER OF KF(I).
C
      COMMON  /AB/A1,B,/YS/Y10,/KK/KS,KF
C
C KS1E AND KS2E ARE KS(1) AND KS(2) AT EQUILIBRIUM TEMPERATURE;
C E1S AND E2S  ARE EXPONENTIAL PARAMETER FOR KS(1) AND KS(2)
C  AS FUNCTION OF TEMP.
C
       COMMON /KE/ KSIE,KS2E,E1S,E2S,Y12
       COMMON /HH/THH,HE
       COMMON /DEGNAC/TA,GE,/DEGN/NA
C
C    SAT IS SUPERSATURATION AND T IS TEMPERATURE
       EXTERNAL FCN,DIVPAG,SSET,UMACH,PARAFG,PARAKF,FCNJ,SPLFIT,YZERO
C  .             INITIALIZE
C  BS=S=(X1)T=0/(X1)EQ.
       HINT=1.0D-12
       MXSTEP=1000000000
        INORM=2
        MITER=2
C FOR Gear methad MAXORD= 5 IMETH=2 ; For Adams methad MAXORD=12
```

```
C IMETH=1

      MAXORD=4
      IMETH=2
      IATYPE=0
      MTYPE=0
      HMAX=0.0D-0
      HTRIAL=0.0D0
      CALL SSET(NPARAM,0.0,PARAM,1)
      PARAM(1)=HINT
      PARAM(3)=HMAX
      PARAM(4)=MXSTEP
      PARAM(6)=MAXORD
      PARAM(10)=INORM
      PARAM(12)=IMETH
      PARAM(13)=MITER
      PARAM(14)=MTYPE
C     PARAM(18)=EPSJ
      PARAM(31)=HTRIAL
      PARAM(19)=IATYPE
C
C     READ THE DATA IN
C
      NLIMIT=900
      TINI=293.3D0
      READ(5,*)SAT,Y(11),Y(12), PPOST
      READ(5,*)A1,B,TOLR,K2F
      READ(5,*)KS1E,KS2E,E1S,E2S
C     READ(5,*)(Y(I),I=1,5)
C     READ(5,*)(Y(I),I=6,10)
      NO=30
      N=30
      Z0=0.0D0
     BETA=1.0D-3
C Y12 , THE INITIAL VALUE OF Y(12), IS THE TEMPERATURE AT WHICH THE
C  INTEGRATION START. it is used in calculation of KF(i).
      Y12= Y(12)
      READ(3,*)
      READ(3,200) SATT
      IF (ABS(SATT-SAT) .GE. 1.0D-3) THEN
     WRITE(8,888)
888   FORMAT( 'CHECK THE SAT IN DATA FILE')
      END IF
      DO 8 I=1,N
8        READ(3,300)T0(I),G2(I),G3(I),G4(I),G5(I),BS(I)
     NA=16
     READ(1,*)
     DO 6 I=1,NA
6    READ(1,*)TA(I),GE(I)
     WM=137.39D-3
     READ(4,*)
     READ(4,*)
     READ(4,*)
C PVA IS VAPOR PRESSSURE IN Pa. Vl is mole volume in M**3/mol
C Hv is enthalpy of evaporation inj/mol;S0 evaporation entropy j/molK
      DO 12 I=1,30
```

```
          READ(4,400)TH(I),PVA(I),VL(I),VG,HL,HG,HV(I),SL,SG
             TH(I)=TH(I)+273.15D0
             PVA(I)=PVA(I)*1.0D05
             VL(I)=VL(I)*WM*1.0D-03
             HV(I)=HV(I)*WM*1.0D03
             S0(I)=(SG-SL)*WM*1.0D03
C       WRITE(8,*)I
  12    CONTINUE
        READ(2,*)
        READ(2,*)
        DO 9 I=1,N
   9      READ(2,300)T0(I),F1(I),F2(I),F3(I),F4(I),F5(I)
C INPTERPRETE THE F(I), G(I) ,S , EVIB AND THERMODYNAMIC DATA
        CALL SPLFIT
C CALCULATTHE INITIAL VALUES OF Y(I) I=1 .. 10
        CALL YZERO(TINI,PVA(1),VL(1),HV(1),S0(1),SAT,Y)
C Y10 is the mole fraction of excited monmer at initial condition, a
C  CONSTANT USED IN ODES.
        Y10=Y(6)
C CINI IS THE INITIAL CONCENTRATION OF EXCITED MONOMER IN MOL/LITER
C PPOST IS THE POST SHOCK PRESSURE.
        CINI=Y10*PPOST/(760.D0*0.082056826*Y12)
C       WRITE(8,152)Y
 152    FORMAT(5E14.5/5E14.5)
        IDO=1
  103   FORMAT(5D14.5)
C  X IS THE INITIAL TIME WHEN  INTEGRATION START.
        X  =0.0D0
        TOL=TOLR
100     FORMAT(4D12.4)
C                    WRITE TITLE
C       WRITE(6,800)A1,B,C,D
C       WRITE(6,801)C,D
C       WRITE(7,800)SAT,T,A1,B
C       WRITE(7,801)C,D
C       WRITE(4,800)SAT,T,A1,B
C       WRITE(4,801)C,D
C       CALL UMACH(2,NOUT)
C       WRITE (10,96)
C       WRITE (9,99)
C       WRITE (7,98)
C        WRITE(8,*)THH,HE
        ZND=-11.0D0
        XEND =0.0D0
C                     INTEGRATE ODE
      DO 10 IEND=1,7000
        IF (XEND .LE. 0.1D-3) THEN
          ZND=ZND+1.0D-2
         ZZ=DEXP(ZND)
        XEND=ZZ
    ELSE IF (XEND .LE. 5.0D0) THEN
      XEND=XEND*(1.0D0+0.035D0)
 ELSE
   C                WRITE(8 ,1) CHECK
                  XEND=XEND*(1.0D0+0.25D-0)
            END IF
```

```
C 10     CONTINUE
C        WRITE(8,*) XEND
         CALL DIVPAG(IDO,NEQ,FCN,FCNJ,A,X,XEND,TOL,PARAM,Y)
CALCULATION THE YPRIME AT POINT XEND.
          CALL FCN (NEQ,XEND,Y,YDOT)
C          WRITE(8,*) YDOT
C       WRITE(8,*) PARAM(31),PARAM(3)
C      TYPRIM=YDOT(1)+2.0D0*YDOT(2)+3.0D0*YDOT(3)+4.0D0*YDOT(4)+
C     &         5.0D0*YDOT(5)+1.0D0*YDOT(6) +2.0D0*YDOT(7)
C     &         +3.0D0*YDOT(8)+4.0D0*YDOT(9)+5.0D0*YDOT(10)
C          YT=Y(1)+Y(6)+2.0D0*(Y(2)+Y(7))+3.0D0*(Y(3)+Y(8))
     &        +4.0D0*(Y(4)+
C    &        Y(9))+5.0D0*(Y(5)+Y(10))
          YT1=Y(1)+Y(6)+(Y(2)+Y(7))+(Y(3)+Y(8))+(Y(4)+
     &        Y(9))+(Y(5)+Y(10))
          SIG=(-YDOT(12)/(Y(12)**2))*CINI*K2F
C TIME IS IN GAS TIME SCALE IN SECOND.
          TIME=X/(CINI*K2F)
C DLCT = YPRIME(11)
C          DLCT=(-TYPRIM*Y(11)/YT)
           WRITE(9,990) TIME,Y(1),Y(2),Y(3),Y(4),Y(5)
           WRITE(7,990) TIME,Y(6),Y(7),Y(8),Y(9),Y(10)
C          WRITE(11,999)X,PARAM(31),PARAM(33),PARAM(10)
C    &                  KF(5)
           WRITE(11,999)TIME,KS    , KF
           WRITE(10,997)TIME,YDOT(11),Y(11),YDOT(12)*CINI*K2F,Y(12),YT1
           WRITE(12,966)X,SIG,TIME
C
C
           ENERG=Y(1)*THH(1)+Y(2)*THH(2)+Y(3)*THH(3)
     +      +Y(4)*THH(4)+Y(5)*THH(5)+
C    +      Y(6)*HE(1)+Y(7)*HE(2)+Y(8)*HE(3)+Y(9)*HE(4)+Y(10)*HE(5)
C
       IF (TIME*1.0E6 .GT. 200.00) GOTO 666
  10   CONTINUE
C                  FINISH UP
       IDO=3
        CALL DIVPAG(IDO,NEQ,FCN,FCNJ,A,X,XEND,TOL,PARAM,Y)
C
 96    FORMAT(6X,'time',8X,'d(c/c0)/dt',8X,'c/c0',10X,'dT/dt',
     &          10X,'TEMPERATURE',3X,'sum of Y(i)')
 99
FORMAT(6X,'time',12X,'Y(1)',10X,'Y(2)',11X,'Y(3)',11X,'Y(4)',11X,
     &  'Y(5)')
 98
FORMAT(6X,'time',10X,'Y(1)*',10X,'Y(2)*',10X,'Y(3)*',10X,'Y(4)*'
     &       , 10X ,'Y(5)*')
   1     FORMAT (A20)
   999   FORMAT(D13.4,5D15.6/5D15.6)
   990   FORMAT(D13.4,5D15.6)
   997   FORMAT(D16.6,5D16.6)
   800   FORMAT('SUPERSATURATION = ',F5.1,5X,'TEMPERATURE = ',F7.2,1X,
     & 'K',3X,   'A = ',E13.4,3X,'B = ',E13.4)
   801   FORMAT('KS(1) = ',E13.4,4X,' KS(2) = ',E13.4)
   300    FORMAT(F8.2,5E23.15)
   400    FORMAT(D13.4,8D14.5)
```

```
  500    FORMAT(10E13.4)
  200    FORMAT(D14.4)
  966    FORMAT(3D14.4)
  666    STOP
         END
C
         SUBROUTINE FCN (NEQ,X,Y,YPRIME)
        COMMON    /YS/ Y60,/KK/ KS,KF
        COMMON /TOFCN/G,F,S,/DHCP/DELTH,CP,DH
        COMMON /MIX/Z0,BETA
         INTEGER     NEQ
         REAL *8     X,Y(NEQ),YPRIME(NEQ),KS(5),KF(5),F(5),G(5),S,Y60,
       &             LNY ,DCDT,TYPRIM ,DELTH(4),CP(10),DH(5),Z0,CPAR
       &  TA
       CPAR=5.0D0*8.314D0/2.0D0
C DH(n)=H*(n)-H(n);    DELTH(n)=H(n)+H*(1)-H*(n+1)
C      WRITE(8,*)DH
C      WRITE(8,*)G,S
C      WRITE(8,*)F
C
C     CALCULATE THE PARAMETER FN(I),GN(I) ,S FOR ODES;
C
       CALL PARAKF  (Y(12))
C
C    CALCULATION KS(I) AND KF(I) FOR ODES;

        CALL PARAFG(Y(12))
C
C    CALCULATE THE CP(I) AND DELTH(I) FOR YPRIME(12) (dT/dt')
C
       CALL DTDT(Y(12))

       YPRIME(1)=KS(1)*(BETA*Z0+Y(11)/Y60)*(Y(6)-F(1)*Y(1))
     &            +Y(1)*(KF(2)*(Y(6)*Y(6)*Y(11)/Y60-Y(7)/(S*G(2)))
     &   +KF(3)*(Y(2)*Y(6)*Y(11)/Y60-Y(8)/(S*F(2)*G(3)))
     &    +KF(4)*(Y(3)*Y(6)
     &   *(Y(11)/Y60)-Y(9)/(S*F(3)*G(4)))+KF(5)*(Y(4)*Y(6)*(Y(11)/Y60)
     &   -Y(10)/(S*F(4)*G(5))))
       YPRIME(2)=KS(2)*(BETA*Z0+Y(11)/Y60)*(Y(7)-F(2)*Y(2))-KF(3)*(
     &         Y(2)*Y(6)*Y(11)/Y60-Y(8)/(S*F(2)*G(3)))
     &            +Y(2)*(KF(2)*(Y(6)*Y(6)*Y(11)/Y60-Y(7)/(S*G(2)))
     & +KF(3)*(Y(2)*Y(6)*Y(11)/Y60-Y(8)/(S*F(2)*G(3)))+
     &       KF(4)*(Y(3)*Y(6)
     &   *(Y(11)/Y60)-Y(9)/(S*F(3)*G(4)))+KF(5)*(Y(4)*Y(6)*(Y(11)/Y60)
     &   -Y(10)/(S*F(4)*G(5))))
       YPRIME(3)=KS(3)*(BETA*Z0+Y(11)/Y60)*(Y(8)-F(3)*Y(3))-KF(4)*(
     &          Y(3)*Y(6)*Y(11)/Y60-Y(9)/(S*F(3)*G(4)))
     &            +Y(3)*(KF(2)*(Y(6)*Y(6)*Y(11)/Y60-Y(7)/(S*G(2)))
     & +KF(3)*(Y(2)*Y(6)*Y(11)/Y60-Y(8)/(S*F(2)*G(3)))
     &      +KF(4)*(Y(3)*Y(6)
     &   *(Y(11)/Y60)-Y(9)/(S*F(3)*G(4)))+KF(5)*(Y(4)*Y(6)*(Y(11)/Y60)
     &   -Y(10)/(S*F(4)*G(5))))
       YPRIME(4)=KS(4)*(BETA*Z0+Y(11)/Y60)*(Y(9)-F(4)*Y(4))-KF(5)*(
     &          Y(4)*Y(6)*Y(11)/Y60-Y(10)/(S*F(4)*G(5)))
     &            +Y(4)*(KF(2)*(Y(6)*Y(6)*Y(11)/Y60-Y(7)/(S*G(2)))
     &     +KF(3)*(Y(2)*Y(6)*Y(11)/Y60-Y(8)/(S*F(2)*G(3)))
```

```
     &     +KF(4)*(Y(3)*Y(6)
     &   *(Y(11)/Y60)-Y(9)/(S*F(3)*G(4)))+KF(5)*(Y(4)*Y(6)*(Y(11)/Y60)
     &   -Y(10)/(S*F(4)*G(5))))
        YPRIME(5)=KS(5)*(BETA*Z0+Y(11)/Y60)*(Y(10)-F(5)*Y(5))
     &           +Y(5)*(KF(2)*(Y(6)*Y(6)*Y(11)/Y60-Y(7)/(S*G(2)))
     & +KF(3)*(Y(2)*Y(6)*Y(11)/Y60-Y(8)/(S*F(2)*G(3)))
     &    +KF(4)*(Y(3)*Y(6)
     &   *(Y(11)/Y60)-Y(9)/(S*F(3)*G(4)))+KF(5)*(Y(4)*Y(6)*(Y(11)/Y60)
     &   -Y(10)/(S*F(4)*G(5))))
        YPRIME(6)=(-KS(1)*(BETA*Z0+Y(11)/Y60))*(Y(6)-F(1)*Y(1))- KF(2)*(
     &          Y(6)*Y(6)*Y(11)/Y60-Y(7)/(S*G(2)))
     &           +(Y(6)-1)*(KF(2)*(Y(6)*Y(6)*Y(11)/Y60-Y(7)/(S*G(2)))

      & +KF(3)*(Y(2)*Y(6)*Y(11)/Y60-Y(8)/(S*F(2)*G(3)))
      &   +KF(4)*(Y(3)*Y(6)
      &   *(Y(11)/Y60)-Y(9)/(S*F(3)*G(4)))+KF(5)*(Y(4)*Y(6)*(Y(11)/Y60)
      &   -Y(10)/(S*F(4)*G(5))))
      YPRIME(7)=KF(2)*(Y(6)*Y(6)*Y(11)/Y60-Y(7)/(S*G(2)))-KS(2)*
      &           (BETA*Z0+Y(11)/Y60)*(Y(7)-F(2)*Y(2))
      &            +Y(7)*(KF(2)*(Y(6)*Y(6)*Y(11)/Y60-Y(7)/(S*G(2)))
      &   +KF(3)*(Y(2)*Y(6)*Y(11)/Y60-Y(8)/(S*F(2)*G(3)))
      &   +KF(4)*(Y(3)*Y(6)
      &   *(Y(11)/Y60)-Y(9)/(S*F(3)*G(4)))+KF(5)*(Y(4)*Y(6)*(Y(11)/Y60)
      &   -Y(10)/(S*F(4)*G(5))))
      YPRIME(8)=KF(3)*(Y(2)*Y(6)*Y(11)/Y60-Y(8)/(S*F(2)*G(3)))-KS(3)*
      &           (BETA*Z0+Y(11)/Y60)*(Y(8)-F(3)*Y(3))
      &            +Y(8)*(KF(2)*(Y(6)*Y(6)*Y(11)/Y60-Y(7)/(S*G(2)))
      &   +KF(3)*(Y(2)*Y(6)*Y(11)/Y60-Y(8)/(S*F(2)*G(3)))
      &   +KF(4)*(Y(3)*Y(6)
      &   *(Y(11)/Y60)-Y(9)/(S*F(3)*G(4)))+KF(5)*(Y(4)*Y(6)*(Y(11)/Y60)
      &   -Y(10)/(S*F(4)*G(5))))
      YPRIME(9)=KF(4)*(Y(3)*Y(6)*Y(11)/Y60-Y(9)/(S*F(3)*G(4)))-KS(4)*
      &           (BETA*Z0+Y(11)/Y60)*(Y(9)-F(4)*Y(4))
      &            +Y(9)*(KF(2)*(Y(6)*Y(6)*Y(11)/Y60-Y(7)/(S*G(2)))
      &   +KF(3)*(Y(2)*Y(6)*Y(11)/Y60-Y(8)/(S*F(2)*G(3)))
      & +KF(4)*(Y(3)*Y(6)
      &   *(Y(11)/Y60)-Y(9)/(S*F(3)*G(4)))+KF(5)*(Y(4)*Y(6)*(Y(11)/Y60)
      &   -Y(10)/(S*F(4)*G(5))))

         YPRIME(10)=KF(5)*(Y(4)*Y(6)*Y(11)/Y60-Y(10)
      &     /(S*F(4)*G(5)))-KS(5)*
      &          (BETA*Z0+Y(11)/Y60)*(Y(10)-F(5)*Y(5))
      &           +Y(10)*(KF(2)*(Y(6)*Y(6)*Y(11)/Y60-Y(7)/(S*G(2)))
      &   +KF(3)*(Y(2)*Y(6)*Y(11)/Y60-Y(8)/(S*F(2)*G(3)))
      &    +KF(4)*(Y(3)*Y(6)
      &   *(Y(11)/Y60)-Y(9)/(S*F(3)*G(4)))+KF(5)*(Y(4)*Y(6)*(Y(11)/Y60)
      &   -Y(10)/(S*F(4)*G(5))))
C yprime(11) = d(C/C0)/dt'
        YPRIME(11)=(-Y(11)*(KF(2)*(Y(6)*Y(6)*Y(11)/Y60-Y(7)/(S*G(2)))

      &      +KF(3)*(Y(2)*Y(6)*Y(11)/Y60-Y(8)/(S*F(2)*G(3)))
      &    +KF(4)*(Y(3)*Y(6)
      &   *(Y(11)/Y60)-Y(9)/(S*F(3)*G(4)))+KF(5)*(Y(4)*Y(6)*(Y(11)/Y60)
      &   -Y(10)/(S*F(4)*G(5)))))

C YPRIME(12) = dT/dt'; CPAR is heat capacity of diluent i.e. argon.
```

```
      YPRIME(12)=((DH(1)*KS(1)*(Y(6)-F(1)*Y(1))+DH(2)*KS(2)*(Y(7)-
     &            F(2)*Y(2))+DH(3)*KS(3)*(Y(8)-F(3)*Y(3))+DH(4)*
     &          KS(4)*(Y(9)-F(4)*Y(4))+DH(5)*KS(5)*(Y(10)-F(5)*Y(5)))*
     &    (BETA*Z0+Y(11)/Y60)+DELTH(1)*KF(2)*(Y(6)*Y(6)*Y(11)/Y60-Y(7)/
     &          (S*G(2)))+DELTH(2)*KF(3)*(Y(2)*Y(6)*Y(11)/Y60-Y(8)/
     &           (S*F(2)*G(3)))+DELTH(3)*KF(4)*(Y(3)*Y(6)
     &           *(Y(11)/Y60)-Y(9)/(S*F(3)*G(4)))+DELTH(4)*
     &           KF(5)*(Y(4)*Y(6)*(Y(11)/Y60)-Y(10)/(S*F(4)*G(5))))/
     & (Y(1)*CP(1)+Y(2)*CP(2)+Y(3)*CP(3)+Y(4)*CP(4)
     &   +Y(5)*CP(5)
     &           +Y(6)*CP(6)+Y(7)*CP(7)+Y(8)*CP(8)+Y(9)*CP(9)+
     &            Y(10)*CP(10)+Z0*Y60*CPAR/Y(11))
C     WRITE(8,*)YPRIME

 100  FORMAT(5D12.4)
     RETURN
      END


C-----------------------------------------------------------------


C IN YZERO THE S0 IS THE ENTROPY OF EVAPORATION
C S IS THE SATURATION DEGREE
      SUBROUTINE YZERO(T,PVA,V,H1,S0,S,YON)
      COMMON /DEGNAC/TA,GE,/DEGN/NA,/DEGFIT/ AG,BG,CG
      DOUBLE PRECISION YO(5),YOE(5),FN(5),YON(10),A0(5),Q,SEVAL,
     & X,S,ENO,DH,E1,R,T,YT,YOT,YOET,EN,PVA,V,H1,S0,AA(6),YOP,
     & TA(16),GE(16),AG(16),BG(16),CG(16),AE(16),DEG,EVB
      1NTEGER NDEG,M,N,I,J,K,NA
      PARAMETER(NDEG=5)
      EXTERNAL DZPORC,THERM
      COMPLEX*16  Z(5)
C     WRITE(8,150) T,PVA,V,H1,S0,S
150   FORMAT(5E13.4/5E13.4)
C M is the biggest cluster size
      M=5
      N=M+1
      R=8.314D0
      AA(1)=-1.0D0
      A0(1)=1.0D0
      DO 10 I=2,M
      CALL THERM(I,T,PVA,V,H1,S0,S,X,DH)
      A0(I)=A0(I-1)/X
C     WRITE(8,*)X,A0(I)
  10  CONTINUE
      DO 30 J=2,6
      AA(J)=A0(J-1)
  30  CONTINUE
      CALL DZPORC(NDEG,AA,Z)
      YOP =REAL(Z(1))
      DEG=SEVAL(NA,T,TA,GE,AG,BG,CG)
      EVB=9*R*T
C     Q=1.0D0/(1.0D0+DEG*DEXP(-EVB/(R*T)))
```

```
      YO(1)=YOP*DEG
C     EXCITED MONOMER
C     E1=-4560.181846D0+26.078275D0*T+0.033411D0*T**2.0D0
C     FN(1)=DEXP(-E1/(R*T))
C     YOE(1)=YO(1)*FN(1)
C    CALCULATION OF EXCITED MONOMER
      YOE(1)=YOP-YO(1)
      YOE(1)=YOP*DEG*DEXP(-EVB/(R*T))/Q
      YOET=YOE(1)
      YOT=YO(1)
C     EXCITED CLUSTER DISTRIBUTION (DIMER TO M-MER )
      DO 20 K=2,5
      YO(K)=A0(K)*YO(1)**(K)
      YOT=YOT+YO(K)
      CALL THERM(K,T,PVA,V,H1,S0,S,X,DH)
      ENO=DH/(R*T)
      EN=ENO+(3.0D0/2.0D0)
      FN(K)=DEXP(-EN)
      YOE(K)=YO(K)*FN(K)
      YOET=YOET+YOE(K)
   20 CONTINUE
C NORMALIZATION
      YT=YOET+YOT
      DO 50 L=1,5
      YON(L)=YO(L)/YT
      YON(5+L)=YOE(L)/YT
   50 CONTINUE
C     WRITE(8,200)YON
  200 FORMAT(5E14.5/5E14.5)
      RETURN
      END
C  ------------------------------------------------


      SUBROUTINE THERM(N, T, PV ,VOL, H0,S0,S,X,DH)
      INTEGER N,N1,NA
      DOUBLE PRECISION S,X,DH,R,EP,WM,TB,T,PV,P, SEVAL,
     &  VOL,H0,S0,PARA,DS,DG,DNS,DG1,DH1,DN ,HE1,HUE,HUE0, EVB
      R=8.314D00
      EP=R*399.0D0
      WM=137.39D-3
      TB=296.85D00
      P=PV
C PARA= a**4; a=eta/r0
      PARA=2.45D0**4
C     PARA=(2.0D0*(H0+P*VOL-R*T)/EP+1.0D0)**(4.0D0/3.0D0)
      EVB=9*R*T
      HE1=DBLE(4)*R*T+(EP/2.0D0)*(PARA**(3.0/4.0)-1.0D0)+EVB
      IF (N .LE. 2)THEN
      HUE=(12.0D0*DBLE(N)-2.0D0)*R*T+(EP/64.0D0)*(18.0D0*DBLE(N)**(
     &     2.0D0/3.0D0)-PARA**(1.0D0/2.0D0))*PARA
      DH=2.0D0*HE1-HUE
C     DH=2.D0*(H0+P*VOL+R*T)-EP*PARA*(28.6-PARA**0.5D0)/6.4D01
      DS=S0+R*5.0D0*DLOG(0.5D0)-R*DLOG(S)
      DG=P*VOL+3.0D0*R*T+(EP/2.0D0)*(PARA**(3.0/4.0)-1.0D0)
     &-(EP/64.D0)*PARA*(18.D0*2.0D0**(2.0D0/3.0D0)-PARA**(0.5D0))
```

```
     &-R*T*5.0D0*DLOG(0.5D0)-R*T*DLOG(P*0.986842105D-5)
      ELSE
      N1=N-1
      DN=DBLE(N)**(2.0D0/3.0D0)-DBLE(N1)**(2.0D0/3.0D0)
C     DH=H0+P*VOL-9.0D0*EP*PARA*DN/32.0D0
      HUE0=(12.0D0*DBLE(N1)-2.0D0)*R*T+(EP/64.0D0)*(18.0D0*DBLE(N1)**
     &     (2.0D0/3.0D0)-PARA**(1.0D0/2.0D0))*PARA
      HUE=(12.0D0*DBLE(N)-2.0D0)*R*T+(EP/64.0D0)*(18.0D0*DBLE(N)**(
     &      2.0D0/3.0D0)-PARA**(1.0D0/2.0D0))*PARA
C
      DH=HUE0+HE1-HUE
      DNS=(DBLE(N1)/DBLE(N))**(3+N)
      DS=S0+R*DLOG(DNS)-R*DLOG(S)
      DG=P*VOL-R*T*DLOG(P*0.986842105D-5)-9.0D0/32.D0*EP*PARA*DN
     & -R*T*DLOG(DNS)
      END IF
      DG1=(DG/(R*T))
      DH1=(1.0D0/T-1.0D0/TB)*H0/R
      X=(DEXP(-DG1))/(S*DEXP(-DH1))
C      WRITE(4,*)X
       RETURN
       END
C-----------------------------------------------------------------------


       SUBROUTINE PARAFG (T)
       INTEGER N
       DOUBLE PRECISION
      1         T0(30),G5(30),G2(30),G3(30),G4(30),BS(30),F1(30),F2(30),
      1 F3(30),F4(30),F5(30),G5A(30),G5B(30),G5C(30),G2A(30),G2B(30)
      1 ,G2C(30),G3A(30),G3B(30),G3C(30),G4A(30),G4B(30),
      1 G4C(30),BSA(30),BSB(30),BSC(30),F1A(30),F1B(30)
      1,F1C(30),F2A(30),F2B(30),F2C(30),
      1 F3A(30),F3B(30),F3C(30),F4A(30),F4B(30),F4C(30),F5A(30),F5B(30)
      1 ,F5C(30),G(5),F(5),BST,T ,SEVAL
       COMMON /GNDATA/T0,G2,G3,G4,G5,BS,N
       COMMON /FNDATA/F1,F2,F3,F4,F5
       COMMON /GNFIT/G5A,G5B,G5C,G2A,G2B,G2C,G3A,G3B,G3C,G4A,G4B,G4C
       COMMON /FNFIT/F1A.F1B,F1C,F2A,F2B,F2C,F3A,F3B,F3C,F4A,F4B,F4C,
      1 F5A,F5B,F5C
       COMMON /BSFIT/BSA,BSB,BSC
C      BST IS S IN SUBROUTINE FCN
       COMMON /TOFCN/G,F,BST
         BST=SEVAL(N,T,T0,BS,BSA,BSB,BSC)
         G(2)=SEVAL(N,T,T0,G2,G2A,G2B,G2C)
         G(3)=SEVAL(N,T,T0,G3,G3A,G3B,G3C)
         G(4)=SEVAL(N,T,T0,G4,G4A,G4B,G4C)
         G(5)=SEVAL(N,T,T0,G5,G5A,G5B,G5C)
         F(1)=SEVAL(N,T,T0,F1,F1A,F1B,F1C)
         F(2)=SEVAL(N,T,T0,F2,F2A,F2B,F2C)
         F(3)=SEVAL(N,T,T0,F3,F3A,F3B,F3C)
         F(4)=SEVAL(N,T,T0,F4,F4A,F4B,F4C)
         F(5)=SEVAL(N,T,T0,F5,F5A,F5B,F5C)
C       WRITE(11,300)T,G(2),G(3),G(4),G(5),BST
C       WRITE(11,300)T,F
C       WRITE(9,400)T,H1
```

```
  300   FORMAT(F8.2,5E15.6)
  400   FORMAT(E14.5,E15.6)
        RETURN
        END


C


        SUBROUTINE FCNJ (NEQ,X,Y,DYPDY)

        INTEGER    NEQ
        DOUBLE PRECISION    X,Y(NEQ),DYPDY(*)
C        COMMON  /AB/ A1, B,C,D, /YS/ Y10,S, // F,G,/CLNY/ LNY,TYPRIM,
C     &          /KK/ KS,KF,DCDT
        RETURN
        END


C
C   DELTH(N)=H(N)+H*(1)-H*(N+1) ;DHE=H(N)* -H(N)
C H(N)* IS ENTROPY OF EXCITED N-MER; H(N) IS FOR UNEXCITED N-MER
C subroutine DTDT calculate the DELTH(4),DH(5) and Cp(5) for Y(12)
C


        SUBROUTINE DTDT(T)

C
      COMMON /ENTHA/TH,HV,PV,VL,NO
      COMMON /ENFIT/HA,HB,HC,PA,PB,PC,VA,VB,VC
      COMMON /DHCP/DELTH,CP,DHE
      COMMON /HH/H,HE
      REAL *8 CP(10),H(5), EP,T,HVAP,PARA,R,DHE(5),DH,E1,PVAP,VLIQ,
      &          TH(30),HV(30),HA(30),HB(30),HC(30),DELTH(4),DH2,DN
      &         ,PV(30),PA(30),PB(30),PC(30),VL(30),VA(30),VB(30),VC(30)
      &         ,SEVAL,HE(5)
        INTEGER I,J,NO,NI,NI1,NA
        R=8.314D0
        EP=R*399.0D0
C ENTHALPY  OF EVAPRATION IN J/mol; Pvap in Pa; vliq in M**3/mol
        HVAP=SEVAL(NO,T,TH,HV,HA,HB,HC)
        PVAP=SEVAL(NO,T,TH,PV,PA,PB,PC)
       VLIQ=SEVAL(NO,T,TH,VL,VA,VB,VC)
C       WRITE(8,*)HVAP,PVAP,VLIQ
C PARA =  A=ETA/R0
C      PARA=(2.0D0*(HVAP+PVAP*VLIQ-R*T)/EP+1.0D0)**(1.0D0/3.0D0)
C        PARA=(2.0D0*HVAP/EP+1.0D0)**(1.0D0/3.0D0)
        PARA=2.450D0
C       WRITE(8,*)PARA,T
C THE DHE(I) IS THE ENERGY DIFFERENCE BETWEEN THE EXCITED AND
C  UNEXCITED
C N-MER
C
        E1=9*R*T
C       E1=-4560.181846D0+26.078275D0*T+0.033411D0*T**2.0D0
```

```
C CALCULATION  THE H(I) THAT IS THE ENTHALPY OF UNEXCITED CLUSTER
C
      H(1)=DBLE(4)*R*T+((EP/2.0D0)*(PARA**3-1.0D0))
      DO 20 J=2,5
      H(J)=(12.0D0*DBLE(J)-2.0D0)*R*T+(EP/64.0D0)*(18.0D0*
     +     DBLE(J)**(2.0D0/3.0D0)-PARA**2)*PARA**4
  20  CONTINUE
C CALCULATE ENTHALPY FOR EXCITED CLUSTER
         HE(1)= H(1)+E1
         HE(2)=2.0D0*HE(1) +1.5*R*T
         HE(3)=H(2)+HE(1)+1.5D0*R*T
         HE(4)=H(3)+HE(1)+1.5D0*R*T
         HE(5)=H(4)+HE(1)+1.5D0*R*T
C CALCULATION THE DHE(1) TO DHE(5)
      DHE(1)=E1
      DO 22 I=2,5
         DHE(I)=HE(I)-H(I)
  22  CONTINUE
C  CALCULATION OF HEAT CAPACITY OF UNEXCITED CLUSTER
      CP(1)=4.0D0*R
      DO 10 I= 2 ,5
          CP(I)=(12.0D0*DBLE(I)-2.0D0)*R
  10  CONTINUE
C      WRITE(8,*)CP
C THE HEAT CAPACITY OF EXCITED CLUSTER
     CP(6)= CP(1)*  = CP(1) + DE(1)*/DT  =4*R+26.078275+0.066822*T
C              =4*R+26.078275+0.066822*T
      CP(6) =13.0D0*R
      CP(7) =3.0D0*R/2.0D0+2.0D0*CP(6)
      DO 12 I=3,5
          CP(5+I)=CP(I-1)+CP(6)+3.0D0*R/2.0D0
  12  CONTINUE
C     WRITE(8,*)CP
C     WRITE(8,888)T,H,HE
      DELTH(1)=2.0D0*HE(1)-HE(2)
      DELTH(2)=H(2)+HE(1)-HE(3)
      DELTH(3)=H(3)+HE(1)-HE(4)
      DELTH(4)=H(4)+HE(1)-HE(5)
C     WRITE(8,*) DELTH
C 100 FORMAT(D13.4)
  888 FORMAT(D16.6,5D13.4/5D13.4)
      RETURN
      END


C


      SUBROUTINE PARAKF (T)
      COMMON  /AB/A1,B,/KK/KS,KF
      COMMON /KE/ KS1E,KS2E,E1S,E2S,Y12
      INTEGER   I
      REAL *8 KS(5),KF(5),A1,B,X,Y1,KS1E,
     &        KS2E,E1S,E2S,R,DT,T ,Z,Y12
       R=8.314D0
C      WRITE(8,100) T
```

```
 100    FORMAT(2F7.2)
           KS(1)=KS1E*DEXP((-E1S/R)*(1.0D0/T))
           KS(2)=KS2E*DEXP((-E2S/R)*(1.0D0/T))
C ASSUMING THAT THE TEMPERATURE DEPENDENCE OF KS(N) IS SAME AS THAT
C FOR
C KS(2)
           DO 81 I=3,5
              X=DBLE(I)
              KS(I)=KS(2)*DEXP(A1*(X-2.0D0))
 81        CONTINUE

C ASSUME THAT KF(N) IS TEMPERATURE INDEPENDENT
C KF(1) IS NOT APPEARED IN THE DIFFERENTIAL EQUATIONS.
      KF(1)=0.0D00
C KF(2) IS EQUAL TO ONE BECAUSE IT IS THE RATIO OF k2/k2e.

      DO 20 K=2,5
      Z=DBLE(K)
      Y1=(1.0D0+Z**(1.0D0/3.0D0))/(1.0D0+2.0D0**(1.0D0/3.0D0))
      KF(K)=Y1*((2.0D0/3.0D0)*((Z+1)/Z))**0.5D0*DEXP(B*(Z-2.0D0))
      KF(K)=KF(K)*DSQRT(T/Y12)
  20  CONTINUE
C     WRITE(8,*)KF,KS
C100  FORMAT(4D12.4)
      RETURN
      END
C-----------------------------------------------------------------


       SUBROUTINE SPLFIT
C        THIS PROGRAM FITS DATA WITH A CUBIC INTERPOLATING SPLINE.
C        USING PARABOLIC END CONDITION: S(0)=S(1),S(N-1)=S(N).
        COMMON /DEGNAC/TA,GE,/DEGN/NA,/DEGFIT/ AG,BG,CG
        COMMON /ENTHA/TH,H,P,V,NO
        COMMON /ENFIT/HA,HB,HC,PA,PB,PC,VA,VB,VC
        COMMON /GNDATA/T0,G2,G3,G4,G5,BS,N
        COMMON /FNDATA/F1,F2,F3,F4,F5
        COMMON /GNFIT/G5A,G5B,G5C,G2A,G2B,G2C,G3A,G3B,G3C,G4A,G4B,G4C
        COMMON /FNFIT/F1A,F1B,F1C,F2A,F2B,F2C,F3A,F3B,F3C,F4A,F4B,F4C,
       1 F5A,F5B,F5C
        COMMON /BSFIT/BSA,BSB,BSC
        INTEGER N,NO,NA
        DOUBLE PRECISION
       &        T00),G5(30),G2(30),G3(30),G4(30),BS(30),F1(30),F2(30),
       & F3(30),F4(30),F5(30),G5A(30),G5B(30),G5C(30),G2A(30),G2B(30)
       & ,G2C(30),G3A(30),G3B(30),G3C(30),G4A(30)
       & ,G4B(30),G4C(30),BSA(30),BSB(30),BSC(30),F1A(30),F1B(30),
       & F1C(30),F2A(30),F2B(30),F2C(30),  F3A(30),F3B(30),F3C(30)
       &,F4A(30),F4B(30),F4C(30),F5A(30),F5B(30)
       & ,F5C(30),G2S(30),G3S(30),G4S(30),G5S(30),BSS(30),F1S(30),
       & F2S(30),F3S(30),F4S(30),F5S(30),H(30),HA(30),HB(30)
       & ,HC(30),HS(30),TH(30),P(30),PA(30),PB(30),PC(30)
       & ,PS(30),V(30),VA(30),VB(30),
       & VC(30),VS(30),TA(16),GE(16),AG(16),BG(16),CG(16),SG(16)

C
```

```
      CALL CUBSPL(TA,GE,NA,AG,BG,CG,SG)
C
C     CALL CUBSPL(TA,VE,NA,AE,BE,CE,SE)
      CALL CUBSPL(T0,F1,N,F1A,F1B,F1C,F1S)
C
      CALL CUBSPL(T0,F2,N,F2A,F2B,F2C,F2S)
C
      CALL CUBSPL(T0,F3,N,F3A,F3B,F3C,F3S)
C
      CALL CUBSPL(T0,F4,N,F4A,F4B,F4C,F4S)
C
      CALL CUBSPL(T0,F5,N,F5A,F5B,F5C,F5S)
C
      CALL CUBSPL(T0,BS,N,BSA,BSB,BSC,BSS)
C
      CALL CUBSPL(T0,G2,N,G2A,G2B,G2C,G2S)
C
      CALL CUBSPL(T0,G3,N,G3A,G3B,G3C,G3S)
C
      CALL CUBSPL(T0,G4,N,G4A,G4B,G4C,G4S)
C
      CALL CUBSPL(T0,G5,N,G5A,G5B,G5C,G5S)
C
      CALL CUBSPL(TH,H,NO,HA,HB,HC,HS)
C
C
      CALL CUBSPL(TH,P,NO,PA,PB,PC,PS)
C
      CALL CUBSPL(TH,V,NO,VA,VB,VC,VS)
C
C     DO 90 I=1,30
C90   WRITE(8,500)G5A(I),G5B(I),G5C(I)
  500 FORMAT(E14.5,2E15.6)
      RETURN
      END


C-----------------------------------------------------------------
C
C
C-----------------------------------------------------------------
C
C
      SUBROUTINE CUBSPL(X,Y,N,A,B,C,S)
C  THIS SUBROUTINE COMPUTES THE MATRIX FOR FINDING THE COEFFICIENTS OF
C CUBIC SPLINE THROUGH A SET OF DATA.
      INTEGER N,NM1,NM2,I,J,FIRST,LAST
      REAL *8 X(N),Y(N),S(N),A(N),B(N),C(N),SMATRX(0:26,4)
     +     ,DX1,DY1,DX2,DY2,DXN1,DXN2
      REAL H(26)
C
C  COMPUTER FOR THE N-2 ROWS
C
      NM2=N-2
```

```
      NM1=N-1
      DX1=X(2)-X(1)
      DY1=(Y(2)-Y(1))/DX1*6.0D0
      DO 10 I=1,NM2
          DX2=X(I+2)-X(I+1)
          DY2=(Y(I+2)-Y(I+1))/DX2*6.0D0
          SMATRX(I,1)=DX1
         SMATRX(I,2)=2.0D0*(DX1+DX2)
          SMATRX(I,3)=DX2
          SMATRX(I,4)=DY2-DY1
          DX1=DX2
          DY1=DY2
 10     CONTINUE
        FIRST=2
        LAST=NM2
C    FOR END CONDITION=3
  80   DX1=X(2)-X(1)
       DX2=X(3)-X(2)
       SMATRX(1,2)=(DX1+DX2)*(DX1+2.0D0*DX2)/DX2
       SMATRX(1,3)=(DX2*DX2-DX1*DX1)/DX2
       DXN2=X(NM1)-X(NM2)
       DXN1=X(N)-X(NM1)
       SMATRX(NM2,1)=(DXN2*DXN2-DXN1*DXN1)/DXN2
       SMATRX(NM2,2)=(DXN1+DXN2)*(DXN1+2.0D0*DXN2)/DXN2
C
C     PRINT OUT TRIDIAGONAL MATRIX IN COMPACT FORM
C
C      DO 11 I = FIRST-1,LAST
C II    PRINT*,(SMATRX(I,J),J=1,4)

C NOW SOLVE THE TRIDIAGONAL SYSTEM.
       DO 110 I= FIRST,LAST
         SMATRX(I,1)=SMATRX(I,1)/SMATRX(I-1,2)
        SMATRX(I,2)=SMATRX(I,2)-SMATRX(I,1)*SMATRX(I-1,3)
         SMATRX(I,4)=SMATRX(I,4)-SMATRX(I,1)*SMATRX(I-1,4)
 110   CONTINUE
C
C-------------------------------------------------------------
C
C NOW WE BACT SUBSTITUTE
       SMATRX(LAST,4)=SMATRX(LAST,4)/SMATRX(LAST,2)
       DO 120 J=LAST-1,FIRST-1,-1
         SMATRX(J,4)=(SMATRX(J,4)-SMATRX(J,3)*SMATRX(J+1,4))
     +       /SMATRX(J,2)
120   CONTINUE
C
C NOW PUT THE VALUES INTO THE S VECTOR
C
       DO 130 I=FIRST-1,LAST
          S(I+1)=SMATRX(I,4)
 130   CONTINUE
C
C---------------------------------------------


c GET S(1) AND S(N) ACCORDING TO END CONDITIONS
```

```
      S(1)=((DX1+DX2)*S(2)-DX1*S(3))/DX2
      S(N)=((DXN2+DXN1)*S(NM1)-DXN1*S(NM2))/DXN2
C
C WRITE OUT COEFFICIENTS OF THE POLYNOMIALS
C
C     PRINT 99
C99   FORMAT(/T2,60('*')//T10,'THE CUBIC POLYNOMIALS, G(X)'
C    +,'DEFINED ON THE INTERVALS',//)
C     PRINT 101
      DO 200 I=1,N-1
         H(I)=X(I+1)-X(I)
         A(I)=(S(I+1)-S(I))/(6.0D0*H(I))
         B(I)=S(I)/2.0D0

        C(I)=((Y(I+1)-Y(I))/H(I))-((2.0D0*H(I)*S(I)+H(I)*S(I+1))/6.0D0)
C
C     PRINT 102,I,A(I),B(I),C(I),Y(I)
C101  FORMAT(T5,'I',T17,'I',T27,'B',T37,'C',T47,'D'/)
C102  FORMAT(T5,I1,T12,F8.4,T22,F8.4,T32,F8.4,T42,F8.4)
 200  CONTINUE
      RETURN
      END
C
C

      REAL FUNCTION SEVAL(N,U,X,Y,A,B,C)
      INTEGER N
      REAL*8 U,X(N),Y(N),B(N),C(N),A(N)
C
C THIS SUBROUTINE EVALUATE THE CUBIC SPLINE FUNCTION
C SEVAL=Y(I)+C(I)*(U-X(I))+B(I)*(U-X(I)**2+A(I)*(U-X(I))**3
C
      INTEGER I,J,K
      REAL*8 DX
      SAVE I
      DATA I/1/
      IF (I.GE.N) THEN
         I=1
      END IF
      IF (U.GE.X(N)) THEN
        DX=U-X(N-1)
         SEVAL=Y(N-1)+DX*(C(N-1)+DX*(B(N-1)+DX*A(N-1)))
         RETURN
      ENDIF
      IF(U.GE.X(I)) THEN
        IF(U .LE. X(I+1)) THEN
           DX=U-X(I)
           SEVAL=Y(I)+DX*(C(I)+DX*(B(I)+DX*A(I)))
         RETURN
        END IF
      ENDIF
      I=1
      J=N+1
 10   K=(I+J)/2
C     WRITE(8,*)K
      IF(U .LT. X(K)) THEN
```

```
          J=K

       ELSE
          I=K
      END IF
        IF (J .GT. I+1) THEN
           GOTO 10
        ELSE
C
C       EVALUATE SPLINE
C
            DX=U-X(I)
             SEVAL=Y(I)+DX*(C(I)+DX*(B(I)+DX*A(I)))
             RETURN
        END IF
C       END
         RETURN
         END
```

BIBLIOGRAPHY

1. J. J. Burton, in B. J. Berne (ed.), Modern Theoretical Chemistry, Vol. 5, Plenum, New York, (1977), p. 195.
2. R. H. Doremus, Rates of Phase Transformations, Academic Press, New York, (1985), p. 171.
3. D. P. Woodruff, The Solid-Liquid Interface, Cambridge University Press, New York (1973), p. 171.
4. G. W. Sears, J. Chem. Phys. Solids, 2, 37 (1957).
5. P. W. Atkins, Physical Chemistry 4 edition, W. H. Freeman and Company N.Y. (1991).
6. F. A. Lindemann, Phys. Z. 11, 609 (1910).
7. S. Khaikin, S. C. R. Ac. Sci. U. R. S. S. 23 (1937).
8. J. Frenkel, Kinetic Theory of Liquids , Dover Publications, New York, (1946).
9. J. W. Gibbs, "The Scientific Papers of J. Willard Gibbs " vol. 1, pp. 55-353. Dover Publications, New York, (1961).
10. M. Volmer and A. Weber, Z. Physik. Chem. (Leipzig), 119, 277 (1926).
11. L. Farkas, Z. Phys. Chem. (Leipzig) A125, 236 (1927).
12. R. Becker and W. Doring, Ann. phys. (Leipzig) ,24,719(1935).
13. J. B. Zeldovich, Acta Physicochim (U.R.S.S.), 181(1943).
14. D. B. Dawson, E. J. Wilson, P. G. Hill and K. C. Russell, J. Chem. Phys. 51, 5389, (1969).

15. A. C. Zettlemoyer, ed., Nucleation, Marcel Dekker, New York, (1969).

16. M. A. Sharaf and R. A. Cobbs, J. Chem. Phys. , 77, 1517 (1982).

17. B. N. Hale, Phys. Rev. A, 33, 4156(1986).

18. C-H. Hung, M. J. Krasnopoler and J. L. Katz, J. Chem. Phys. 90, 1856(1989).

19. F. Peters and B. Pakert, J. Chem. Phys. 91, 5672(1989).

20. J. Z. McDonald, Am. J. Phys. 31, 31(1963).

21. W. Band, J. Chem. Phys. 7, 324, (1939).

22. F. F. Abraham, J. Appl. Phys. , 39, 3287(1968).

23. R. T. V. Kung and S. H. Bauer, "Shock Tube Research" 8th International Symposium, Chapman and Hill, London (1971), Paper number 61.

24. J. L. Katz and M. D. Donohue , Adv. Chem. Phys. 40,137(1979).

25. J. Lothe and G. M. Pound, in Nucleation, ed A. C. Zeffelmoger, Dekker, New York, (1969).

26. J. Feder , K. C. Russell, J. Lothe, and G. M. Pound, Advan. Phys.,15, 111(1966).

27. F. F. Abraham, Homogeneous Nucleation Theory, Academic Press New York (1974).

28. D. Turnbull, Trans. AIME, 175, 774 (1948).

29. M. Volmer and H. Flood, Z. Phys. Chem., A, 170, 273 (1934).

30. H. L. Jaeger, E. J. Willson, P. G. Hill, J. Chem. Phys. 51, 5380(1969).

31. J. L. Katz, J. Chem. Phys. 52, 4933 (1970) .

32. J. Lothe and G. M. Pound, J Chem. Phys. 36, 2080(1961).

33. P. E. Wagner and R. Strey, J. Phys. Chem. 75, 2694(1981).

34. P. P. Wegener and B. J. C. Wu, Adv. Colloid Interface Sci 7, 325 (1977).

35. H. Reiss J. Statist. Phys. 2, 83(1970).

36. A. Langsdorf, Rev. Sci. Instr. 10, 91 (1939).

37. J. L. Katz, C. J. Scoppa II , N. G. Kumar and P. Mirabel, J. Chem. Phys., 62, 448 (1975).

38. J. L. Katz, P. Mirabel, C. J. Carman and T. L. Virkler, J. Chem. Phys. , 65, 382 (1976)

39. H. Reiss, J. L. Katz and E. R. Cohen J. Chem. Phys. 48, 1968(1968).

40. R. Nishioka, Phys. Rev. A16, 2143(1977).

41. D. J. Frurip and S. H. Bauer, J. Phys. Chem. 81, 1015 (1977).

42. P. Hamill, D. Stuffer and C. S. Kiang, Chem Phys. Lett. 28, 209(1974).

43. M. E . Fisher, Physics, 3,255(1967).

44. C. F. Wilcox Jr. and S. H. Bauer, J. Chem. Phys. 94, 8302 (1991).

45. J. L. Katz and H. Wiedersich, J. Colloid Interface. Sci., 61, 351(1966).

46. H. Reiss and J. L. Katz, J. Chem. Phys. 46, 2496 (1967).

47. F. F. Abraham and J. V. Dover, J. Chem. Phys., 55, 1587(1971).

48. S. Grishick and Chia-Pin Chiu, J. Chem. Phys. 93, 1273 (1990).

49. B. Nowakowski and E. Ruckenstein, J. Chem. Phys. 94, 1397 (1991).

50. S. H. Bauer and C. F. Wilcox, Jr. J. Phys. Chem. , 97, 271 (1993).

51. W. R. Creasy , J. Chem. Phys. 92, 7223 (1990).

52. C. H. Yang and H. Qiu, J. Chem. Phys. 84, 416 (1986).

53. J. L. Schmitt G. W. Adams and K. A. Zalabsky, J. Chem, Phys.77, 2089 (1982).

54. J. L. Schmitt, R. A. Zalabsky and G. W. Adams, J. Chem. Phys. 81, 5074 (1984).

55. H. Reiss, A. Tabazadek and J. Tabot, J. Chem. Phys. 92 1266 (1990).

56. P. E. Wagner and R. Strey, J. Chem. Phys. 80, 5266 (1984).

57. F. Peters and B. Peikert, J. Chem. Phys. 91, 5672 (1989).

58. G. Gyarmathy and H. Myer, VDI Forschungsh. 508,1 (1965).

59. C. F. Powell, Proc. R. Soc. London Ser.A 119, 553 (1928).

60. J. I. Yellot, Trans. ASME 56, 411 (1934).

61. I. Scazzer, Ann. Phys. 35, 619 (1939).

62. J. L. Katz and B. J. Ostermeir, J. Chem. Phys. , 47, 478 (1967).

63. H. L. Jaeger, E. J. Wilson, P. G. Hills and K. C. Russell, J. Chem. Phys. 51, 5380 (1969).

64. I-H. Hung, M. J. Krasnopoler and J. L. Katz, J. Chem. Phys. 90, 185 (1989).

65. P. E. Wagner and R. Strey, J. Phys. Chem. 85, 2694 (1981).

66. W. R. Creasy and J. T. Brenna , J. Chem. Phys. 92, 2269(1990).

67. A. O'Keefe, M. M. Ross and A. P. Baronavski, Chem. Phys. Lett. 130, 17(1986).

68. R. E. Honig, J. Chem. Phys. 22, 126, (1954).

69. J. Drowart, R. P. Burns, G. DeMaria and M. G. Inghram, J. Chem. Phys. 31, 1131 (1959).

70. C. T. R. Wilson, Phil. Trans. Roy. Soc. A189, 265 (1897); A193, 289 (1900).

71. P. P. Wegener and G. J. Lundquist, J. Applied Phys., 22, 233 (1951).

72. J. B. Homer "Shock Tube Research" 8th International Symposium, Chapman and Hill, London (1971), Paper number 62.

73. F. Peters and B. Paikert, Exp. Fluids. 7, 521(1989).

74. E. Peters, Exp. Fluids 1, 143 (1983).

75. R. Goldstein, J. Chem. Phys., 40, 2793(1964).

76. W. R. Smith, Proc. 9th Int. Shock Tube Symp. (eds. D. Bershader, and W. Griffith) Stanford University, Stanford (1967).

77. M. Maerefat, S. Fujikawa, T. Akamatsu, T. Goto and T. Mizutani, Exp. Fluids, 7, 513 (1989).

78. S. Fujikawa, M. Okuda, Akamatsu, T. Goto, J. Fluid Mech. 183, 293, (1986).

79. J. L. Kassner, Jr. and R. J. Schmitt, J. Chem. Phys. 44, 4166(1966).

80. D. Barschdorff, Phys. Fluids, 18, 529 (1975).

81. R. C. Miller, Ph. D. Thesis , University of Missouri, Rolla, MO, (1976).

82. R. J. Anderson, R. C. Miller, J. L. Kassner, Jr and D. E. Hagen , J. Atoms, Sci. 37, 2509, (1980).

83. G. K. Vemulapalli, Physical Chemistry, Prentice Hall, Englewood, Cliffs, New Jersey, (1993).

84. A. M. Zhabotinskii, in Oscillations and Travelling Waves in Chemical Systems, ed. R. J. Field and M. Burger, John Wiley & Son, (1985), p. 1.

85. R. J. Field, E. Koros, and R. M. Noyes, J. Am. Chem. Soc. 94, 8649, (1972).

86. R. B. Lam , R. C. Wieboldt and T. L. Isenhour, Anal. Chem. 53, 889A, (1981).

87. I. E. Saal'nikov Zh. Fiz. Khim., 23, 258, (1949).

88. B. F. Gary and C. H. Yang, J. Phys. Chem, 69,2747, (1965);

89. B. F. Gary and C. H. Yang, J. Phys. Chem, 73, 3795, (1969).

90. R. J. Field and M. Burger, eds., Oscillations and Travelling Waves in Chemical Systems, John Wiley & Sons, (1985).

91. A. C. Tam, H. Sontag and P. Hess, Chem. Phys. Letters, 120, 280 (1985).

92. A. G. Gaydon, I. R. Hurle, The Shock Tube in High Temperature Chemical Physics, Chapman and Hall Ltd. London (1963).

93. N. J. Edward, Chemical Kinetics: A Modern Survey of Gas Reactions. N. Y. (1976).

94. V. S. Rao and G. B. Skinner, J. Phys. Chem. 93, 1869, 1989.

95. M. Braun-Unkhoff , P. Frank and Th. Just, 22nd Symp.(Int.) on Combustion, pp. 1053-61, Pittsburgh: Combustion Inst., 1989.

96. S. C. Khandelwal and G. B. Skinner, in Shock Waves in Chemistry, ed. A. Lifshitz, Marcel Dekker Inc. N. Y. 1981, p. 1.

97. K. Saito, R. Ito, T. Kukumoto and A. Imamura, J. Phys. Chem. 90, 1422, 1986.

98. M. Yasuhaza, K. Yoneda, and S. Sato, J. Phys. Soc. Japan, 36, 535, 1974.

99. J. H. Kiefer and R. W. Lutz, J. Chem. Phys 44, 658, 1966.

100. J. E. Dove and H. Teitelbaum, Chem. Phys. 6, 431, 1974.

101. J. E. A. John, Gas Dynamics, Allyn and Bacon, Inc., Boston, 1987.

102. R. L. Belford and R. A. Strehlow, Ann. Rev. Phys. Chem. 20, 247, 1969.

103. H. Teitelbaum, Ph. D. Thesis, University of Toronto, 1974.

104. J. H. Kiefer and R. W. Lutz, J. Chem. Phys. 44, 658, 1966.

105. J. H. Kiefer, in Shock Waves in Chemistry, ed. A. Lifshitz, Marcel Dekker Inc, N. Y. 1981, p. 219.

106. J. R. Partington, An Advanced Treatise on Physical Chemistry, vol. 4; Longmans, Green and Co., London (1953) pp.9-20.

107. R. C. Weasst (ed.), Handbook of Chemistry and Physics, CRC Press, Cleveland (1974), p. E222.

108. N. B. Vargaftik, Tables on the Thermophysical Properties of Liquids and Gases, John Wiley & Sons, Inc. New York, 1964.

109. C. F. Gerald and P. O. Wheatley, Applied Numerical Analysis, 4th Ed., Addison-Wesley Publishing Corp., 1989.

110. T. Boublik, V. Fried and E. Hala, The Vapour Pressures of Pure Substances, Elsevier Publisher, 1984 .

111. W. C. Gardiner, Jr., B. F. Walker and C. B. Wakerfield, in Shock Waves in Chemistry, Ed. A. Lifshitz, Marcel Dekker Inc., N. Y., 1981, p. 319.

112. D. R. Lide (chief ed.) ,CRC Handbook of Chemistry and Physics, 73rd edition, 1992-1993, Boca Raton, p. 14-31.

113. D. M. Considine, Van Norstrand's Scientific Encylopedia, Seventh Edition, Van Nostrand Reinhold New York, (1984). p. 1189.

114. H. Mirrels, NACA, TN3401, Washington (1955).

115. S. H. Bauer, Ann. Rev. Phys. Chem. 16, 245, (1965).

116. J. C. Breeze and C. C. Ferriso, Phys. Fluids, 7, 1071, (1964).

117. H. Teitelbaum, C. Carruthers and K. Francoeur, 16th Symp.(Int.) on Shock Tubes and Shock Waves, Aachen, W. Germany (1988). p. 327.

118. W. J. Moore, Physical Chemistry, Englewood Cliffs, N. J. (1973).

119. H. Teitelbaum, P. Hamilton and Z. Cheng, J. Phys. Chem. 95, 4929, (1991).

120. J. E. Dove and H. Teitelbaum, in Shock Tube and Shock Wave Research, Proceedings of the 11th Symp. (Int.) on Shock Tubes and Waves, Seattle, (1977), p. 474.

121. D. R. Lide (chief ed.), CRC Handbook of Chemistry and Physics, 73rd edition, 1992-1993, Boca Raton, p. 6-27 .

122. B. Heijmen, C. Liedenbaum, S. Stolte and J. Reuss, Laser. Chem., 8, 275, (1988).

123. G. A. Morris Two-Dimensional Fourier Transform NMR Spectroscopy in Fourier, Hadamard, and Hilbert Transforms in Chemistry (ed. A. G. Marshall) Plenum Press, New York, (1982), p. 271.

124. P. R. Griffiths, Fourier Transform Infrared spectrometry: Theory and Instrumentation, in Transform Techniques in Chemistry (ed. P. R. Griffiths), Plenum Press, New York, (1978). p.109

125. L. M. Faires, Anal. Chem. 58, 1923A, (1986).

126. P. Berge, Y. Pomeau and C. Vidal, Order within Chaos, John Wiley & Sons, New York, (1984).

127. R. S. Dumont and D. Brumer, J. Chem. Phys., 88, 1481, (1988).

128. E. O. Brigham, The Fast Fourier Transform and its Applications, Englewood Cliffs, New Jersey, (1988).

129. P. R. Griffiths, ed. Transform Techniques in Chemistry, Plenum, New York, (1978).

130. M. Cartwright, Fourier Methods for Mathematicians, Scientists and Engineers,

Ellis Horwood Chiuchester, (1990).

131. W. H. Press, S. A. Teukolsky, W. T. Vetterling and B. P. Flannery, Numerical Recipes in C, Cambridge University Press, New York, (1992).

132. S. K. Scott, Chem. Britain, 23, 1183, (1987).

133. M. Alamgir and I. R. Epstein, J. Am. Chem. Soc., 105, 2500, (1983).

134. P. Rehmus and J. Ross, Periodically Perturbed Chemical Systems, Oscillations and Traveling Waves in Chemical Systems, ed. R. J. Field and M. Burger, John Wiley & Son, (1985), p. 287.

135. A. G. Marshall (ed.), Fourier, Hadamard, and Hilbert Transforms in Chemistry Plenum Press, New York, (1982).

136. J. M. Smith, Mathematical Modeling and Digital Simulation for Engineers and Scientists, John Wiley & Son, New York, (1987).

137. S. E. Stein and B. S. Rabinovitch , J. Chem. Phys, 58, 2438, (1973).

138. T. Beyer and D. F. Swinehart, Commun. Assoc. Comput. Machin. 16, 379, (1973).

139. J. Phys. Chem. Ref. Data, Vol. 14, Suppl. 1. (1985).

140. J. O. Hirschfelder, C. F. Curtiss and R. B. Bird, Molecular Theory of Gases and Liquids, John Wiley & Son, New York , (1952).

141. L. K. Nash, Elements of Statistical Thermodynamics, 2nd ed. Addison Wesley, California, (1972).

142. L. F. Shampine and C. W. Gear, SIAM Review, 21, 1, 1979.

143 C. W. Gear, Numerical Initial Value Problems in Ordinary Differential Equations,

Prentice-Hall, Englewood Cliffs, NJ, (1971).

144. I. Gladwell, D. K. Sayers, ed. Computational Techniques for Ordinary Differential Equations, Academic Press, (1980).

145. R. L. Burden and J. Douglas Faires, Numerical Analysis, PWS-KENT, Boston, (1989).

146. C. F. Curtiss and J. O. Hirschfelder, Proc. Nat. Acad. Sci. U.S. 38, p. 235, (1952).

147. L. Lapidus and W. E. Schiesser, eds. Numerical Methods for Differential systems, Academic Press, (1976).

148. G. Dahlquist, BIT, 3, 27, (1963).

149. J. C. Butcher, Math. Comp. 18, 50, (1964).

150. C. W. Gear, e-mail communication to H. Teitelbaum. Nov. (1992).

151. P. P. Wegener, Nonequilibrium Flow, Marcel dekker, New York (1969).

152. L. A. Curtiss and M. Blander, Chem. Rev. 86, 827, (1988).

153. M. R. Hoare and P. Pal, Adv. Phys. 20, 161, (1971).

154. R.J. Kee, L. R. Petzold, M. D. Smooke and M. D. Grear, Multiple Time Scales, ed. J. V. Brackbill and B. I. Cohen, Academic, New York,(1985).